

**Modular Tools for High Throughput Process Development of
Polysaccharide Vaccines**

A thesis submitted to University College London (UCL) for the degree of

ENGINEERING DOCTORATE

by

Aaron R. Noyes

The Advanced Centre for Biochemical Engineering, Department of Biochemical Engineering,
University College London, Bernard Katz Building, Gordon St., WC1E 7JE, United Kingdom

Abstract

Polysaccharide conjugate vaccines are typically comprised of several different polysaccharides produced with distinct and complex production processes. Clarification and primary recovery operations, such as particle conditioning are integral to purification. Efficient process development of these two unit operations has been constrained by lab-scale models that require large volumes and considerable time to evaluate. A modular approach to develop rapidly purification processes for polysaccharides at the micro-scale would greatly enhance productivity and speed the development of novel conjugate vaccines.

To enable high throughput screening, a suite of high throughput analytics was assembled for polysaccharide-containing feedstreams. Three orthogonal generic assays were developed for the high throughput determination of product titre. Assays for clarity and impurity determination were also optimized. The final comprehensive suite of high throughput analytics was qualified for analysis of product titre, product quality, impurity clearance, clarification efficiency, and particle size characterisation.

We developed a novel system for high throughput particle conditioning. With this system, 96 individual reaction conditions can be evaluated in parallel, including downstream centrifugal clarification. The scalability of particle conditioning was evaluated between USD reactors with less than 1 mL of volume up to Pilot-scale reactors of 14 L for several biological feedstreams derived from three host species. Product yield, impurity clearance, and product quality were comparable between scales. An engineering characterisation of the reactors was performed and several approaches for scaling particle conditioning processes were evaluated. To support this platform, a custom-built, modular system for depth filtration of eight conditions/filters in parallel was developed using 0.2 cm² area of media per channel. The reproducibility and scalability of this technology was demonstrated with several filtration media.

With this integrated approach to particle conditioning and depth filtration, we have shortened the process development time. The engineering scale up models developed in this thesis will facilitate the creation of more robust processes at pilot and commercial scales of operation.

Signed Declaration

I, Aaron R. Noyes, confirm that the work presented in this thesis is my own. Where information has been derived from other sources, I confirm that this has been indicated in the thesis.

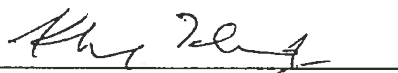
Aaron R. Noyes 03 Oct 14

Aaron R. Noyes

03 October 2014

Signed Declaration

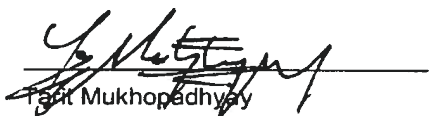
We, Khurram Sunasara and Tarit Mukhopadhyay, affirm supervision of the work presented in this thesis and the interpretation of the results.



Khurram Sunasara

19 FEB 2015

Date



Tarit Mukhopadhyay

20/02/2015

Date

Dedication

This journey would have been impossible but for my family. My incredible wife has been an unwavering source of inspiration, support, and love from the inception. Countless times, she has picked up the slack that I paid out, neither with hesitation nor complaint. My beautiful daughter has brightly dealt with the frequent travels and retreats to home office, becoming inspiration and motivation as she provided company seated atop piled books and papers. Amy and Brinley, this thesis is for you.

Acknowledgments

Raising a family of seven is no small feat but my parents managed to make it look easy, judiciously balancing support and autonomy while encouraging adventure. I am grateful for my parents and siblings, who conditioned me to believe that anything is possible. From a tender age when they reinforced my dream to become an astronaut (and a cow); I have always been taught that with hard work, you can do anything. It is a profound lesson and one with which I feel blessed to have been instilled.

This thesis was an incredible journey that will not soon fade from memory. Along the way, I have been helped by so many. Jon Coffman had the audacity to think that this collaboration was possible and Ranga Godavarti had the vision to make it happen. Khurram Sunasara stepped in admirably and has become a trusted supervisor and friend. I also owe a debt to Khurram's lab group who have patiently put up with my data reviews and telephone voice for the last few years.

UCL feels like home to me. For that, I am grateful to the community of friends, faculty, and staff. In particular, I will miss Nigel Titchener Hooker's uncanny capacity to rapidly frame a problem and see solutions clearly, always with a twinkle in his eye.

And Tarit, what can I say? You have been excellent. You have coached me and given me the guidance I needed to improve. I will miss your wit and intelligence. It is said that mimicry is the most sincere form of flattery and with that,

To my friends who made this incredible journey possible,

It was the best of times.

Table of Contents

1	Introduction	30
1.1	<i>Vaccinology History</i>	30
1.2	<i>Polysaccharide Vaccines</i>	32
1.3	<i>Market Information</i>	34
1.3.1	Current Vaccine Market	34
1.3.2	Drug Pipeline	35
1.3.3	Cost Considerations	37
1.4	<i>Vaccine Immunology</i>	38
1.5	<i>Polysaccharide Biology</i>	39
1.6	<i>Polysaccharide Stability</i>	41
1.6.1	Hold Time Stability of Purified Polysaccharides	41
1.6.2	Hydrolysis	42
1.6.3	Acetylation	43
1.6.4	Miscellaneous Degradation Pathways	44
1.7	<i>Vaccine Manufacturing</i>	44
1.7.1	History	44
1.7.2	Fermentation	45
1.7.3	Downstream Processing	45
1.7.3.1	Historical Methods	46
1.7.3.2	Primary Recovery and Dissociation from Cell Envelope	48
1.7.3.3	Holistic Process Research	49
1.8	<i>Particle Conditioning and Filtration Unit Operations</i>	50
1.8.1	Precipitation	50
1.8.1.1	Scaling Heuristics	52
1.8.2	Centrifugation	56

1.8.3	Filtration	58
1.9	<i>High Throughput Process Development</i>	59
1.9.1	Automation	61
1.9.2	Particle Conditioning	61
1.9.3	Integrated High Throughput Centrifugation	62
1.9.4	Integrated High Throughput Filtration	62
1.9.5	Impediments to Deployment of High Throughput Process Development	63
1.9.5.1	High Throughput Analytics	64
1.9.5.2	System and Hardware Constraints	65
1.9.5.3	Scaling Heuristics	65
1.9.5.4	Remaining Challenges	65
1.10	<i>Research Objectives</i>	66
1.10.1	Specific Objectives	67
2	Characterisation and Adaptation of Impurity Analytics to HTPD	68
2.1	<i>Introduction</i>	68
2.1.1	Impediments to High Throughput Process Development	68
2.1.2	Unique Requirements for Purification Process Development	68
2.1.3	Current Practise	69
2.1.3.1	Standard Reference Tests	69
2.1.4	Impurity Assays	71
2.1.4.1	Endotoxin	71
2.1.4.2	Protein	72
2.1.4.3	DNA	72
2.1.4.4	Rheology	73
2.1.4.5	Particle Characterisation	74
2.1.5	Interference	74
2.2	<i>Aim and Objectives</i>	74

2.3	<i>Materials and Methods</i>	75
2.3.1	Materials	75
2.3.2	Absorbance Spectra	76
2.3.3	Endotoxin Assay	76
2.3.4	Protein Assays	77
2.3.4.1	Bradford Assay	77
2.3.4.2	Bicinchoninic Acid Assay	77
2.3.5	DNA Assay	77
2.3.6	Rheology	78
2.3.7	Micro Flow Imaging	78
2.3.8	Nephelometry	79
2.3.9	Assay Reproducibility	79
2.4	<i>Results and Discussion</i>	80
2.4.1	Absorbance Spectra	80
2.4.2	Endotoxin Assay	81
2.4.3	Protein Assays	85
2.4.3.1	Accuracy and Precision	85
2.4.3.2	Interference	86
2.4.4	DNA Assay	88
2.4.5	Rheology	89
2.4.6	Micro Flow Imaging	92
2.4.7	Nephelometry	95
2.4.8	Assay Robustness	96
2.4.8.1	Standard Curve Reproducibility	96
2.4.8.2	Precision	98
2.4.9	Automation	100
2.5	<i>Chapter Summary</i>	100
3	Characterisation and Adaptation of Product Analytics to HTPD	102

3.1	<i>Introduction</i>	102
3.1.1	Carbohydrate Titre Assays	102
3.1.2	High Throughput Titre Assays	103
3.1.3	Phenol Sulphuric Acid Assay	104
3.1.4	Cationic Surfactants and Phase Separation	104
3.1.5	SEC-MALS	105
3.2	<i>Aim and Objectives</i>	106
3.3	<i>Materials and Methods</i>	107
3.3.1	Materials	107
3.3.2	Modified Phenol Sulphuric Acid Assay	108
3.3.3	Phase Separation Assay	109
3.3.3.1	Desalting	109
3.3.3.2	Enzymatic Treatments	110
3.3.4	SEC-MALS	110
3.3.4.1	HPLC-SEC-MALS	110
3.3.4.2	UPLC-SEC-MALS	111
3.4	<i>Results and Discussion</i>	111
3.4.1	Modified Phenol Sulphuric Acid Assay	111
3.4.2	Phase Separation Assay	120
3.4.2.1	Robustness	120
3.4.2.2	Reactivity with Bacterial Species	123
3.4.2.3	Interference from Impurities	124
3.4.2.4	Complex In-Process Samples	126
3.4.3	SEC-MALS	130
3.4.3.1	Optimization	130
3.4.3.2	Root Mean Square Radius	130
3.4.3.3	Molecular Weight	132
3.4.3.4	Conformation Slope Gradient Functions	133

3.4.3.5	Titre Measurements	135
3.5	<i>Chapter Summary</i>	136
4	High Throughput Particle Conditioning	139
4.1	<i>Introduction</i>	139
4.2	<i>Aim and Objectives</i>	139
4.3	<i>Materials and Methods</i>	140
4.3.1	Materials	140
4.3.2	High Throughput Particle Conditioning System	140
4.3.3	General Flocculation Procedure	143
4.3.3.1	S. aureus	144
4.3.3.2	N. meningitidis	144
4.3.3.3	S. pneumoniae	145
4.3.4	Core Suite of HTPC Assays	146
4.3.4.1	DNA	147
4.3.4.2	Turbidity	147
4.3.4.3	Protein	147
4.3.4.4	CPS Yield and Quality	147
4.3.4.5	UPLC-SEC-MALS	147
4.3.4.6	HPLC-SEC-MALS	148
4.3.4.7	Phase Separation Assay	148
4.3.4.8	Particle Sizing and Characterisation	148
4.3.5	Kinetics	148
4.3.6	Mixing Studies	149
4.3.7	Heat Transfer Characterisation	149
4.4	<i>Results and Discussion</i>	150
4.4.1	USD Platform Description	150
4.4.2	Blend Times	151

4.4.3	Engineering Characterisation	152
4.4.3.1	Regime Analysis	153
4.4.3.2	Power Number (N_p)	154
4.4.3.3	Heat Transfer	156
4.4.3.4	Hydrodynamics	157
4.4.4	Demonstrating Industrial Platform Scalability	159
4.4.5	Particle Conditioning with Polysaccharides	160
4.4.5.1	Flocculation with Staphylococcal CPS (SA1)	160
4.4.5.2	Flocculation with Staphylococcal CPS (SA2)	164
4.4.5.3	Flocculation with Meningococcal CPS	166
4.4.5.4	Flocculation with Pneumococcal CPS	171
4.4.5.5	Do All Floccs Have the Same Composition?	178
4.4.6	Sources of Scaling Discrepancies	179
4.5	<i>Chapter Summary</i>	181
5	High Throughput Depth Filtration	182
5.1	<i>Introduction</i>	182
5.1.1	Scale-down Models	183
5.1.2	Challenges	184
5.1.2.1	Commercial	184
5.1.2.2	Engineering	184
5.1.2.3	Scalability	185
5.1.2.4	Predicting Filterability	186
5.1.2.5	Clarity Assays	186
5.2	<i>Aim and Objectives</i>	187
5.3	<i>Materials and Methods</i>	187
5.3.1	Materials	187
5.3.2	Filtration Systems	188

5.3.2.1	Load Material	188
5.3.2.2	Laboratory-scale Filtration	188
5.3.2.3	Filterplates	189
5.3.2.4	Pre-existing Pfizer Device	190
5.3.2.5	UCL Constant Vacuum USD Device	190
5.3.2.6	Novel Constant Flux USD Device	191
5.3.2.7	Sterile Filtration at Constant Pressure	195
5.3.3	Generation of Filtrate Samples for Clarity Measurements	189
5.3.4	Clarity Measurements	196
5.3.4.1	Turbidity	196
5.3.4.2	Spectrophotometric (A_{405} , A_{600})	196
5.3.4.3	Particle Characterisation by Micro Flow Imaging	196
5.4	<i>Results and Discussion</i>	197
5.4.1	Correlates of Filterability	197
5.4.1.1	Particle Characterisation	198
5.4.1.2	Filterplates	200
5.4.2	Pre-existing Scale-down Options	201
5.4.2.1	Pre-existing Pfizer Device	202
5.4.2.2	UCL Constant Vacuum Device	203
5.4.3	Novel Micro-scale Depth Filtration Device	207
5.4.3.1	Device Design and Engineering	207
5.4.3.2	Filtration Performance	208
5.4.4	Micro-scale Clarity Measurements	216
5.5	<i>Chapter Summary</i>	217
6	Conclusions and Future Work	219
6.1	<i>Conclusion</i>	219
6.1.1	High Throughput Analytics	219

6.1.1.1	Product Quantification and Quality	219
6.1.1.2	Impurity Determination	220
6.1.2	High Throughput Particle Conditioning	220
6.1.3	High Throughput Depth Filtration	221
6.1.4	Final Conclusion	222
6.2	<i>Future Work</i>	223
6.2.1	High Throughput Analytics	223
6.2.2	High Throughput Particle Conditioning	223
6.2.2.1	Deepening Understanding of Scalability	223
6.2.2.2	Measuring Clarity	224
6.2.2.3	Predicting Clarification	224
6.2.2.4	Structure-function Relationships	224
6.2.2.5	Expand Applications	225
6.2.3	High Throughput Depth Filtration	225
6.2.4	Final Thoughts	225
7	References	226
8	Appendix A - Validation	243
8.1	<i>Research Objectives</i>	243
8.2	<i>Significance of Research</i>	243
8.3	<i>Key Validation Issues</i>	244
8.3.1	Overview	244
8.3.2	High Throughput Particle Conditioning Case Study	245
8.3.2.1	Quality by Design	246
8.3.2.2	Windows of Operation	247
8.4	<i>Regulatory Concerns</i>	249
8.4.1	Scaling Models	249

8.4.2	Limitations to Scale Equivalence	250
8.4.3	Looking to the Future	251
8.5	<i>Chapter Summary</i>	252
9	Appendix B – Supplementary Data	253
9.1	<i>Neisseria Meningitidis Case Study</i>	253
9.1.1	Meningococcal Pathogenesis	253
9.1.2	Meningococcal Epidemiology	253
9.1.3	Meningococcal Glycobiology	255
9.2	<i>Holistic Purification Process Development for CPS</i>	257
9.3	<i>Protein Assays</i>	259
9.4	<i>Differential Assay for Carbohydrates</i>	262
9.5	<i>Phase Separation Assay</i>	264
9.6	<i>Flocculation Kinetics at the Micro-scale</i>	267
9.7	<i>Engineering of USD Depth Filtration Device</i>	268
9.7.1	Tubing Diameter	268
9.7.2	Solids Holding Capacity	270
9.8	<i>Correlations between Clarity Measurements</i>	271
9.8.1	Nephelometry	272
9.8.2	Particle Characterisation	273
9.8.3	Comparison of Clarification Measurements	275
9.8.4	Clarity Correlations	276

List of Figures

Figure 1.1. Typical production process for meningococcal CPS	46
Figure 2.1. Absorbance spectra of compounds typically found in microbial broths and assorted carbohydrates.....	81
Figure 2.2. Effect of incubation temperature on the relative fluorescence measurements in the Pyrogene™ assay.....	82
Figure 2.3. Interference in the Pyrogene™ assay.	84
Figure 2.4. Absorptivity of various carbohydrates in BCA and Bradford assays.....	87
Figure 2.5. Reactivity of reducing sugars in BCA assay	88
Figure 2.6. Interference in Picogreen assay.	89
Figure 2.7. Rheological power law curves for microbial fermentation broths from different species and pneumococcal serotypes.....	90
Figure 2.8. Effect of hold time, diluent, and broth age on particle diameter (2.8a) and particle concentration (2.8b) of flocculated SA1.....	94
Figure 2.9. Correlation of MFI counts (counts/mL) and A_{600} (AU) with Hach turbidimetric values (NTU).	95
Figure 2.10. Consistency of DNA standard curves in the Picogreen assay across time.	98
Figure 2.11. RSD for duplicate flocculations assayed with six different techniques.....	99
Figure 3.1. Glucose standard curves generated with variants of PHS assay, prepared in triplicate.	112
Figure 3.2. Slopes of standard curves for neutral and anionic hexoses and pentoses in the modified PHS assay.	115
Figure 3.3. Reaction of carbohydrates listed in Figure 3.2, plotted as a function of common reactive sugars.	116
Figure 3.4. Dynamic linear range for concentration measurements in modified PHS assay.....	118
Figure 3.5. Concentration of interfering species required to effect 20% shift in the PHS assay response	119
Figure 3.6. Effect of Hb reagent concentration on turbidity of Mn C samples prepared in 25 mM sodium phosphate, pH 7.2 or RODI.....	122

Figure 3.7. Reactivity of bacterial CPS from <i>S. pneumoniae</i> in the precipitation assay, with serotype identified in the legend.	123
Figure 3.8. Elimination of DNA interference from the phase separation assay.	126
Figure 3.9. Robustness of titre assay to samples taken from different locations in the purification trains for two CPS from <i>S. aureus</i>	128
Figure 3.10. Enhancement in assay performance with DNase treatment of fermentation broth samples	129
Figure 3.11. Effect of buffer and column on r_{rms} for CPS serotypes from two bacterial species.	131
Figure 3.12. Effect of buffer and column on MW for CPS serotypes from two bacterial species.....	132
Figure 3.13. Effect of buffer and column on conformation slope for CPS serotypes from two bacterial species.....	134
Figure 3.14. Accuracy of UPLC-MALS for titre measurements using SA1 CPS from an intermediate in-process pool.....	136
Figure 4.1a, b. Schematic of the USD flocculation device (4.1a) and flow diagrams for HTPC (4.1b).	141
Figure 4.2. Mixing constants (95% mixed) as a function of Reynolds number (N_{Re}), measured in duplicate in the USD system using iodometry	152
Figure 4.3. Heat transfer in the microplate for different volumes with various insulation configurations.	157
Figure 4.4a, b. CPS yield (percentage of load control) in the supernatant as a function of the floc agent concentration and pH during the flocculation process for staphylococcal CPS SA1.	161
Figure 4.5a, b. CPS MW (relative to the mean MW for both scales at 2.5% floc agent concentration/pH 5.5) in the supernatant as a function of the floc agent concentration and pH during the flocculation process for staphylococcal CPS SA1.	162
Figure 4.6a, b. DNA clearance (percentage of load control) in the supernatant as a function of the floc agent concentration and pH during the flocculation process for staphylococcal CPS SA1.....	163
Figure 4.7a, b. DNA clearance (percentage of load control) in the supernatant as a function of the floc agent concentration and pH during the flocculation process for staphylococcal CPS SA2.....	165
Figure 4.8a, b, c. Scaling by N_{js} , P/V_{avg} , λ_K , E_{fr} , Ca , or v_{tip} , P/V_{imp} , λ_{Kimp} : Effect of scaling meningococcal flocculation using different scaling rules on MFI-derived particle characterisation.	169

Figure 4.9. Scaling by P/V_{avg} , λ_{kavg} , E_{fr} and/or Ca: Flocculations with a neutral pneumococcal CPS were performed at the 13 L scale and centrifuged in a semi-continuous disk-stack (dark gray bars) or in a swinging bucket (light gray bars) centrifuge.	172
Figure 4.10. Statistical analyses from the full factorial HTPC with the neutral pneumococcal CPS (see Table 4.2).	175
Figure 4.11. Scale-up of impurity removal from a particle conditioning step for a neutral pneumococcal CPS at 0.6 mL to 700 L.	177
Figure 5.1a, b. Media substrate after laser cutting of 255 filter discs (left: 6.1a). Filter pucks: depth filter discs embedded in epoxy with an embedded flat plastic washer serving as the top sealing surface (right: 6.1b).	192
Figure 5.2a, b, c, d. Final micro-scale depth filtration device.	194
Figure 5.3. Changes in filtration flux at nominal constant feed pressure with four staphylococcal centrate samples at 17 cm ² -scale (47 mm discs).	198
Figure 5.4a, b, c. Correlating particle properties measured with MFI with 0.22 μ m filterability.	199
Figure 5.5. Relative filterability of samples A-D in various filterplates.	201
Figure 5.6. Hydraulic profiles for 270 cm ² lab-scale pods (LSP), 23 cm ² Micropods, and 2.6 cm ² internal Pfizer device (Bend device) replicates.	202
Figure 5.7a, b. A1HC depth filtration in constant vacuum USD device.	205
Figure 5.8. Correlation of water permeability of A1HC with the filtration performance obtained with CHO centrate.	206
Figure 5.9. Water permeability of steric depth filtration media.	209
Figure 5.10a, b, c. Hydrodynamics during centrate filtration at USD- (solid lines) and lab-(dashed lines) scales for 30SP (5.10a), 60SP with freshly thawed centrate (5.10b), and 60SP with thawed centrate held for several hours at room temperature (5.10c).	210
Figure 5.11. Throughput achieved at 172 kPa pressure with steric depth filters at two scales.	211
Figure 5.12a, b. Filtrate clarity of filtration scale-down. Mean turbidity of 30SP filtrate (5.12a) and 60SP filtrate (5.12b) at two scales.	213
Figure 5.13a, b. X0HC filtration at USD- and lab-scale.	215
Figure 5.14. Filtrate clarity of X0HC runs.	216

Figure 8.1. Pareto plot for percentage of load control A_{600} remaining (data in Table 4.3)	246
Figure 8.2. Contour plot model of DNA clearance (percentage of load control) for HTPC with neutral pneumococcal CPS.	247
Figure 8.3. Window of operation for a particle conditioning operation with a neutral pneumococcal CPS where $Ca = 6.5 \times 10^5$	248
Figure 9.1. Distribution of <i>N. meningitidis</i> serotypes around the world.....	254
Figure 9.2. Outer cellular structure of <i>N. meningitidis</i>	256
Figure 9.3. Standard curves (9.3a) and statistical effect (9.3b) of adjusting the dynamic range of BSA in the protein assays.	260
Figure 9.4. Relative standard deviation of two different measurement parameters for generating standard curves with the Bradford assay.	260
Figure 9.5a, b. Standard curves generated with the Bradford assay for assorted carbohydrates and compounds typically found in microbial broths.....	261
Figure 9.6. Determination of reducing sugar concentration through differential analysis of orthogonal protein assays.	263
Figure 9.7a, b. Precision (n=6) and dynamic range of phase separation assay for Mn C (9.7a) and Mn Y (9.7b).	265
Figure 9.8a b. Figure 9.7 plotted on a semi-log-transformed plot	266
Figure 9.9a, b. Kinetic curves for the flocculation of staphylococcal CPS SA1 (9.9a) and SA2 (9.9b) during dynamic aging steps.	267
Figure 9.10. Hydraulic profiles for filtration performed with X0HC, C0HC, D0HC, and CE50 depth filters.	272
Figure 9.11. Hach turbidity values for filtrate samples during four filter trials.	273
Figure 9.12a, b. Particle characterisation of filtrate samples.....	274
Figure 9.13a, b, c, d. Responses of clarity assays across four filtration runs	276
Figure 9.14a, b. Correlation of Hach NTU with MFI particle counts.	278
Figure 9.15. Correlation between two nephelometric turbidity measurements.	279
Figure 9.16. Correlations between Hach turbidity and absorbance at two wavelengths: A_{405} (green) and A_{600} (blue).....	280

Figure 9.17. Correlations between A_{600} and two nephelometric turbidity measurements: Nephelostar
NTU (blue) and Hach NTU (red). **281**

List of Tables

Table 1.1. Chronology of key milestones in human vaccine development	30
Table 1.2. Chronology of the evolution of vaccine classes	32
Table 1.3. CPS vaccines licensed in the United States	33
Table 1.4. Recently approved polysaccharide conjugate vaccines	34
Table 1.5. Polysaccharide vaccines in development.....	36
Table 1.6. Repeating units of CPS for selected bacterial pathogens	40
Table 1.7. Overview of manufacturing purification processes for CPS from <i>N. meningitidis</i>	47
Table 2.1. WHO and European Pharmacopeia specifications for polysaccharide components of vaccines	70
Table 2.2. Reference assays for vaccine products as indicated in WHO and European Pharmacopeia documentation	71
Table 2.3. Maximum endotoxin clearance values that can be measured in the presence of interfering species.....	85
Table 2.4. Viscosity and Ostwald-de Waele parameters for polysaccharide-containing fermentation broths	91
Table 3.1. Comparison of PHS methods.....	108
Table 3.2. Column and chromatographic properties for SEC-MALS screening.	111
Table 3.3. Absorbance maxima for carbohydrates and other molecules commonly found in in-process pools of CPS production processes	114
Table 3.4. Molar absorptivity of reactive sugars in proposed PHS assay.....	117
Table 4.1. Engineering characterisation of the flocculation reactors.	142
Table 4.2. Mixing constants (θt) in the USD system.	154
Table 4.3. A full factorial flocculation study at the 0.8 mL scale was performed with a neutral pneumococcal CPS.	174
Table 5.1. Available options for scale-down of depth filtration.	183
Table 5.2. Filterplates used for filterability correlation work.....	190

Table 9.1. Chronology of meningococcal vaccine development **255**

Table 9.2. Repeating structures of pathogenic *N. meningitidis* CPS. **257**

Table 9.3. Summary of research into downstream processing of meningococcal polysaccharide **257**

Table 9.4. Amount of glucose calculated from differential method..... **263**

Table 9.5. Engineering characteristics of depth filtrations systems at several scales **269**

Table 9.6. Effect of percentage solids and filter throughput on the height of the solids holding area
 required..... **271**

Nomenclature

<i>A</i>	empirical constant
<i>A_{XXX}</i>	optical absorbance measured at a wavelength of XXX nm (AU)
<i>HAc</i>	acetic acid
<i>Ara</i>	L-arabinose
<i>AU</i>	absorbance units
<i>BARDA</i>	Biomedical Advanced Research and Development Authority
<i>BCA</i>	bicinchoninic acid
<i>BLOQ</i>	below the limit of quantification
<i>BSA</i>	bovine serum
<i>C</i>	impeller clearance off tank bottom (m)
<i>Ca</i>	Camp number ($\bar{G}t$)
<i>C_{BT}</i>	correction factor to compensate for flow patterns not included in initial Σ derivation
<i>C_{DSC}</i>	correction factor to compensate for flow patterns not included in initial Σ derivation
<i>CD</i>	circular dichroism
<i>CDC</i>	Centre for Disease Control
<i>CHO</i>	Chinese Hamster Ovary cell culture
<i>CMC</i>	critical micelle concentration
<i>COGs</i>	cost of goods
<i>cP</i>	centipoise
<i>CPS</i>	capsular polysaccharide
<i>CRM</i>	cross-reactive material; a non-toxic mutant of diphtheria toxin, with glutamic acid substituted for glycine
<i>CSA</i>	cross-sectional area
<i>CTAB</i>	cetyl trimethylammonium bromide, Hb
<i>D</i>	impeller diameter (m)
<i>DOE</i>	Design of Experiments
<i>D/T</i>	ratio of impeller diameter to tank diameter

<i>DF</i>	diafiltration
<i>DLS</i>	dynamic light scattering
<i>DNA</i>	deoxyribonucleic acid
<i>DOE</i>	Design of Experiment
d_p	particle diameter
<i>DSC</i>	disc-stack centrifuge
E_f	time-integrated fluid stress (W s m^{-3})
<i>EDTA</i>	ethylenediaminetetraacetic acid
<i>EtOH</i>	ethanol
<i>EU/mL</i>	endotoxin units per mL
G	gravitational acceleration (m s^{-2})
\bar{G}	mean velocity gradient (s^{-1})
$\bar{G}_{imp}t$	time-integrated mean velocity gradient in impeller zone
<i>Gal</i>	galactose
<i>GAVI</i>	global Vaccine Alliance
<i>Glc</i>	glucose
<i>GlcA</i>	glucuronic acid
<i>GSK</i>	GlaxoSmithKline plc
<i>GulA</i>	glucuronic acid
H	tank height (m)
h	hour; height of channel (μm)
<i>HA</i>	hyaluronan
<i>Hb</i>	hexadecyltrimethylammonium bromide, CTAB
<i>Hib B</i>	a capsular polysaccharide serotype from <i>H. influenzae</i>
<i>HPAEX-PAD</i>	high pressure anion exchange chromatography with pulsed amperometric detection;
<i>HPLC</i>	high pressure liquid chromatography
<i>HT</i>	high throughput
<i>HTDF</i>	high throughput depth filtration
<i>HTPC</i>	high throughput particle conditioning

<i>HTPD</i>	high throughput process development
<i>HTS</i>	high throughput screening
<i>IgG</i>	Immunoglobulin G
<i>IgM</i>	Immunoglobulin M
K_1	empirical constant in Mark-Houwink-Sakurada equation
K_2	consistency index in Ostwald-de Waele relationship ($N s^n m^{-2}$)
<i>kDa</i>	kiloDalton
<i>LAL</i>	<i>Limulus</i> amoebocyte lysate, a method for quantifying endotoxin
<i>LMH</i>	filtration flux ($L s^{-1} m^{-2}$)
<i>LOQ</i>	limit of quantification
<i>LPS</i>	lipopolysaccharide
<i>LRV</i>	log reduction value
<i>LSP</i>	lab-scale pods, depth filtration devices with 270 cm ² area
<i>M</i>	molarity
<i>m</i>	metre
<i>m/v</i>	mass per volume
<i>MALS</i>	multi-angle static light scattering
<i>Man</i>	mannose
<i>MDa</i>	megaDalton
<i>MFI</i>	Micro Flow Imaging
<i>mg</i>	milligram
<i>min</i>	minute
<i>mL</i>	millilitre
<i>mM</i>	millimolarity
<i>Mn A</i>	capsular polysaccharide serotype A from <i>N. meningitidis</i>
<i>Mn C</i>	capsular polysaccharide serotype C from <i>N. meningitidis</i>
<i>Mn W135</i>	capsular polysaccharide serotype W135 from <i>N. meningitidis</i>
<i>Mn Y</i>	capsular polysaccharide serotype Y from <i>N. meningitidis</i>
<i>MOPS</i>	3-(N-morpholino)propanesulfonic acid

<i>MPa</i>	megapascal
<i>MW</i>	molecular weight (kDa)
<i>n</i>	number of impellers; flow behaviour index
<i>N</i>	stirrer speed (s^{-1})
<i>NaAc</i>	sodium acetate
<i>NANA</i>	N-acetyl neuraminic acid
<i>N_{js}</i>	suspended speed
<i>nm</i>	nanometre
<i>NOR</i>	normal operating range
<i>N_p</i>	Power number
<i>N_{Re}</i>	Reynolds Number ($\frac{ND^2\rho}{\eta}$)
<i>NTU</i>	Nephelometric turbidity units
<i>NMR</i>	nuclear magnetic resonance
<i>NMWCO</i>	nominal molecular weight cut-off (kDa)
<i>OD</i>	optical density, synonymous with absorbance (AU)
<i>PAR</i>	proven acceptable range
<i>P/V</i>	power input per liquid volume ($W m^{-3}$)
<i>P/V_{avg}</i>	average power input per liquid vessel volume ($W m^{-3}$)
<i>P/V_{imp}</i>	power input per impeller swept volume ($W m^{-3}$)
<i>PBS</i>	phosphate buffered saline
<i>pH</i>	measure of acidity or basicity of a solution
<i>PHS</i>	phenol sulphuric acid method
<i>pp</i>	polypropylene
<i>ppm</i>	parts per million
<i>Ppt</i>	precipitation
<i>PTFE</i>	polytetrafluoroethylene
<i>PVDF</i>	polyvinylidene fluoride
<i>Q</i>	feed flow rates ($mL min^{-1}$)

<i>QbD</i>	Quality by Design
Q/Σ	centrifugal scaling method of maintaining flow rate (Q)/settling area (Σ)
R^2	correlation coefficient
<i>RCF</i>	relative centrifugal force
<i>RFU</i>	relative fluorescent unit
<i>RI</i>	refractive index
r_i	inner radii (m)
<i>Rib</i>	ribose
r_o	outer radii (m)
<i>RODI</i>	water purified by reverse osmosis filtration and deionization
r_{rms}	root mean square radius (nm)
<i>RSD</i>	relative standard deviation
<i>RT</i>	room temperature
<i>s</i>	second
<i>SA1</i>	capsular polysaccharide serotype from <i>S. aureus</i>
<i>SA2</i>	capsular polysaccharide serotype from <i>S. aureus</i>
<i>SEC</i>	size exclusion chromatography
<i>SDQ</i>	scale-down qualification
<i>SPa</i>	capsular polysaccharide serotype from <i>S.pneumoniae</i>
<i>SPb</i>	capsular polysaccharide serotype from <i>S.pneumoniae</i>
<i>SPc</i>	capsular polysaccharide serotype from <i>S.pneumoniae</i>
<i>SPd</i>	capsular polysaccharide serotype from <i>S.pneumoniae</i>
<i>SPe</i>	capsular polysaccharide serotype from <i>S.pneumoniae</i>
<i>SPf</i>	capsular polysaccharide serotype from <i>S.pneumoniae</i>
<i>SPg</i>	capsular polysaccharide serotype from <i>S.pneumoniae</i>
<i>t</i>	time; aging time (s)
<i>T</i>	tank diameter (m)
<i>TE buffer</i>	10 mM Tris-HCl, 1 mM EDTA, pH 7.5
<i>TFF</i>	tangential flow filtration

<i>TT</i>	tetanus toxoid
<i>UF</i>	ultrafiltration
<i>UPLC</i>	ultra high pressure liquid chromatography
<i>USD</i>	ultra scale-down
v_{tip}	impeller tip speed ($m\ s^{-1}$)
<i>V</i>	liquid volume (m^3)
v/v	volume per volume
V_{imp}	liquid volume in the impeller swept volume (m^3)
V_{max}	total volume of filtrate that can pass through a given filter area before it plugs (mL)
v_s	sedimentation velocity ($m\ s^{-1}$)
v_{tip}	impeller tip speed ($m\ s^{-1}$)
<i>w</i>	width of channel (μm)
<i>WHO</i>	World Health Organization
<i>Z</i>	liquid height (m)
<i>Z/T</i>	ratio of liquid height to tank height

Greek Letters

γ	shear rate (s^{-1})
γ_{app}	apparent shear rate for Newtonian fluids (s^{-1})
ϵ_{avg}	average energy dissipation rate ($W\ m^{-2}$)
ϵ_{imp}	minimum local energy dissipation rate ($W\ m^{-2}$)
ϵ_{max}	maximum local energy dissipation rate ($W\ m^{-2}$)
$(\epsilon_{loc}/\epsilon_{avg})_{max}$	maximum value of local energy dissipation rate
η	dynamic viscosity (Pa s)
ϑ	angle of discs relative to the vertical axis ($^\circ$)
$\vartheta_{0.95}$	blend time for 95% homogeneity (s)
$\vartheta_{0.95} t$	mixing constants for 95% homogeneity
λ_K	Kolmogorov length scale (m)
λ_{Kavg}	average Kolmogorov length scale (m)

λ_{kimp}	Kolmogorov length scale in impeller zone (m)
λ_{max}	maximum Kolmogorov length scale (m)
ν	kinematic viscosity (η/ρ)($m^2 s^{-1}$)
μL	microlitre
μg	microgram
μm	micron
ρ	liquid density ($kg m^{-3}$)
ρ_f	density of the fluid ($kg m^{-3}$)
ρ_p	density of the particle ($kg m^{-3}$)
τ	shear stress ($N m^{-2}$)
$\tau_{turb}/\rho v_{tip}^2$	maximum turbulent shear stress normalized by v_{tip} ($N m^{-2}$)
ω	angular velocity ($radian s^{-1}$)
Σ	centrifuge sigma factor (m^2)

1 Introduction

1.1 Vaccinology History

Vaccine technology has undergone a slow evolution since the initial vaccine trial in 1796 (Table 1.1)(Plotkin, 2005). Smallpox notwithstanding, early vaccines consisted of attenuated microorganisms or viruses that had been weakened with heat, desiccation, chemical treatment, or multiple exposures to high temperature. A major breakthrough occurred with the discovery that inoculation with discrete components of the original microorganism or virus, otherwise known as subunit vaccines, was effective in providing immunological protection. The earliest of these subunit vaccines consisted of extracts of infectious organisms such as anthrax, diphtheria, tetanus, and influenza.

Table 1.1. Chronology of key milestones in human vaccine development

Date	Advance	Details
1796	Vaccination with virus	Inoculation of cowpox in young boy is shown to protect against smallpox (Jenner, 1798)
1885	Attenuated vaccine	Inoculation of desiccated rabies virus protects against potential rabies infection (Mandell et al., 2004)
1896	Inactivated whole microorganism	Typhoid vaccine of inactivated whole cells (Plotkin, 2005)
1936	Growth of viruses in cell culture	Poliomyelitis virus cultivated in human embryos (Plotkin, 2005)
1969	Polysaccharide subunit	<i>N. meningitidis</i> Group A and Group C vaccine tested in humans (Gotschlich et al., 1969b)
1977	Multivalent polysaccharide	A multivalent capsular polysaccharide vaccine comprised of 14 <i>S. pneumoniae</i> serotypes is licensed in the U.S. (Robbins et al., 1983)
1980	Conjugate	<i>H. influenzae</i> Type B polysaccharide coupled to diphtheria toxoid (Granoff et al., 1984)
1984	Recombinant vaccine	Hepatitis B grown in <i>S. cerevisiae</i> (McAleer et al. 1984)
1986	Protein subunit	Hepatitis B protein vaccine is developed (Bae et al., 2009)
2005	Multivalent polysaccharide conjugate	A tetravalent polysaccharide conjugate vaccine against meningococcal meningitis is licensed in US (Meningitis Vaccine Project, 2011)

The first vaccines employing purified molecules were toxoid based vaccines using non-specific alum-protein precipitation to concentrate and purify the vaccine. However, as more sophisticated purification methods were developed, it became possible to isolate and purify capsular polysaccharides (CPS) to protect against typhoid, pneumococcal, and meningococcal infections (Table 1.2)(Genco et al., 1976).

Soon thereafter, proteins were isolated and employed as vaccines against Hepatitis B and Lyme disease (Bae et al., 2009; Plotkin, 2005). Genetic engineering improved the manufacturability of vaccine components by enabling expression in non-virulent host organisms (McAleer et al., 1984). As understanding progressed, vaccine manufacturers combined antigens representing several diseases into a single vaccine formulation, as was the case with measles, mumps, and rubella (Plotkin, 2005). An analogous strategy was pursued for multivalent CPS vaccines against infectious microorganisms, in which multiple strain-specific components were included to protect against the most prevalent pathogenic serotypes.

Table 1.2. Chronology of the evolution of vaccine classes (adapted from (Plotkin, 2005))

Vaccine Strategy	Date	Vaccine or Target
Inactivated whole organisms	1896	Typhoid
	1896	Cholera
	1897	Plague
	1926	Whole-cell pertussis
	1938	Influenza
	1955	Inactivated polio vaccine
	1995	Hepatitis A
Use of extracts, toxoids, subunits	1944	Japanese encephalitis
	1970s	Influenza
	1960	Anthrax
	1976	Cell-culture rabies
	1923	Diphtheria
	1927	Tetanus
Use of capsular polysaccharides	1977	Pneumococcal
	1974	Meningococcal
	1995	Typhoid
Use of protein-conjugated capsular polysaccharides	1987	<i>H. influenzae</i> type b
	2002	Pneumococcal
	2002	Meningococcal
	Future	Staphylococcal
	1986	Hepatitis B ^a
	1996	Acellular pertussis ^b
	1998	Lyme disease

^aPlasma-derived vaccine in 1981 ^bEarlier in Japan

1.2 Polysaccharide Vaccines

In recent decades, the pharmaceutical industry has shifted away from naked CPS vaccines towards producing conjugate vaccines that can be administered to infants within the typical immunization schedule for improved longevity of the immune response (Astronomo and Burton, 2010). CPS conjugate vaccines link covalently the carbohydrate to an adjuvant, typically a protein. The first CPS conjugate vaccine was targeted against *Haemophilus influenzae* type B (Hib B)(Schneerson et al., 1980). The success of this formulation compelled manufacturers to create vaccines against several serotypes of *Neisseria meningitidis* and *Streptococcus pneumoniae* (Frasch, 1990; Jones, 2005a). In recent years, additional polysaccharide-based vaccines have been produced. Table 1.3 lists the vaccines that have been approved by the Food and Drug Administration for sale in the United States.

Table 1.3. CPS vaccines licensed in the United States (adapted from (Astronomo and Burton, 2010))

Indication	Vaccine	Manufacturer (Trade name)
<i>Haemophilus influenzae</i> type b (Hib)	Glycoconjugate, polysaccharide with tetanus toxoid (TT)	Sanofi Pasteur (ActHIB); GlaxoSmithKline Biologicals (Hiberix)
	Diphtheria toxoid (DT), TT and acellular pertussis adsorbed, inactivated poliovirus and Hib-TT conjugate vaccine	Sanofi Pasteur (Pentacel)
	Hib conjugate (meningococcal protein conjugate)	Merck & Co (PedvaxHIB)
	Hib conjugate (meningococcal protein conjugate) and hepatitis B (recombinant) vaccine	Merck & Co (Comvax)
<i>Neisseria meningitidis</i> A, C, Y and W-135	Glycoconjugate, meningococcal polysaccharide with DT	Sanofi Pasteur (Menactra)
	Glycoconjugate, meningococcal polysaccharide with CRM197	Novartis (Menveo)
	Meningococcal polysaccharide	Sanofi Pasteur (Menomune-A/C/Y/W-135)
<i>Salmonella typhi</i>	Vi capsular polysaccharide	Sanofi Pasteur (TYPHIM Vi)
<i>Streptococcus pneumoniae</i> 4, 6B, 9V, 14, 18C, 19F and 23F	Pneumococcal polysaccharide 7-valent-CRM197 conjugate	Pfizer (Prennar-7)
<i>Streptococcus pneumoniae</i> 1, 3, 4, 5, 6A, 6B, 7F, 9V, 14, 18C, 19A, 19F and 23F	Pneumococcal polysaccharide 13-valent-CRM197 conjugate	Pfizer (Prennar-13)
<i>Streptococcus pneumoniae</i> 1, 2, 3, 4, 5, 6B, 7F, 8, 9N, 9V, 10A, 11A 12F, 14, 15B, 17F, 18C, 19F, 19A, 20, 22F, 23F and 33F	Pneumococcal polysaccharide, 23-valent	Merck & Co (Pneumovax 23)

CRM197 = cross reactive material: diphtheria toxin engineered to be nontoxic by substitution of glutamic acid for glycine

The number of serotypes included in a CPS conjugate vaccine is largely dependent on the epidemiology of the disease. Bacterial meningitis provides an illustrative example. This disease is most commonly caused by *H. influenzae*, *N. meningitidis*, and *S. pneumoniae*. A monovalent Hib B vaccine against meningitis was highly effective, resulting in greater than 99% reduction in the incidence of invasive disease in children less than five years of age (Centers for Disease Control, 2002). Meningococcal meningitis is caused primarily by five serotypes of *N. meningitidis* (*i.e.* A, B, C, Y, and

W135) and 83% of pneumococcal meningitis in children under four years of age is caused by seven serotypes of *S. pneumoniae* (Black et al., 2000; Joshi et al., 2009). The breadth of disease-causing strains has necessitated that many contemporary CPS conjugate vaccines are multivalent.

1.3 Market Information

1.3.1 Current Vaccine Market

In 2013, the worldwide vaccine market was estimated at \$32 billion dollars (Markets and Markets, 2013). Within the CPS polysaccharide conjugate segment, most of the revenue was derived from the licensure of competing vaccines against a few key bacterial infections (Table 1.4).

Table 1.4. Recently approved polysaccharide conjugate vaccines (adapted from (Frasch, 2009))

Organism	Vaccine manufacturer	First licensed	Saccharide	Carrier protein	Vaccine dose (μg)
H. influenzae type b	Pfizer	1988	Hib oligo	CRM 197	10
	Merck & Co.	1989	Hib size reduced	OMPC	7.5
	Sanofi Pasteur	1993	Hib PS	Tetanus toxoid	10
	GSK	1996	Hib PS	Tetanus toxoid	10
Meningococcus	Pfizer	1999	C size reduced	CRM 197	10
	Baxter	2000	C De-OAc PS	Tetanus toxoid	10
	Novartis	2000	C oligosaccharide	CRM 197	10
	Sanofi Pasteur	2005	A, C, Y, W size reduced	Diphtheria toxoid	4 each
Meningococcal/Hib	GSK	2005	Hib, Men C	Tetanus toxoid	5 each
Pneumococcal	Pfizer	2000	4, 6B, 9V, 14, 18C, 19F, 23F PS except 18C (oligosaccharide)	CRM 197	2 (4 μg 6B)

OMPC = outer membrane complex of *N. meningitidis*

With a projected compound annual growth rate of 11.4%, the vaccine market is expected to expand to \$84 billion dollars in 2022. Projections indicate that multivalent CPS conjugate vaccines will eventually occupy more than 50% of the world market (Bae et al., 2009).

With the exception of the US, the vaccine market is largely driven by growth based on the public health policies of national governments. While we accept this growth is projected on nation-state actors who will most likely expand the immunization schedule, it does require the final cost-per-dose to be affordable for each geographic territory. As such, the population served by vaccines is, in part, dependent on the cost of the vaccine.

1.3.2 Drug Pipeline

The growing vaccines sector has revived vaccine research and development, leading to a proliferation of polysaccharide vaccine candidates in the industry's pipeline (Table 1.5). As of 2013, vaccines against bacterial infections comprised 15%, by project number, of the industrial vaccine pipeline (Stephens, 2014). The evidence suggests that multivalent conjugate vaccines will form an increasingly large share of future approved vaccines (Astronomo and Burton, 2010; Bae et al., 2009; Hecht et al., 2009).

Table 1.5. Polysaccharide vaccines in development (adapted from (Astronomo and Burton, 2010))

Indication	Vaccine	Phase
Enterohaemorrhagic <i>Escherichia coli</i>	O-specific polysaccharide-protein conjugate	Phase I
Group A <i>Streptococcus</i> spp.	Glycoconjugate of Group A polysaccharide with TT	Preclinical
Group B <i>Streptococcus</i> spp.	Glycoconjugate of type 1a, 1b, II, III and V polysaccharides linked to carrier proteins	Phase II
<i>Haemophilus influenzae</i> (non typeable)	Subunit-detoxified lipooligosaccharide conjugate	Preclinical
<i>Pseudomonas aeruginosa</i>	Octavalent glycoconjugate of O-polysaccharide with toxin A	Phase III
<i>Salmonella typhi</i>	rEPA-Vi conjugate vaccine	Phase III
<i>Shigella dysenteriae</i>	O-specific polysaccharide-protein conjugate	Preclinical
<i>Shigella flexneri</i>	O-specific polysaccharide-protein conjugate	Phase II
<i>Shigella sonnei</i>	O-specific polysaccharide-protein conjugate	Phase III
<i>Streptococcus pneumoniae</i>	Glycoconjugates of synthetic 6B polysaccharide motifs	Preclinical
<i>Vibrio cholera</i>	Lipopolysaccharide-protein conjugate	Phase I
<i>Aspergillus fumigates</i>	β -glucan-CRM 197 conjugate	Preclinical
<i>Candida albicans</i>	Cell surface oligomannosyl epitope (various conjugates) β -glucan-CRM 197 conjugate	Preclinical Preclinical
<i>Cryptococcus neoformans</i>	Glycoconjugates of capsular polysaccharide with TT β -glucan-CRM 197 conjugate	Phase I Preclinical
<i>Leishmania</i> spp.	Lipophosphoglycan Lipophosphoglycan conjugates	Preclinical Preclinical
<i>Plasmodium falciparum</i>	Glycosylphosphatidylinositol-KLH conjugate	Preclinical
HIV-1	Man $\alpha(1 \rightarrow 2)$ Man oligomannosyl epitope (various conjugates, engineered yeast strains and modified glycoproteins)	Preclinical
Breast cancer	Unimolecular hexavalent conjugates (Globo H-GM2-Lewis ^Y -sTn-TF-Tn-R) sTn(c)-KLH plus QS-21 as adjuvant	Preclinical Phase I
Epithelial cancer	Globo H-GM2-Lewis ^Y -MUC1-32(aa)-sTn(c)-TF(c)-Tn(c)-KLH conjugate vaccine plus QS-21 as adjuvant	Phase I
Melanoma	GM3NPhAc-KLH	Preclinical
Prostate cancer	Unimolecular hexavalent conjugates (Globo H-GM2-Lewis ^Y -sTn-TF-Tn-R) TF(c)-KLH plus QS-21 as adjuvant Tn(c)-KLH and Tn(c)-palmitic acid Globo H-GM2-Lewis ^Y -MUC1-32(aa)-TF(c)-Tn(c)-KLH conjugate vaccine plus QS-21 as adjuvant	Preclinical Phase I Phase I Phase II

1.3.3 Cost Considerations

The capability of vaccines to prevent disease is greater than ever but the full global health benefit has not been realized. Every year, 1.5 million children die from vaccine-preventable diseases, many of whom die from underuse of available but cost-prohibitive vaccines (Bill and Melinda Gates Foundation, 2014). Multivalent conjugate vaccines are time-consuming and complex to manufacture and thus, are expensive relative to other vaccines. Indeed, multivalent pneumococcal CPS conjugate vaccines are designated as \$83 per dose in the United States Centre for Disease Control (CDC) cost-benefit analysis (Centers for Disease Control, 2005). Although many vaccine manufacturers, including Pfizer, donate and offer vaccines at discounted prices in developing countries, there remains a chronic lack of availability due to the high costs of developing, producing, storing, transporting, and administering vaccines. Currently, multivalent pneumococcal conjugate vaccines are sold to the GAVI alliance at \$3.30 and \$3.40 per dose by Pfizer and GSK, respectively (GAVI Alliance Secretariat, 2014). However, with an estimated 150 million doses required in 2015 and demand growing to over 250 million doses by 2022, the initial \$1.5 billion in initial GAVI funding cannot meet demand. Clearly, there are enormous humanitarian benefits that can be realized through the reduction in the cost of goods (COGs) for polysaccharide conjugate vaccines.

An examination of the published costs of polysaccharide vaccines against *N. meningitidis* serotype A (Mn A) provides insight into the opportunity for production cost reductions and the potential associated public health benefit. Over many decades, production processes of meningococcal vaccines have evolved, leading to lower COGs. Naked CPS vaccines against meningococcal serotypes A/C and A/C/W135, are sold in Africa for \$0.66/dose and \$1.30 per dose, respectively (LaForce et al., 2007). As part of MenAfriVac, a recent non-profit effort to produce inexpensive Mn A vaccine, Synco BioPartners and the Serum Institute were able to manufacture the Mn A active pharmaceutical intermediate (*i.e.* polysaccharide) for \$0.02 per dose (BioPartners, 2011). Factoring in the cost of protein and conjugation, the MenAfriVac program has succeeded in decreasing the cost of polysaccharide conjugate vaccine production to \$0.50 per dose for mass vaccination against this endemic disease (Mayor, 2010). It is estimated that the widespread implementation of the low cost

vaccine against Mn A will prevent 50,000 cases of meningitis each year and save 5,000 lives (Mayor, 2010).

The convergence of drug pipelines swollen with polysaccharide vaccine candidates, the increasingly prominent competitive imperative to reduce manufacturing costs, and the unmet global medical need have created strong demand for improved, high yielding, CPS production processes with low COGs. The opportunity is greatest for multivalent vaccines, where generic approaches for vaccine production can be designed and leveraged. As companies invest more heavily in vaccine development and gain a greater understanding of vaccine production, development and manufacturing costs will be reduced. This thesis represents one element in a broader investment to improve the state-of-the-art in vaccine production.

1.4 Vaccine Immunology

Although they have been incorporated in vaccines, polysaccharides exhibit limitations as immunogens. Inoculation with naked polysaccharide stimulates B cells and produces a T cell-independent response, yielding predominantly IgM and relatively low affinity IgG antibodies (Reingold et al., 1985; Schneerson et al., 1980). This response is poorly immunogenic in infants, induces only short duration immunological memory, and does not decrease nasalpharyngeal carriage so as to facilitate herd immunity (Centers for Disease Control, 2005). In conjugate vaccines, polysaccharides are linked covalently to a protein with proven T cell epitopes, such as tetanus toxoid or modified diphtheria toxin. As a result, conjugate vaccines elicit a T-cell dependent immune response yielding higher antibody titres. The avidity of the antibodies is increased through affinity maturation and isotype switching. T cell-dependent immune responses exhibit memory, most probably due to antigen migration to the germinal centres of the lymphatic system, thereby conferring longer lasting protection, which is particularly important in the prime vaccination cohort: children younger than 2 years old. Public health is further increased through the reduction of carriage rates and the provision of herd immunity to unvaccinated individuals.

In Appendix 9.1: *Neisseria Meningitidis* Case Study, meningococcal meningitis is used as a case study to examine the intricacies inherent in developing a multivalent polysaccharide vaccine for humans.

1.5 Polysaccharide Biology

Capsular polysaccharides are highly diverse carbohydrate polymers that surround bacteria from many genera. Both Gram-negative (*e.g. Escherichia coli, Haemophilus influenzae, Neisseria meningitidis, Pseudomonas aeruginosa, Salmonella typhi, Klebsiella pneumoniae*) and Gram-positive bacteria (*e.g. Streptococcus pneumoniae, Staphylococcus aureus, Streptococcus agalactiae* (Group B)) produce capsular polysaccharides (Astronomo and Burton, 2010). The functions of these carbohydrates are to assist in hydration and adherence of the bacterial cell and to assist the cell in evading host immune responses (Roberts, 1996). Capsular polysaccharides cloak peripheral cellular structures, obscuring peripheral and transmembrane proteins, LPS in Gram-negative bacteria, and lipoteichoic acid in Gram-positive bacteria (Bae et al., 2009; Lindberg et al., 1977). The concealment of extracellular antigens has hindered the development of protein-based vaccines with adequate coverage for encapsulated pathogenic bacteria. However, effective human immune responses can be raised against capsular polysaccharides.

Capsular polysaccharides exhibit vast structural diversity. Heterogeneous polymers, they are generally composed of monosaccharide units joined through glycosidic and phosphodiester bonds in repeating oligosaccharide units (Roberts, 1996). Native capsular polysaccharides are comprised of tens to thousands of these oligosaccharide 'monomers' linked together, ranging from kDa to MDa in molecular weight (MW). Due to the large number of hydroxyls on each oligosaccharide, covalent bonds can form at an array of locations, resulting in a highly complex and variable macromolecular structure. O- and N-acetylation patterns can also differ but usually maintain a characteristic consensus pattern (Jones and Lemercinier, 2002). The particular monosaccharide units are often generally conserved within a species. In contrast, the underlying oligosaccharide repeat unit can be specific to a particular bacterial species, to differentiated serotypes within a species, or to structurally differentiated strains, as outlined in Table 1.6.

Table 1.6. Repeating units of CPS for selected bacterial pathogens (Jones, 2005a)

Organism	Structure
Haemophilus influenzae type b	→3)-β-D-Ribf-(1→1)-D-Ribitol-(5→OPO ₃ →
Neisseria meningitidis Group A	→6)-α-D-ManpNac(3/4OAc)-(1→OPO ₃ →
Neisseria meningitidis Group B	→8)-α-D-Neup5Ac-(2→
Neisseria meningitidis Group C	→9)-α-D-Neup5Ac(7/8OAc)-(2→
Neisseria meningitidis Group W135	→6)-α-D-Glcp-(1→4)-α-D-Neup5Ac(9OA)-(2→
Neisseria meningitidis Group Y	→6)-α-D-Galp-(1→4)-α-D-Neup5Ac(9OAc)-(2→
Salmonella typhi Vi	→4)-α-D-GalpNacA(3OAc)-(1→
S. pneumoniae Type 1	→3)-D-AAT-α-Galp-(1→4)-α-D-GalpA(2/3OAc)-(1→3)-α-D-GalpA-(1→
S. pneumoniae Type 2	→4)-β-D-Glcp-(1→3)-[α-D-GlcpA-(1→6)-α-D-Glcp-(1→2)] -α-L-Rhap-(1→3)-α-L-Rhap-(1→3)β-L-Rhap-(1→
S. pneumoniae Type 3	→3)-β-D-GlcA-(1→4)-β-D-Glcp-(1→
S. pneumoniae Type 4	→3)-β-D-ManpNac-(1→3)-α-L-FucpNac-(1→3)-α-D-GalpNac-(1→4) -α-D-Galp2,3(S)Py-(1
S. pneumoniae Type 5	→4)-β-D-Glcp-(1→4)-[α-L-PnepNac-(1→2)-β-D-GlcpA-(1→3)] -α-L-FucpNac-(1→3)-β-D-Sugp-(1→
S. pneumoniae Type 6B	→2)-α-D-Galp-(1→3)-α-D-Glcp-(1→3)-α-L-Rhap-(1→4)-D-Rib-ol-(5→P→
S. pneumoniae Type 9N	→4)-α-D-GlcpA-(1→3)-α-D-Glcp-(1→3)-β-D-ManpNac-(1→4) -β-D-Glcp-(1→4)-α-D-GlcpNac-(1→
S. pneumoniae Type 9V	→4)-α-D-GlcpA(2/3OAc)-(1→3)-α-D-Galp-(1→3)-β-D-ManpNac(4/6OAc)-(1→4)-β-D-Glcp-(1→4)-α-D-Glcp-(1→
S. pneumoniae Type 12F	→4)-[α-D-Galp-(1→3)]α-L-FucpNac-(1→3)-β-D-GlcpNac-(1→4)-[α-D-Glc-(1→2-α-D-Glc-(1→3)]-β-D-ManNacA-(→
S. pneumoniae Type 14	→4)-β-D-Glcp-(1→6)-[β-D-Galp-(1→4)]-β-D-GlcpNac-(1→3)-β-D-Galp-(1→
S. pneumoniae Type 18C	→4)-β-D-Glcp-(1→4)-[α-D-Glcp(6OAc)(1→2)][Gro-(1→P→3)]-β-D-Galp-(1→4)-α-D-Glcp-(1→3)-β-L-Rhap-(1→
S. pneumoniae Type 19F	→4)-β-D-ManpNac-(1→4)-α-D-Glcp(1→2)-α-L-Rhap-(1→P→
S. pneumoniae Type 23F	→4)-β-D-Glcp-(1→4)-[α-L-Rhap (1→2)]-[Gro-(2→P→3)] -β-D-Galp-(1→4)-β-D-Galp-(1→4)-β-L-Rhap-(1→
Staphylococcus aureus Type 5	→4)-β-D-ManNacA-(1→4)-α-L-FucNac(3OAc)-(1→3)-β-D-FucNac-(1→
Staphylococcus aureus Type 8	→3)-β-D-ManNacA(4OAc)-(1→4)-α-L-FucNac-(1→3)-α-D-FucNac-(1→

1.6 Polysaccharide Stability

Ensuring the long-term stability of a vaccine drug product is essential; however, understanding and maintaining short-term stability is critical for purification development. The unique chemistries of polysaccharides present an array of structural features that can be altered, intentionally or inadvertently, during processing and analysis. The conditions required for purification can stress biological molecules, resulting in changes in product quality. In-process pools are generated at several points in a purification process and may need to be held for several days. During process development, many experiments may employ a single feedstream stored at 5°C and purified pools may need to be stored for prolonged periods prior to analysis.

The key routes of degradation are hydrolysis of the backbone glycosidic/phosphodiester bonds and the scrambling of O-acetylation sites. Product literature and published articles provide insight into specific stability attributes.

1.6.1 Hold Time Stability of Purified Polysaccharides

Much information on stability can be gleaned from product regulatory documents. Meningococcal serotypes C, W, W135, and Y (*i.e.* Mn C, Mn W135, and Mn Y, respectively) are provided in Menveo as liquid vials of 10 µg/mL each in phosphate-buffered saline (10 mM phosphate, 77 mM NaCl)(Centers for Disease Control, 2010a). Stability of these liquid formulation at 2-8°C is specified for two years (European Medicines Agency, 2009). Mn A is more labile and is provided in a lyophilized form, with post-reconstitution stability assured at ≤ 25°C for eight hours (Centers for Disease Control, 2010a; European Medicines Agency, 2009; Food and Drug Administration United States, 2010b). The Hib B drug substance liquid is stable at 2-8°C and unspecified higher temperatures for 3 months (Food and Drug Administration United States, 1993). When frozen at < -15°C, 36 months of stability are specified for the four aforementioned meningococcal serotypes, except for Mn C for which 30 months are provided (European Medicines Agency, 2009). In addition, the drug substances for all four serotypes are resilient to at least two cycles of freezing and thawing. Since all of these reports employed relatively low concentrations of polysaccharides, some of which were conjugated to

proteins, the higher concentrations routinely encountered in intermediate pools will likely be characterised by inferior stability.

1.6.2 Hydrolysis

For most capsular polysaccharides, hydrolysis of glycosidic and phosphodiester bonds is a significant factor in polysaccharide production (Costantino et al., 1992; Plumb and Yost, 1996; Ravenscroft et al., 2007). Hydrolysis can be introduced by design in a process or as an inadvertent by-product of purification operating conditions (e.g. extreme pH, high temperature, etc.) where CPS are susceptible to hydrolysis. Reducing end groups are typically preserved in hydrolysis reactions but alternatively, can be added as has been observed with Mn C. Other ancillary effects of hydrolysis include a decrease in the degree of polymerization, increased solubility, and reduced viscosity (Jones, 2005a). Some polysaccharides, such as staphylococcal serotypes, have few free hydroxyl groups and are extremely resistant to hydrolysis.

The specific conditions required for hydrolysis of phosphodiester and glycosidic bonds depend on the structure of the carbohydrate but in general are catalyzed through an exposure to acidic or alkaline conditions (Bardotti et al., 2005; Dascenzi, 2006; Gudlavalleti et al., 2007). 1% acetic acid (HAc) hydrolyzed *Klebsiella pneumoniae* exopolysaccharide after 2 hours at 90°C (Adam et al., 1995). Costantino *et al.* showed that incubation of Mn A in 10 mM HAc at 50°C for 12 hours and Mn C in 10 mM HAc (pH 5) at 100°C for 8 hours caused significant cleavage of the polysaccharides (Costantino et al., 1992). Partial hydrolysis of Mn A, Mn C, Mn W135, and Mn Y was effected by incubation in 0.1 M HCl at 60°C for 4 hours (Bardotti et al., 2008). Hib B CPS was also fully degraded to its base subunits when stored in 0.1 M NaOH at room temperature for 16 hours (Tsai et al., 1994). Pujar et al. performed a thorough study of base hydrolysis, employing all the phosphodiester bond-containing polysaccharides of a 23-valent *S. pneumoniae* vaccine (Pujar et al., 2004). Cleavage rates were found to be polysaccharide-dependent and pH-dependent, with CPS structures containing hydroxyl groups adjacent to phosphate predisposed to cleave. Other studies found that the presence of divalent cations enhanced degradation rates (Pujar et al., 2004; Zon et al., 1982). Similar susceptibility to hydrolysis was observed for Hib B CPS, which is comprised of repeating ribitol ribiose-3-phosphate

units. Understanding hydrolysis is important as it is also utilised in the manufacturing process to size correctly the various CPS streams.

1.6.3 Acetylation

The bonding of acetyl groups to oxygen substituents is referred to as O-acetylation. Patterns of O-acetylation represent a differentiating characteristic for many vaccine polysaccharides though some capsular polysaccharides, including those associated with *S. aureus*, possess no O-acetylation (Jones, 2005a). The sites possessing O-acetylation can be variable across a population for a given CPS (Lemercinier and Jones, 1996). Production variables such as fermentation conditions and processing environment can also affect the pattern of O-acetylation (Kao, 2004). Typically, O-acetylation is not a significant factor in eliciting an immune response but has been found to be immunologically significant with Mn A (Gudlavalleti et al., 2007; Jódar et al., 2004). Owing to potential immunological significance, structural prominence, and sensitivity to manufacturing conditions, O-acetylation has become an important quality attribute for polysaccharide vaccines. Accordingly, it is often used as a measure of process consistency.

The O-acetyl groups are labile moieties on CPS. Acetyl groups have a propensity to migrate between proximal intra- and inter-chain hydroxyl groups, although reaction from the former position is more common (Jones, 2005b). O-acetylation is susceptible to hydrolysis, particularly under alkaline conditions and at elevated temperatures (Kamerling et al., 1987). Indeed, the log half-lives of certain O-acetyl transmigrations in neuraminic acid variants were found to correlate to pH across the 7-9 range. Even when incubated in mild conditions of pH 7.4 and 30°C for a few days, Mn C converted from a 5:1 ratio of acetylation at two adjacent oxygen atoms to a 1:3 ratio (Lemercinier and Jones, 1996). More extreme conditions can promote de-O-acetylation as observed with *S. pneumoniae* serotypes 17F and 20, where one to six hours at pH 10.5 yielded full de-O-acetylation (Pujar et al., 2004). Indeed, exposure to 10 mM NaOH for four hours at 37°C is sufficient to release all O-acetylation (as acetate) from Mn A, Mn W135, Mn Y, typhoid Vi, pneumococcal 9V and pneumococcal 18C CPS (Kao, 2004). Mn C required 48 h of incubation in these conditions to complete de-O-acetylation, perhaps due to electrostatic or steric hindrance.

1.6.4 Miscellaneous Degradation Pathways

Myriad other pathways can lead to degradation of CPS. In the presence of amides, reducing sugars can be converted into Schiff bases (Brons and Olieman, 1983). Thermal effects are well-documented; elevated or sub-freezing temperatures can lead to a range of deleterious structural effects on vaccines (World Health Organization, 2006). Finally, there are many undesirable reaction pathways specific to the linkages present in each particular capsular polysaccharide. It is evident that an understanding of CPS stability is requisite for the development of robust manufacturing options.

1.7 Vaccine Manufacturing

1.7.1 History

Vaccine process development and manufacturing have faced several unique challenges. Vaccines are highly complex, comprised of many diverse antigens that must be individually purified prior to activation, conjugation, and formulation in a single product. As a class, vaccines are highly diverse, hindering industry-wide bootstrapping that has proven so fruitful for the evolution of mAb production processes. Project resources have rarely been scaled with the number of sub-components, resulting in project teams tasked with daunting technical and logistical hurdles. Moreover, vaccines are often developed in response to public health crises, leading to additional strain on project teams and necessitating the evolution of efficient practises.

In this environment, vaccine development has made impressive achievements. Platform processes have been developed for a variety of vaccine classes, even if details are not always available in peer-reviewed literature (Buckland, 2014). Timelines from vaccine definition to investigational new drug applications have decreased to as little as 6 months, substantially faster than documented for mAb processes (Washabaugh, 2014). These advances have enabled the efficient production of increasingly complex vaccine products with fewer resources and less time. The resulting decreased COGS have increased the accessibility of vaccines to less affluent regions of the world.

Additional efforts to simplify the development and manufacturing of multivalent polysaccharide vaccines are needed. Through continued investment in partnerships with government, academia, and nonprofits, industry can advance the field. Complementing these initiatives, the United States Biomedical Advanced Research and Development Authority (BARDA) has launched three Centres for Innovation in Advanced Development and Manufacturing to combine public/private/academic expertise to advance the state-of-the-art for manufacturing and to create a deeper pool of applicable skills. In combination, these approaches will build on the foundation of historical vaccine knowledge and continue the evolution towards ever more sophisticated and effective production practises.

1.7.2 Fermentation

The production of CPS is mainly achieved through the fermentation of pathogenic microbes. There are a few examples of synthetically generated polysaccharides, such as Quimi-Hib, which utilises a fully synthetic version of Hib CPS and has been part of the Cuban vaccination program since 2004; however, fermentation is still the main method of generating CPS (Verez-Bencomo et al., 2004). Hence, fermentation will determine the type and concentrations of impurities and excipients that the downstream process will be tasked with removing. Unfortunately, there is a dearth of information published on the pertinent fermentation processes employed at manufacturing-scale. Most of the peer-reviewed literature describes research performed at ≤ 80 L-scale (Paz et al., 2003). A recent review by Joshi *et al.* examined fermentation production of meningococcal CPS (Joshi et al., 2009). Typical fermentations produced 1-2 g/L of biomass and 0.1-0.2 g/L CPS. Given the likelihood of advances in fermentation since publication, this information provides guidance for analytical ranges, providing a lower estimate of CPS titre and an upper boundary for impurity quantification that downstream analytics must be capable of characterising.

1.7.3 Downstream Processing

Several production methods for meningococcal CPS have been described in the literature. Due to a lack of adequate alternatives, these studies will serve as benchmark processes for discussion. After a review of historical purification methods, typical unit operations will be examined in the context of a literature review of past applications, applicability to the described purification challenge, and

available scale-down rules. These analyses culminate in an assessment of the potential to deploy an operation as part of a high throughput workflow.

1.7.3.1 Historical Methods

Early vaccine production processes relied heavily on extraction, precipitation, centrifugation, and filtration. A typical production process for a capsular polysaccharide is provided in Figure 1.1 with process details from the relevant research described in Table 1.7.

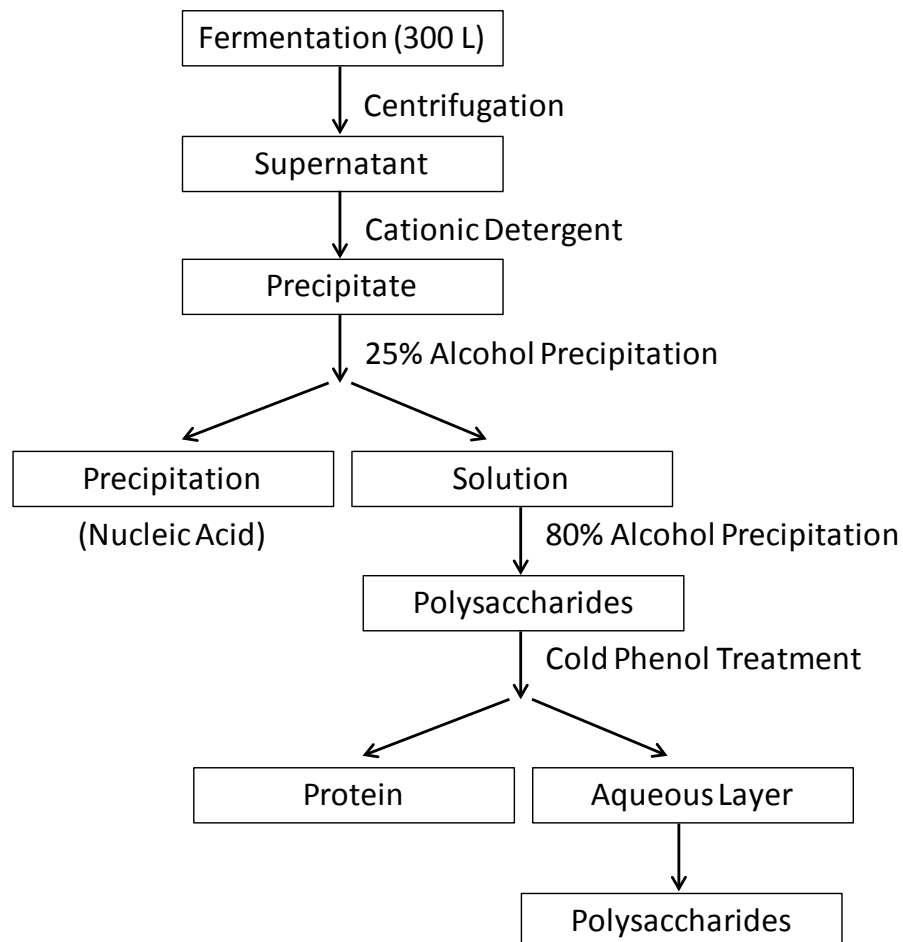


Figure 1.1. Typical production process for meningococcal CPS (Laskin, 1988)

Table 1.7. Overview of manufacturing purification processes for CPS from *N. meningitidis* (European Medicines Agency, 2009; Food and Drug Administration United States, 2010b; Frasch, 1990; Gotschlich et al., 1969a; Preaud, 2010). (s) indicates solid is product-containing and (l) indicates liquid is product-containing. Centrifugation is integral to each precipitation step. Table is colour-coded per this legend:

Chromatography Precipitation Tangential Flow Filtration Extraction

Manuf. Process	Standard Chiron/Novartis (Mn A/Mn C) ¹	Brazil process (all serotypes)	MenAfriVac (Mn A)	Menveo (Mn A, Mn Y, Mn W135)	Menveo (Mn C)
Growth media-Inactiv.	N/A	N/A	N/A	Franz-formaldehyde	Franz-formaldehyde
Order of Operations	Microfiltration	Ppt with CTAB; CF(s)	Extraction with CTAB; CF (s)	CF (l)	CF (l)
	Ppt with CTAB; CF (s)	Resuspension in 1 M CaCl ₂ ; CF (l)	UF	UF/DF with H ₂ O	UF/DF with H ₂ O
	Resuspension in 1 M CaCl ₂	Ppt DNA with 25% EtOH; CF(l)	Ppt; CF (s)	Ppt; CF (s)	Ppt; CF (s)
	Ppt DNA with 25% EtOH; CF (l)	Ppt with 80% EtOH; CF(s)	DF	Extraction with alcohol; CF (l)	Extraction with alcohol; CF (l)
	Ppt with 80% EtOH; CF (s)	Cold phenol washes in 10% NaAcet to remove protein	Ppt; CF	Ppt; CF (s)	Ppt; CF (s)
	Extract protein with cold phenol	DF with H ₂ O		Hydrolysis	Chromatography
	UltraCF to remove LPS (l?)	CF to separate LPS		Sizing with TFF	Hydrolysis
	Ppt with 80% EtOH; CF (s)				Sizing with TFF

¹Process is followed by hydrolysis of pure polysaccharide at 10 mg/mL in 0.01 M HAc at 50°C for 13 hours. CTAB = cetyltrimethylammonium bromide; EtOH = ethanol; NaAc= sodium acetate; UF = ultrafiltration; DF = diafiltration; TFF = tangential flow filtration; Ppt = precipitation, LPS = lipopolysaccharide; Inact. = inactivation agent; CF = centrifugation.

Although details for current processes are unavailable and have advanced beyond those reported in the published domain, it is instructive to consider the unit operations and the linkages between the steps using the available research. Killing the cells (*e.g.* with detergent, heat, phenol, formaldehyde, etc.) effectively terminates the fermentation. Chemical extraction may be required to liberate CPS but is unnecessary if CPS titres are high (Frasch, 1990). Size-based technologies such as centrifugation and filtration can be leveraged to purify the desired polysaccharides from the extracts. Hydrolysis can be employed where necessary to liberate free polysaccharide and to reduce the mean MW of the polysaccharide populations.

Traditional CPS purification processes suffered from several weaknesses. Foremost, the DSP process was saddled with long processing times and many operations. The precipitation and extractions were often carried out with high concentrations of organic solvents such as phenol, ethanol, and methanol. The flammability of the solvents required processing in explosion-proof rooms. Moreover, the handling, disposing, and recycling of toxic components presented major safety and regulatory challenges. Ultracentrifugation is extremely energy-intensive and expensive, with limited options for scale-up. Replacement of these traditional approaches with improved or alternative purification technology will lead to more cost-effective, efficient, higher yielding, and scalable processes. An examination of select unit operations follows.

1.7.3.2 Primary Recovery and Dissociation from Cell Envelope

The primary recovery operation has often been highly variable and low yielding. At the termination of fermentation, capsular polysaccharides are bound to the bacterial outer membrane and free in solution. For select bacterial species, such as *N. meningitidis*, once the fermentation reaches stationary phase, the CPS become dissociated from the cellular envelope. If additional dissociation is required, two common methods are to homogenize the cells and chemically dissociate the sugar from the cell surface (Gotschlich et al., 1969b; Pato et al., 2006; Tanizaki et al., 1996). Following dissociation, the population of carbohydrates is often heterogeneous, comprised of diverse sizes and structures, including capsular polysaccharides, polysaccharides covalently bond to (phospho) lipids

and complexes of outer membranes vesicles. Centrifugation is subsequently applied to isolate the CPS.

Positively charged detergents (*e.g.* cetyl trimethylammonium bromide (CTAB, Hb)) have been employed to segregate capsular polysaccharides from cell culture fluids and impurities such as DNA (World Health Organization, 1967). Most commonly, the detergent has been added with the cells present, inducing the precipitation of CPS. With this treatment, the cells can be homogenized to maximize polysaccharide liberation or left intact for easier removal (Baruque-Ramos et al., 2005; Gotschlich et al., 1969b). Some researchers have opted to concentrate the cell culture prior to the addition of detergent (Gotschlich et al., 1969b). This manipulation can have the ancillary effect of reducing the mean MW of the final purified polysaccharides, with reductions in MW from > 2 MDa to < 50 kDa reported (Gotschlich et al., 1969b). This phenomenon was likely due to enzymes that could degrade the polysaccharides as opposed to chemical instability of the polysaccharides. Improvements in fermentation have led to increasing cell density and sufficient free CPS titre in the cell culture broth to enable purification without cell lysis. In this scenario, it is preferable to remove the cells prior to further purification. Indeed, Pato *et al.* eliminated the positively-charged detergent extraction step through such an approach (Pato et al., 2006).

Centrifugation is effective at removing cells and segregating polysaccharide, making it a key element of primary recovery. This operation is usually placed immediately downstream of fermentation or the CPS liberation step. When used at subsequent points in the process, centrifugation can separate precipitate from supernatant.

1.7.3.3 Holistic Process Research

Several research groups have proposed improvements to conventional purification process trains for CPS. While interesting, the particular research falls slightly outside the scope of this thesis as the approaches are impractical given cGMP facility constraints or not amenable to high throughput processing. An overview of the research is provided in Appendix 9.2: Holistic Purification Process Development for CPS.

1.8 Particle Conditioning and Filtration Unit Operations

1.8.1 Precipitation

Particle conditioning comprises a series of operations wherein insoluble particulates are formed, dynamically conditioned to improve particle characteristics for subsequent processing, and then separated from the clarified liquid. Insoluble material is produced via modulation of environmental properties such as temperature, pH, and/or through the addition of one or more chemical agents. While precipitation describes the formation of insoluble solids from dissolved species, flocculation is the agglomeration of colloids and precipitates. As such, flocculation can be viewed either as an independent process or as the final stages of a precipitation process. From a practical standpoint, both methods are equivalent in that the solute is altered in some manner, an increasing amount of solid phase develops, and the resulting solids must then be separated from the liquid. A typical particle conditioning sequence is flocculation followed by centrifugation and then filtration.

Particle conditioning steps such as flocculation have been used for the clarification of biological products for over a century (Bonnerjea, 1988; Cohn, 1925; Cuo, 1977; Gotschlich et al., 1969b; Milburn et al., 1990; Osborne and Harris, 1903; Roush and Lu, 2008; Salt et al., 1995; Thommes and Etzel, 2007). More recently, flocculation has been used for the clarification of vaccines (Bonnerjea, 1988; Cuo, 1977; Gotschlich et al., 1969b; Milburn et al., 1990; Salt et al., 1995). The principal objectives of flocculation have been the removal of contaminants and the formation of larger particulates for enhanced downstream removal via centrifugation and filtration. For the purification of CPS, a common strategy has been to agglomerate the polysaccharide while leaving impurities in solution (Cuo, 1977; Frasch, 1990; Gotschlich et al., 1969b; Preaud, 2010). Published purification processes for *N. meningitidis* (i.e. A, C, W-135, and Y) and *H. influenzae* type-B strains employed positively charged detergents to precipitate anionic CPS that contained sialic acids or phosphate. The utility of this approach should extend to other microbes since many CPS are acidic as are most bacteria (Harden and Harris, 1952; Jones, 2005a). The literature is less prescriptive for applications where the solids and impurities are flocculated while the CPS remains soluble. Higher resolution purification from impurities such as protein, DNA, and endotoxin has also been achieved (Brodsky et

al., 2012; Shan et al., 1996). A variety of flocculation agents have been employed, including detergents, salts, alcohols, polyions, multivalent ions, polymers, and organic solvents. The selection of the agent and operating conditions has generally been empirical or based on historical protocols. A means to screen rapidly for the optimal flocculant or precipitation agent would be useful.

Flocculation is a complex phenomenon that involves the interplay of many parameters. At a minimum, to define conditions for equilibrium partitioning between the solid and liquid phases, the practitioner must specify the pH, floc agent(s), floc agent concentration(s), ionic strength, and temperature (Fisher et al., 1986; Fisher and Glatz, 1988a; Iyer and Przybycien, 1995). The particle characteristics of the flocs will then be dictated by the kinetics of floc formation and the impact of aging, which are in turn driven by the dynamic response to addition rates, diffusivity, reaction rates, kinetics, local shear gradients, collisions, turbulent eddies, and the physicochemical properties of the solution. Given the myriad variables involved, an empirical approach to defining flocculation conditions has typically been followed (Belter et al., 1988).

The efficient development of unit operations for flocculation has been constrained by lab-scale models that require large volumes and considerable time to evaluate. A jar test is often used to screen floc agents but this is low throughput and can require over 1 L per condition (Camp and Conklin, 1970). Small-scale systems for particle conditioning employing only 200-400 mL of feed have been described and exhibit good scalability with Pilot-scale (Berrill et al., 2008; Neal et al., 2003). Kang et al. performed flocculations for hundreds of conditions with 5-10 mL aliquots, scaling a subset of conditions up to the 2 L scale (Kang et al., 2013). An engineering characterisation of the system was not provided but the performance of downstream depth filtration was thoroughly explored. A 25 mL system was used to examine the flocculation of yeast cells and debris, though neither the impact of the solid-liquid separation step nor correlations with larger scale performance were included (Wickramasinghe et al., 2005). For precipitation scouting, myriad lab-scale configurations utilising single vessels have been detailed, ranging from reaction volumes of 1.5 mL up to hundred of mL (Gagnon, 2012; Liu et al., 2010; Sieberz et al., 2014). However, these precipitation studies have

focused on the assessment of equilibrium conditions and excluded characterisation of the particle aging steps and their subsequent impact on downstream operations.

1.8.1.1 *Scaling Heuristics*

The scale-up of particle conditioning processes is based largely on heuristics derived from precipitation operations, which seek to match the Camp number between mixing vessels, thereby maintaining floc strength. Since scaling rules for the particle conditioning of vaccine streams, such as polysaccharides, have not been established, inferences from investigations into protein precipitation and water treatment scale-up were utilised in the present study. Many guidelines have been proposed to improve the consistency of mixing and performance across scales (Hemrajani and Tatterson, 2004). These scaling rules are based on geometric similarity of tank design, assume fluid flows are in the turbulent regime, and depend on the specific properties of the floc system. Many useful scaling rules seek to maintain energy dissipation, shear rate, and time-integrated permutations of these properties as one scales up. The mathematical descriptions of select scaling rules are described below.

1.8.1.1.1 Energy Dissipation

- P/V_{avg} (Belter et al., 1988; Kresta and Brodkey, 2004) Scaling by power per liquid volume (P/V_{avg}),

$$\frac{P}{V} = \frac{n_4 N_p \rho N^3 D^5}{\pi T^2 H} \quad (1)$$

equates to matching the average energy dissipation (ϵ_{avg}) between reactors. Zwietering demonstrated that scaling by P/V_{avg} provided a conservative estimate of the stirrer speed required for complete suspension (Zwietering, 1958). Maintaining P/V_{avg} across scales has been frequently employed for scale-up of many mixing applications, including protein precipitation and cell culture (Atiemo-Obeng et al., 2004; Hemrajani and Tatterson, 2004; Löffelholz et al., 2013). Scaling by mean P/V can be misleading; however, as the levels of energy dissipation are not homogeneous throughout the tank.

- P/V_{imp} (Kresta and Brodkey, 2004; Zhou and Kresta, 1996) Turbulence is not homogeneous in a baffled reactor leading to local P/V levels that can be much higher than the average P/V. The local P/V reaches a maximum in the trailing vortices of the impeller and most particles will eventually encounter this impeller discharge region (V_{imp}) during recirculation. As a result, P/V in the impeller swept zone (P/V_{imp}),

$$\frac{P}{V_{imp}} = \frac{N_p \rho N^3 D^5}{D^3} \quad (2)$$

is equivalent to the maximum local energy dissipation rate (ϵ_{max}) and can be a useful scaling metric.

- $\epsilon_{max}/\epsilon_{avg}$ (Geisler et al., 1994) The maximum ratio of the local to average energy dissipation rate is referred to as $\epsilon_{max}/\epsilon_{avg}$. This value offers a measure of the diversity of hydrodynamic fields in a stirred tank and is defined by,

$$\frac{\epsilon_{max}}{\epsilon_{avg}} = \left[0.1 N_p^{0.33} \left(\frac{D}{T} \right)^{-3} \left(\frac{Z}{T} \right) \right] \quad (3)$$

This ratio increases as N_p increases or as D/T decreases. Elevated ratios benefit systems where high ϵ are required such as dispersion processes but are not ideal for shear-sensitive applications such as floc aging.

1.8.1.1.2 Shear

- v_{tip} (Batchelor, 1947; Hemrajani and Tatterson, 2004) The tip speed (v_{tip}),

$$v_{tip} = \pi N D \quad (4)$$

experienced at the termini of an impeller represents the highest local flow rates and maximum shear imparted into a stirred tank. The v_{tip} at lab-scale and smaller tend to be lower than the v_{tip} generally found at large scale, even for low (*i.e.* $< s^{-1}$) stirrer speeds at production-scale.

- λ_k (Batchelor, 1947; Kolmogorov and Levin, 1991; Kresta and Brodkey, 2004) The total energy imparted through an impeller into a tank is converted to kinetic energy, and transferred through

a turbulent eddy cascade of decreasing length scale until the energy is dissipated. One measure for the size of the smallest eddies in a liquid system was determined by Kolmogorov. The Kolmogorov length scale (λ_K),

$$\lambda_K = \left(\frac{v^3}{\varepsilon_{avg}} \right)^{\frac{1}{4}} \quad (5)$$

is based on the eddy size where the inertial and viscous forces are equivalent. Particles smaller than the characteristic eddy size can be convected within the eddy. As dispersion processes generate eddies approaching the size of the particles, eddies can produce significant shear forces on the particle, leading to breakage.

- λ_{Kimp} (Geisler et al., 1994; Kresta and Brodkey, 2004; Townsend, 1976) The Kolmogorov characteristic scale was extended to define the local isotropic turbulence in V_{imp} , where $\varepsilon = \varepsilon_{max}$. In these regions, the eddy micro-scale will be smaller, as defined by,

$$\lambda_{Kimp} = \left(\frac{v^3}{\varepsilon_{imp}} \right)^{0.25} \quad (6)$$

and will have the greatest deteriorative effect when the eddy size drops below 1/2 to 1/3 the size of the particle.

- \bar{G} (Bell and Dunnill, 1982; Boychyn et al., 2000; Camp and Stein, 1943; Crittenden et al., 2005; Letterman et al., 1973) In a turbulently stirred tank, the velocity gradients associated with eddies fluctuate in time and space. The mean velocity gradient (\bar{G}) averages this value over the volume of the tank and accounts for viscosity,

$$\bar{G} = \left(\frac{P}{\eta V_{avg}} \right)^{0.5} \quad (7)$$

- $\tau_{turb}/\rho v_{tip}^2$ (Geisler et al., 1994) The fluctuating velocities inherent in turbulent regimes give rise to shear stress. Turbulent shear stress is in addition to laminar shear stress, which is dominant in regions adjacent to vessel walls and baffles. The maximum turbulent shear stress,

$$\frac{\tau_{\text{turb}}}{\rho v_{\text{tip}}^2} = \left(\frac{4N_p}{\pi^4 \left(\frac{5}{7}\right)} \right)^{0.67} \left(\frac{D}{T} \right) \left(\frac{Z}{T} \right) \left(\frac{\varepsilon_{\text{max}}}{\varepsilon_{\text{avg}}} \right)^{0.67} \quad (8)$$

is normalized by v_{tip} to enable a comparison of larger vessels and varied impellers. $\tau_{\text{turb}}/\rho v_{\text{tip}}^2$ is found in the impeller discharge zone and being larger than laminar shear stress, it plays a substantial role in floc break-up dynamics.

1.8.1.1.3 Time-Integrated Factors

- $\bar{G}t$ (Bell and Dunnill, 1982; Camp and Stein, 1943) The Camp number (Ca), is well-established for flocculation and augments \bar{G} by adding in the duration of shear:

$$\text{Ca} = \bar{G}t = \left(\frac{P}{\frac{V_{\text{avg}}}{\eta}} \right)^{0.5} t \quad (9)$$

$\bar{G}t$ is often used to provide an estimate of the effect of aging on floc strength, with $\text{Ca} \geq 10^5$ associated with strong floc particles.

- $\bar{G}_{\text{imp}}t$ (Ducoste and Clark, 1998; Francois, 1987) Several authors have found that particle size varies when Ca is maintained, both within a given system and upon scale-up. Since the evolution of floc size is dependent on aggregation and breakup processes, the zone that contains ε_{max} , the impeller swept volume, should be an element represented in a scaling factor. In this region, shear and turbulence will be maximized while eddy sizes will be minimized. Modification of Ca to incorporate this constrained volume yields,

$$\bar{G}_{\text{imp}}t = \left(\frac{P}{\frac{V_{\text{imp}}}{\eta}} \right)^{0.5} t \quad (10)$$

- E_f (Neal et al., 2003) The time-integrated fluid stress, E_f ,

$$E_f = \left(\frac{P}{V} \right) t \quad (11)$$

can be viewed as the total work performed on the flocs. For flocs, it is reasonable to assume that the duration of exposure will influence the particle characteristics and E_f can be viewed as an

extension of common P/V_{avg} scaling practises. This definition can also be extended to substitute P/V_{imp} for P/V_{avg} .

1.8.1.1.4 Empirical Heuristics

- θ_B (Hemrajani and Tatterson, 2004) Very fast reactions can benefit from scaling by mixing time,

$$\theta_B = V/Q \quad (12)$$

This approach maintains stirrer speed (N) upon geometric scale-up, necessitating very large motors at the largest scales, effectively limiting the size of the largest scale.

- N_{js} (Atiemo-Obeng et al., 2004; Ibrahim and Nienow, 1999) The minimum stirrer speed required to suspend solid particles is referred to as the just suspended speed (N_{js}). N_{js} is the lowest stirrer speed where the maximum surface area of substrate is exposed to the fluid for reaction. Diffusional mass transfer increases with increasing N up to N_{js} , beyond which it becomes independent of vessel, impeller, or power consumption. Increasing stirrer speed beyond N_{js} increases convective mass transfer slightly.

While this list is not exhaustive, it covers the main scaling heuristics that will be considered for the precipitation and flocculation steps employed in this thesis and will form the basis of further scaling methodologies.

1.8.2 Centrifugation

The scaling of centrifugation incorporates a combination of theory and empiricism. The theoretical aspect is based on Stokes' law for settling,

$$v_s = \frac{\rho_p - \rho_f}{18\mu} d_p^2 g \quad (13)$$

where v_s is sedimentation velocity, ρ_p is the density of the particle, ρ_f is the density of the fluid, d_p is the particle diameter, and g is gravitational acceleration (Doran, 1995). Since a particle will travel

farther in a greater period, longer centrifugation times will result in increased sedimentation. In a continuous centrifuge, residence time is modulated by varying feed flow rates (Q).

To obtain similar performance in centrifuges with different sizes and/or designs, Sigma theory utilises the concept of equivalent settling area (Σ) (Ambler, 1959; Maybury et al., 2000). For a disc-stack centrifuge (DSC),

$$\Sigma_{DSC} = \frac{2\pi n \omega^2 (r_o^3 - r_i^3) V}{3g \tan \theta} \quad (14)$$

where n is the number of discs, ω is angular velocity, r_o is the outer radii of the disc, r_i is the inner radii of the disc, and θ is the angle of discs relative to the vertical axis (Russell et al., 2007). For a bench-top centrifuge (*e.g.* swinging bucket, microplate),

$$\Sigma_{bench-top} = \frac{\omega^2 (3 - 2x - 2y) V}{\ln \frac{2r_2}{(r_1 + r_2)} 2g} \quad (15)$$

where x and y are the time fractions required for acceleration and deceleration, respectively, and r_1 and r_2 are the radii at the surface and base of the centrifuge liquid, respectively (Russell et al., 2007). Using Sigma theory, DSC conditions can be translated to the equivalent operating conditions in a bench-top centrifuge using the relationship,

$$\frac{Q_{DSC}}{C_{DSC} \Sigma_{DSC}} = \frac{V_{BT}}{t_{C_{BT}} \Sigma_{BT}} \quad (16)$$

where V is the bench-top centrifugation volume, t is centrifugation time (Russell et al., 2007; Tait et al., 2009). C_c and C_b are experimentally determined calibration factors that compensate for flow patterns not included in generic form of Σ . Values for C_c and C_b are 0.4 and 1.0, respectively (Tait et al., 2009). Although the only centrifuges employed in this study were swinging bucket microplate centrifuges and a single DSC, using calibration factors, Sigma theory can be adapted for characteristic flow patterns inherent in centrifuges of different sizes and designs. The relative location of a well on a microplate can also complicate implementation of scaling with Sigma theory. The effect of well location on a microplate was found to be significant but only contributed 16% of the total noise in 96 parallel measurements of percentage solids.

Local shear rates can be extremely high in feed zones in disc stack centrifuges, a characteristic not replicated in swinging bucket centrifuges (Boychyn et al., 2001; Hutchinson et al., 2006; Zaman et al., 2009). The energy dissipation rate in this zone exceeds the highest zones found in conventional stirred tanks. The turbulence and shear in this zone can fracture particles (*e.g.* cells, flocs, precipitates, debris, etc.) greatly increasing the percentage solids in the centrate, consequently reducing downstream filtration performance (Chatel et al., 2014; Hutchinson et al., 2006; Kempken et al., 1995; Lau et al., 2013; Tait et al., 2009). This phenomenon has been particularly well-studied for protein precipitates (Bell et al., 1982; Bell et al., 1983; Bell and Dunnill, 1982; Chatel et al., 2014; Hoare et al., 1983). A USD device based on a spinning disc enabled the application of energy dissipation rates to feed samples that are similar to process-scale centrifuges (Boychyn et al., 2001; Boychyn et al., 2004; Tait et al., 2009). This approach has been demonstrated to provide clarification performance representative of DSCs (Titchener-Hooker et al., 2008). Others have used capillary devices to impart shear to particles to simulate the effects of large scale processing (Chan et al., 2006). The shear-sensitivity of diverse products and feedstreams differs in significant ways that are not well understood (Tait et al., 2009; Titchener-Hooker et al., 2008). Shear-sensitivity can determine the success of Q/Σ -based scaling approach and to what extent empirical studies will be required to supplement theoretical scaling bases.

1.8.3 Filtration

In both depth and sterile filtration, the flux and volumetric capacity per unit filter area are held constant upon scale-up with a maximum pressure specified.

The standard method for sizing sterile filtration is to conduct constant-pressure filtration runs on 47 mm diameter (17 cm²) or 25 mm diameter (4.9 cm²) membranes. The V_{max} represents the total volume of filtrate that can pass through a given filter area before it plugs at a constant pressure. This value is measured as the area under the flux versus time curve (Badmington et al., 1995). Smaller syringe filters are commercially available for scaling down further, but in general, suffer from too much imprecision to be useful for scaling studies (personal communication: MerckMillipore R&D). Membranes affixed to microplates offer areas as small as 0.3 cm² but feed volumes are limited and

reports are mixed as to the precision that can be obtained (Chandler and Zydney, 2004; Jackson et al., 2006). Membrane quality, type, and manufacturer all contribute to this variability. In addition, filter microplates are only available for a limited selection of membrane types.

The standard method for sizing depth filtration is to process at constant flux. The P_{max} represents the total volume of filtrate that can pass through a filter before it plugs at a constant flow or flux. Constant flux operation is critical as many depth filters have adsorptive capabilities (*e.g.* diatomaceous earth) and exhibit residence time-dependent performance. The smallest commercially available devices for depth filters contain areas of 23 cm^2 (Merck Millipore, Micropods) and 25 cm^2 (3M, ZetaPlus capsules). Achieving typical capacity of $100\text{-}400\text{ L m}^{-2}$ would require approximately $230\text{-}1000\text{ mL}$ of feed per run.

1.9 High Throughput Process Development

Traditional development of purification processes for biological molecules, vaccines or otherwise, has been a resource-intensive effort requiring a great deal of experimentation by many skilled scientists to find acceptable operating conditions. Often, this approach has been limited by the availability and cost of early phase feedstocks. As biological therapeutics become more numerous in companies' pipelines, there has been enormous pressure to reduce the duration required to develop an optimized process and to do so with less material and fewer people. Concomitant with this change, there have been dramatic advances in both the commercial technologies available to perform high throughput screening (HTS) and the field's understanding of how to translate performance consistently between very small scale and manufacturing-scale.

The advent of high throughput process development (HTPD) has created opportunities for streamlining purification development of biological candidates (Titchener-Hooker et al., 2008). The capability to screen many conditions in parallel is central to maximizing productivity with micro-scale studies. Adsorption experiments in a 96-well microplate format were first described in 1990 (Merson and Bojanic, 1990). Methods soon emerged for purifying an assortment of molecules on microplates using various purification techniques. Applications ranged from removing the by-products of

combinatorial chemical syntheses to purifying arrays of proteins to optimizing downstream processing conditions for biological therapeutics (Bhambure et al., 2011; Irving et al., 1998). Much progress has been made in designing high throughput (HT) methods for the purification optimization of a single protein with microfiltration, extraction, solubilization, refolding, centrifugation, precipitation, filtration, and chromatography (Aucamp et al., 2005; Balasundaram et al., 2011; Chhatre and Titchener-Hooker, 2009; Coffman et al., 2008; Kong et al., 2010; Peng et al., 2001; Tait et al., 2009; Treier et al., 2012; Tustian et al., 2007; Walther et al., 2014). HT technology has also been utilised for stability studies, where it can be effective for *in vitro*, non-invasive assessment and subsequent identification of conditions of exceptional protein stability (Aucamp et al., 2005). The current state-of-the-art involves the integration of various automated steps into a cohesive automated approach requiring no manual intervention (Ma et al., 2008). Many authors have shown how data attained with HTPD can be used to predict performance at much larger scales.

As liquid handling technology has improved, the volumes manipulated have decreased to the point where it is common for purification experiments to be conducted with microlitre (μL) quantities of material, giving rise to the descriptor, micro-scale. Systems designed to enable process development at the micro-scale are termed ultra scale-down (USD). For many purification unit operations, an understanding has been assembled that allows for the translation of findings made at the micro-scale into predictable and robust results at large scale (Jackson et al., 2006; Kramarczyk et al., 2008; Siddiqi et al., 1997; Tustian et al., 2007). A fundamental model system for purification is the evaluation of a single stage equilibrium condition. The specific methods employed depend on the mode of purification and are well-established or can be conceived readily (Bhambure et al., 2011).

Chromatography modelling relies on small-scale batch binding experiments with an adsorptive surface. Precipitation/flocculation can also be evaluated at the micro-scale, after the addition of an agglomeration agent. To effect solid-liquid separations, centrifugation can be carried out in microplates. The approach for micro-scale filtration differs, in that a force gradient must be applied against a sample trapped in front of a porous size-selective medium. Much of the development of purification processes can now occur at the micro-scale, constrained only by the number of conditions that can be generated and analysed rapidly.

HTPD will be central to the improvement of existing polysaccharide manufacturing processes. Currently, the development of purification processes for vaccine polysaccharides is complex and laborious. HTPD of polysaccharides has lagged significantly behind current developmental archetypes for other biologicals such as monoclonal antibodies. Advancements in approaches for parallel processing and the standardization of platform technologies would benefit vaccine process development. In particular, the advent of high throughput tools to optimize primary recovery would have a large impact, given the prominence of this unit operation in polysaccharide purification. It will be employed to identify critical process parameters that potentially impact the quality attributes of the vaccine and to develop purification processes for clinical candidates.

1.9.1 Automation

In purification process development, several HTS can be run to evaluate different unit operations or distinct modes within a given unit operation. In addition, multivalent products such as many CPS vaccines, present the need for parallel screening between allied feedstreams. The complexity inherent in performing these operations heralds an era when purification development benefits greatly from the utilization of robotics to manipulate microlitre volumes of samples. The availability of a fast and automated analytics platform will expand the scope, robustness, and evolution of Design of Experiment (DOE) studies. It is envisaged that this will lead to expanded use of Quality by Design (QbD) approaches in vaccine process development.

1.9.2 Particle Conditioning

Substantial progress has been made in using microplate-based, HTS to optimize precipitation and flocculation unit operations. Such HT approaches are preferred for the high degree of parallelization and the compatibility with microplate-based analytical techniques that they offer. The earliest examples of microplate-based precipitation focused on sample prep applications and the elimination of protein and nucleic acids (Biddlecombe and Pleasance, 1999; Kachel et al., 2006; Rouan et al., 2001; Walter et al., 2001). Additionally, solubility screening with precipitation was evaluated by several groups (Ahmad and Dalby, 2011; Kramarczyk et al., 2008; Nfor et al., 2011; Wiendahl et al., 2009; Yoshimoto et al., 2013). More recently, reports have aimed at optimizing precipitation and

flocculation conditions for the recovery of mAbs and Fc-fusion proteins (Sheth et al. 2013; Ma et al. 2010; Balasundaram et al. 2011; Knevelman et al. 2010). These studies employed a broad range of precipitation agents and conditions to identify regions of superior clarity, yield, quality, and impurity clearance.

The preceding HT studies did not present scalability data nor provide an engineering context for the USD system design. Pilot- and commercial-scale reactors typically consist of baffled systems with central impellers. In the aforementioned studies, the widespread utilisation of orbital shaking for agitation complicated scale-up due to limited applicable engineering correlations and scale-up rules. In addition, the integration of downstream solid separation steps was not explored in these studies.

1.9.3 Integrated High Throughput Centrifugation

Solids removal via centrifugation is critical to the success of particle conditioning operations and often a difficult aspect to scale-down satisfactorily (Boychyn et al., 2004). While methods based on Sigma theory are broadly applicable, scaling down the shear present in the feed zone to swinging bucket centrifuge is more challenging. The USD technology for shearing samples requires ≥ 20 mL and has specified centrifugation in tubes that are not amenable to HT processing. Tait et al. described methods to enable the assessment of centrifugation and feed zone shear in 96 well microplates, although imparting controlled shear still required ≥ 20 mL of feed material (Tait et al., 2009). Thus, there is opportunity for the further development of USD centrifugation and integration with HT particle conditioning.

1.9.4 Integrated High Throughput Filtration

HT filtration requires the development of USD filtration devices and a system to enable the parallel operation of these filters. Several groups have made important progress in this area and in general, these can be categorized by whether the filtration substrate was a membrane or lenticular depth media.

Chandler and Zydney devised a system for performing constant-flux or constant-pressure filtration on a 96 well microplate with integrated membrane, utilizing pressure transducers in a novel way to measure filtrate accumulation (Chandler and Zydney, 2004). Consistent permeability profiles were observed and were representative of larger scale syringe filters. The technology is dependent on the availability of commercial filterplates, restricting this approach to a few membranes. Another group manufactured a steel holder that was capable of accommodating 16 membrane discs in parallel with constant pressure operation and mixing of the feed zone (Vandezande et al., 2005). Microfiltration has been scaled down recently by Rayat et al., who used a thorough engineering characterisation to design a USD system that emulated many geometric and hydrodynamic properties of large scale systems (Rayat et al., 2014).

A previous group in the Department of Biochemical Engineering at UCL invented a novel 8-channel USD filtration device (Jackson et al., 2006). This apparatus was mounted to a Tecan vacuum manifold, enabling operation under constant vacuum. Flux and capacity were measured through an elegant utilisation of the liquid height-sensing capability of the Tecan. The filter sealing configuration accommodated diverse media heights. Indeed, a subsequent group demonstrated depth filtration and the removal of significant levels of impurities with this device (Lau et al., 2013). With this system, constant flux operation is not possible and spatial heterogeneity in media permeability suggests that filters tested in parallel might experience different residence times. The further development of USD filtration to enable constant flux will be explored within this thesis.

1.9.5 Impediments to Deployment of High Throughput Process

Development

Currently, HTPD of polysaccharide vaccines is rarely practised, primarily due to a lack of suitable HT analytics, lack of qualified systems and hardware to control and measure the performance of unit operations, and the lack of established scaling methodologies for particle conditioning.

1.9.5.1 High Throughput Analytics

The rapid development of purification processes for polysaccharide vaccines is constrained by a lack of simple, HT analytical tools. Most of the published analytical literature encompasses methods assessing small molecules, proteins, or nucleic acids. Limited research has been presented on the HT quantification of polysaccharides. Current technologies for the measurement of polysaccharide recovery and process-related impurity clearance are complex, time-consuming, and generally not amenable to HTPD. Moreover, the compatibility of polysaccharides and in-process sample matrices with various HT technology and the implicit methodological assumptions have not been tested. A major bottleneck has been the identification of relevant product assays that can be performed in a highly automated fashion and are resilient to the diverse conditions typically found in developmental studies. Thoroughly resolving these issues is a pre-requisite to the implementation of a HT analytical platform to support HTPD.

Assays for purification process development have contrasting demands compared to assays for release testing. In purification development, feedstocks are usually in short supply so volume requirements for the assays must be minimal. Second, the assay should ideally be microplate-based to facilitate parallel processing. The assays should be fast and straightforward as multiple assays may be performed to support a single screen. Integration with robotic liquid handling systems and the typical room temperature environment of the robots is also desired. Another significant issue is assay interference because in-process samples typically have high levels of impurities that can interfere with assays. When combined with lower polysaccharide titres than are found in pure drug substance, this puts stringent demands on assay robustness. Fortunately, the requirements for accuracy are less rigorous than for a release assay. Moreover, as purification HTPD favours the screening of purification conditions in a 96-well microplate, the precision of an assay is often more important than the accuracy. The results from a single screen might be compared only within the screen with the best conditions subsequently verified at larger scale.

1.9.5.2 System and Hardware Constraints

There are no qualified systems for inducing flocculation or precipitation in a high throughput format. Such a system must offer fine control over liquid addition and particle aging processes while being underpinned by data showing consistency of results when scaling up.

Depth filtration performance is a critical output of successful flocculation. There are no available technologies to provide representative depth filtration from small volume pools produced with high throughput particle conditioning (HTPC). A system is needed that enables depth filtration of 8-12 streams in parallel with constant flux operation. For instance, if HTPC were employed to screen 12 different conditions in replicate, a 96-well microplate would generate approximately 8 mL per condition. Assuming enough load material from each flocculation condition is needed to challenge a filter to 200 L m⁻², depth filter areas ≤ 0.4 cm² would be required. In order to make such a high throughput depth filtration (HTDF) system tenable, system control and data collection would need to be automated. As detailed earlier, although other systems for HT filtration have been described, each suffer weaknesses that exclude them from consideration for HTDF.

1.9.5.3 Scaling Heuristics

Scaling rules for purification unit operations such as chromatography and filtration are straightforward. There is no consensus as to the most effective way to scale particle conditioning. The addition of flocculants can be scaled on a concentration basis or relative to the product titre, impurity concentration, or percentage solids. Ensuring consistent hydrodynamic environments across scales during initial mixing and particle aging is even more challenging, with many scaling heuristics proffered but none substantiated for CPS vaccines in the peer-reviewed literature. Finally, a representative and scalable approach for effecting solid-liquid separations (*i.e.* centrifugation) after particle aging has not been described.

1.9.5.4 Remaining Challenges

Several challenges remain in the arena of HT and USD purification technology. Very little research has been presented on merging of polysaccharide production processes with high throughput technology.

In this niche, a major challenge is the identification of relevant product assays that can be assayed in a highly automated fashion and are resilient to the diverse conditions desirable in a developmental microplate. Moreover, the compatibility of CPS with various HT technologies, assays and implicit methodological assumptions have not been tested. The best practises for handling CPS and for mitigating interactions between fermentation sample matrices and CPS during hold times have not been established. These factors highlight the challenges inherent in developing appropriate and robust HT processing and detection technology for polysaccharides at the micro-scale.

1.10 Research Objectives

As have been discussed, multivalent polysaccharide vaccines are highly complex substances comprised of several different polysaccharides. These vaccines have proven challenging, both to develop production processes for and to manufacture. Although certain unit operations have been common to multiple polysaccharide serotypes and standardization has been practised where possible, custom processes are required for many polysaccharide serotypes. In addition, it has been observed that particular serotypes can present unique and unforeseen challenges (*e.g.* high viscosity, poor stability, inconsistent behaviour, etc.) to the project teams.

A modular approach for developing rapidly purification processes for polysaccharides at the micro-scale would greatly enhance productivity, reduce development costs, and speed the development of novel polysaccharide vaccines. This research aims to accelerate this effort by creating tools for the streamlined development of more efficient and productive polysaccharide purification processes, which can be generically employed across varied polysaccharide entities. The development of HT analytics must precede the development of HTPD of unit operations or else design decisions will be made with unreliable premises. Demonstrating the predictable scalability of processes developed at the micro-scale will be a critical element of this study. In this research, commercially available polysaccharides and relevant internal products will be used to generate modular and scalable methods for the rapid development of polysaccharide purification processes.

1.10.1 Specific Objectives

The specific research aims of this dissertation are:

- Development of HT analytical methods that can be utilised for rapid analyses in screening experiments.
- Development of HTS for primary recovery operations:
 - Flocculation and precipitation (HTPC)
 - Centrifugation (HTPC)
 - Depth filtration (HTDF)

For HTPC or HTDF to be considered a successful scale-down model, it is desirable to achieve, in order of increasing difficulty, faithful prediction of effect directionality, magnitude of response, and predictive accuracy.

2 Characterisation and Adaptation of Impurity

Analytics to HTPD

2.1 Introduction

2.1.1 Impediments to High Throughput Process Development

Currently, high throughput processing and development of polysaccharide vaccines is rarely practised, primarily due to a lack of suitable high throughput analytics. Most of the published analytical literature encompasses methods assessing small molecules, proteins, or nucleic acids. Many high throughput assays are available for the quantification of various classes of impurities but the compatibility of these technologies with polysaccharides and in-process sample matrices have not been established. Thoroughly resolving these issues is a pre-requisite to the implementation of a high throughput analytical platform to supported HTPD.

2.1.2 Unique Requirements for Purification Process Development

Assays to support purification process development have contrasting demands to methods employed for release testing. The assays should be simple, straightforward, and rapid because often, multiple assays will be performed to support a single screen. In purification development, feedstocks are usually in short supply so sample volume requirements must be minimal. Excluding affinity separations, the maximum purification factor that can be achieved in a single-stage equilibrium experiment is typically 2 log removal value (LRV). Hence, the exquisite accuracy demanded from release assays is unnecessary. Moreover, since HTPD of purification steps favours the screening of purification conditions in a highly parallel fashion, the precision of an assay is often more important than the accuracy. The results from a single screen are often compared only within the screen, with the best conditions subsequently scaled up for verification. Ideally, the assay should be 96-well microplate-based to facilitate parallel processing. Integration with robotic liquid handling systems and compatibility with typical laboratory room temperature environment of the robots is also desired.

Assay interference is another significant issue because in-process samples typically have high levels of impurities that can impair assay fidelity. When combined with lower polysaccharide titres than are typically found in pure drug substance, this puts stringent demands on assay robustness.

2.1.3 Current Practise

2.1.3.1 *Standard Reference Tests*

Polysaccharides, endotoxin, proteins, and nucleic acids are the major components found in bacterial fermentation broths employed in industrial polysaccharide vaccine manufacturing. Their critical importance is underscored by the inclusion of the respective assays in the batch release package for product characterisation. Although national health agencies must authorise approval, the World Health Organization plays an active role in providing specific guidance for protocols and acceptance criteria for vaccine purity. Typical release specifications and in-process concentration limits provide insight into the analytical requirements for vaccines. Table 2.1 lists the level of required purity for a broad panel of polysaccharide vaccines and provides a general target for the development of purification unit operations.

WHO-recommended vaccine release tests can be categorized into purity, identity, and molecular weight. For background and insight, it is instructive to be familiar with the standard reference assays. Table 2.2 lists the reference assays utilised to measure the properties listed in Table 2.1. The reference assays in Table 2.1 are highly accurate for the testing of highly concentrated, relatively pure formulations; however, they are also laborious, complex, and/or lengthy assays. With the exception of A_{260} for nucleic acids, these assays are poorly suited for integration in a high throughput purification context. The intensive characterisation and high sensitivity provided by the assays specified in Table 2.2 is neither required nor desired for purification HTPD. Indeed, with release specifications generally $\leq 1\text{-}3\%$ protein or DNA and ≤ 100 IU/mg polysaccharide for endotoxin, detecting minute quantities of impurities is not necessary (WHO 2009; WHO 2006; WHO 2004; WHO 2000; WHO 1980; European Pharmacopoeia 2005a,c,d). Assuming a product titre of ≥ 1 mg/mL and the modest equilibrium purification factors, quantifying less than 0.01 mg/mL is rarely necessary.

To support purification HTPD, a set of analyses is required for product titre (3.3), product quality (3.3), impurity amount (*i.e.* endotoxin, nucleic acids, protein), and physicochemical properties of the stream (*e.g.* pH, viscosity, clarity, particle characterisation, filterability, etc.). This latter subset of properties is particularly important when developing procedures for primary recovery, the central focus of this thesis, where the level of particulates is high and the physicochemical properties of streams can vary substantially.

Table 2.1. WHO and European Pharmacopeia specifications for polysaccharide components of vaccines (European Pharmacopoeia, 2005a; European Pharmacopoeia, 2005b; European Pharmacopoeia, 2005c; European Pharmacopoeia, 2005d; WHO, 1980; WHO Expert Committee on Biological Standardization, 2006; WHO Expert Committee on Biological Standardization, 2009; WHO Technical Report Series, No. 897, 2000; WHO Technical Report, Series No. 924, 2004)

Species	<i>S. pneumoniae</i>	<i>N. meningitidis</i>	<i>H. Influenzae</i>	<i>S. typhi</i>
Serotype	23 different	A,C,Y,W-135	B	Vi
Identity	reference	reference	reference	reference
Protein	≤ 2% ^a	≤ 1%	≤ 1%	≤ 1%
Nucleic Acids	≤ 3% ^a	≤ 1%	≤ 1%	≤ 2%
Pyrogen	2.5 mg/kg	≤ 100 IU/mg	≤ 25 IU/mg	N/A
Molecular Size (Main peak Kd)	^a	≤ 0.65; ≤ 0.75; ≤ 0.57; ≤ 0.31	consistent with reference	50% before Kd = 0.25
Inactivation Agent Removal	≤ 2.5 g/L	N/A	N/A	≤ 0.2 g/L
C-polysaccharide	^a	N/A	N/A	N/A
Saccharide Content	^a	phosphorus/sialic acid	phosphorus/ribose 9% ≥	Immuno-chemical
Phosphorus	N/A	≥ 8% (Group A)	x ≥ 6.8%	N/A
Sialic Acid (% of monomers)	N/A	≥ 80%, ≥ 56% (Group C, Y, W-135)	N/A	N/A
Group-heterologous polysaccharide	N/A	≤ 1%	≤ 1%	N/A
O-acetylation (Group A,C,Y,W-135)	^a	≥ 2 mmol/g, ≥ 1.5 mmol/g, ≥ 0.3mmol/g, ≥ 0.3mmol/g	N/A	≥ 2 mmol/g

^aserotype specific

Table 2.2. Reference assays for vaccine products as indicated in WHO and European Pharmacopoeia documentation (Chen et al., 1956; European Pharmacopoeia, 2005a; European Pharmacopoeia, 2005b; European Pharmacopoeia, 2005c; European Pharmacopoeia, 2005d; Hestrin, 1949; Ricci et al., 2001; Svennerholm, 1957; WHO, 1980; WHO Expert Committee on Biological Standardization, 2006; WHO Expert Committee on Biological Standardization, 2009; WHO Technical Report Series, No. 897, 2000; WHO Technical Report, Series No. 924, 2004)

Property	Assay
Identity	Pneumococcal: chemical composition with wet chemistry; HPAEX-PAD; others: NMR, (immuno)electrophoresis or colorimetry
Protein	Lowry
Nucleic Acids	UV ₂₆₀
Pyrogen	LAL or rabbit injections
Molecular Size (Main peak kDa)	Sepharose CL-4B, -6B w/RI or colorimetric detection and SEC w/RI or MALLS detection
Inactivation Agent Removal	Pneumococcal: phenol; A,C,Y,W-135: heat/CTAB; B:phenol, others; Vi: formaldehyde/CTAB
C-polysaccharide	NMR or HPAEX-PAD
Saccharide Content	Pneumococcal: chemical composition; A,C,Y,W-135:NMR, AEX-CD, or AEX-PAD; B: ribose via Bial reaction or HPAEX-PAD; Vi: appropriate
Phosphorus	Colorimetric
Sialic Acid	Resorcinol assay
Group-heterologous polysaccharide	Unidentified
O-acetylation (Group A,C,Y,W-135)	Hestrin method

HPAEX-PAD: high pressure anion exchange chromatography with pulsed amperometric detection;
NMR: nuclear magnetic resonance

2.1.4 Impurity Assays

2.1.4.1 Endotoxin

Endotoxin assays have been historically enzymatic, time-consuming, and rarely automated. For instance, endotoxin assays require live animals or complex enzymatic cascades coupled to fickle kinetic measurements. A recent addition to the panel of commercially available assays offers the promise of rapid measurement (Lonza, 2007). As opposed to kinetic assays based on *Limulus* amebocyte lysate, the Pyrogene™ assay is an endpoint assay. The Pyrogene™ assay utilises a

recombinant protease zymogen, Factor C, which is activated upon endotoxin binding. The activated enzyme then cleaves a fluorogenic substrate that is quantified spectroscopically.

2.1.4.2 Protein

For protein quantification, bicinchoninic acid (BCA) and Bradford assays for protein concentration can be readily performed in a microplate format (Thermo Scientific, 2007). In the BCA assay, proteins reduce Cu^{+2} to Cu^{+1} in alkaline conditions. A proprietary BCA-containing reagent then reacts with the cuprous ion to form a purple colour, absorbing at 562 nm (Thermo Scientific, 2007). The extent of reaction depends on the macromolecular structure, number of peptide bonds, and the amount of C, Y, and W residues in the protein (Wiechelman et al., 1988). The Bradford assay employs an acidic solution of Coomassie Brilliant Blue G-250 that absorbs at 595 nm when incubated with proteins containing basic and aromatic residues (Bio Rad, 2008; Bradford, 1976; Compton and Jones, 1985). In this study, the Lowry assay was not tested due to its relative complexity, the multitude of substances that interfere (*e.g.* detergents), and poor reagent stability (Brown et al., 1989).

2.1.4.3 DNA

Several high throughput methods exist for measuring DNA concentration. A simple method based on absorbance at 260 nm or the ratio of absorbance at 260 nm and 280 nm are excellent for relatively pure samples. Where a complex absorbance background precludes the use of absorbance measurements for DNA quantification, fluorescent assays with Picogreen have proven exceptionally useful (Singer et al., 1997).

The PicoGreen assay is based on the high affinity binding of the unsymmetrical cyanine dye, PicoGreen to DNA. Upon binding, there is a 1000X increase in fluorescence with excitation at 480 nm and emission at 520 nm. The exact binding mechanism is unknown but believed to involve intercalation of dye into the nucleic acids and/or interactions with the molecule surface and grooves. Binding is not sequence-specific but dependent on conformation. This renders the assay much more sensitive to non-specific double stranded DNA than single stranded DNA or RNA.

2.1.4.4 Rheology

Capsular polysaccharides tend to be characterised by a higher viscosity than typical biotechnological products. Viscosity (η) is the ratio of shear stress (τ) to shear rate (γ), as given by

$$\eta = \frac{\tau}{\gamma} \quad (17)$$

Viscosity can be a critical physicochemical measurement because it affects all downstream operations. Flow patterns, Reynolds number, and many other hydrodynamic properties important for mixing are influenced by viscosity. For instance, pressure differentials in downstream operations, including filtration (mass transfer-controlled region) and chromatography exhibit a linear dependency on viscosity. It is imperative to increase our understanding of the range and magnitude of the rheological properties of CPS.

The rheological behaviours of capsular polysaccharides are complex. Solution properties such as pH, ionic strength, specific multivalent ions, molecular conformation, CPS concentration, and impurities such as DNA can affect the viscosity of CPS (Doran, 1995). Viscosity has also been shown to be dependent on molecular weight, as described by the Mark-Houwink-Sakurada equation,

$$\mu = K_1(MW)^\alpha \quad (18)$$

where K_1 and α are empirical constants and MW is the molecular weight of the CPS. Probing the impact of these substituent parameters is beyond the scope of this thesis. However, most capsular polysaccharides are non-Newtonian fluids, defined as having a viscosity that is dependent on shear rate. The rheological behaviour of all fluids is characterised by the Ostwald-de Waele relationship,

$$\mu_{app} = K_2\gamma^{n-1} \quad (19)$$

where K_2 = consistency index, a reflection of absolute viscosity, γ = shear rate, and n = flow behaviour index, the extent of divergence from Newtonian behaviour ($n=1$). With this power law relationship, $n < 1$ for non-Newtonian pseudoplastic fluids and $n > 1$ for non-Newtonian dilatant fluids.

2.1.4.5 Particle Characterisation

Many methods for particle characterisation exist and an excellent review on the subject was produced by J. Gregory (Gregory, 2009). For the operations of primary recovery, particles in the sub-visible range, 1-100 μm , are most critical. This is the range driven by orthokinetic processes and is where the impact of particle conditioning is readily apparent. Particles < 1 μm can be important, particularly for the plugging of sterile filters but the technologies available for investigating this range are less useful for the complex samples employed in this thesis.

2.1.5 Interference

A thorough understanding of assay interference is critical to the success of high throughput process development. The process streams created by unit operations occurring immediately downstream of a bacterial fermentor may have impurity concentrations 10-100 fold higher than that of the product. Challenges also exist further downstream where impurity loadings can still exceed the product concentration. For polishing operations, concerns about the levels of interference are redirected towards the potential presence of high concentrations of added excipients that can impair assays.

2.2 Aim and Objectives

This chapter describes the development of rapid and simple assays to enable the evolution of HTPD for the generation of novel polysaccharide purification processes. More specifically, a set of analytical methods is described that yield information on:

- Endotoxin
- Nucleic acids
- Protein
- Clarity
- Particle characteristics
- Viscosity

Accuracy, precision, robustness, reproducibility, modularity, and interference from sample matrix were examined. To facilitate future integration in a platform purification process, emphasis was given to developing methods that were versatile and would accommodate many different feedstreams, Along with bacterial CPS, a broad range of commercially available carbohydrates were screened in order to thoroughly evaluate potential interferences from vaccine streams.

2.3 Materials and Methods

The identity of select capsular polysaccharides were redacted in Figures 2.7, 2.8, and 2.11 and in Tables 2.4 and 2.7

2.3.1 Materials

All common chemicals were commercial analytical grade. Lysozyme from chicken egg white, albumin from bovine serum (BSA), L-arabinose, glycogen from oyster, chondroitin sulphate A sodium salt from bovine trachea, α -lactose monohydrate, glucose, N-acetyl neuraminic acid (NANA) from *E. coli*, Type II ι -carrageenan, 3-(N-morpholino)propanesulfonic acid (MOPS), and dextran were obtained from Sigma-Aldrich (United Kingdom). Deoxyribonucleic acid (DNA) sodium salt from salmon sperm was purchased from Fisher Bioreagents (United Kingdom). Sodium alginate from *L. hyperborea* came from BDH (United Kingdom). Lonza Walkersville (Walkersville, MD) provided the endotoxin from *E. coli*. Gellan gum was produced by Applichem Biochemica (United Kingdom). High molecular weight hyaluronan (hyaluronic acid, HA) was purchased from R&D Systems (United Kingdom). Endotoxin standards and stocks were purchased from Lonza Walkersville (Walkersville, MD). All reagents were used as purchased. All sugars are D isomers except where otherwise noted. Solutions were filtered with 0.22 μ m filters (GV PVDF, PES Express, Millipore, Billerica, MA) where appropriate. A Safire II microplate spectrophotometer (Safire II, Tecan, Switzerland) was used for all absorbance and fluorescence measurements except for the Picogreen data and wherever CPS are referenced, and for absorbance measurements where noted. In these instances, a fluorescence-enabled spectrophotometric plate reader (Molecular Devices, Spectramax M3) was employed using top reads

with liquid height-compensation disabled. Costar 3635 or 3596 acrylic microplates from Corning were used (Corning, NY) for all UV measurements, except where noted.

Capsular polysaccharides from various serotypes of *S. pneumoniae*, *S. aureus*, and *N. meningitidis* were kindly provided by Pfizer R&D. All sugars have D and α structural configuration.

The identity of select capsular polysaccharides were redacted in Figures 2.7, 2.8, and 2.11 and in Table 2.4 and 2.7

2.3.2 Absorbance Spectra

Absorbance spectra of pure carbohydrates and proteins were measured in solutions buffered with 20 mM MOPS, pH 7.2. Absorbance spectra were measured from 230-1000 nm in ≤ 3 nm increments using a microplate reader.

2.3.3 Endotoxin Assay

A pyrogen assay (PyroGene™, Lonza, Walkersville MD) based on recombinant Factor C for endotoxin was qualified. The instructions provided by the assay kit manufacturer (version: 08299P50-658U/NV-612/07) were followed except where noted. Pyrogen-free consumables including reagent reservoirs, pipette tips, conical tubes, Limulus Amebocyte Lysate (LAL) Reagent Water, and serological pipettes were purchased from Lonza Walkersville. Samples were diluted into LAL Reagent Water and standard curves were run in triplicate. For assay interference testing and positive product controls, 10 μ l of a 10 EU/mL standard solution was added to 90 μ l of sample, yielding a 1 EU/mL reference standard concentration. Endotoxin samples and standards were vortexed vigorously for the prescribed amount of time. Generally, microplates were incubated for 1 hour at 37°C inside the plate reader prior to reading. In certain instances, incubations at 22°C, 26°C, and 37°C were evaluated for varying durations. The log amount of endotoxin present is proportional to the log change in the relative fluorescent unit (RFU), with second order polynomial fits the most accurate.

The excitation and emission wavelengths were set to 380 nm (± 20 nm) and 440 nm (± 20 nm), respectively, with an integration time of 40 μ s. A single measurement was taken approximately 60

minutes after the start of incubation at 37°C instead of the manufacturer's recommended two-point measurement.

2.3.4 Protein Assays

2.3.4.1 Bradford Assay

The Bio-Rad protein assay (Hercules, CA) based on Bradford's method was employed to measure protein concentration (Bradford, 1976)(Bio Rad, 2008). The instructions provided by the reagent manufacturer were followed utilizing microtitre plates (Corning Costar #3596, Lowell, MA). Samples were diluted in 20 mM MOPS, pH 7.0. Absorbance measurements were made at 595 nm and 990 nm. Blank-corrected standard curves were run in triplicate with absorbance at 990 nm subtracted from absorbance at 595 nm. Linear regression was used to fit the standard curve.

2.3.4.2 Bicinchoninic Acid Assay

The bicinchoninic acid (BCA) assay kit (Pierce Thermo Scientific, Rockford IL, version: 1296.7) was employed to measure protein concentration (Smith et al., 1985). The microplate instructions provided by the assay kit manufacturer were followed. Samples were diluted into 20 mM MOPS, pH 7.0. Absorbance was measured at 562 nm and 990 nm. Blank-corrected standard curves were run in triplicate with a second order polynomial fit employed.

2.3.5 DNA Assay

The Quant-it Picogreen double-stranded DNA kit (Q33130; Life Technologies, Grand Island, NY) based on the original method by Singer et al. was used for DNA quantification (Singer et al., 1997). A dynamic linear range of 8-2000 ng/mL was found to be achievable. The single DNA standard included in the kit was diluted in 1X TE buffer (10 mM Tris-HCl, 1 mM EDTA, pH 7.5) to prepare 2000, 1000, 500, 250, 125, 62, 31, 16, and 8 ng/mL standards, with TE buffer employed as the blank. Typically, standards were prepared in triplicate with single measurements of each standard. To initiate the binding reaction, 150 µL of sample was combined with 150 µL of Picogreen reagent, using 4 cycles of pipettor aspiration/dispense for mixing. Samples were incubated at room temperature in the dark for 5 minutes before being read at excitation and emission wavelengths of 480 nm and 520 nm,

respectively. For instrument settings, an auto cut-off of 515 nm, a sensitivity of 12, the photo-multiplier tube set to auto were specified. Black Costar 3915 microplates from Corning were used (Corning, NY) for all Picogreen measurements.

2.3.6 Rheology

An mVROC viscometer (Rheosense, San Ramon, CA) was employed to measure the viscosity of samples. The instrument is comprised of a pressure transducer array integrated with a microfluidic fluid path. With this technology, the pressure drop created by a laminarly flowing liquid is measured. The slope of the pressure versus flow path distance is used to calculate the wall shear stress (τ),

$$\tau = -slope \frac{wh}{(2w+2h)} \quad (20)$$

where the width of the channel (w) is constant for the instrument and the channel depth (h) was fixed at 50 μm for this testing. The flow rate (Q) is used to calculate the apparent shear rate for Newtonian fluids (γ_{app}),

$$\gamma_{\text{app}} = \frac{6Q}{wh^2} \quad (21)$$

and the true shear rate for non-Newtonian fluids,

$$\gamma = \frac{\gamma_{\text{app}}}{3} \left(2 + \frac{d \ln \gamma_{\text{app}}}{d \ln \tau} \right) \quad (22)$$

Viscosity (μ) is then determined as described in Equation 17.

'A' and 'B' microfluidic cells were used for viscosity measurements, depending on the range required by the sample. Replicate measurements were made with 100 μL and/or 500 μL syringes. For determination of the Ostwald-de Waele relationship, viscosity versus shear rate curves were generated across the range where $268 \leq \gamma \leq 13,880 \text{ s}^{-1}$.

2.3.7 Micro Flow Imaging

Micro Flow Imaging (MFI) is an image-based, sub-visible particle analyser (MFI 5200, 1-70 μm , Protein Simple, Santa Clara, CA) that measures particle size, particle counts, and morphologic properties.

Samples are aspirated and dispensed through a capillary, in which the entire sample volume is captured via images from a high-resolution, high-speed camera. In this study, the Bot1 attachment enabled automated sample pick-up from microplates in the native buffer system. 0.7 mL of each sample was analysed, edge particles were ignored, and to expedite processing, analysis was restricted to 50,000 particles per sample. Particulates for analysis were generated through the flocculation of hydrolyzed SA1 fermentation broth with 2% floc agent, pH 5.5. Prior to flocculation, broths were stored for 2 or 5 days at 5°C. Dynamic aging at 37°C for 60 min was employed prior to analysis. Floc samples were diluted 100-fold with PBS, RODI, or a custom, process-specific diluent of 300 mM NaCl, 50 mM HEPES, 2.5% floc agent, pH 5.5. Diameters reported in μm refer to the equivalent circular diameter and represent number-averaged values.

2.3.8 Nephelometry

Filtrate samples were collected from several similar depth filtration operations. Nephelometric measurements were made with three different technologies:

1. Turbidity measurements were made with a 2100P portable turbidimeter (Hach, Loveland, CO), using 7 mL of sample. Duplicate measurements of the same sample were averaged.
2. The absorbance at 600 nm (A_{600}) was measured with a microplate spectrophotometer (Molecular Devices, Spectramax M3). 300 μL of each sample was measured in a 96-well Costar 3635 microplate.
3. Particle counts were measured with the MFI using the procedures in 2.3.7.

Samples were analysed within 3 hours of sample generation, with samples stored statically at room temperature.

2.3.9 Assay Reproducibility

To provide a realistic analysis of the robustness of the HT analytical suite, duplicate flocculations of fermentation broth were performed with 2% floc agent, pH 4.0 with ten pneumococcal serotypes and with 2% floc agent, pH 5.5 for two staphylococcal serotypes. Individual wells were then agitated at one of four stirrer speeds for one hour before centrifugation and subsequent sampling of the

supernatant. Several assays were run with the supernatant from each duplicate flocculation. This entire process was repeated at two different temperatures and with the order of titrant addition reversed to yield 144 independent conditions run in duplicate (precipitation was duplicated, not the analytics). Assays for absorbance and DNA were performed as described in 2.3.2 and 2.3.5. SEC-MALS-derived measurements such as titre, MW, and r_{rms} were run as later described in 3.3.4.2. One key permutation was that the 'large proteins' data was derived from integration of the A_{280} UV signal across the elution window between the void volume of the column and the elution point of BSA, for the aforementioned SEC-MALS method. This measurement was designed to exclude small UV-absorbing metabolites and was predicated on the CPS not adsorbing at 280 nm. Although there was no systematic qualification of this method, it was found to correlate roughly to Bradford assay results (data not shown). Depending on the assay, a few data points were excised due to operational errors during execution of the screen, leading to the total number of duplicates being approximately 144.

2.4 Results and Discussion

2.4.1 Absorbance Spectra

Absorbance spectra of various carbohydrates, proteins, and model mixtures are shown in Figure 2.1. This characterised the most common impurities found in the process and their impact on absorbance profiles. Many of the molecules absorb significantly in the ultraviolet range from 230-310 nm, owing to the presence of aromatic groups. This property was expected for proteins, DNA, and for polysaccharides such as chondroitin sulphate, which are conjugated to proteins. All compounds except dextran had minor, albeit similar absorbance in the near infrared spectrum, 900-1000 nm.

These absorbance spectra demonstrate that A_{280} and A_{260} remain effective ways to assay crudely for protein and DNA respectively in relatively pure samples of polysaccharides. The negligible absorbance present for any sample from 400-900 nm is advantageous since many commercial assays, including ones employed in this chapter, employ reagents that specify measurements in this region.

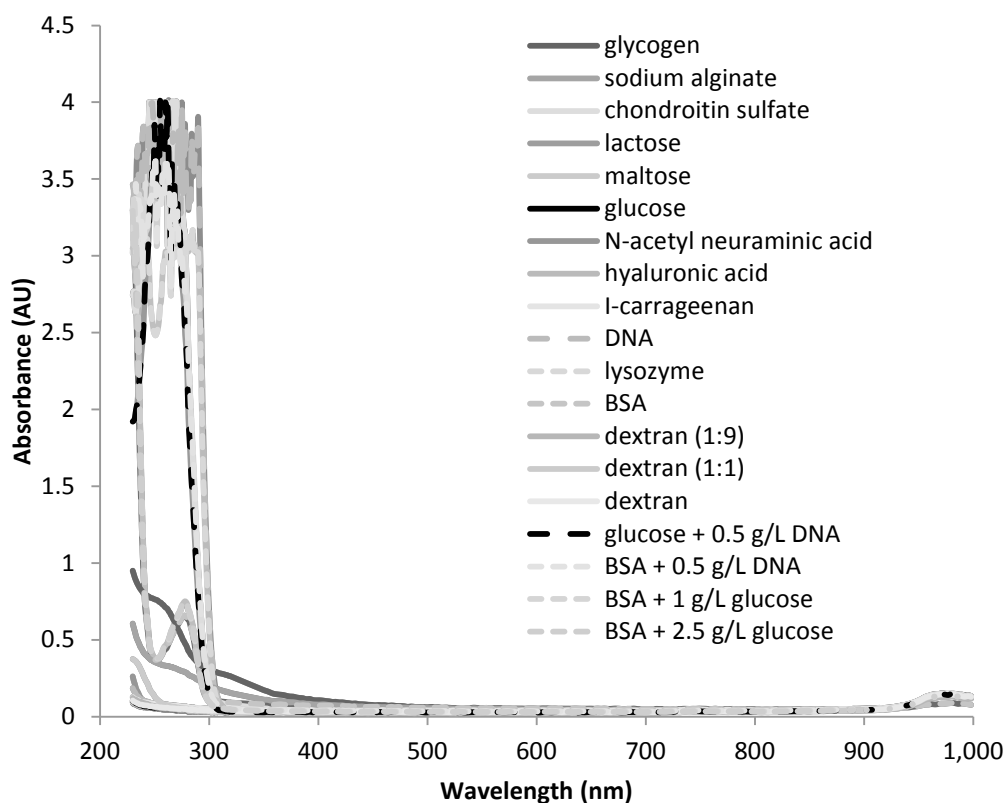


Figure 2.1. Absorbance spectra of compounds typically found in microbial broths and assorted carbohydrates. Delineation of individual plots is not required where the set of molecules identified in the legend have negligible absorbance (*i.e.* 400-900 nm)

2.4.2 Endotoxin Assay

The Pyrogene™ assay was qualified as the principal endotoxin assay (Ding and Ho, 2001). This assay was selected for its simplicity and ease of automation, particularly when compared to kinetic assays (*e.g.* kinetic QCL). In the standard assay, the log amount of endotoxin present is proportional to the log change in the relative fluorescent unit (RFU) signal after 60 minutes. To improve operational flexibility, the reaction incubation step was performed at temperatures below the recommended temperature of 37°C (Figure 2.2).

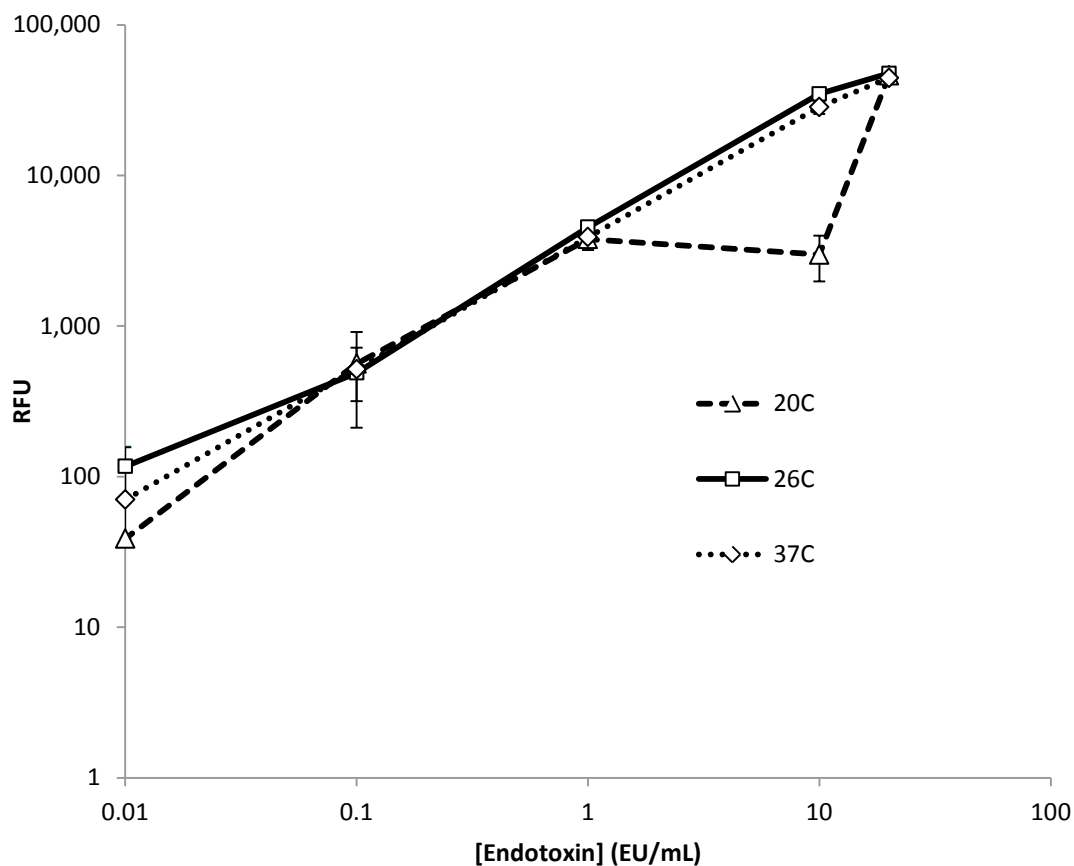


Figure 2.2. Effect of incubation temperature on the relative fluorescence measurements in the Pyrogene™ assay. The incubation duration was 1 h. No significant differences in measurements were noted for 2 h incubations. Standard curves were run in triplicate with the error bars denoting the standard deviation.

The log-log standard curves were consistent and exhibited good fits with $R^2 > 0.99$ across a range of 0.01-20 endotoxin units (EU/mL). The 10 EU/mL sample tested at 20°C was anomalous. This experimental condition was not rerun but a pipetting error is believed to be the cause of the deviation, given that the sample at 26°C exhibited the expected fluorescence. The average precision was 7% RSD across the tested range. Enabling the incubation period to occur at room temperature is helpful when automating assays with liquid-handling robots situated in room temperature environments.

The potential for various substances to interfere with the Pyrogene™ assay was evaluated through positive product controls. In these samples, endotoxin was spiked to a final concentration of 1 EU/mL in the presence of a concentration series of various impurities (*i.e.* proteins, sugars, or DNA). Several of the tested substances (*i.e.* BSA, HA, lysozyme, and dextran) exhibited apparent enhancement when tested initially. As these liquid samples had been stored non-sterile at 5°C for two weeks, fresh stocks were prepared. Using the fresh stocks, no enhancement was observed, highlighting the importance of mitigating potential Gram-negative bacteria contamination. None of the tested species consistently interfered except for those shown in Figure 2.3.

Fresh lysozyme artificially increased the signal intensity of the assay. The dry chemical stock of lysozyme may have harboured Gram-negative microbes or pyrogenic by-products. Unlike with the LAL assay, high molecular weight carbohydrates such as carrageenan were not found to enhance the Pyrogene™ assay (Pearson et al., 1984).

Chondroitin sulphate, DNA, sodium alginate, ι -carrageenan, and several anionic capsular polysaccharides (CPS data not shown) inhibited the Pyrogene™ assay. The severity of the inhibition was high, with dilutions to $< 1 \mu\text{g/mL}$ required to abolish the inhibition. The inhibition was consistent across assays performed on multiple days with freshly made solutions, with a multi-day variability of $\sim 27\%$. Each of these inhibitors is an anionic polysaccharide but other anionic polysaccharides such as HA, gellan gum, and NANA did not react, nor did the acidic protein, BSA. A common structural feature between the DNA, ι -carrageenan, and chondroitin sulphate is the presence of sulphates. Every species with a sulphate that was tested was found to inhibit the assay. However, other anionic groups did not inhibit consistently. For example, none of the uronic acid-containing polysaccharides reacted except for sodium alginate and chondroitin sulphate, the latter possessing sulphate groups. The mechanisms for inhibition are unknown but could be due to electrostatic interactions with the zwitterionic endotoxin. Inhibition of the recombinant Factor C through the active site is unlikely as the lipid domain of endotoxin serves as the substrate (Ding and Ho, 2001).

Utilisation of the Pyrogene™ assay will necessitate extensive dilution (*i.e.* 10^{-3} - 10^{-4}) to eliminate interference. The level of dilution will be predicated on the concentration and nature of components

in the sample background, with samples taken from upstream in the process requiring greater dilution than the samples taken from more purified streams found further downstream in the process.

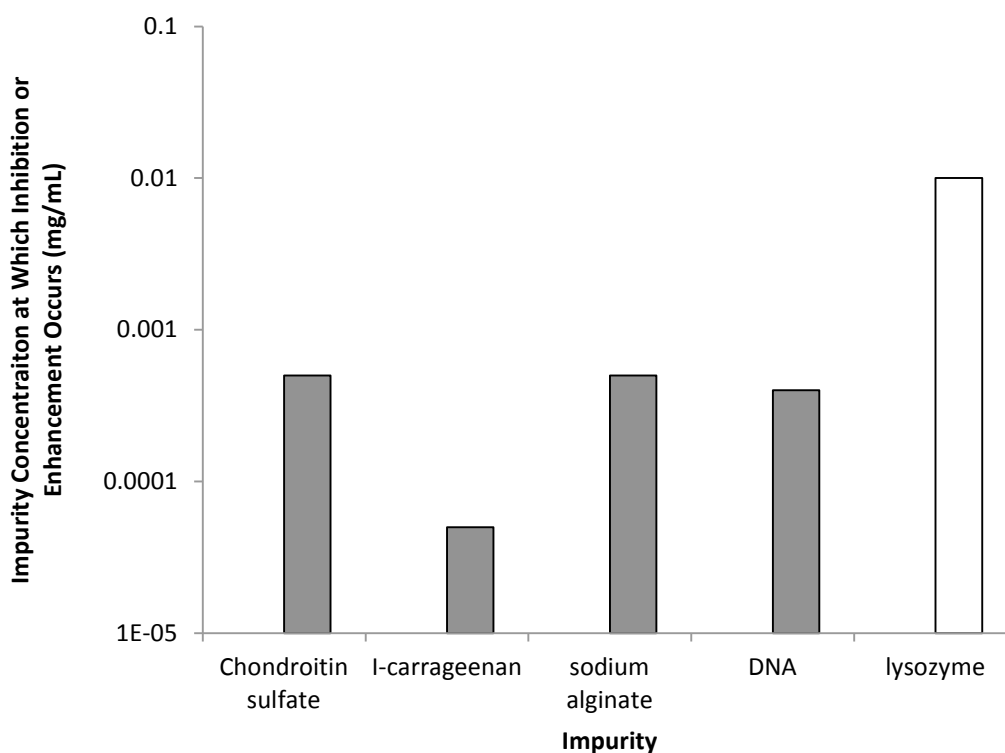


Figure 2.3. Interference in the Pyrogene™ assay. Gray and white bars denote inhibition and enhancement, respectively. Endotoxin concentration was 1 mg/mL in 20 mM MOPS, pH 7.0. Interference was defined as a shift in the measurement of an endotoxin concentration from a 1 EU/mL standard to ≥ 5 EU/mL or ≤ 0.5 mg/mL. Interfering substances were added from freshly prepared liquid stocks and diluted into depyrogenated H₂O prepared to give a fixed endotoxin standard concentration. All substances inhibited the assay except for lysozyme, which enhanced the assay.

Although the magnitude of the inhibition is large, the Pyrogene™ assay is still suitable for measuring endotoxin in in-process pools. In polysaccharide process streams derived from Gram-negative

bacteria, the starting concentrations of endotoxin are extremely high. These values often exceed 20,000,000 EU/mL (personal communication Pfizer R&D). However, the linear range of the Pyrogene™ assay is 0.01-10 EU/mL, necessitating multiple serial dilutions for a typical sample to fall within the standard curve. Because of the large difference between the range of the Pyrogene™ assay and in-process endotoxin concentrations, it is possible to measure adequate LRV of endotoxin, even when factoring in dilution to eliminate interference (Table 2.3).

Table 2.3. Maximum endotoxin clearance values that can be measured in the presence of interfering species. Assumes polysaccharide concentration is 1 mg/mL and endotoxin assay dynamic range is 0.01-10 EU/mL.

	[Endotoxin] (EU/mL)	[Endotoxin] with Assay Dilution (EU/mL)	Available Log Removal Value (LRV)
Post-harvest	> 20,000,000	2,000-20,000	~5-6
Post-primary recovery	20,000	2-20	~2-3

With such high amounts of endotoxin present, dilution to 10^{-3} - 10^{-4} should still enable the demonstration of 5-6 LRV of endotoxin clearance for harvest samples and 2-3 LRV of endotoxin clearance for polishing steps. These potential clearance values are sufficient for purification process development. Paradoxically, the demonstration of adequate clearance may be a greater problem in purer samples taken downstream of polishing steps, where endotoxin concentration is lower and therefore allows for less dilution.

2.4.3 Protein Assays

2.4.3.1 Accuracy and Precision

Two protein assays were qualified for suitability for integration with polysaccharide HTPD: the BCA and the Bradford assays. Results are elaborated in Appendix 9.3: Protein Assays. The standard curves generated with both protein assays exhibited good fits. For the BCA assay, a $R^2 > 0.99$ for the 0.025-2 mg/mL range was achieved with a relative standard deviation of 4%. Second-order polynomial fitting

improved the accuracy. Correction for absorbance at 990 nm decreased the precision slightly and was therefore eliminated from the procedure. With the Bradford assay, the correlation coefficient was found to be a function of the range. Employing 0.025 mg/mL as the lowest non-zero concentration tested, linearly fit standard curves with an upper range of 0.5, 1.0, and 2.0 mg/mL were generated. The R^2 values for these curves were > 0.99 , > 0.98 , and > 0.95 , respectively, with curves based on the broader ranges overestimating the highest concentrations. The subtraction of the absorbance at 990 nm from the absorbance at 595 nm improved mean precision from 6% to 3% RSD and was instituted as standard practise.

2.4.3.2 Interference

Each protein assay had a unique interference pattern (Figure 2.4). Concentrated DNA (5 mg/mL) yielded a significant response in the Bradford assay but did not react in the BCA assay. In the Bradford assay, DNA was the only sugar-containing species to form absorbing species, although this was only substantial at > 1 mg/mL, consistent with product literature (Bio Rad, 2008). An increase in absorbance at 595 nm due to shifts in the charged dye equilibria may underlie this observation (Compton and Jones, 1985). In the Bradford assay, the relative response of lysozyme and BSA to DNA was 28-fold and 11-fold, respectively. This finding suggests that relative to the signal from proteins, any DNA interference would be manageable in a process development scheme. Endotoxin, up to 2.5% flocculent agent, and up to 2 mg/mL purified SA2 and SA1 did not react and did not interfere in either assay. The standard curves for the full set of molecules that were tested in the Bradford assay are provided in Appendix 9.3: Protein Assays.

Carbohydrates did not exhibit any reactivity in the Bradford assay but reducing sugars were oxidized in the BCA assay (Figure 2.5).

Monosaccharide and disaccharide reducing sugars exhibited the highest absorptivity with no clear difference between hexoses or pentoses. Polysaccharides were characterised by lower absorptivity, due to the localization of the reducing groups at the termini and the low relative number of reducing groups per polysaccharide. Indeed, dextran exhibited negligible reactivity due to the reducing groups

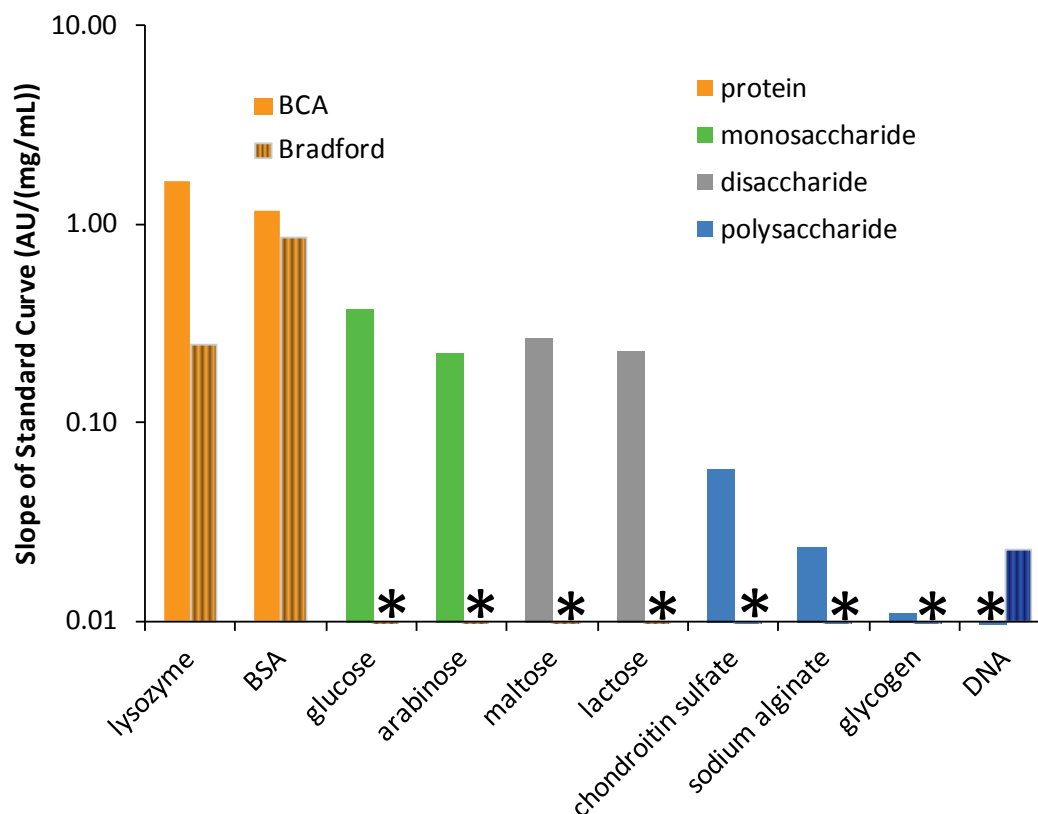


Figure 2.4. Absorptivity of various carbohydrates in BCA and Bradford assays. Standard curves in both assays were fit with linear regression although second order polynomial fitting produced slightly better fits for the BCA assay. For Bradford and BCA assays, all curves were characterised by $R^2 > 0.92$ and $R^2 > 0.98$, respectively. * denotes samples with absorbivity below the limit of quantification (BLOQ) or that did not signal.

being confined to a limited number of branched termini and representing a small proportion of the total hexoses comprising the polysaccharide. Non-reducing carbohydrates including glycogen, HA, chondroitin sulphate, NANA, and sodium alginate did not react in the BCA assay (data not shown). The net result of these interference studies is that depending on whether the carbohydrate or DNA concentration is known, the Bradford or BCA assay can both be used for in-process samples. Utilisation of differential response of these two protein assays for sugar quantification was pursued but suffered from inadequate accuracy and precision (Appendix 9.4: Differential Assay for Carbohydrates).

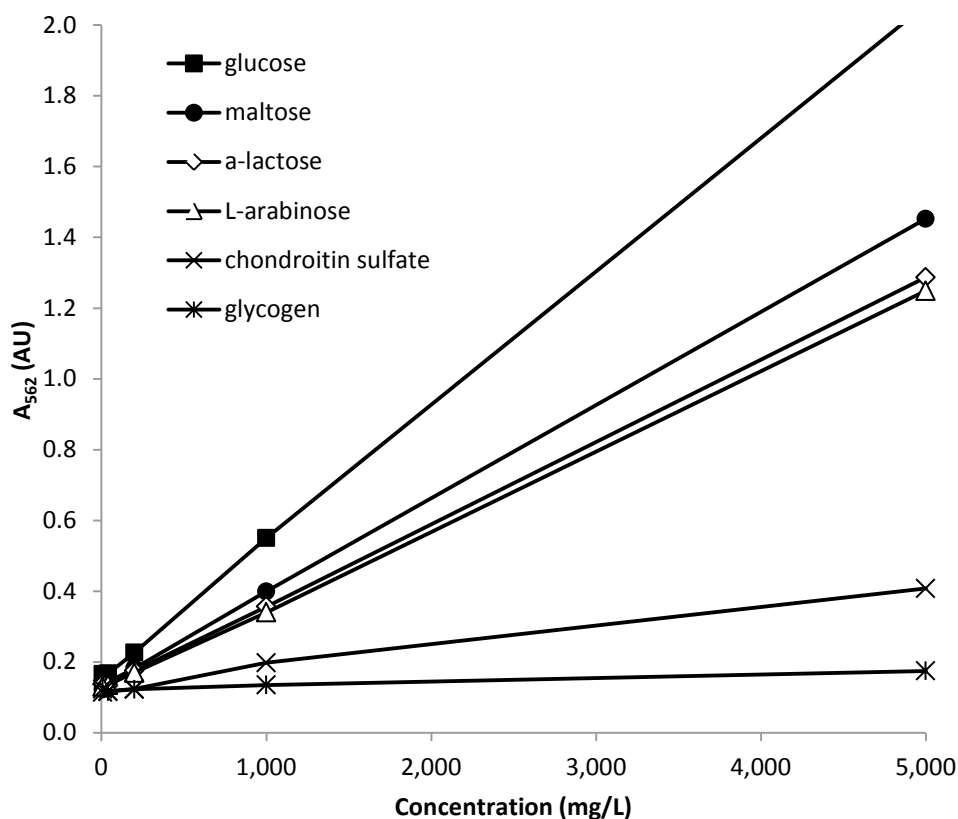


Figure 2.5. Reactivity of reducing sugars in BCA assay

2.4.4 DNA Assay

The use of Picogreen with recombinant protein products is well established internally. Therefore, it was only necessary to assess the compatibility of the assay with polysaccharides and any reagents utilised specifically for HTPD. The initial effort was to identify false positives and determine whether the flocculant and capsular polysaccharides exhibited positive interference. Neither these compounds nor PBS signalled in the assay. The latter observation enabled the substitution of PBS for TE buffer as the assay diluent. Next, positive product controls were generated through the spiking of different concentrations of a panel of compounds into DNA standards to ascertain if interference was observed. The result was that while CPS did not affect DNA quantification, the flocculant was shown to inhibit (Figure 2.6).

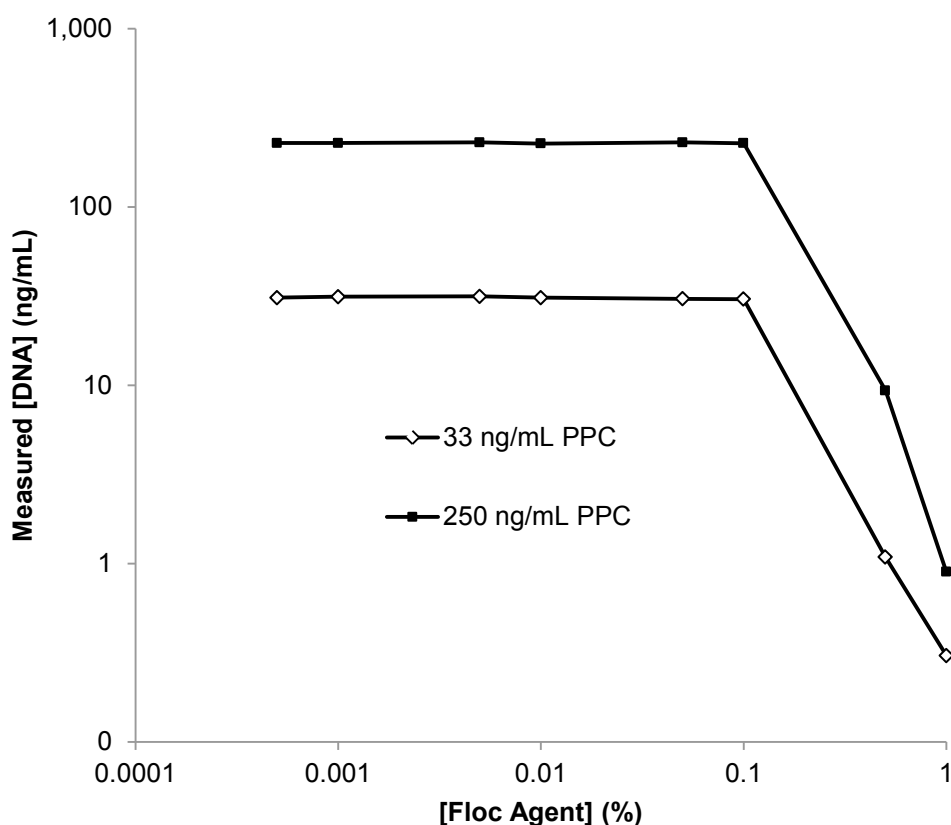


Figure 2.6. Interference in Picogreen assay. Effect of a range of floc agent concentration on the quantification of positive product controls where [double stranded DNA] = 33 and 250 ng/mL.

Interference abated when the floc agent was diluted to ≤ 0.1 mg/mL. Assuming a working floc agent concentration range of 1-5%, flocculation samples would need to be diluted 10-fold to 50-fold.

Ultimately, a dilution range of 20-fold to 600-fold was found to be suitable for most experiments and could be addressed satisfactorily via serial dilution protocols.

2.4.5 Rheology

The rheological properties of fermentation broths have proven to be limiting factors in downstream processing. Specifically, shear-thinning fluids are more difficult to mix during early downstream steps (*e.g.* flocculation/precipitation, filtration, etc.) because the viscosity will be lowest in the impeller zone of reactors, leading to the development of stagnant zones on the sides and corners of the tanks.

Solutions of extreme viscosity may necessitate special impellers (e.g. anchor impellers) to effect a well-mixed tank or alternatively, require viscosity mitigation strategies, such as heating or enzymatic treatment. To survey rheological properties, a diverse set of killed fermentation broths containing CPS was characterised, with a set of the samples plotted in Figure 2.7, including those serotypes that exhibited the strongest non-Newtonian behaviour.

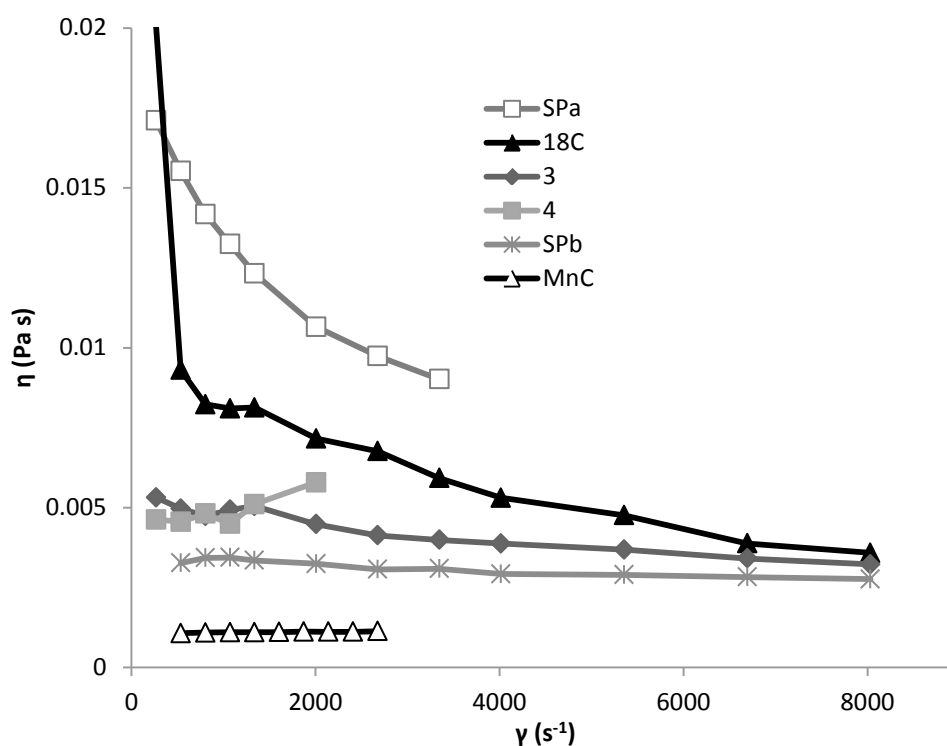


Figure 2.7. Rheological power law curves for microbial fermentation broths from different species and pneumococcal serotypes. The CPS identified in the legend are derived from *S. pneumoniae* except for Mn C. SPb and SPa are pneumococcal CPS with serotypes blinded due to commercial sensitivity. Shear rates (γ) are plotted on the x-axis and the corresponding apparent viscosity (η) is plotted on the y-axis. Shear rate was varied by modulating flow rate through the microfluidic cell of the viscometer. SPx denotes blinded capsular polysaccharides from *S. pneumoniae*.

The rheological behaviour shown in Figure 2.7 was reversible, suggesting that re-orientation of CPS occurred rapidly following exposure to a shear field. Serotype 18C exhibited the sharpest pseudoplastic behaviour as indicated by the sharp gradient function and high viscosity. From plots

similar to Figure 2.7, parameters for the Ostwald-de Waele relationship (19) were extracted from the shear-viscosity curves and are reported in Table 2.4.

Table 2.4. Viscosity and Ostwald-de Waele parameters for polysaccharide-containing fermentation broths. The dotted line demarcates pseudoplastic from dilatant fluids. The apparent viscosity calculated for a shear rate of 1000 s^{-1} is given in the final column. SPa, SPb, SPc, SPd, SPe, SPf, and SPg are pneumococcal CPS with serotypes blinded due to commercial sensitivity.

Γ	K_2	n	η (at $\dot{\gamma}=1000 \text{ s}^{-1}$)
18C	0.16	0.59	0.0090
SPa	0.079	0.74	0.0129
3	0.013	0.85	0.0047
SPb	0.0058	0.92	0.0033
SPc	0.0058	0.93	0.0035
SPd	0.0033	0.96	0.0024
SPe	0.0030	0.96	0.0022
SA1	0.0032	0.96	0.0024
SA2	0.0043	0.97	0.0035
SPf	0.0031	0.98	0.0026
SPg	0.0021	0.99	0.0019
Mn C	0.0009	1.03	0.0011
4	0.0026	1.09	0.0050

The vast majority of polysaccharide broths were mildly pseudoplastic, which generally facilitate good mixing. Serotypes 18C, SPa, and 3 were the most pseudoplastic of the broths. When viscosities are $> 5 \text{ cP}$ as with serogroups 18C and SPa, downstream processing can benefit from viscosity-mitigation strategies. Nevertheless, of the set of tested broths, none has a viscosity $> 100 \text{ cP}$ or $n < 0.3$ (classification for highly pseudoplastic), either of which would warrant consideration of specialized impellers for mixing (Doran, 1995). The dataset in Table 2.4 lends itself to probing why serotypes 18C, SPa, and 3 are the most pseudoplastic of the tested CPS. Few structural similarities or shared broth attributes are present that might underpin the extraordinary rheology of this group (data not shown). A common repeating component is however shared between serotypes 3 and SPa. This structural element may contribute to the adoption of a CPS morphology that favours interactions with other CPS

or otherwise supports higher viscosity and pseudoplastic characteristics. Additional characterisation is needed to understand better the significance of this commonality.

2.4.6 Micro Flow Imaging

Micro flow imaging (MFI) is the only sub-visible particle sizing technology that offers high throughput analysis, sample volumes less 1 mL, and options for automated sample resuspension. Importantly for labile samples such as flocs, the system enables a set of samples to be run with different sample backgrounds, thereby preserving any initial solution-dependent macromolecular structure. This feature is of particular interest for flocculation where agglomeration processes tend to be reversible. Since the analysis cycle for a sample takes approximately 8 minutes and a half microplate batch requires 6 hours to run, this static holding period could lead to altered structures even if dissociation kinetics were slow. To evaluate the effects of static holds while in the MFI microplate and the diluent composition on particle properties, flocculated SA1 was diluted in several reagents and then repeatedly analysed over several hours (Figure 2.8).

In Figure 2.8, the age of the broth has minimal effect but the effect of diluent is striking. Dilution into RODI leads to the largest particles and fewest particle counts, consistent with a diluent-induced aggregation phenomenon. Conversely, PBS yields the smallest particles but highest particle concentrations. Of moderate particle size and concentration are the samples diluted in the custom diluent, which had been designed to match the conductivity, pH, and flocculation agent concentration of the flocculation conditions. So which diluent provides the truest representation of the pre-dilution particle population? The custom diluent is the more appropriate diluent. An examination of time-dependent changes in particle properties further corroborates this finding. Samples diluted in PBS and RODI are initially characterised by moderate sizes and concentration but with additional incubation time, progressively shift to a size and count plateau that is characteristic of the respective diluent. This observation corroborates an intuitive preference for the custom diluent and highlights the necessity of using custom diluents for this flocculation process (and probably others). The data in Figure 2.8 also demonstrates measurement stability because the samples run at the end of batch

yield approximately the same data as samples run at the outset of the batch, when prepared with the custom diluent.

In Figure 2.8, the age of the broth has minimal effect but the effect of diluent is striking. Dilution into RODI leads to the largest particles and fewest particle counts, consistent with a diluent-induced aggregation phenomenon. Conversely, PBS yields the smallest particles but highest particle concentrations. Of moderate particle size and concentration are the samples diluted in the custom diluent, which had been designed to match the conductivity, pH, and flocculation agent concentration of the flocculation conditions. So which diluent provides the truest representation of the pre-dilution particle population? The custom diluent is the more appropriate diluent. An examination of time-dependent changes in particle properties further corroborates this finding. Samples diluted in PBS and RODI are initially characterised by moderate sizes and concentration but with additional incubation time, progressively shift to a size and count plateau that is characteristic of the respective diluent. This observation corroborates an intuitive preference for the custom diluent and highlights the necessity of using custom diluents for this flocculation process (and probably others). The data in Figure 2.8 also demonstrates measurement stability because the samples run at the end of batch yield approximately the same data as samples run at the outset of the batch, when prepared with the custom diluent.

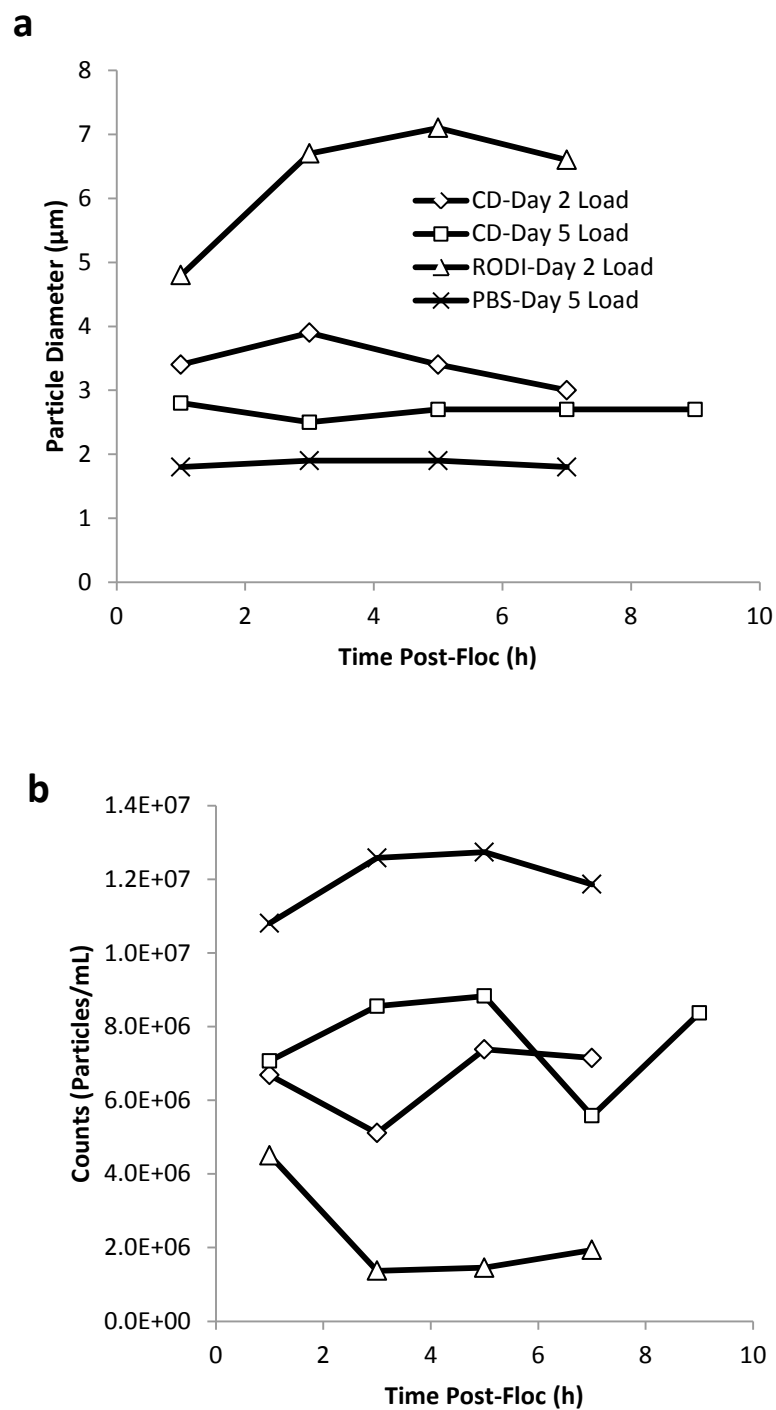


Figure 2.8. Effect of hold time, diluent, and broth age on number-averaged, equivalent particle diameter (2.8a) and particle concentration (2.8b) of flocculated SA1. CD is the custom diluent described in 2.3.7.

2.4.7 Nephelometry

Tracking the clarity of solutions is critical for assessing particle conditioning, depth filtration, and sterile filtration operations. For in-process solutions, the standard instrument for this purpose is the Hach turbidimeter. The portable Hach turbidimeter employed in this study requires a minimum of 7 mL for accurate measurement. Alternative approaches that require less than 1 mL are necessary for HTPD. Two orthogonal measurements, particle concentration obtained with MFI and A_{600} acquired via a microplate-spectrophotometer, were compared directly against Hach measurements for a set of samples (Figure 2.9)

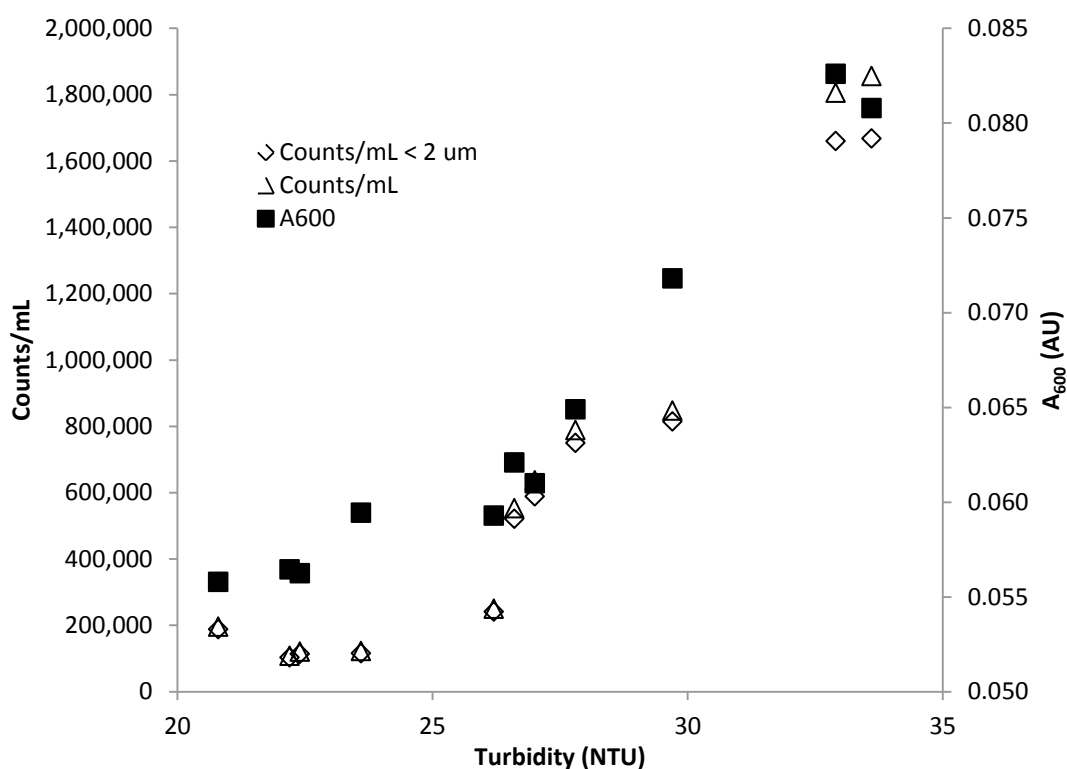


Figure 2.9. Correlation of MFI counts (counts/mL) and A_{600} (AU) with Hach turbidimetric values (NTU). MFI-derived particle concentrations were reported for the full 1-70 μ m range and for particles with 1 μ m \leq ECD < 2 μ m to see if a particular range more closely tracked NTU measurements.

The samples were designed to vary only slightly in their turbidity to provide a high-resolution comparison of these three nephelometric approaches. Across this very tight fine NTU range, generally, all three measurements were well correlated. The MFI data exhibited a marginally better correspondence to the Hach NTU data when the full size range of particles was utilised and not restricted to particles < 2 μm . These findings are important as they create options for turbidimetric measurements with sub-mL volumes and connect results to nephelometric properties (*i.e.* Hach NTU) that are meaningful at larger scale. It also substantiates internal data connecting A_{600} and NTU for samples of moderate to high turbidity. It is notable that below 22-24 NTU, the correspondence appeared to diverge. Additional data is needed to increase confidence in the result and to understand this behaviour better. This result corroborates previous experiences where the NTU of fine pad filtrate (*i.e.* X0HC) and the supernatant from aggressively spun flocs have not correlated with A_{600} . In all of these instances, the turbidity was low, suggesting that these optical properties were changing disproportionately.

2.4.8 Assay Robustness

2.4.8.1 Standard Curve Reproducibility

Understanding the reproducibility of standard curves with respect to time, age of standards, and reagent batch is important for HTPD for multiple reasons. The standards used to generate prescribed standard curves require multiple dilutions and are time-consuming to prepare. Standard curves for most of the qualified assays require up to ten concentrations and it is desirable to run at least one replicate set of standards. Running duplicates of a standard curve on each microplate (as opposed to using a prior standard curve), would use > 20% of the available wells, reducing the number of HTPD samples that could be screened per microplate. Proving adequate stability of standard curves would enable a reliance on historical standard curves, thereby requiring fewer batches of standards to be made, fewer standards per standard curve, and potentially eliminating the need to run replicates of the standard curve on each plate.

Stability must be assessed individually for each assay. With respect to protein assays, protein stability is well-understood, commercial assays are highly reliable, and sterile standard vials are readily

available. Indeed, excellent reproducibility for standard curves was observed with both the BCA and Bradford assays when the same standards were run on multiple days on different microplates.

Conversely, there is a paucity of stability data regarding the storage of dilute DNA standards at 5°C, jeopardizing plans to make a single batch of standards and draw from it over the course of several months. Figure 2.10 depicts a compilation of standard curves run over several months using different combinations of Picogreen reagent batches, DNA standards, and microplates.

Figure 2.10 provides evidence for the reproducibility of standard curves in the Picogreen assay. All standard curves generated with the first batch of reagent had a mean slope of 1.48 RFU mL ng⁻¹ with a RSD of 5.5%. DNA standards diluted in TE buffer were stable for ≥ 1 month when stored at 5°C. Standard curves were comparable except for when the Picogreen reagent batch was changed, in which case a substantial shift was demonstrated. These findings enable a HTPD practitioner to maximize the number of process samples screened on a plate, provided a few wells are left for verification of a previously generated, reagent lot-specific, standard curve.

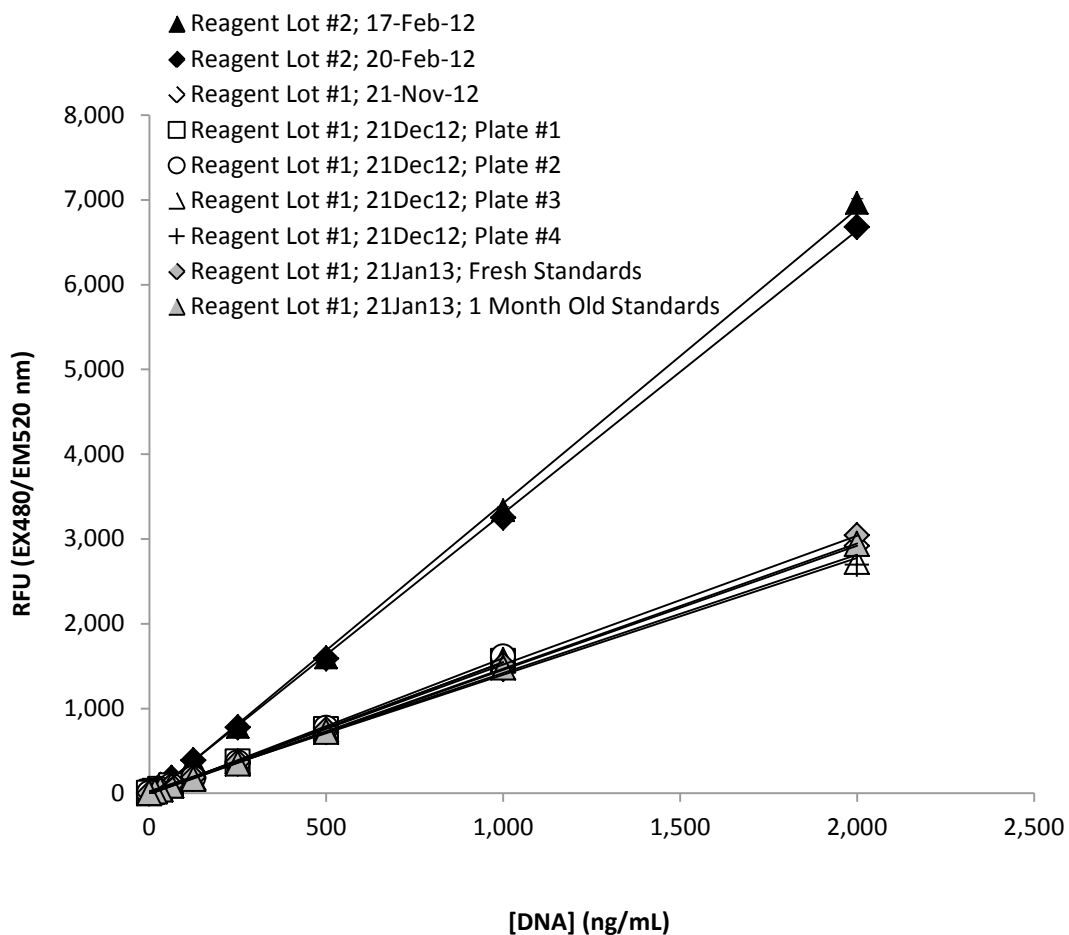


Figure 2.10. Consistency of DNA standard curves in the Picogreen assay across time. White- and gray-filled data points were generated with one lot of Picogreen reagent. Gray-filled points were generated with the same DNA standards. Black-filled points were generated with different lot of Picogreen reagent. Each curve had $R^2 > 0.99$. Standard curves were run in duplicates except for “reagent Lot #2; 17Feb12” which was run in triplicate. The error bars denote the standard deviation.

2.4.8.2 Precision

For any of the described assays, the precision for replicate measurements of a given standard is very high, typically $\leq 5\%$. Generally, excursions from this level of consistency can be attributed to operator variation or error. However, what is most salient is not the precision of well-behaved standards but the reproducibility of measurements produced in a representative system. The contribution of potentially minor sample matrix interferences, multiple sample manipulations,

evaporation, etc. can have detrimental effects on precision. Moreover, the errors associated with the execution of duplicate purification unit operation such as flocculations are expected to exceed greatly the error inherent in the assay measurements alone. To provide a realistic analysis of the robustness of the high throughput analytical suite, 144 flocculations were run in duplicate and assayed with a suite of high throughput assays. The assay RSDs for each duplicate are given in Figure 2.11.

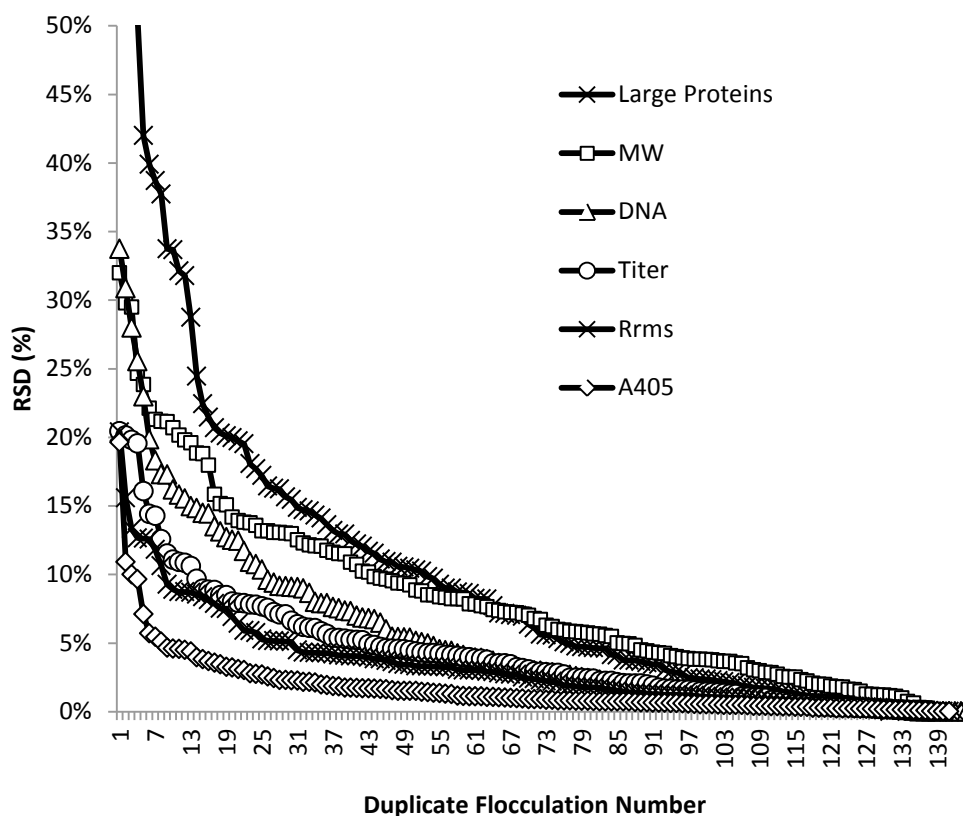


Figure 2.11. RSD for duplicate flocculations assayed with six different techniques. Errors are sorted from highest to lowest. Flocculations were renumbered during generation of this plot, as there was no apparent run order basis for error. Each flocculation condition was carried out in duplicate. Every well used for flocculation was measured once in each assay.

Overall, the combined precision of flocculation, solids removal, handling, and assays was excellent. All duplicates were defined by RSD < 35%. The average RSDs of the assays for “large proteins”, MW, DNA, titre, r_{rms} , and A_{405} were 11, 8, 5, 4, 3, and 2%, respectively. The quantification of “large

proteins” was the least reproducible of the assays listed in Figure 2.11, which is believed to be due to the variability in chromatographic profiles. However, because it is multiplexed with the SEC-MALS assays for product quality and titre, this UV method still offers the convenience of offering relative protein quantification without the need to run an additional protein assay, which can be an attractive trade-off. Excluding the “large proteins” method, MW was the least precise method, with 10 of 138 duplicates characterised by RSD > 20%. This assay incorporates data from two detectors, MALS and RI, which is probably the principal source of the higher error. The better precision afforded by an orthogonal size measurement, r_{rms} , may be due to its utilisation of a single detector type. The enhanced precision of r_{rms} versus MW was consistently observed throughout this thesis. For a suite of assays capable of assessing impurity clearance (DNA: Picogreen), quality (r_{rms} : SEC-MALS), yield (titre: SEC-MALS), and clarity (A_{405}), RSDs \leq 5% can be achieved.

2.4.9 Automation

The capability to automate assays used to inform purification process development is clearly an important attribute. All of the described assays can be integrated into an automated analytical platform, enabling multi-faceted characterisation of product yield and impurity clearance in less than one day by a single scientist. The availability of a fast and automated analytics platform will expand the scope, robustness, and evolution of Design of Experiment (DOE) and Quality by Design (QbD) approaches in vaccine process development.

2.5 Chapter Summary

In the current work, analytical techniques for quantifying polysaccharides, endotoxin, and proteins were qualified. Micro-scale methods for establishing rheological properties and particle characterisation were also evaluated. These methods comprise the core analytical techniques needed to support HTPD. In selecting methods, emphasis was given to procedural simplicity, amenability to automation, robustness, and precision over accuracy. In addition, the qualification process included screening the impact of a diverse library of polysaccharides and the impurities commonly encountered in relevant vaccine streams.

Simple and automatable procedures were described that are compatible with in-process samples from polysaccharide production processes. The Pyrogene™ assay was streamlined from a differential assay to a single measurement while removing a heated incubation step. This modified assay was demonstrated to determine robustly the broad spectrum of endotoxin concentrations present in samples drawn from harvest, clarification, and most polishing unit operations. For protein determination, the BCA assay was shown to be superior to the Bradford assay in terms of sensitivity although the presence of specific interferences may justify the Bradford assay. Using the differential signal from these two protein assays, the amount of reducing sugar present could be quantified, though it was characterised by inferior accuracy and precision relative to other CPS titre assays and will not be pursued further. A Picogreen-based procedure for DNA quantification was proven robust to complex in-process samples and reproducible across time and within the same reagent lot. A system for high throughput particle characterisation was optimized and provides microplate-based analysis. A rapid, micro-scale technique for viscosity measurements was used to characterise a library of polysaccharides and led to potential structure-behaviour insights. The described suite of analytics enables the rapid quantification of key molecular classes in a microplate-based format that is amenable to automation. The deployment of these analytics will enable the development of high throughput processing platforms to speed the development of polysaccharide manufacturing processes.

3 Characterisation and Adaptation of Product

Analytics to HTPD

3.1 Introduction

The increasing requirement for multivalent vaccines containing diverse capsular polysaccharides has created an unmet need for a fast and straightforward assay for polysaccharide titre. In particular, the evolution of HTPD for CPS vaccines has been impeded by the lack of rapid assays for CPS quantitation. Consistent measurement of polysaccharide quantity has proven historically to be a challenging measurement. The challenge in designing streamlined titre assays lies in the intrinsic complexity of CPS.

3.1.1 Carbohydrate Titre Assays

Assays to quantify the concentrations of capsular polysaccharides typically react with a specific subunit of the repeating structure. Hence, each capsular polysaccharide or subset of serotypes tends to have a custom method for polysaccharide quantification

Many different classes of assays have been utilised to measure polysaccharide titre. These include methods based on ELISA, liquid and gas chromatography, fluorescence, infrared spectroscopy, capillary electrophoresis, mass spectrometry and colorimetry (Cruz-Leal et al., 2006; Frasc, 2009; Guo et al., 1998; Kim et al., 2005; Lee and Frasc, 2001; Nunnally and Yao, 2007; Ricci et al., 2001; Stone and Szu, 1988; Trautmann et al., 1991; WHO Expert Committee on Biological Standardization, 2006; WHO Expert Committee on Biological Standardization, 2009; WHO Technical Report Series, No 840, 1994; WHO Technical Report Series, No. 897, 2000; WHO Technical Report, Series No. 924, 2004). Refractive index (RI) has been used in conjunction with HPLC for many years to estimate sugar content. However, chromatography is time-consuming with many procedures requiring thirty minutes or more. Without the added purification and normalization provided by chromatography, RI has proven exceedingly sensitive to chemical, thermal, and hydraulic interference (Cepria and Castillo,

1997; Hanning and Roeraade, 1997; Liu and Dasgupta, 1994). Due to the ubiquity of spectrophotometers and relative simplicity of the measurement, colorimetric assays have remained popular and include assays based on phenol sulphuric acid for hexoses/pentoses, anthrone for hexoses/pentoses, resorcinol for sialic acid, ascorbic acid for phosphates, and purpald for glycols (Chen et al., 1956; DuBois et al., 1956; Lee and Frasch, 2001; Roe, 1955; Svennerholm, 1957). Other methods involving phenol, 1-naphthosulfonate, and aniline phthalate/TCA have been proposed but suffer from toxicity, interference, and limited reactivity with ketoses, respectively (DuBois et al., 1956). In addition, all of the aforementioned methods suffer from a combination of large sample requirements, complex sample preparations and derivatization, highly toxic chemicals, low throughput, insufficiently broad reactivity and substantial interference. Many of these assays involve complex colorimetric procedures but research groups have found alternative approaches for measuring polysaccharide quantity (Laurentin and Edwards, 2003; Lee and Frasch, 2001; Turula et al., 2010).

3.1.2 High Throughput Titre Assays

Several authors have recognized the analytical bottleneck posed by sugar quantitation and devised high throughput methods. Methods based on anthrone have been developed and further scaled-down to microplates (Dreywood, 1946; Laurentin and Edwards, 2003; Turula et al., 2010). This assay's limitations include reagent instability, poor reactivity with pentoses and methylated sugars, interference by process substances such as phenol, and issues with consistency (DuBois et al., 1956; personal communication from Tom Emmons, Pfizer R&D. Refractive index has been used in conjunction with HPLC for many years to estimate sugar content but this method is customized for each CPS serotype and requires lengthy processing times. For a microplate of 96 samples, HPLC-RI would introduce lengthy hold times for samples with unknown stability, as each well may comprise a unique buffer condition. Other methods involving phenol, 1-naphthosulfonate, or aniline phthalate/trichloroacetic acid have been proposed but suffer from toxicity, interference, and limited reactivity with ketoses, respectively (DuBois et al., 1956).

3.1.3 Phenol Sulphuric Acid Assay

The phenol sulphuric acid method (PHS) is a promising assay for integration with high throughput screening. This method is based on a colorimetric product formed from the reaction of phenol, sulphuric acid, and sugar and was first described by Dubois et al. in 1951 (Dubois et al., 1951). This assay is broadly applicable and measures hexoses and pentoses in a variety of oligosaccharides, making it useful for quantifying neutral sugars (DuBois et al., 1956; Saha and Brewer, 1994). The broad carbohydrate specificity of this assay underlies its attractiveness but the measurement may be confounded by the reaction of heterogeneous carbohydrate-containing substances, such as glycoproteins. In one permutation of the original method, the PHS procedure was refined by reversing the sequence of reagent addition to improve sensitivity for glycosylated proteins and uniformity with respect to sugar type (Rao and Pattabiraman, 1989). Saha et al. removed the heating step and reduced volumes to 2.5 mL total per sample (Saha and Brewer, 1994). Subsequent efforts have focused on reducing the volume further and/or improving throughput but have required cumbersome heating and/or specialized pipetting not amenable to automation (Cuesta et al., 2003; Fox and Robyt, 1991; Masuko et al., 2005; Saha and Brewer, 1994). To further optimize and minimize interference, procedures for cleaning up protein interference have been described (Agbenorhevi and Kontogiorgos, 2010; Xi et al., 2010). However, none of the described methods minimizes sample utilisation or is microplate-based, while concurrently simplifying the heating procedures sufficient for transfer to a liquid-handling robot for automation.

3.1.4 Cationic Surfactants and Phase Separation

The cationic detergent, hexadecyltrimethylammonium bromide (Hb) has been used in multiple applications. For purification, Hb has been shown to improve glycoprotein resolution in gel electrophoresis and to facilitate DNA precipitation (Buxbaum, 2003). Hb has also been cited extensively as a precipitation agent for the purification of CPS (Anderson and Smith, 1977; Costantino, 2002; Costantino, 2006; Gotschlich et al., 1969b; Tanizaki et al., 1996). However, to the best of our knowledge, the interaction of Hb with anionic polysaccharides has never been exploited analytically for quantifying polysaccharide content.

The interactions between Hb and polyelectrolytes have been studied extensively (Bao et al., 2008; Biswas and Chatteraj, 1997; Chakraborty et al., 2006; Fundin et al., 1997; Hansson and Almgren, 1996; Konop and Colby, 1999; Li et al., 2007; Maulik et al., 1995). The binding of Hb to polyanions is an entropically driven process, principally mediated by electrostatic interactions via charge effect neutralization (Chakraborty et al., 2006; Fundin et al., 1997; Maulik et al., 1995). Procedurally, as the Hb concentration is increased past the critical micelle concentration (CMC) and approaches saturation, the free charge on the polyanionic CPS is neutralized. This change initiates precipitation, which continues until large particles are formed that are capable of obscuring visible light (Li et al., 2007). Hydrophobic interactions between the surfactant tail and uncharged regions of the polymer can also be significant, particularly at pH < 3 but are usually secondary to charge-charge interactions (Bao et al., 2008; Chakraborty et al., 2006; Wang et al., 1991; Yang et al., 2009; Zubay and Strominger, 1988).

3.1.5 SEC-MALS

HPLC coupled with RI and multi-angle light scattering (HPLC-MALS) has been routinely used to measure CPS titre with size exclusion chromatography (SEC-MALS) (Dambra et al., 1997; Helting and Kumpe, 1978; Komorowska-Rycerz et al., 1966; McCauley et al., 1981). In addition, CPS quality has been informed by SEC-MALS-derived biophysical parameters such as molecular weight (MW) and root mean square radius (r_{rms}), which is the mass-centred radius, often referred to as the radius of gyration (Dambra et al., 1997; Dambra et al., 2000; Jumel et al., 2002). While insight into molecular conformation can be gleaned from SEC-MALS, there does not appear to be any instances where this property has been reported.

Ultra high pressure liquid chromatography (UPLC) was introduced ten years ago. Since that time, many applications have taken advantage of its exquisite resolution, particularly with the reversed phase mode. UPLC-SEC applications for CPS have not been published, presumably due to the limited selection of UPLC columns available and the accompanying small pore sizes designed for recombinant protein applications. The issue has a mechanical basis as the UPLC bead sizes are 1.7 μm and HPLC-SEC columns for CPS typically have pore sizes up to 0.1 μm . Designing such a porous sorbent would

leave scant material available to provide the mechanical support to withstand the 103,421 kPa pressure maximum of UPLC.

3.2 Aim and Objectives

The aim of this chapter is to describe the development and performance of several high throughput assays for polysaccharide titre. Emphasis was given to developing methods that were simple, rapid, versatile, and would accommodate many different feedstreams to facilitate integration into a platform purification process. The specific procedures are:

1. Phenol sulphuric assay: A colorimetric assay with nearly universal reactivity but requires handling of highly toxic reagent.
2. Hb phase separation assay: The binding of Hb to anionic CPS results in a precipitation reaction wherein the suspension turbidity is proportional to polysaccharide titre. This assay offers the fastest plate-based analysis but is limited to anionic CPS and can have complex interference patterns.
3. UPLC-SEC-MALS: This method consists of refractive index following size exclusion chromatography using an ultra high pressure chromatographic system and column. Integrating static light scattering in the analysis offers product quality measurements such as MW, r_{rms} , and conformation and will be referred to as UPLC-SEC-MALS.

Accuracy, precision, robustness, sample matrix interference, sample conditioning, and modularity will be evaluated using CPS derived from a variety of bacterial species and where stated, with representative levels of process contaminants. Additional assay-specific evaluations of robustness will be evaluated as appropriate. This body of work relies on the evaluation of a combination of commercially available and clinically relevant polysaccharides to ensure maximum versatility and reactivity of the final assay suite.

3.3 Materials and Methods

The identity of polysaccharides were redacted in Figures 3.9 and 3.11-3.14.

3.3.1 Materials

All common chemicals were commercial analytical grade. Albumin from bovine serum (BSA), L-arabinose, glycogen from oyster, chondroitin sulphate A sodium salt from bovine trachea, α -lactose monohydrate, glucose, N-acetyl neuraminic acid from *E. coli*, Type II ι -carrageenan, 3-(N-morpholino)propanesulfonic acid (MOPS), and dextran were obtained from Sigma (United Kingdom). Deoxyribonucleic acid (DNA) sodium salt from salmon sperm was purchased from Fisher Bioreagents (United Kingdom) and Fisher Scientific (Pittsburgh, PA). Sodium alginate from *L. hyperborea* came from BDH (United Kingdom). Lonza Walkersville (Maryland, USA) provided endotoxin derived from *E. coli*. Gellan gum was produced by Applichem Biochemica (United Kingdom). High molecular weight hyaluronan (HA) was purchased from R&D Systems (United Kingdom). Endotoxin standards and stocks were purchased from Lonza Walkersville (Maryland, USA). All reagents were used as purchased. All sugars are D isomers except where noted otherwise. Hexadecyltrimethylammonium bromide, sodium azide, bovine serum albumin, and protease from *S. griseus* were purchased from Sigma (St. Louis, Missouri). Amresco (Solon, OH) provided DNase I (ultra pure grade), trypsin (USP grade), and proteinase K (biotechnology grade) enzymes. Merck KGaA (Darmstadt, Germany) supplied Benzonase. 0.22 μ m polyethersulfone or cellulose acetate filters were used interchangeably to sterile filter buffer solutions (Millipore, Billerica, MA). Biological solutions (enzymes, proteins, DNA) were not filtered. 96-well, desalting microplates (G-25, 500 μ L) were purchased from GE Healthcare (Uppsala, Sweden). Costar 3635 acrylic microplates from Corning were used (Corning, NY) for all UV measurements. All spectroscopic measurements were made with a Safire II spectrophotometer (Tecan, Switzerland), except where noted. Standard abbreviations for L-arabinose (Ara), ribose (Rib), glucose (Glc), galactose (Gal), glucuronic acid (GlcA), guluronic acid (GulA), N-acetyl neuraminic acid (NANA), mannose (Man) were selectively used to reduce graphical clutter.

Capsular polysaccharides from various serotypes of *S. pneumoniae*, *S. aureus*, and *N. meningitidis* were kindly provided by Pfizer R&D. All sugars have D and α structural configuration. CPS were sterile filtered as part of their respective manufacturing process but were not filtered after receipt from manufacturing. The titres of stock solutions of *S. pneumoniae* and *S. aureus* CPS were derived from SOP-based serotype-specific SEC-RI assays of process intermediate and purified drug substance stock obtained from Pfizer manufacturing. For *N. meningitidis* CPS, the titres of stock solutions were derived from a SOP-based colorimetric assay employing the reaction of 4-(dimethylamino) benzaldehyde with N-acetyl neuraminic acid under acidic conditions. For all serotypes, dilutions were performed with 25 mM sodium phosphate, pH 7.2.

3.3.2 Modified Phenol Sulphuric Acid Assay

The procedures described by (DuBois et al., 1956; Masuko et al., 2005; Saha and Brewer, 1994) were used as reference points to develop a modified PHS assay. The methods of Saha *et al.* formed the basis for the advent of a modified method as described in Table 3.1.

Table 3.1. Comparison of PHS methods. The ‘proposed’ method is described in more detail in the accompanying text. ‘RT’ refers to room temperature, 18-25°C operation.

Source	Dubois et al.	Saha et al.	Masuko et al.	Proposed
Year	1956	1994	2005	2012
Volume (μL)	7050	3500	230	175
[Sugar] ($\mu\text{g/mL}$)	5-35	10-100	4-585	10-1000
Method	Add 50 μL 80% phenol to 2 mL sugar	Add 0.5 mL 5% phenol to 0.5 mL sugar	Add 150 μL H_2SO_4 to 50 μL sugar	Add 25 μL 5% phenol to 25 μL sugar
	Add 5 mL H_2SO_4	Add 2.5 mL H_2SO_4	Add 30 μL 5% phenol	Add 125 μL H_2SO_4
	Incubate 10 min	Vortex	Incubate 5 min in 90°C water bath	Incubate for 30 min at RT
	Shake	Incubate 30 min at RT	Cool to RT for 5min in RT water bath	Read UV
	Cool in 25-30°C water bath	Read UV	Wipe microplate dry	
	Read UV		Read UV	

In the modified method, 25 μL of 5% (m/v) phenol was added to 25 μL of sugar solution previously aliquoted into the microplate, followed by mixing with a pipettor. Next, 125 μL of H_2SO_4 was added to each well, followed by rapid mixing with a pipettor. Solutions were incubated for 30 minutes at

room temperature (18-25°C) before the absorbance was read at 485 nm in the microplate reader. Where applicable, samples were diluted in reverse osmosis-purified, distilled water. Except for the comparative study performed with glucose as a test sample, all PHS measurements were made with the modified method. All mixing was performed via five aspiration cycles with a pipettor. Standard curves were run in triplicate with absorbance values corrected for the blank. The final yellow colour was found to be stable for 1 hour, although slight development occurred with prolonged incubation following the reaction. Phenol solution was stored in the dark when not in use.

In certain circumstances with the modified PHS assay, a glass microplate (Zinsser, Germany) was evaluated.

3.3.3 Phase Separation Assay

100 µL of desalted (except where noted) capsular polysaccharide sample was dispensed into each well of a 96-well acrylic microplate. Hb to achieve 100 mM was dissolved in 25 mM sodium phosphate, pH 7.2 at 37°C before 100 µL of 100 mM Hb was dispensed into each well. Five cycles of slow pipettor aspiration/dispensing were executed immediately upon addition of Hb reagent to effect the requisite mixing. Care was taken to ensure that no air was evacuated from the tip or expelled into any microwell. Following 15 minutes of incubation at room temperature, absorbance values were read at 320 nm using a spectrophotometric plate reader (Molecular Devices, Spectramax M3) with well height compensation disabled. Permutations on the aforementioned standard method are described in the 3.4.2.

3.3.3.1 Desalting

Desalting plates were equilibrated with 25 mM sodium phosphate, pH 7.2 according to the manufacturer's instructions. 130 µL of sample was added to the centre of the top of each bed in the desalting microplate. Centrifugation at 700g relative centrifugal force (RCF) for 2 minutes was sufficient to elute the conditioned sample.

3.3.3.2 Enzymatic Treatments

Proteinase K, trypsin, and *S. griseus* proteases were dissolved in separate 1 mL aliquots of 25 mM sodium phosphate, pH 7.2 to achieve an activity of 200 units/mL for each protease. DNase I and Benzonase were separately formulated in 25 mM MgCl₂, 5 mM CaCl₂, 25 mM sodium phosphate, pH 7.2 to a concentration of 3000 Kunitz activity units., where a Kunitz unit is the amount of DNase required to increase A₂₆₀ by 0.001 AU min⁻¹ mL⁻¹ at 25°C at pH 5.0. An aliquot of 10% (v/v) of the appropriate enzyme solution was added to each sample. Treated samples were then incubated for 1 h at 37°C prior to the execution of the standard assay method. In parallel with treated samples, negative controls were incubated with the respective enzyme-free sample buffer.

3.3.4 SEC-MALS

SEC-MALS with RI detection is routinely used for the quantification of diverse polysaccharides. Titre can be calculated from an integration of the RI signal. MW is calculated from the RI and MALS signals. The mass centred radius of gyration, r_{rms} , is derived from the angular dependency of the MALS signals. Both MW and r_{rms} are descriptors of the CPS size and are representations of quality.

3.3.4.1 HPLC-SEC-MALS

HPLC-SEC-MALS was used to measure CPS titre and quality. A high pressure liquid chromatography system (2795 Alliance; Waters, Milford, MA) was employed. MALS (DAWN HELEOS II) and RI (Optilab T-rEX) equipment were provided by Wyatt (Santa Barbara, CA). Several combinations of columns and buffers were screened as shown in Table 3.2.

Table 3.2. Column and chromatographic properties for SEC-MALS screening. Injection volume was 50 μ L (10 μ L for UPLC), temperature was 25°C and mobile phases were: PBS= phosphate buffered saline, pH 7.2, Ace = 294 mM HAc, 1 mM EDTA, pH 6.7, Zwit = PBS, 0.75% Zwitterion 3-10, pH 7.2. An additional 200 ppm sodium azide served as a bacteriostat.

Column	Mfg	Bead Size	Pore Size	Support	Buffer	Flow Rate	Run Time	Reference
GMPWxL	Tosoh	13 μ m	10-100 nm	methacrylate	Zwit	0.5 mL/min	31 min	GMP-Zwit
GMPWxL	Tosoh	13 μ m	10-100 nm	methacrylate	PBS	0.5 mL/min	31 min	GMP-PBS
TSKgel G4000SWxl	Tosoh	8 μ m	45 nm	silica	PBS	0.5 mL/min	27 min	4000sw-PBS
TSKgel G4000SWxl	Tosoh	8 μ m	45 nm	silica	Ace	0.5 mL/min	27 min	4000sw-Ace
SynChroPak GPC 1000, 100	Eprogen	7, 5 μ m	100, 10 nm	silica with glycerol propyl bonded phase	Ace	0.5 mL/min	17 min	Syn-Ace
BEH200 SEC	Waters	1.7 μ m	<20 nm	bridged ethylene hybrid	Ace	0.4, 0.2 mL/min	8 min	UPLC-Ace

3.3.4.2 UPLC-SEC-MALS

UPLC-SEC-MALS, was used to measure CPS titre and quality. An ultra high pressure liquid chromatography system (UPLC Acquity; Waters, Milford, MA) was employed. MALS and RI detectors were identical to those used for HPLC-SEC-MALS. Following screening and development work, the final mobile phase employed for standard curve generation was 0.15 M NaCl, 0.1 M NaH₂PO₄, 0.1 mM EDTA, 200 ppm sodium azide, pH 6.2 \pm 0.1.

3.4 Results and Discussion

3.4.1 Modified Phenol Sulphuric Acid Assay

Several permutations of the original PHS method for sugar quantitation have been described. In order to establish a benchmark and compare the methods to the modified method described here, standard curves were generated with each method, using glucose as the standard carbohydrate (Figure 3.1).

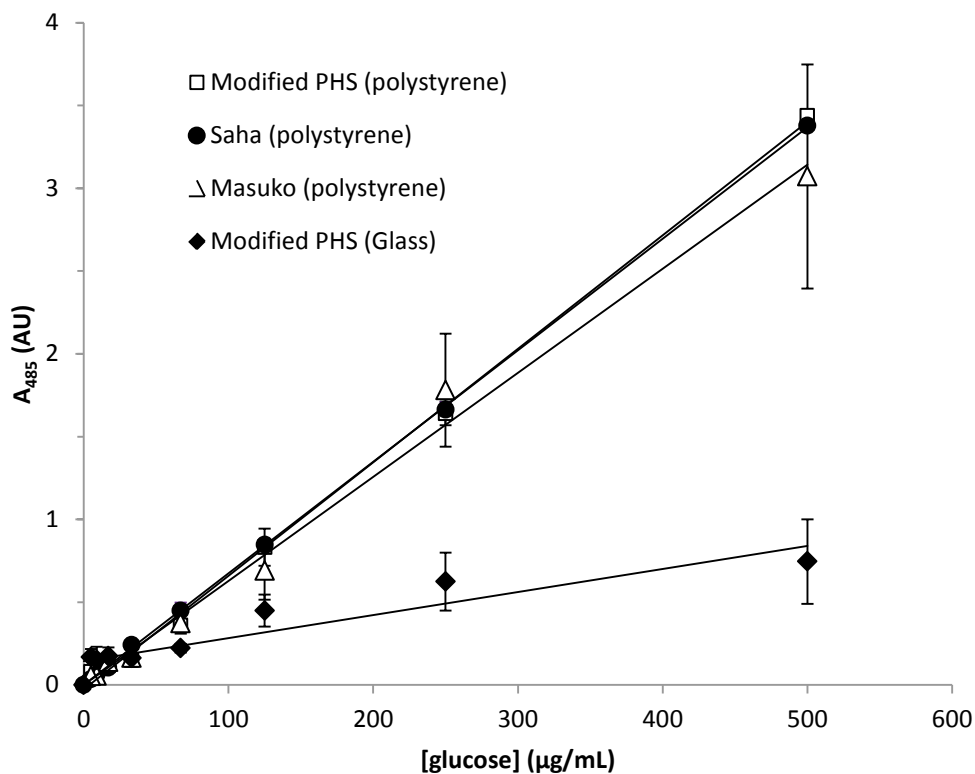


Figure 3.1. Glucose standard curves generated with variants of PHS assay, prepared in triplicate.

“Masuko” refers to method described in Masuko et al., “Saha” refers to method described in Saha et al., “Modified PHS” refers to method as described in Materials and Methods, and material in parentheses refers to the microplate material employed during the reaction (DuBois et al., 1956; Masuko et al., 2005; Saha and Brewer, 1994). The volumes prescribed in the original citations were followed. Standard curves were run in triplicate with the error bars denoting the standard deviation. Absorbance was normalized to 300 µL per well. R^2 for each linear regression fit line was > 0.99 , except for “Modified PHS (Glass)” where $R^2 = 0.87$.

As shown in Figure 3.1, the absorbance intensity attained for each method was very similar, irrespective of the specific PHS method employed. This observation suggests that the extent of reaction in each microwell was comparable. The Masuko method was expected to yield higher absorbance values due to a rearrangement of the reagent addition sequence but these signal

increases were not realized (Masuko et al., 2005). Therefore, it appears that previously observed sulphonated phenol-mediated attenuation was either consistent or insignificant.

The precision of the reported PHS procedures differed significantly. Across the 17-500 $\mu\text{g/mL}$, the mean relative standard deviation (RSD) for the Saha, optimized PHS, and Masuko assay were 6%, 10%, and 22%, respectively. While the Saha method exhibited the best precision, it required the most material (*i.e.* 0.5 mL). The decreased reproducibility of the Masuko method may be due to increased sensitivity to unintended variability in the time lapsed from sulphuric acid addition (*i.e.* the heat generation step) to the addition of phenol. In this work, the order of addition was found to be important, with better precision observed when the heat generation step was the final step, presumably leading to a more uniform reaction temperature.

A consistent reaction was generated by careful consideration of the factors affecting the temperature of reaction. In contrast to the method described here, which used a polystyrene microtitre plate, a reduced signal was observed when the glass microplate was used (Figure 3.1). This attenuated signal was likely due to the higher thermal conductivity and specific heat of borosilicate glass as well as the greater volume of material contained in the glass microplate relative to the polystyrene microplate. These factors presumably prevent the solution from attaining the high temperature required for robust reaction.

The testing with glucose established that the modified PHS assay had satisfactory accuracy and precision. This method was comparable to the method of Saha et al. and was characterised by superior precision to the method of Masuko et al (Masuko et al., 2005; Saha and Brewer, 1994). The reproducibility was particularly strong for higher polysaccharide concentrations, which is the region in which most samples derived from typical purification HTPD will likely reside. The greater simplicity, speed, and ease of automation afforded by the elimination of the discrete heating steps warranted further qualification of the modified PHS method.

A diverse library of mono-, di-, and poly-saccharides were assayed with the modified PHS assay. The carbohydrates tested included glucose, α -lactose monohydrate, L-arabinose, maltose, hyaluronic acid, chondroitin sulphate, sodium alginate, gellan gum, dextran, ι -carrageenan, glycogen, DNA, endotoxin,

and N-acetyl neuraminic acid. Initially, absorbance scans of the reacted sample were made to identify the wavelength at which maximum absorbance (λ_{\max}) was measured. As displayed in Table 3.3, the λ_{\max} fell in the range 477-487 nm which corroborates with the range of 480-490 nm published for more limited subsets of carbohydrates (DuBois et al., 1956; Masuko et al., 2005; Saha and Brewer, 1994).

Table 3.3. Absorbance maxima for carbohydrates and other molecules commonly found in in-process pools of CPS production processes

Composition	λ Maximum (nm)
glucose	487
α -lactose monohydrate	486
dextran	487
maltose	490
glycogen from oyster	485
I-carrageenan	487
L-arabinose	476
gellan gum	485
DNA (salmon sperm)	477
sodium alginate	480
chondroitin sulfate	482
hyaluronic acid	482
endotoxin	483
N-acetyl neuraminic acid	482
lysozyme	482
BSA	482
BSA (Ecol2) 5 g/L + 1.0 g/L DNA	478
BSA (Ecol2) 5 g/L + 2 g/L glucose	488
blank (MOPS)	482
AVERAGE	483

For hexose sugars (n=11), the mean λ_{\max} = 485 nm \pm 3 nm and for pentose sugars (n=2), the mean λ_{\max} = 477 nm \pm 1 nm. From this dataset, a fixed value of 485 nm was determined to provide robust measurement of diverse polysaccharides in the modified PHS assay.

Using a wavelength of 485 nm, standard curves were generated for the library of polysaccharides (Figure 3.2).

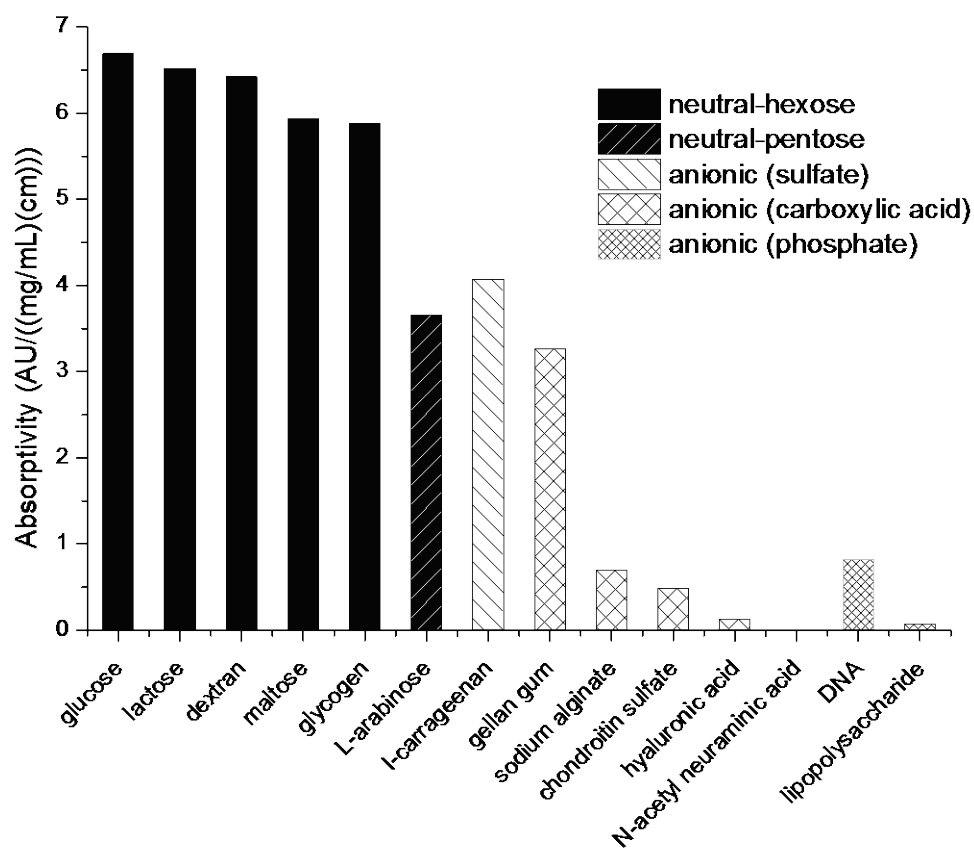


Figure 3.2. Slopes of standard curves for neutral and anionic hexoses and pentoses in the modified PHS assay. The standard curves for the carbohydrate library were linear with $R^2 > 0.95$ for each species tested. The legend describes the repeating monosaccharide for neutral sugars and the charged group for anionic sugars.

In the modified PHS assay, hexoses absorb more strongly than pentoses at 485 nm. This order is maintained even if the λ_{\max} for pentoses is used for the absorbance measurement (data not shown). The anionic polysaccharides absorb far less per unit mass than do the neutral carbohydrates. In large part, this is due to the presence of non-signalling anions such as sulphate.

It has been previously shown that for complex oligosaccharides containing different hexoses, the summed contribution of the reactive hexoses equates to the approximate reactivity of the

polysaccharide (Saha and Brewer, 1994). Moreover, as N-acetyl galactosamine, N-acetyl glucosamine, and N-acetyl neuraminic acid have been demonstrated to insignificantly react in the PHS assay (data not shown), the contributions of certain structures can be discounted if other reactive pentoses and hexoses are present (Masuko et al., 2005). Similarly, the organic and inorganic anion groups do not signal and can be disregarded. After applying these data transformations to oligosaccharides comprised of similar repeating sugar components, the absorbance response converges on a single line as a function of the concentration of particular reactive monosaccharide (Figure 3.3).

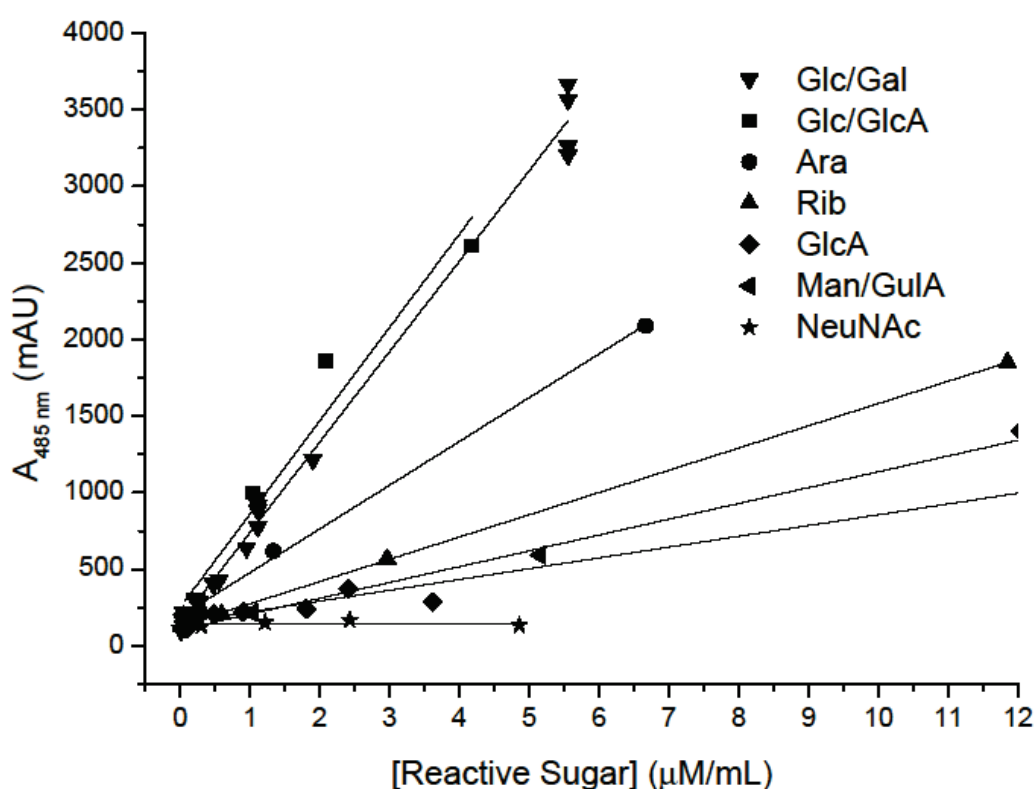


Figure 3.3. Reaction of carbohydrates listed in Figure 3.2, plotted as a function of common reactive sugars. Unreactive structural components were ignored. $R^2 > 0.95$ for each fit line. Carbohydrates with glucose and galactose were co-plotted as the relative reactivity of these hexoses was found to be statistically similar when plotted independently (data not shown).

The data in Figure 3.3 can be used to approximate the expected reactivity of diverse carbohydrates based on their underlying molecular structures. Of the carbohydrate classes tested, the hexoses produced the highest absorptivity in the modified PHS assay. The absorbance of

heteropolysaccharides can be approximated by the addition of the reactive components. However, it was noted that addition was imperfect when heteropolysaccharides composed of both glucuronic acid and glucose were summed, as the polysaccharide containing both units reacted slightly less than the sum of the independently generated glucose and glucuronic acid curves.

To facilitate appropriate comparisons, the molar absorptivity of the reactive units are displayed in Table 3.4

Table 3.4. Molar absorptivity of reactive sugars in proposed PHS assay. N-acetyl neuraminic acid is representative of a non-reactive carbohydrate.

Sugar	Molar Absorptivity (AU((μmol/mL)(cm)))
Glc and Gal	1.135
Glc/GlcA	1.171
Ara	0.550
Rib	0.279
GlcA	0.198
ManA/GulA	0.135
NANA	0.002

The absorptivity values in the modified PHS method are consistent with those described in the original PHS papers by DuBois et al. (DuBois et al., 1956). The range of absorptivity gives rise to the dynamic linear ranges depicted in Figure 3.4. Having an elevated lower limit of quantification (LOQ) is advantageous when monitoring the array of concentrations across a microplate where the titre of the load material may be 0.5-5 mg/mL. The loss of low-end sensitivity (*i.e.* < 10 mg/L) is acceptable as detecting such minute concentrations is not practically relevant, particularly in purification HTPD, where concentration changes greater than 100-fold are rarely encountered.

Polysaccharide titre measurements will be required for impure samples possessing a complex background. DNA, protein, and endotoxin are impurities present in virtually all in-process samples. Therefore, a key element of the robustness of the any in-process sugar assay is the propensity of

typical impurities to interfere. The interference generated by a panel of typical impurities is quantified in Figure 3.5.

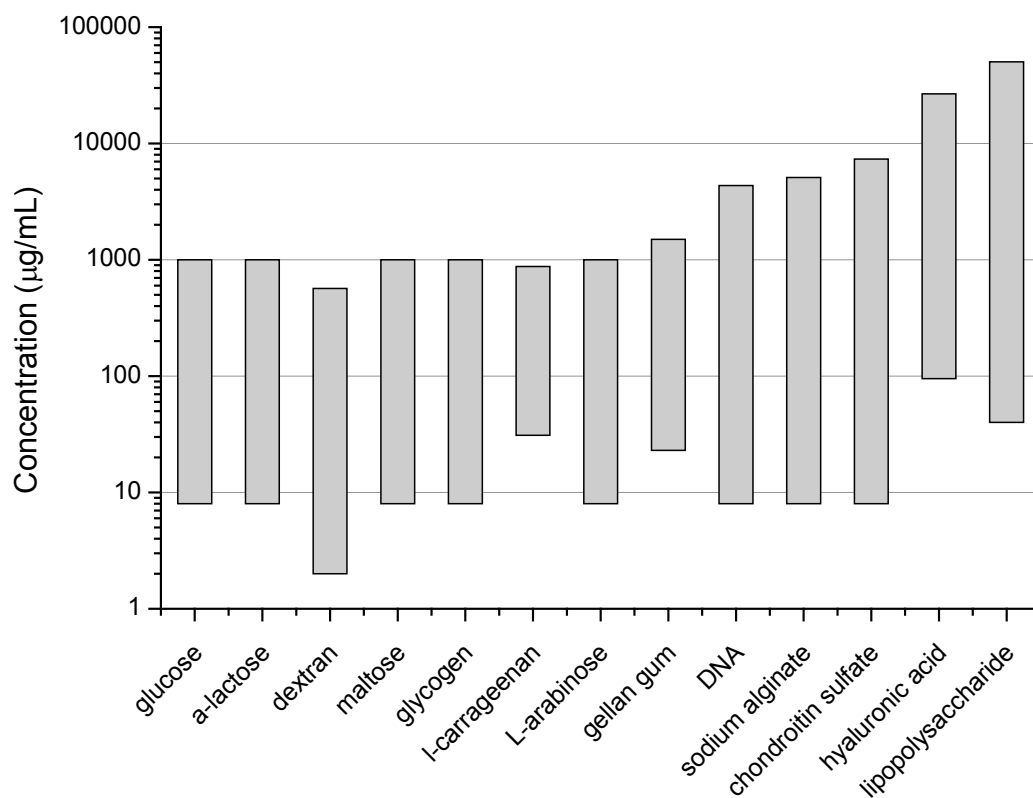


Figure 3.4. Dynamic linear range for concentration measurements in modified PHS assay. All $R^2 > 0.95$ when fit with linear regression. Range is linear up to $A_{485} = 2.0$ AU.

Interference in the modified PHS assay was minor. As the assay is colorimetric and designed for in-process samples, a shift in measurements of $\geq 20\%$ was deemed to represent significant interference. Every sample in Figure 3.5 reacted more weakly than glucose. Although proteins did not react strongly, the test proteins were not glycosylated. Therefore, based on the reactivity of the constituent glycan, an estimate was made of the interference posed by a glycosylated 20 kDa protein possessing one trisaccharide glycan per protein molecule. The interference calculated for this composition was slight due to the low molarity of the pendant oligosaccharide. Based on Figure 3.5,

only far upstream in the purification process would samples be likely to contain concentrations of interfering species (*i.e.* simple sugars from broth/media, DNA) high enough relative to the target carbohydrate concentration to cause problematic interference. In such a case, a high throughput desalting step using a microtitre plate could be utilised to reduce interference

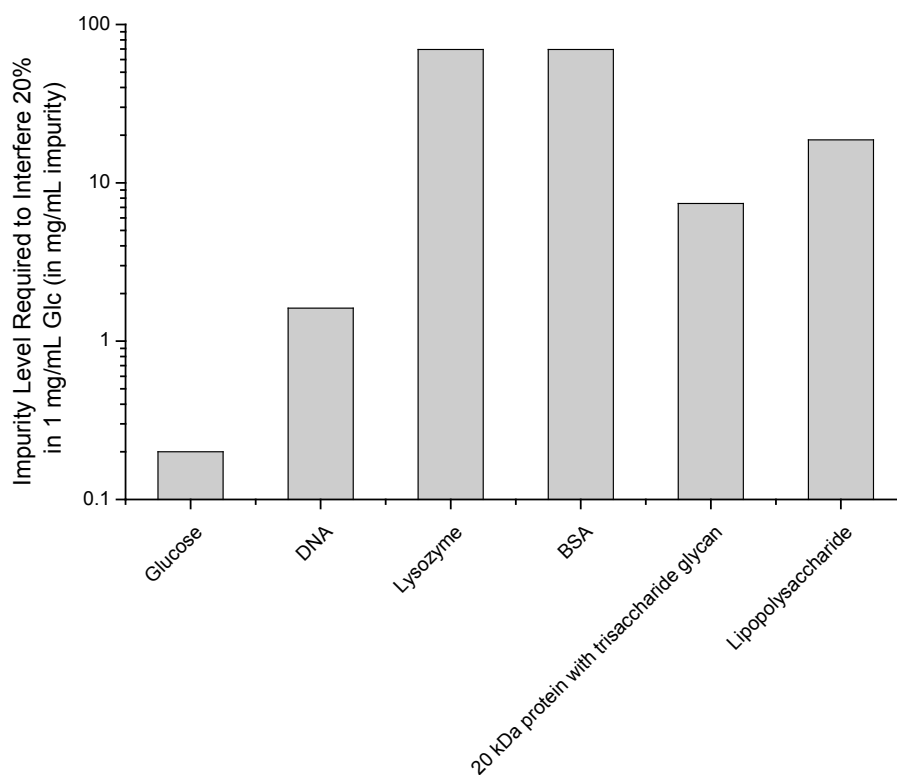


Figure 3.5. Concentration of interfering species required to effect 20% shift in the PHS assay response. All molecules enhanced assay response. Y-axis values assume the desired analyte is 1 mg/mL glucose. The lower LOQ for the slope is 0.01 AU/(mg/mL), equating to 69.6 mg/mL impurity on the y-axis. The hypothetical tri-hexose glycan, Glc-Glc-Glc, represented the worst-case interference.

3.4.2 Phase Separation Assay

Two anionic serogroups from *N. meningitidis* were used to define the operating parameters for the phase separation assay. Serogroup C (Mn C) is comprised of a repeating unit of (2,9)N-acetylneuraminic acid with two sites possessing nearly 100% O-acetylation (Lemerclinier and Jones, 1996). Serogroup Y (Mn Y) consists of repeating units of (4)N-acetylneuraminic acid (2→6)-glucose-(1→ with two sites possessing O-acetylation occupancy of approximately 50% (Lemerclinier and Jones, 1996). Due to the neuraminic acid, each CPS has one anion (*i.e.* carboxylic acid) per repeating unit.

Standard curves with the Hb phase separation assay were generated for Mn C and Mn Y. (Appendix 9.5: Phase Separation Assay). The assay provided a dynamic range of approximately 2 logs, spanning the 0.016-1.28 mg/mL range. Across this working range of Mn C, a linear regression analysis of the logarithmically transformed data yielded a R^2 of 0.99 and a mean RSD of 2.6%. For Mn Y, $R^2 = 0.96$ with a mean RSD of 3.6%. Mn Y exhibited a lower reactivity than the Mn C, resulting in a reduced sensitivity for dilute sample but a potentially increased upper limit LOQ. The reduced charge density of Mn Y is thought to underpin the contrasting reactivity with Mn C.

3.4.2.1 Robustness

3.4.2.1.1 Operational Parameters

The absorbance at wavelengths of 320 nm (A_{320}), 405 nm (A_{405}), and 600 nm (A_{600}) was examined. A similar mean precision was observed for each wavelength but the sensitivity was inversely proportional to wavelength. In order to achieve improved accuracy at a low LOQ, A_{320} was selected for the standard procedure. For circumstances where an elevated upper LOQ is desired or where background substances interfere, longer wavelengths can be utilised.

A total reaction volume of 200 μ L was selected to ensure that the CPS concentrations measured at the upper LOQ (*i.e.* 2 AU) were close to the expected concentrations present in process samples. The total reaction volume per well can be increased to 300 μ L to increase the sensitivity or reduced using half area microplates to conserve sample. The number of aspiration cycles employed to mix the

samples was found to have a minor effect on precision, with 5 cycles found to be more precise than 8 cycles, particularly for more concentrated samples.

The addition of the Hb reagent to a solution containing Mn C initiated a dynamic precipitation reaction that matured over a 16 hour interval. While the extent of reaction for most samples was nearly complete in the first few seconds following addition, low starting concentrations of CPS kinetically limited the reaction. Therefore, the result of immediate measurement was inferior sensitivity and greater imprecision. To address this issue, a minimum precipitation development time of 15 minutes is recommended. After 15 minutes and before approximately two hours, very precise and accurate titre measurements can be made spectrometrically ($RSD \leq 5\%$). If the precipitate is allowed to continue to mature, the smaller particulates gradually flocculate with other particulates and settle to the bottom of the microwell. The result is attenuated light scattering, leading to a reduced signal range and inferior precision ($RSD \leq 10\%$). Resuspension of precipitate through orbital mixing of the microplate did not recover the signal range or precision.

3.4.2.1.2 Reagent Concentration

The method is insensitive to the concentration of the Hb reagent across the 20-80 mM range (Figure 3.6). From a 100 mM stock solution, 50 mM was specified as the concentration of diluted Hb in the final assay mixture. The target concentration of Hb is well above its CMC and ensures a significant molar excess of surfactant when incubated with typical polysaccharide process concentrations. These attributes decrease the risk that inaccurate reagent formulation or CPS mass variability will significantly skew the titre results.

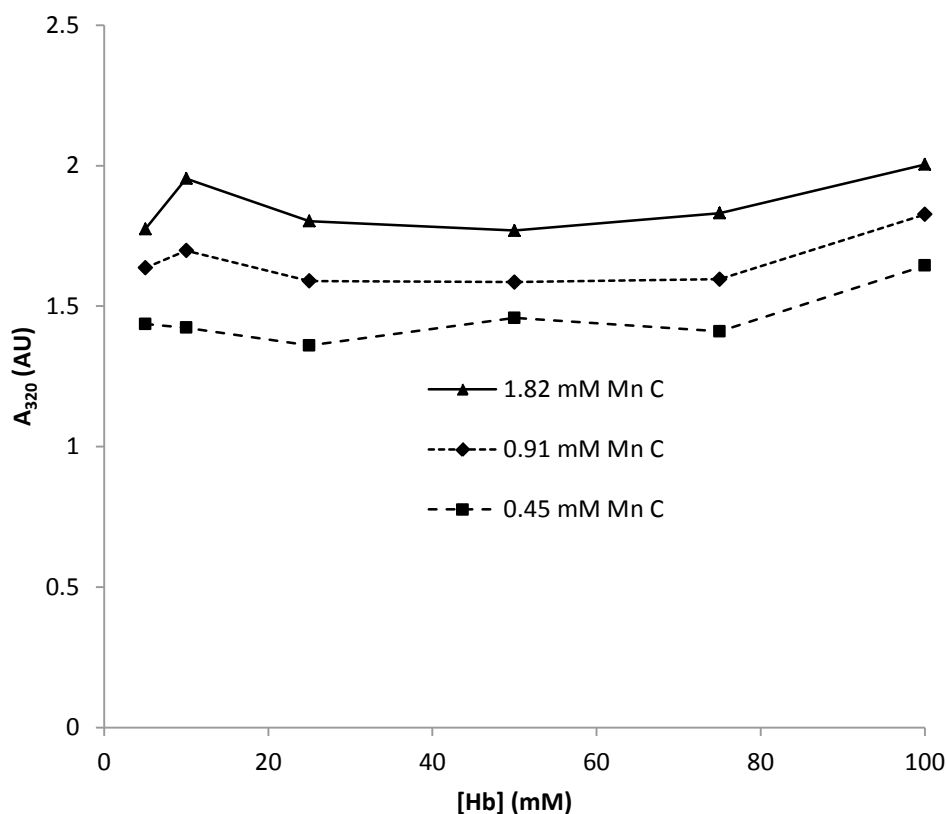


Figure 3.6. Effect of Hb reagent concentration on turbidity of Mn C samples prepared in 25 mM sodium phosphate, pH 7.2 or RODI. The legend data corresponds to 0.64, 0.32, and 0.16 mg/mL. A 20-fold range of Hb:CPS ratios was examined. Each point was assayed in quadruplicate.

3.4.2.1.3 Physicochemical Effects

The principal interaction between the Hb and the CPS relies on charge-charge interactions.

Accordingly, the effect of ionic strength ([I]) on the precipitation reaction was assessed (*i.e.* without batch-desalting) and found to attenuate Mn C and Mn Y reactivity when $[I] \geq 200$ mM, with NaCl as the salt. When batch-desalted with the prescribed gel filtration microplate, the impact of [I] on precipitation was eliminated across a range of 10-400 mM NaCl (Appendix 9.5: Phase Separation Assay). The meningococcal CPS recovery across the G-25 microplate was greater than 95% with Mn C or Mn Y.

An ancillary benefit of the desalting step is broad robustness with respect to sample pH and buffer system. Buffers including formate, imidazole, HEPES, tris, acetate, MES, and phosphate were

evaluated with buffer concentrations ranging from 25-100 mM and pH from 3.0-8.75. No significant interference was noted for any of these buffer systems or pH ranges, demonstrating the chemical compatibility of the phase separation assay.

3.4.2.2 Reactivity with Bacterial Species

A key assay property is the capacity to react modularly with anionic capsular polysaccharides.

Standard curves for CPS from serogroups of *S. pneumoniae* were generated (Figure 3.7).

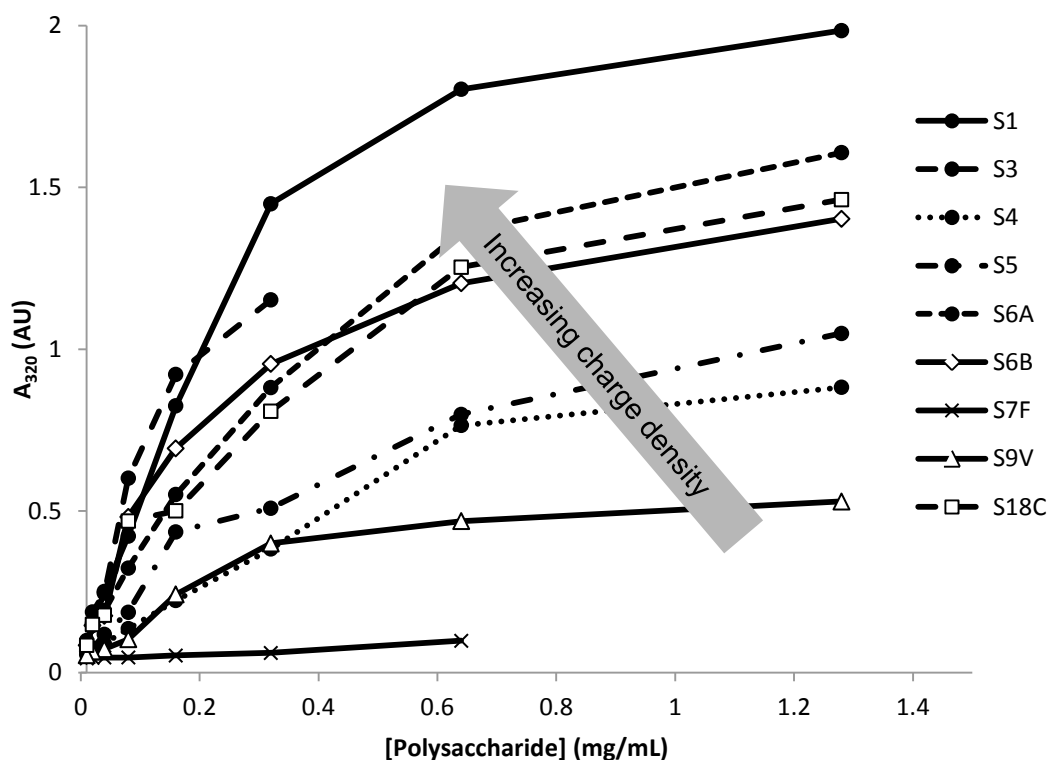


Figure 3.7. Reactivity of bacterial CPS from *S. pneumoniae* in the precipitation assay, with serotype identified in the legend. Purified CPS was serially diluted in 25 mM sodium phosphate, pH 7.2. Each line represents a distinct anionic CPS, except for serotype 7F, which is neutral. The pneumococcal polysaccharides are comprised of linear repeating units except for serotypes 5, 7F, and 18C, which are branched.

The repeating units were linear or branched and contained from 2-7 monosaccharides (Jones, 2005a). The anionic pneumococcal serotypes possessed either sialic acids or phosphates in their side chain or backbone. Each anionic serotype reacted monotonically in the assay. Linear regression analyses with each serotype were characterised by $R^2 > 0.94$, indicating precipitation that was consistently proportional to CPS titre.

Due to the variety of CPS structures, extensive efforts were made to correlate the signal intensity with myriad structural or chemical properties of the CPS (Figure 3.7). The only statistically significant ($p < 0.1$ level) correlation (positive) with turbidity existed for the charge density of sugar. This finding is corroborated by research showing the higher charge density increases the cooperativity of binding between Hb and polyanions (Hansson and Almgren, 1996). High charge density may mitigate the impact of [I], with polyanions of increased charge density binding to Hb with greater resiliency to elevated [I]. Indeed, a lessened dependency to elevated [I] was observed for Mn C relative to Mn Y, which has a lower charge density (data not shown). A single neutral CPS was included in the reactivity study and exhibited negligible reaction with Hb, except for a slight tendency to precipitate at higher concentrations (Figure 3.7), possibly through hydrophobic interactions with the aliphatic tail domain of Hb (Lundqvist et al., 2002).

3.4.2.3 Interference from Impurities

The most prevalent non-CPS polyanions in bacterial processes are nucleic acids. DNA is frequently released by dying cells, through cell lysis during clarification operations following CPS extractions, and in some cases, by intentional cell lysis to liberate CPS (Ball et al., 1987; Food and Drug Administration United States, 2010b; Frasc, 1990; Tanizaki et al., 1996). DNA titres can be above 1 mg/mL in samples taken from downstream processes (personal communication from Dr. Bernie Violand and Dr. Khurram Sunasara, Pfizer R&D). In isolation, as little as 0.02 mg/mL DNA was found to signal in the assay (data not shown). In the presence of Mn C (> 0.1 mg/mL), > 0.2 mg/mL DNA was required for interference, suggesting a competitive effect. Because of the high levels of DNA in the downstream process and the propensity of polyanions to interfere, enzymatic digestions were explored to mitigate DNA-related interference.

Deoxyribonuclease I (DNase I) and Benzonase are Mg^{2+} -dependent endonucleases that cleave single and double stranded DNA into small oligonucleotides (Ball et al., 1987; Yang, 2011). We hypothesized that by adding endonucleases to a CPS sample at the outset of the assay, the DNA would be cleaved into small fragments. The small fragments could then be removed with the batch-desalting step.

Figure 3.8 illustrates the efficacy of enzymatic sample conditioning in eliminating nucleic acid interference in the phase separation assay. Both DNase I and Benzonase were highly effective in eliminating the signal from DNA. The negligible difference between the endonuclease-treated samples and the control proves the utility of this sample conditioning method for removing nucleic acid interference.

Following clarification, proteins can also be present in high concentrations. In spiking studies with the phase separation assay, basic model proteins did not react and acidic proteins (*i.e.* BSA) reacted mildly when concentrations approached 8 g/L, a value exceeding typical process values.

Experimentation analogous to the endonucleases study but designed to facilitate protein clearance was performed with proteases (*i.e.* trypsin, proteinase K, and protease from *S. griseus*). Only proteinase K exhibited effectiveness in reducing interference from acidic proteins (*i.e.* BSA) at very high concentration (data not shown).

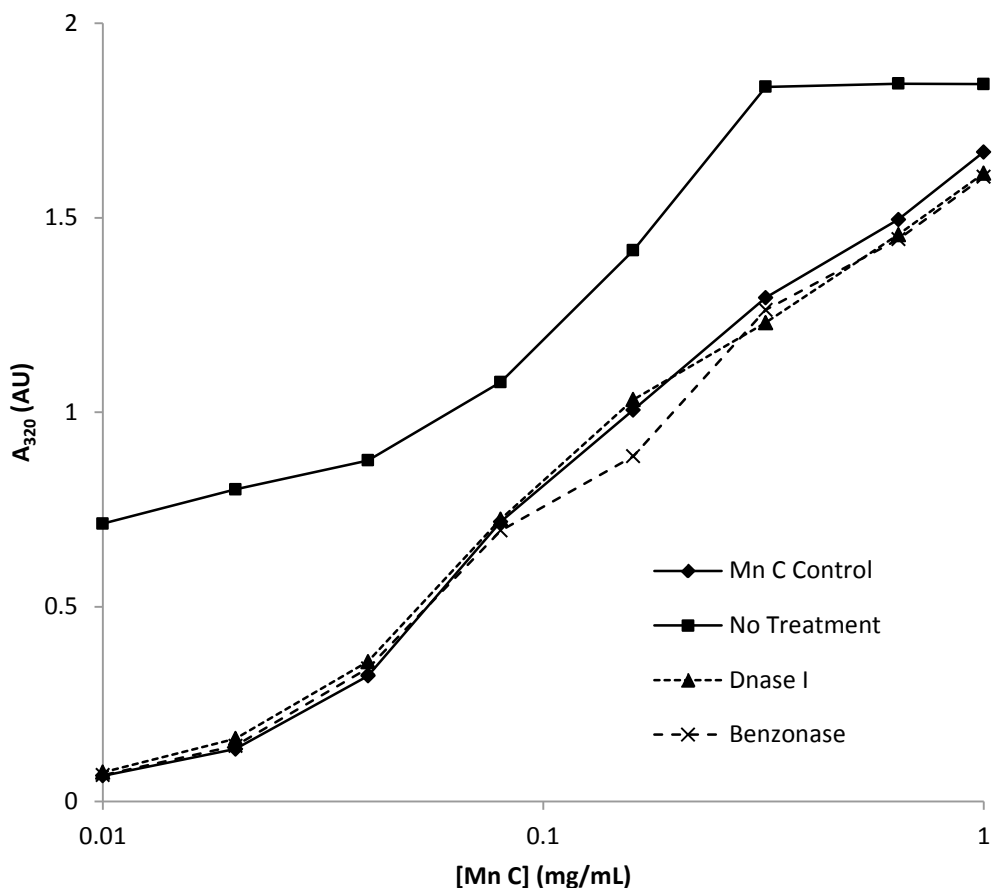


Figure 3.8. Elimination of DNA interference from the phase separation assay. Samples (except for “Mn C Control” which contained no spiked DNA) were formulated in 25 mM sodium phosphate, pH 7.2 with a range of [CPS] and a final [DNA] = 2 mg/mL. The samples were then spiked with 10 % (v/v) of 3000 Kunitz units of DNase I or Benzonase. After mixing via pipettor aspiration/dispensing, the solutions were incubated at 37°C for 1 hour. “Mn C Control” was composed of purified Mn C without added DNA (*i.e.* “No Treatment”) and spiked with the enzyme buffer absent the enzyme. The standard assay procedure was then followed.

3.4.2.4 Complex In-Process Samples

3.4.2.4.1 Primary Recovery and Downstream Unit Operations

To assess the compatibility of the assay with in-process pools from downstream processing, samples were taken at several points in the purification trains for staphylococcal CPS (Figure 3.9).

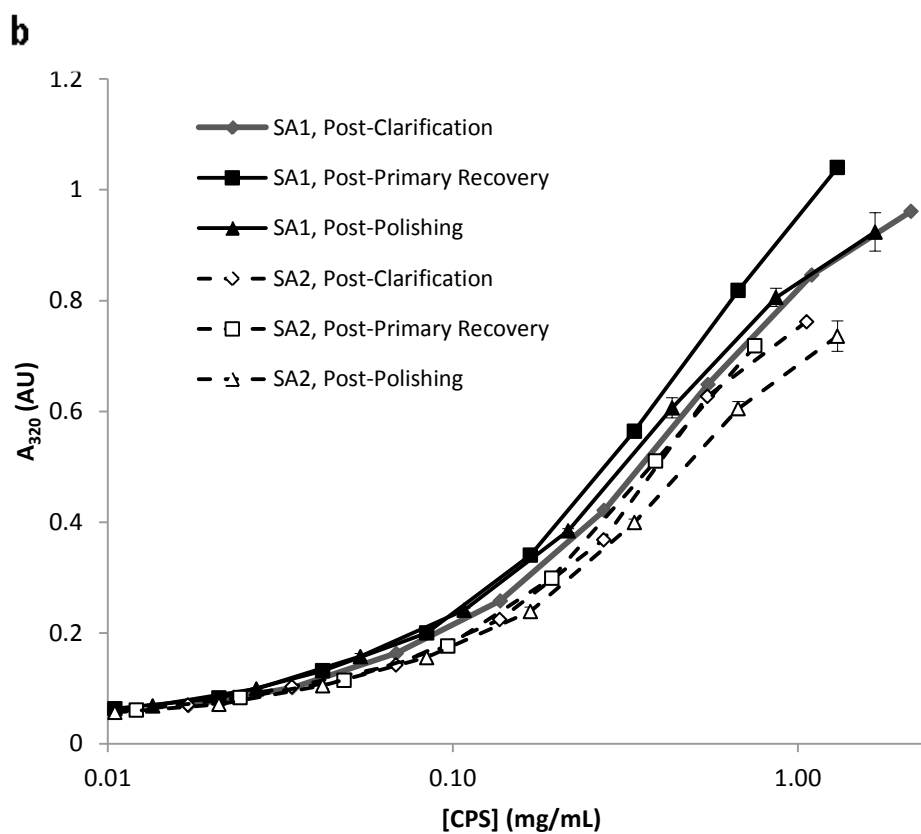
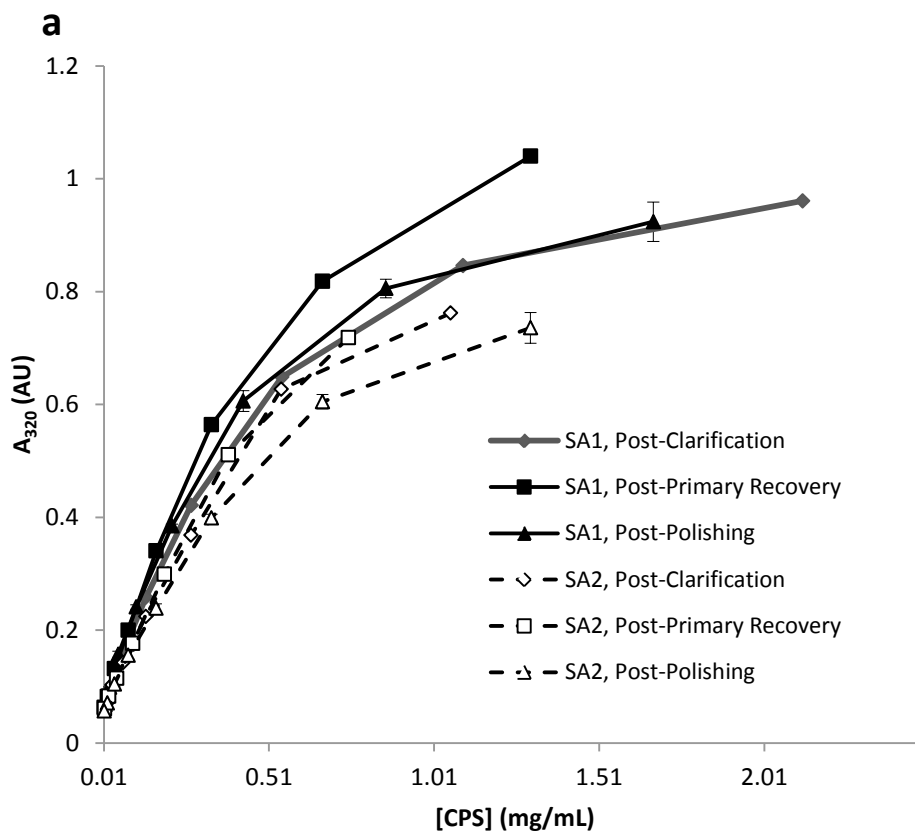


Figure 3.9. Robustness of titre assay to samples taken from different locations in the purification trains for two CPS from *S. aureus*. The identities of the serotypes have been redacted. Serial dilutions in 25 mM sodium phosphate, pH 7.2 were made from bulk pools prior to the addition of Hb. No additional sample pre-treatment was performed. Relative sample impurity is: Post-Clarification > Post-Primary Recovery > Post-Polishing. All curves relied on single measurements except for 'Post-Polishing' samples, which were run in triplicate incorporate error bars denoting the standard deviation. Although samples were sterile-filtered as part of the production process, no sample conditioning besides the integrated batch-desalting step was implemented. Figure 3.9b shows the same data as Figure 3.9a but with log transformed concentration values on the x-axis (for values ≥ 0.1 mg/mL), defined by the following equations: SA2 Post-Clarification: $y = 0.27 \ln(x) + 0.79$, $R^2 = 0.99$; SA2 Post-Primary Recovery: $y = 0.31 \ln(x) + 0.94$, $R^2 = 0.99$; SA2 Post-Polishing: $y = 0.26 \ln(x) + 0.81$, $R^2 = 0.99$; SA1 Post-Clarification: $y = 0.24 \ln(x) + 0.74$, $R^2 = 0.97$; SA1 Post-Primary Recovery: $y = 0.27 \ln(x) + 0.78$, $R^2 = 0.99$; SA1 Post-Polishing: $y = 0.22 \ln(x) + 0.67$, $R^2 = 0.98$; Polynomial fits could be employed to extend the range of the standard curve.

The results from two distinct purification processes suggest that even without any sample pre-treatment, the phase separation assay can be deployed at various points in a downstream process and cope with complex sample matrices.

3.4.2.4.2 Fermentation Broth

The most challenging sample background for assay deployment is fermentation broth. In addition to proteins and DNA, high concentrations of endotoxin, metabolites, growth media, and cell components are among the components in the fermentation milieu. Centrifuged fermentation broth from pneumococcal serotype 6B was screened for its impact on precipitation assay performance (Figure 3.10).

With DNase digestion, the signal from clarified fermentation broth was reduced approximately 50%, from 1.4 AU to 0.7 AU. The decrease in interference improved the slope of the 6B standard curve in the presence of 50% broth from 34% to nearly 80% of the reference slope. Across the 0.1-1.0 mg/ml

6B range, the curves of the standard and the DNase-treated samples were approximately parallel. This result differs from the 0.01-0.1 mg/ml 6B range, highlighting the dependency of the interference on CPS concentration, with higher concentrations yielding better results.

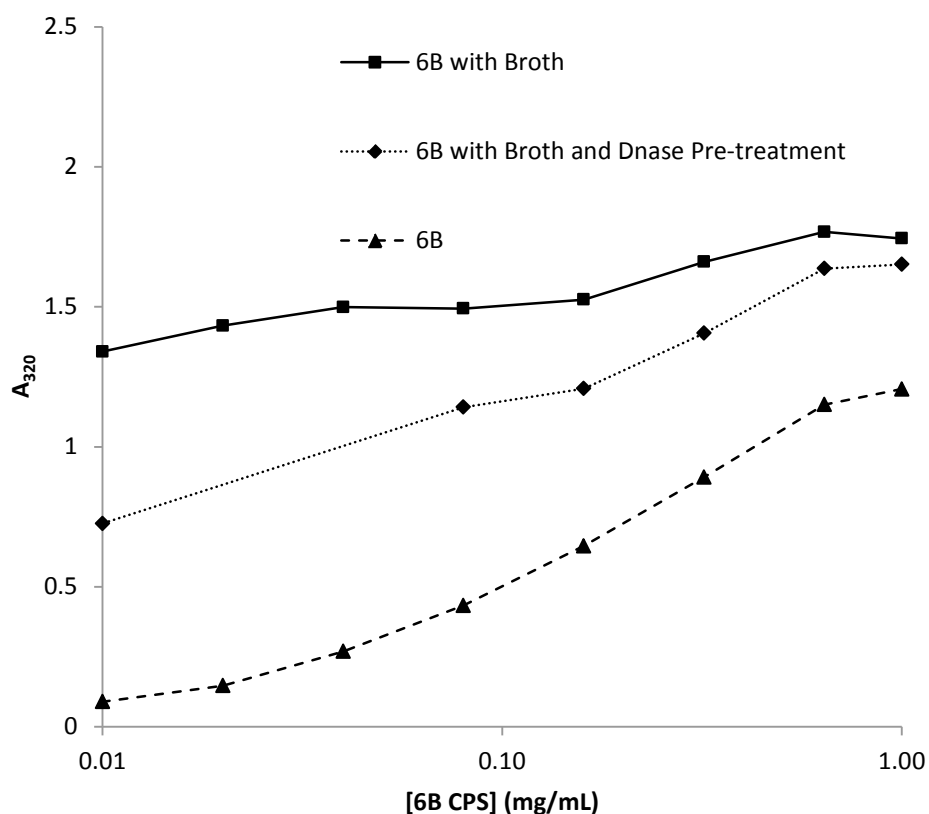


Figure 3.10. Enhancement in assay performance with DNase treatment of fermentation broth samples. Purified pneumococcal serotype 6B was serially diluted in 25 mM sodium phosphate, pH 7.2. Fermentation broth was centrifuged and sterile filtered prior to the addition of 6B. The sample was then diluted with 25 mM sodium phosphate, pH 7.2 to attain a 2-fold dilution. A 50% solution of broth with negligible amounts of CPS was characterised by an absorbance > 1.2 AU and is representative of the sample background signal. DNase pre-treatment constituted incubation of the '6B with Broth' sample for 1 hour at 37°C with 300 Kunitz units/mL of Benzonase prior to execution of the standard assay procedure. Linear regression analysis was performed and the log slopes for the three sample sets were 0.089, 0.20, and 0.26.

It can be challenging to eliminate all the interfering substances in clarified fermentation broth. Moreover, the composition of broth is highly dynamic, making it difficult for an analyst to assure complete removal of matrix inhibition or to have high confidence in the accuracy of the results for a new fermentation batch. In many cases, the benefit of this type of exhaustive work would not justify the investment. However, as depicted in Figure 3.10, even in broth with no enzymatic pre-treatment, the assay response is monotonic with sample concentration. This suggests that at a minimum, the phase separation assay will accurately provide relative measurements of CPS where the sample background is comparable. This property is important for measurements of batch-batch consistency and particularly useful to scientists working in HTPD, where frequently the key aim is to identify rapidly the best subset of experimental combinations on a microplate, for more meticulous development for future scale-up.

3.4.3 SEC-MALS

3.4.3.1 Optimization

To increase sensitivity and robustness, SOPs for SEC-MALS of CPS will often include custom chromatographic parameters (*e.g.* sample prep, mobile phase, temperature, etc.). The capability to analyse myriad CPS with SEC-MALS with a single platform configuration would be highly desirable. To assess the sensitivity of SEC-MALS outputs to assay operational changes, a combinatorial HPLC-SEC-MALS study was performed with a number of candidate mobile phases, SEC columns, and CPS serotypes. In addition, UPLC columns were included, although the pore sizes ensured that many CPS would be excluded and be eluted near the void volume of the column. UPLC utilises smaller bead sizes and a specialized chromatographic system to enhance resolution and provide equivalent performance to a HPLC but with shorter run times. UPLC columns are advantageous for HTPD, as each run requires 8 minutes instead of the 30 minutes per sample common to HPLC procedures. The correspondence between various combinations of CPS, column, and buffer was evaluated using a range of product quality attributes.

3.4.3.2 Root Mean Square Radius

The r_{rms} of the CPS under a range of conditions are delineated in Figure 3.11.

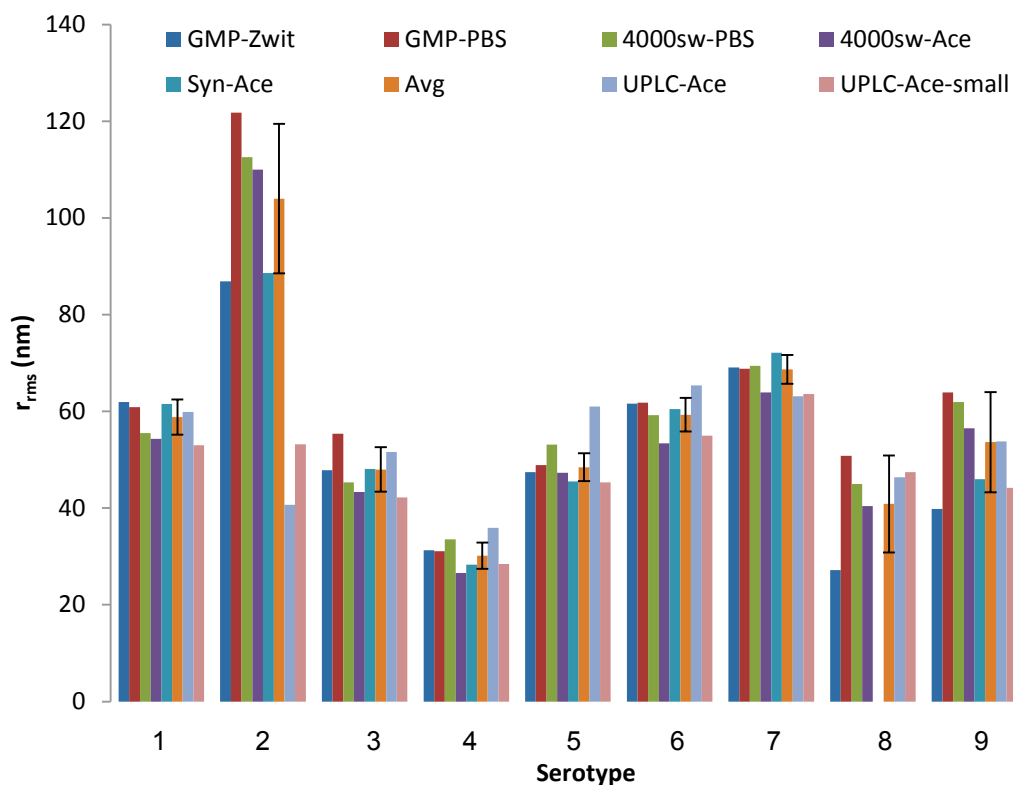


Figure 3.11. Effect of buffer and column on r_{rms} for CPS serotypes from two bacterial species. “Avg” represents the average of the five HPLC values. PBS= phosphate buffered saline, pH 7.2, Ace = 294 mM HAc, 1 mM EDTA, pH 6.7, Zwit = PBS, 0.75% Zwitterion 3-10, pH 7.2. The qualifier “small” on the UPLC values indicates when a smaller peak window (based on starting at RI inflection) was used for MALS calculations. Serotype numbers are blinded references to CPS serotypes from *N.meningitidis* and *S. pneumoniae*.

The broad trends in Figure 3.11 suggest that each pneumococcal CPS is defined by a characteristic size that it is only slightly dependent on the column or the mobile phase. Moreover, the radii measured with UPLC columns did not differ markedly from the average of the HPLC comparators. However, the meningococcal CPS were impacted by the buffer choice, with the addition of zwitterion leading to significantly smaller CPS. This shift is explained by a sharp increase in CPS yield in the presence of zwitterion, whereas with other experimental conditions, significant masses of meningococcal CPS are retained on the column.

3.4.3.3 Molecular Weight

For the r_{rms} values given in Figure 3.11, the corresponding MW values are provided in Figure 3.12.

MW is a standard size measurement for CPS.

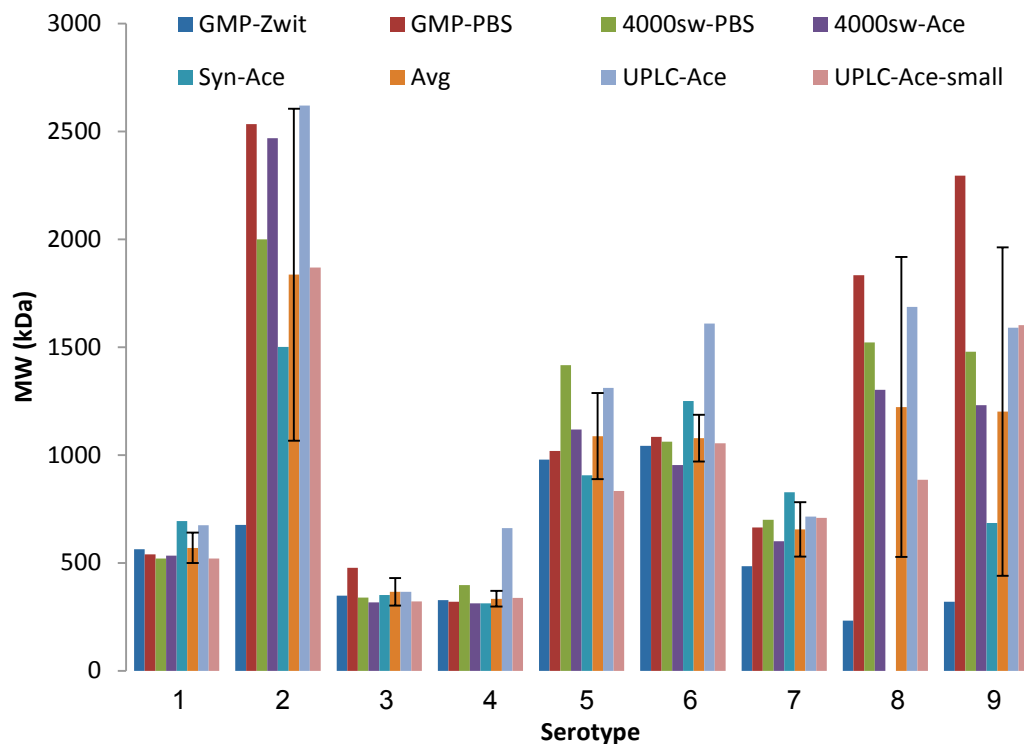


Figure 3.12. Effect of buffer and column on MW for CPS serotypes from two bacterial species. “Avg” represents the average of the five HPLC values. PBS = phosphate buffered saline, pH 7.2, Ace = 294 mM HAc, 1 mM EDTA, pH 6.7, Zwit = PBS with 0.75% Zwitterion 3-10, pH 7.2. The qualifier “small” on the UPLC values indicates when a smaller peak window (based on a peak definition starting at RI inflection) was used for MALS calculations. Serotype numbers are blinded references to CPS serotypes from *N.meningitidis* and *S. pneumoniae*.

In Figure 3.12, the error bars on the HPLC averages are larger than for the r_{rms} averages. In addition, MW measurements for replicate injections generally have a higher RSD than the concurrently calculated root mean square radius. This finding was consistent across a broad range of thesis work,

irrespective of whether automated or manual peak integration methods were employed. There were no discernible patterns between MW values and the buffer or column utilised. R_{rms} is determined from the angular dependency of light scattering whereas MW integrates both the light scattering signal and the RI signal. The addition of a second orthogonal signal (*i.e.* RI) is believed to underlie the differential precision (worse for MW) observed in these two measurements. Additional analyses were performed with the column, buffer, and CPS combinations to assess the impact on other MALS-derived properties.

3.4.3.4 Conformation Slope Gradient Functions

An approximation of the molecular conformation can be inferred from the slopes of log plots of r_{rms} against MW. General conformations are defined by slopes of: 0.33 = sphere (*i.e.* $MW = r^3$), 1.0 = rod (*i.e.* $MW = r^1$), and 0.5-0.6 = random coil (*i.e.* $MW \approx r^2$). The conformation slopes are provided in Figure 3.13.

Conformation plots have more noise than other MALS-derived biophysical measurements. This is due to three signals being integrated and to the potentially faulty assumptions that all the polysaccharides in a sample have the same conformation and that the CPS peak is completely isolated from unrelated co-eluting molecules. The imprecision in the measurements are evident in the error bars associated with the averages in Figure 3.13 and makes interpretation of the trends challenging. Nevertheless, several general characteristics can be extracted. As with size properties, each CPS appears to have a favoured conformation, with most of the CPS being spherical. Serotype 6A has demonstrably more random coil orientation and none of the polysaccharides adopts a rod-like conformation. With respect to the impact of the columns and buffers, there was no clearly discernible pattern between MW values and the buffer or column utilised. Since the UPLC method cannot fractionate all of the CPS population by size (due to pore exclusion), the conformation plots that were generated are unreliable.

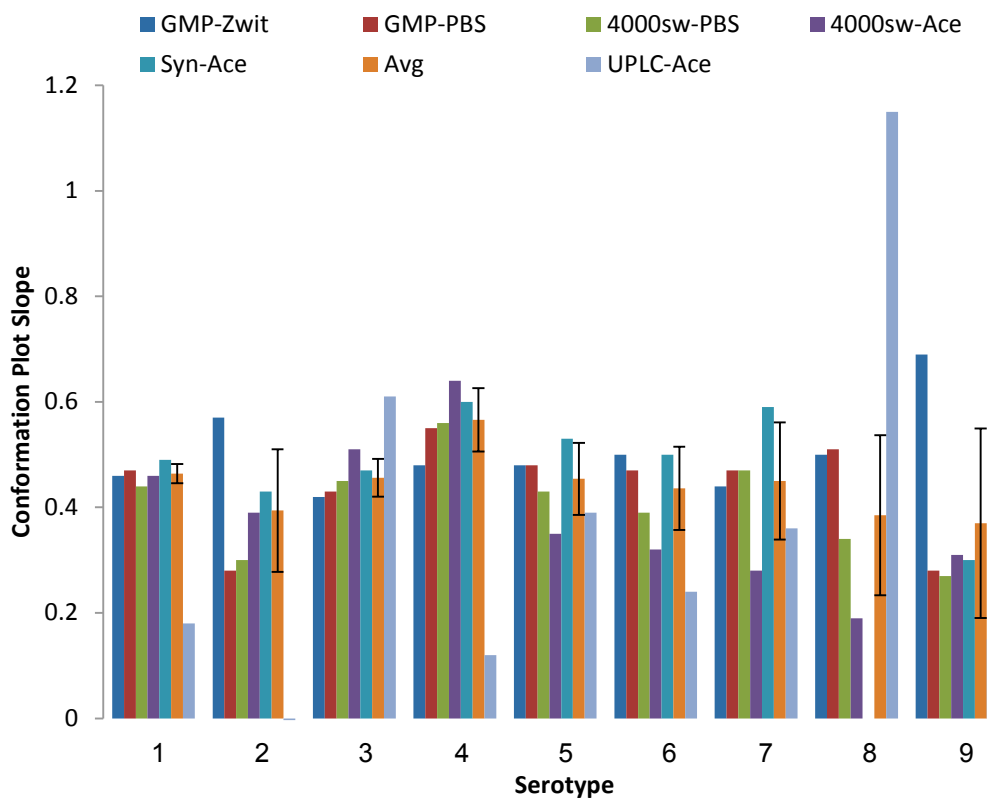


Figure 3.13. Effect of buffer and column on conformation slope for CPS serotypes from two bacterial species. “Avg” represents the average of the five HPLC values. PBS = phosphate buffered saline, pH 7.2, Ace = 294 mM HAc, 1 mM EDTA, pH 6.7, Zwit = PBS with 0.75% Zwitterion 3-10, pH 7.2. Serotype numbers are blinded references to CPS serotypes from *N.meningitidis* and *S. pneumoniae*.

Fortuitously, many conditions and columns were found to offer similar measurements of r_{rms} and MW for a given CPS. Of particular interest, the UPLC method was found to be highly reproducible and robust for determination of r_{rms} and MW, highlighting the potential of this SEC technology to supplant the traditional HPLC version. In subsequent work with SA1 and SA2, UPLC flow rates had to be throttled from 0.4 mL/min to 0.2 mL/min. The amplified pressure and shear associated with the higher flow rate transiently shifted the conformation of these CPS, leading to an apparent increase in MW (data not shown). The revised run time of 16 minutes is still half the duration of an analogous HPLC run, providing sufficient basis for adoption.

The only commercially available UPLC columns for SEC have pores smaller than the CPS, leading to steric exclusion and elution of CPS in the void volume. The result is that the UPLC column is functioning as an enhanced desalting column. This characteristic necessitates a reliance on averaged values for each peak, which is acceptable for r_{rms} and MW but prevent determination of polydispersity or sub-fractionation of different polysaccharide fractions. A column with ≤ 20 nm pore size was used in this study although an UPLC column with ≤ 45 nm pores size was available. Abbreviated testing indicated that many CPS were still excluded from the larger pore size matrix. In addition, the preferred MALS standard, BSA, eluted with mobile phase, complicating instrument standardization.

3.4.3.5 Titre Measurements

The data in Figures 3.11 and 3.12 are evidence of the comparability of size measurements made in UPLC and HPLC systems with a range of CPS types and concentrations. Since SEC-MALS is also relied upon for titre measurements, a brief qualification was performed. The standard curve for an in-process SA1 pool was generated in two different ways: increasing the mass loaded through increasing volumetric injections of a fixed sample concentration or increasing the mass loaded through increasing concentrations of a fixed volume sample injection. The standard curves are compared against an ideal linear curve in Figure 3.14.

For both modes of standard curve generation, the results were linear, similar, and comparable to the expected 'Full Recovery' line. Product did not appear to bind non-specifically to the column or otherwise foul the column. The results in Figure 3.14 indicate that this assay provided accurate mass estimation across the tested range of sample concentrations. This is important as the sample concentrations across a microplate-based purification screen will vary. Further, the insensitivity to injection volume will enable samples outside the tested sample concentration range to be accurately quantified through an adjustment of the volume injected.

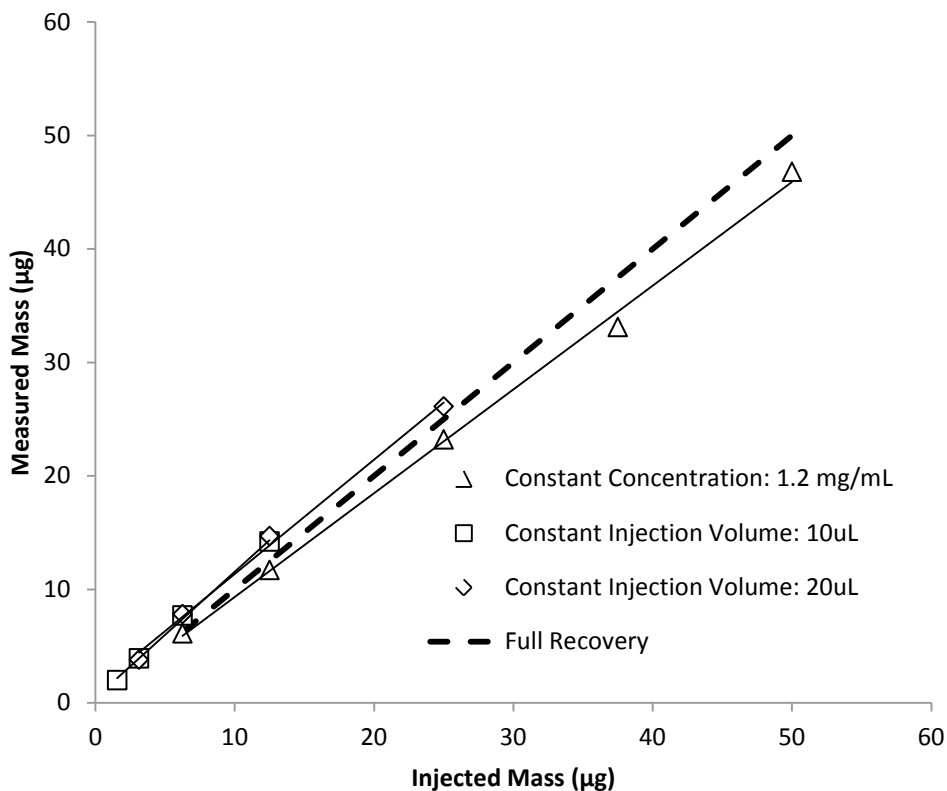


Figure 3.14. Accuracy of UPLC-MALS for titre measurements using SA1 CPS from an intermediate in-process pool. Standard curves were generated by varying injection volume with constant sample concentration or by varying sample concentration with constant injection volume. Equations for the standard curves are Constant Concentration: $y = 0.91X + 0.17$; Constant Injection Volume: 10 μL : $y = 1.01X + 1.30$; and Constant Injection Volume: 20 μL : $y = 1.11X + 0.43$. The R^2 for each line was 1.00.

3.5 Chapter Summary

In this chapter, the development, characterisation, and qualification of three novel assays for measuring the titre of anionic CPS have been described.

A PHS assay was modified and optimized for high throughput quantitation of mono-, di-, and poly-saccharides. The assay requires only 25 μL of sample and involves no heating steps that can complicate automation. The described procedure also reduces the quantities of hazardous chemicals

such as phenol and sulphuric acid, requiring only 150 μL total per sample. A linear range of approximately 2 logs (*e.g.* glucose: 8-1000 $\mu\text{g}/\text{mL}$) was observed for every tested carbohydrate, with the actual range derived from the specific composition of reactive sugars present. The precision of the described assay was found to be 10%. This assay offers universal reaction with reducing sugars but requires the use of highly toxic reagents.

The Hb precipitation assay enables the rapid quantitation of anionic polysaccharides for downstream samples. The resulting procedure can robustly measure the titre of myriad anionic capsular polysaccharides in 96 samples in less than 30 minutes using low toxicity reagents and routine laboratory equipment. A microplate desalting step is integral to the assay and helps minimize assay interference. The assay has been shown to be robust across a pH range of 3-8.75, with samples containing up to (at least) 400 mM of NaCl, in a diverse set of excipients, and in complex in-process backgrounds. The most significant interference encountered was due to nucleic acids, for which a simple, effective enzymatic treatment was prescribed, assisting in the cleanup of samples as complex as fermentation broth.

In the application development of the phase separation assay, 16 unique capsular polysaccharides were screened, of which 13 were anionic. A two-log dynamic range has been established with a mean relative standard deviation less than 10% across this range although inferior performance has been observed in fermentation broth. Every tested anionic CPS reacted in the phase separation assay, independent of whether the acidic moiety was uronic acid, sialic acid, or phosphate and whether the anion resided in the CPS backbone or side chain. Neutral polysaccharides did not react substantially in this assay. These observations suggest that this assay may approach a universal titre assay for anionic CPS in samples, although excessive interference precludes the deployment in fermentation samples.

UPLC was demonstrated to provide CPS titre, r_{rms} , and MW measurements that were equivalent to traditional HPLC-based analogues. With UPLC-MALS, the time to process a sample is approximately one fourth that of existing HPLC procedures. For a microplate of samples, this reduces process time from 2 days to 8 hours.

For an array of CPS, it was demonstrated that buffer and column properties did not substantially affect the integrity of product quality measurements such as MW and r_{rms} . These findings led to the adoption of a single set of chromatographic conditions for all the polysaccharides. Qualification of titre quantification of UPLC-MALS established that the expected spectrum of product concentration that would be encountered in HTPD is encompassed with this assay. UPLC-MALS offers a rapid, universal, and robust assay that is effective for samples ranging in complexity from broth to purified CPS drug substance.

The described suite of analytics enables the rapid quantitation of CPS titre and quality in a microplate-based format that is amenable to automation. The productivity of CPS titre measurements were improved by up to 30-fold. Determination of in-process product concentration can now be made on 96 samples in less than a day and require only 130 μ L of sample per condition, representing a marked improvement over current practises. The capability to measure rapidly microplate quantities of CPS samples, with little customization for the underlying CPS chemistry has the potential to change the way process development of CPS is conducted. These assays, particularly UPLC-MALS and to a lesser extent, the phase separation assay, comprise the analytical cornerstones of the HTPD platform for CPS and will be employed in Chapters 4, 8, and 9.

4 High Throughput Particle Conditioning

4.1 Introduction

A key challenge in designing a high throughput particle conditioning platform is emulating results from larger scales. With particle conditioning, the success of the purification step is additionally dependent upon the capacity to remove the solids produced, whether by downstream settling, centrifugation, or filtration. Indeed, the inclusion of a dynamic aging step following initial precipitation is designed to facilitate subsequent solid-liquid separations by improving the strength and density of the particles. Accordingly, particle characteristics become paramount. These are profoundly influenced by the erosion, fragmentation, and regrowth processes simultaneously competing to establish the characteristics of the average particle.

4.2 Aim and Objectives

We developed an USD particle conditioning system, comprised of off-the-shelf parts and designed to enable automated, temperature-controlled flocculation of 96 different reactors in parallel. A centrally positioned magnetic stirrer provides the agitation for each well and a robotic liquid handling system introduces the feed material, flocculants, and titrants. In this chapter,

1. Through an examination of engineering properties, we compare the hydrodynamic environment in the USD system to the respective conditions found at larger scale.
2. We illustrate the use of HTPC to examine a broad experimental space using a suite of high throughput analytics described in Chapters 2 and 3 for the quantification of clarification, particle characteristics, purity, yield, and product quality.
3. We demonstrate the applicability of HTPC as a platform technology by applying it to diverse capsular polysaccharides from three different species. For each CPS, we scale-up multi-factor experimental spaces to demonstrate how closely HTPC results represent the performance of

several different Pilot-scale reactors. In doing so, we examine the suitability and engineering ramifications of maintaining different factors during scale-up. Scalability is assessed in reactor volumes from 0.8 mL up to 12.9 L, a scaling factor of 4 logs.

4.3 Materials and Methods

The identity of polysaccharides were redacted in Table 4.3, Figures 4.4-4.7, and Figures 4.9-4.11.

4.3.1 Materials

All common chemicals were commercial analytical grade. Nalgene 0.22 μm polyethersulfone filters (Thermo Fisher Scientific, Waltham, MA) were used to filter assay diluents. Benzonase enzymes were supplied by Merck KGaA (Darmstadt, Germany). Biological solutions (CPS broth, DNA, enzymes) were not filtered, except for the meningococcal streams, which were sterilized with 0.22 μm filters. All spectroscopic measurements were made using a spectrophotometric plate reader (Spectramax M3; Molecular Devices, Sunnyvale, CA).

Capsular polysaccharide from various serotypes of *S. pneumoniae* (neutral), *S. aureus* (anionic), and *N. meningitidis* (anionic) were provided kindly by Pfizer R&D. All sugars have D and α structural configuration. Broth was taken from locations early in the process train, prior to the primary recovery of CPS. Fresh material was used for the *S. aureus* and *S. pneumoniae* work, while frozen stocks were employed for *N. meningitidis*. Crossover screens between fresh and previously frozen feedstocks exhibited only minimal differences in HTPC responses. The most significant changes manifested as a slight improvement in clarification and marginally faster kinetics for the previously frozen material.

4.3.2 High Throughput Particle Conditioning System

A schematic diagram of the USD system is given in Figure 4.1a and workflow specifics are provided in Table 4.1b.

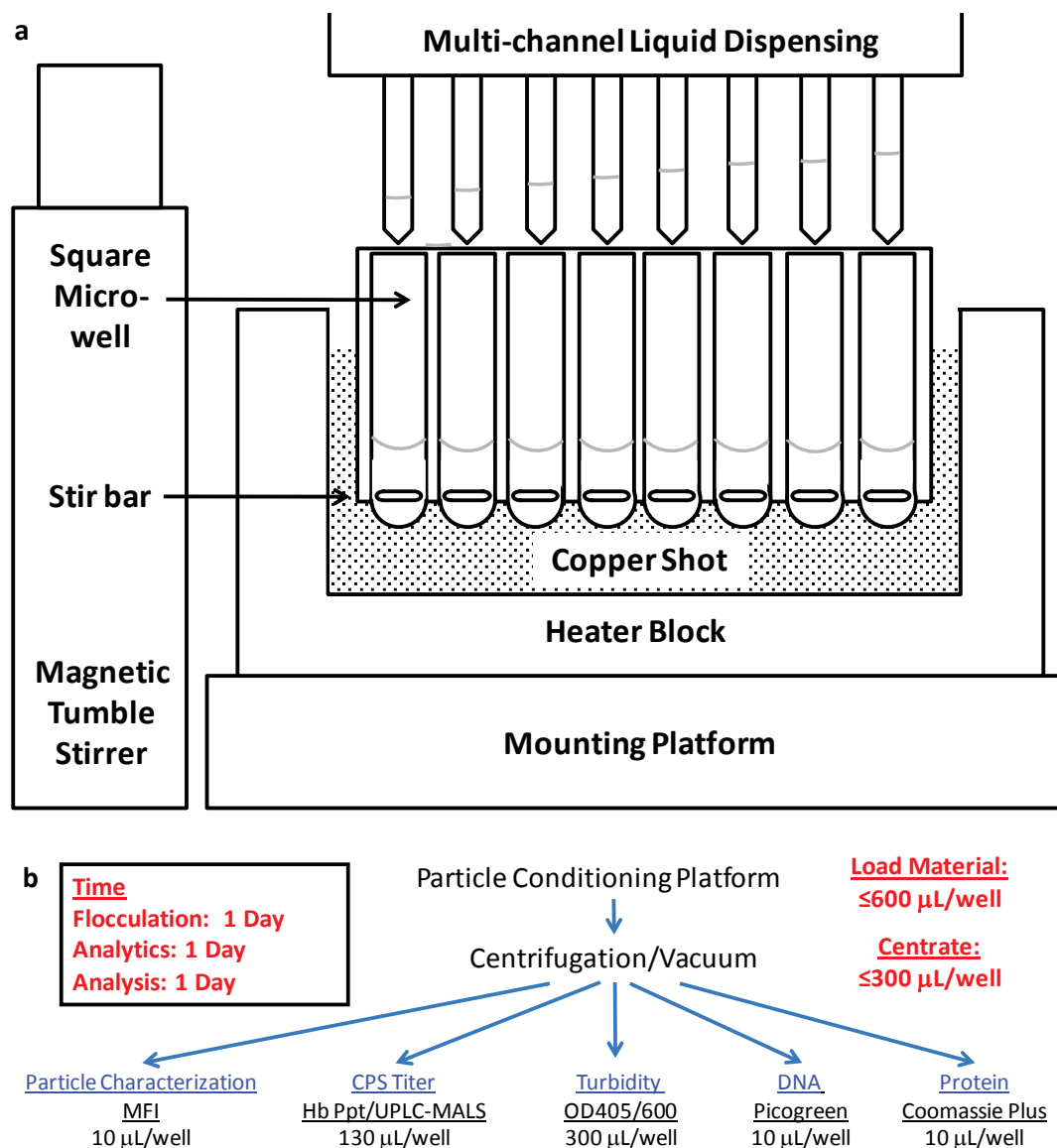


Figure 4.1a, b. Schematic of the USD flocculation device (4.1a) and flow diagrams for HTPC (4.1b).

Details for a typical screen are provided. See 2.3, 3.3, and 4.3 for process set points and specific assays.

Table 4.1. Engineering characterisation of the flocculation reactors. Discussion refers to the reference letter atop each column. ‘A’ is representative of a commercial-scale reactor while ‘B’, ‘D’, and ‘F’ are the Pilot-scale reactors employed in this study. ‘C’ and ‘E’ describe the USD flocculation reactor configurations used in this study, with ‘E’ delineating set points designed to maximize both power input and tip speed. Volumes represent the volumes present at the start of floc aging. Underlined values represent attributes that were held constant during scaling studies. Representative values of $\eta = 0.002 \text{ Pa s}$, $\rho = 1000 \text{ kg m}^{-3}$, and aging time = 4800 s were used for all calculations. Formulae for each parameter are provided in the Introduction and Nomenclature sections.

Reference		A	B	C	D	C	E	F	E
Species		<i>S. aureus</i>			<i>N. meningitidis</i>			<i>S. pneumoniae</i>	
Vessel		Ferm	Ferm	Micro	Ferm	Micro	Micro	Ferm	Micro
V	mL	1,806,000	3,480	1.21	2,350	1.21	0.77	12,900	0.77
T	cm	112	21.0	0.82	13.0	0.82	0.82	21.1	0.82
Baffled	Y, N	Y	Y	Y	Y	Y	Y	Y	Y
D	cm	40.6	8.5	0.64	4.5	0.64	0.64	8.3	0.64
Impeller Type		Rushton	Rushton	Stir bar	Rushton	Stir bar	Stir bar	Rushton	Stir bar
n		3	1	1	1	1	1	3	1
N _p		5.4	5.4	1	5.4	1	1	5.4	1
Z/T		1.65	0.57	2.18	0.99	2.18	1.40	1.75	1.40
D/T		0.36	0.40	0.78	0.35	0.78	0.78	0.39	0.78
N	s ⁻¹	0.83	3.08	10.0	2.50	10.0	16.7	2.42	16.7
N _{Re}		68,682	11,139	205	2,654	205	341	8,244	341
v _{tip}	m s ⁻¹	1.06	0.82	0.2	<u>0.36</u>	0.2	<u>0.34</u>	0.63	0.34
θ _{0.95}	s	50	3	7	<u>15</u>	<u>7</u>	<1	15	<1
P/V _{avg}	W m ⁻³	57	170	9	<u>10</u>	<u>9</u>	65	<u>68</u>	<u>65</u>
λ _{kavg}	m	19 X10 ⁻⁶	15 X10 ⁻⁶	31 X10 ⁻⁶	<u>30 X10⁻⁶</u>	<u>31 X10⁻⁶</u>	19 X10 ⁻⁶	<u>19 X10⁻⁶</u>	<u>19 X10⁻⁶</u>
P/V _{imp}	W m ⁻³	515	1100	41	<u>180</u>	41	<u>190</u>	520	190
λ _{kimp}	m	11 X10 ⁻⁶	9 X10 ⁻⁶	21 X10 ⁻⁶	<u>15 X10⁻⁶</u>	21 X10 ⁻⁶	<u>14 X10⁻⁶</u>	11 X10 ⁻⁶	14 X10 ⁻⁶
E _f	W s m ⁻³	2.7+05	8.1E+05	4.3E+04	<u>4.9E+04</u>	<u>4.3E+04</u>	3.1E+05	<u>3.3E+05</u>	<u>3.1E+05</u>
\bar{C}_t		8.1E+05	1.4E+06	3.2E+05	<u>3.4E+05</u>	<u>3.2E+05</u>	8.6E+05	<u>8.9E+05</u>	<u>8.6E+05</u>
$\bar{C}_{imp,t}$		2.4E+06	3.6E+06	6.9E+05	<u>1.4E+06</u>	6.9E+05	<u>1.5E+06</u>	2.4E+06	1.5E+06
[ε _{loc} /ε _{avg}] _{max}		14	11	3.2	28	3.2	2.1	12	2.1
τ _{turb} /ρv _{tip} ²	N m ⁻²	0.44	<u>0.14</u>	<u>0.15</u>	0.40	0.15	0.072	0.45	0.072

A magnetic tumble stirrer (VP710 C1), heating block (VP741ABZ-R-MB), and a Hall sensor tachometer (VP710-RPM) were purchased from V&P Scientific (San Diego, CA). Flea micro stir bars were procured from Bel-Art Scienceware (F27119-0635; Bel-Art Scienceware, Wayne, NJ). The USD stir bar diameter was 0.64 cm. The heating block used in these studies was modified with a bed of copper shot (0.8-2 mm, 44213; Alfa Aesar, Ward Hill, MA) placed in the heating block cavity. Flocculation experiments were performed in 2 mL, deep, square-well, polypropylene microplates (7701-5200; Whatman,

Maidstone, UK) as outlined in Table 4.1 'B'. Except for the pneumococcal work, duplicate USD flocculations were performed for all scaling experiments with averaged values used for all analyses. The floc agent concentration is reported on a mass/volume percentage based on the starting volume of broth, except for experimentation involving pneumococcal CPS, wherein mass/volume percentage is based on the final volume of broth and excipients, including the added volume of the floc agent. Relative standard deviations for assay responses for duplicate conditions were generally < 10% and approximately < 15% for MALS-based assays, although duplicates in regions of steep changes were occasionally characterised by higher relative standard deviations. To maximize heat transfer, plates were sealed with foil adhesive tape (T592100, E&K Scientific, Santa Clara, CA) and a tent fabricated out of aluminium foil. Acrylic microplates (Costar 3635; Corning, Corning, NY) from Corning were used for all UV measurements. A Tecan (EVO150; Mannedorf, Switzerland) liquid handling robot was used where automated pipetting was employed.

4.3.3 General Flocculation Procedure

Broth was added to the Pilot-scale vessel or microplate and a steady state mixing pattern established through sustained agitation. The broth was titrated with a 10% (m/v) stock of flocculant to a final range of 1-4% (m/v) flocculant. In the Pilot-scale reactor, titration to a final online pH set point was then achieved with either 5 N acid or base titrant. For HTPC, 1 N acid or base was used interchangeably with the respective 5 N concentrate to improve pipetting accuracy. Titration of pH in HTPC relied on percentage by volume additions derived from *a priori* larger scale model titrations. Titrations were made in the centre of the broth volume and were followed by three cycles of aspirate/dispense in order to minimize reagent hold-up in the pipette tip and to promote rapid mixing. After aging for 60-120 minutes, a duration typical of many manufacturing schedules, 10 μ L and 600 μ L of suspension from each condition was sampled for particle sizing and centrifugation, respectively. In all experiments, 0.6 mL samples of raw flocs were centrifuged (3000 g, 60 min, 20°C) in nominal 0.5 mL polypropylene microplates (Costar 3365; Corning, NY). Following centrifugation, the top 300 μ L of supernatant was sampled and used for analysis (Figure 4.1a).

Additional procedural details specific for each CPS are given below:

4.3.3.1 *S. aureus*

4.3.3.1.1 HTPC

The configuration specified in Table 4.1: C was employed. Full factorial HTPC screens were run with two different staphylococcal CPS, SA1 and SA2, with a final volume of 1.2 mL during floc aging.

Duplicate flocculations were performed with averaged values used for all analysis. A Tecan liquid handling robot was used for automated pipetting. Controls of load material were dynamically aged and centrifuged in parallel.

4.3.3.1.2 Pilot-scale

The configuration specified in Table 4.1: B was employed. A subset of the HTPC experimental space was performed in a 20-L baffled Biostat C DCU3 fermenter from Sartorius (Gottingen, Germany; T, Z, and H = 21, 12, and 63 cm, respectively). The 8.5 cm diameter Rushton turbine was mounted centrally with a clearance of 3.5 cm and operated at 3.08 s^{-1} . Titrations were performed via submerged addition. Final volume during floc aging was 3.48 L. For both scales, operational parameters were based on prior experience and no specific scaling rule was employed beyond ensuring that by visual examination, the solution appeared to be well mixed. For both scales, following aging, raw flocs were spun (3000 g, 60 min, 20°C) in 0.5 mL microplates in a swinging bucket centrifuge fitted with microplate adapters (5810R, Eppendorf, Hamburg, Germany).

4.3.3.2 *N. meningitidis*

4.3.3.2.1 HTPC

The configurations specified in Table 4.1: C and E were employed for the first and second meningococcal trials, respectively. Full factorial HTPC screens were run with one anionic meningococcal CPS. The screen was run with two different hydrodynamic conditions (Table 4.1) with final volumes of 1.2 mL and 0.8 mL during aging for the first and second screens, respectively. A Tecan liquid handling robot was used for automated pipetting. Titrations for the first meningococcal HTPC (*i.e.* maintaining N_{js} constant) were performed on the Tecan deck with 10 s^{-1} orbital shaking, immediately followed by mixing at 10 s^{-1} with magnetic stirrers. Titrations for the second

meningococcal HTPC (*i.e.* maintaining P/V_{imp} constant) were performed with a magnetic stirrer integrated on the Tecan deck, enabling stir bars to be used for all mixing operations. Magnetic interference from the stirrer drive necessitated the use of fixed tips with liquid sensing disabled when the stirrer drive was mounted on the Tecan deck. In all other cases, disposable capacitance-sensing pipette tips were employed.

4.3.3.2.2 Pilot-scale

The configuration specified in Table 4.1: D was employed. A subset of the HTPC experimental space was performed in a 2 L baffled fermentation tank (Applikon, Delft, Netherlands; T, Z, H=13, 13, 25 cm, respectively). A 4.6 cm diameter Rushton turbine was mounted centrally on an overhead mixer (BDC2002; Caframo, Warton, Canada) with a clearance of 4.6 cm. Titrations were performed via submerged addition. Final volume during floc aging was 2.35 L. The first trial sought to simultaneously maintain N_{js} , P/V_{avg} , λ_K , E_f , Ca (Table 1: C, D) and the second trial simultaneously held v_{tip} , P/V_{imp} , and λ_{Kimp} constant (Table 1: D, E) between scales. For both scales, following aging, raw flocs were centrifuged (3000 g, 60 min, 20°C) in a Sorvall swinging bucket centrifuge fitted with microplate adapters (Legend RT EASY; Thermo Fisher Scientific, Waltham, MA).

4.3.3.3 *S. pneumoniae*

4.3.3.3.1 HTPC

The configuration specified in Table 4.1: E was employed. Full factorial HTPC screens were run with a neutral pneumococcal CPS with a final volume of 0.77 mL during floc aging. Raw flocs were spun (4750 g, 5 min, 20°C) in a swinging bucket centrifuge fitted with microplate adapters (JS-5.3; Beckman Coulter, Brea, CA). The centrifugation condition was based on conditions experimentally determined to sediment a sample of the 13 L floc suspension in the microplate such that the absorbance of the supernatant at 600 nm (A_{600}) approximated the A_{600} of the large scale, disk-stack centrifuge centrate. Pneumococcal flocculations were performed with a central magnetic stir bar for all phases of mixing.

4.3.3.3.2 Pilot-scale

The configuration specified in Table 4.1: F was employed. A subset of the HTPC experimental space was performed in a 15 L baffled fermenter (Applikon, Delft, Netherlands; T, Z, and H = 21, 37, and 50 cm, respectively). Three 8.3 cm diameter Rushton turbines were mounted centrally in the fermenter. The bottom Rushton had a clearance of 8.3 cm with each impeller separated by 8.3 cm. Titrations were performed via surface addition. Final volume during floc aging was 12.9 L. Semi-continuous centrifugation was performed with a disk-stack centrifuge (CSC-6; GEA Westfalia Separator Group, Oelde, Germany). The CSC-6 was operated at 12,000 g at room temperature with a flow rate of 1 bowl volume/min where bowl volume was 1.8 L. The first and last 5 L of centrate/supernatant were discarded. Separately, flocs generated in the 15 L fermenter were spun as described in the pneumococcal HTPC section.

For both scales, operational parameters were modulated to maintain P/V_{avg} and Ca constant between scales. Because the same feed material was employed for these studies, E_f and λ_{kavg} were also maintained constant for a given flocculation condition.

Permutations on the aforementioned HTPC process were evaluated but yielded results substantially different from larger scale models. Two such examples are summarized as follows. To have adequate buffering at the pH values used in HTPC and to avoid the need to determine titration volumes for each well, a system of stock buffers was employed to achieve a pH set point, similar to Kelley et al. (Kelley et al., 2008). An alternative procedure for HTPC involved reversing the sequence of pH titration and floc agent addition. Both approaches led to results that differed markedly from the larger scale results. These two examples exemplify a key lesson that continually recurred throughout this USD design process: the need to emulate large scale processes as closely as possible even if procedures or set points could be ‘improved’ through apparent enhancement of the USD system.

4.3.4 Core Suite of HTPC Assays

A battery of assays comprised the HTPC analytics platform (Figure 4.1b). A summary of the methods is provided below with additional details available 2.3, 3.3, and in other publications (Noyes et al., 2014).

4.3.4.1 DNA

The standard procedure for Quant-iT Picogreen doubles-stranded DNA Reagent and Kit (Life Technologies, Carlsbad, CA) was followed as per manufacturer's direction. Dilution of samples were performed with Ca²⁺-and Mg²⁺-free phosphate-buffed saline solution, which, in this assay, was found to perform equivalently to the manufacturer-recommended Tris-EDTA buffer.

4.3.4.2 Turbidity

The A₂₆₀, A₄₀₅, and A₆₀₀ of 300 µL of supernatant were read using a spectrophotometric plate reader. Undiluted load controls were centrifuged (3000 g, 20°C, 60 min) in a swinging bucket centrifuge in the standard 0.5 mL polypropylene microplates (Costar 3365; Corning, NY).

4.3.4.3 Protein

The standard procedure for Coomassie Plus (Bradford) protein assay (Thermo Fisher Scientific, Waltham, MA) was followed as described by the manufacturer. The Bradford assay was used for protein quantification as described previously (Noyes et al., 2014).

4.3.4.4 CPS Yield and Quality

Depending on the type of CPS, one of three separate approaches was employed to measure titre and/or quality:

4.3.4.5 UPLC-SEC-MALS

For staphylococcal CPS, UPLC-SEC-MALS was used to measure CPS titre and quality. An UPLC system from Waters (UPLC Acquity; Milford, MA) was employed. MALS (DAWN HELEOS II) and RI (Optilab T-rEX) equipment were provided by Wyatt (Santa Barbara, CA). A 15 cm BEH-200 UPLC (Waters, Milford, MA) column was processed at a flow rate of 0.4 mL/min at 25°C with 10 µL injections. The mobile phase was 0.15 M NaCl, 0.1 M NaH₂PO₄, 0.1 mM EDTA, 200 ppm sodium azide, pH 6.2 ± 0.1. Titre was calculated from RI, while MW and r_{rms} were determined with both MALS and RI.

4.3.4.6 HPLC-SEC-MALS

For streptococcal CPS, HPLC-SEC-MALS was used to measure CPS titre and product quality. A liquid chromatography system from Waters (Alliance 2695, Milford, MA) was used with the same models of RI and MALS detection equipment as for staphylococcal CPS. Column, buffer, and processing parameters were based on species-specific SOPs. Titre was calculated from RI, while MW and r_{rms} were determined with MALS and RI.

4.3.4.7 Phase Separation Assay

For meningococcal CPS, a turbidimetric assay for titre was employed (Noyes et al., 2013). DNase pre-treatment with Benzonase was employed as described in the reference. Neither size nor other product quality data were assessed for meningococcal CPS.

4.3.4.8 Particle Sizing and Characterisation

Particle characterisation and sizing was performed with a Micro Flow Imager with Bot1 autosampler (5200; 1-70 μm ; Protein Simple, Santa Clara, CA). Samples from a given HTPC screen were diluted 1:100 in a single custom diluent. The custom diluent was comprised of a NaCl solution with equivalent conductivity to the undiluted floc suspension, which was then spiked with floc agent and titrant to match the floc agent concentration and pH set points of the centerpoint of the screen. For a given comparison, all scales and conditions utilised the same diluent. The full batch of samples was run and the analysis was repeated in duplicate. Analysis was limited to 50,000 particles per sample with particles excluded that spanned the edge of the micrograph.

4.3.5 Kinetics

A 10 mL, 24-well microplate (7701-5102; Whatman, Maidstone, UK) was utilised for particle conditioning. In each well, 9 mL of SA1 or SA2 fermentation broth was agitated with an ellipsoidal stir bar ($D = 1.0 \text{ cm}$) at approximately 10 s^{-1} at 22°C . The floc agent was added, followed immediately by 5 M base or acid to achieve the target pH. Volumes were determined *a priori* by off-line titrations. A mixing control was created through the volumetric substitution of 5 M NaCl for the titrant and PBS for

the flocculant. At each time point, 0.5 mL was sampled from the reactor. Of the 0.5 mL, 0.2 mL was used immediately for A_{260} , A_{405} , and A_{600} measurements with the remainder of the sample diluted rapidly 20-fold in DNA Assay diluent and spun (13,200g, 20°C, 2 min) in fixed angle centrifuge (5415D, Eppendorf, Hamburg, Germany) to quench the flocculation reaction. The optical densities of the undiluted samples were periodically measured thereafter to allow for detection of continued precipitation and/or signal drift.

4.3.6 Mixing Studies

An iodine/thiosulphate indicator system based on the work of Nagata et al. was employed (Awtrey and Connick, 1951; Nagata et al., 1957; Takahashi et al., 1985). Briefly, a 0.22 μm polyethersulfone-filtered solution of 0.7% starch in 0.6 mM I_2 , 316 mM KI was loaded into a reactor and the flow pattern established. Either 2.5% (v/v) or 10% (v/v) of 379 mM sodium thiosulphate reductant was then added as a single bolus injection in the middle of the stirred vessel contents to decolourize the solution. Mixing studies were performed in HTPC microplates and duplicate mixing trials for each condition were performed. The decolourization process was captured with a digital camera and analysed with CUDA Video Converter (v6.9) after completion of the experiments. Video settings were adjusted to an approximate limit of detection of 95% based on visual calibration against standard dilutions.

4.3.7 Heat Transfer Characterisation

The capability of the USD system to heat 96 wells containing 1.5 mL water per well evaluated. The initial temperature of the water was 25°C and the microplate was then transferred to the heating block, which was preheated to 55°C. Temperature was monitored with thermometers and digital thermocouples, with a range of wells examined periodically to assess spatial non-uniformity. Experiments evaluated combinations of (1) copper shot in a bed beneath the microplate and (2) aluminium foil adhesive tape an aluminium tent over the heating block that housed the sealed plate. The optimal insulation configuration (*i.e.* shot, aluminium covers) was repeated with 0.75 mL of water in each well.

4.4 Results and Discussion

HTPC comprises USD flocculation, centrifugation in microplates, and a suite of high throughput analytics as illustrated in Figure 4.1. The appropriate analytical methods can be selected from a library of high throughput assays qualified for CPS-containing microbial feedstreams (see Methods; (Noyes et al., 2014)). A typical 80-point screen requires 80 mL total volume and can be performed in 2-3 workdays, including setup and multiplexed analyses. The remaining wells on a HTPC plate are necessary for standard curves, blanks, and controls during analysis.

In the following sections, we address the engineering underpinning the USD system and demonstrate the scalability of micro-scale particle conditioning to Pilot-scale with four different capsular polysaccharides. First, the USD system is described along with an engineering characterisation expounding on regime analysis, power number, heat transfer, and hydrodynamics. Second, scale-up studies are utilised to assess different scaling heuristics and show robustness of the HTPC system with diverse CPS. Finally, we holistically interrogate the results to induce mechanistic behaviour and to consider which factors contribute most significantly to variability in performance while scaling.

4.4.1 USD Platform Description

Although not geometrically similar, the USD flocculation system was designed to match key engineering elements of larger scale reactors as closely as possible. Table 4.1 provides a description of the USD system properties along with comparisons to Pilot-scale and commercial-scale reactors. The square well microplate is effectively baffled by the corners present in the cross-section and these enable the employment of and comparison with power numbers (N_p) derived from baffled cylindrical tanks (Kresta et al., 2006; Leentvaar and Ywema, 1980). The base of the microplate is hemispherical which has been shown to offer negligible differences when compared to common ellipsoidal, dished, or parabolic bottoms with respect to suspension of particles or uniformity (Atiemo-Obeng et al., 2004; Zwietering, 1958). Mixing is achieved through rotation of a central impeller. Titrants can be introduced at the surface or via submerged addition. To match typical large-scale reactors fitted with

a single impeller, a liquid height (Z) to tank diameter (T) ratio of unity is preferred, although an exact match is impossible given the range of volumetric conditions tested in a microplate.

There are several key hardware differences between the microplate and larger reactors. The impeller type is a magnetic stir bar instead of a standard shaft-mounted Rushton, marine, or paddle impeller. To maximize energy input into the USD system, a very large diameter (D) stir bar ($D/T=0.8$) is employed. Accordingly, the impeller swept volume is quite large relative to the total tank volume found in conventional floc reactors. The clearance of the magnetic stir bar is very small since the stir bar is not suspended, which will affect flow patterns within the vessel relative to typical reactor dimensions. Abrasion of the stir bar against the floor can potentially lead to anomalous particle distributions, though specific artefacts have not been observed. The single magnetic stir bar also precludes the examination of large Z/T ratios, where additional mixing stages would typically be employed.

4.4.2 Blend Times

To characterise macromixing, the mixing constant ($\theta_{0.95} t$) in the microplate was determined with an iodometric mixing system and is shown as a function of N_{Re} in Figure 4.2. Two different percentage by volume additions and three different Z/T ratios were measured to span the probable range of operating conditions. The evaluation of ranges for percentage addition and Z/T is important as these parameters can vary across a screen and are specific to each flocculation process. In general, 95% homogeneity was achieved rapidly for all conditions where $N_{Re} > 150$ (*i.e.* $\geq 10 \text{ s}^{-1}$; hereafter a recommended boundary) and much more quickly than can be achieved at larger scales. When $N_{Re} > 150$, there exists only minor blend time sensitivity to Z/T and this facilitates inter-well comparisons across a microplate. The 10% addition was characterised by very rapid mixing, owing to the presence of jet mixing from the serological pipette and might not be representative of lower percentage additions. The slowest mixed zones resided at the seams of the baffles, consistent with larger scale reactors, providing additional evidence of similarity with cylindrical stirred tanks that are baffled (Nienow, 1968). Since mixing time is essentially independent of impeller type in these reactor geometries, the results with the magnetic stir bars can be scaled to Rushton turbines and marine

propellers that are more commonly employed at larger scales and were evaluated in our work (Ruszkowski, 1994)

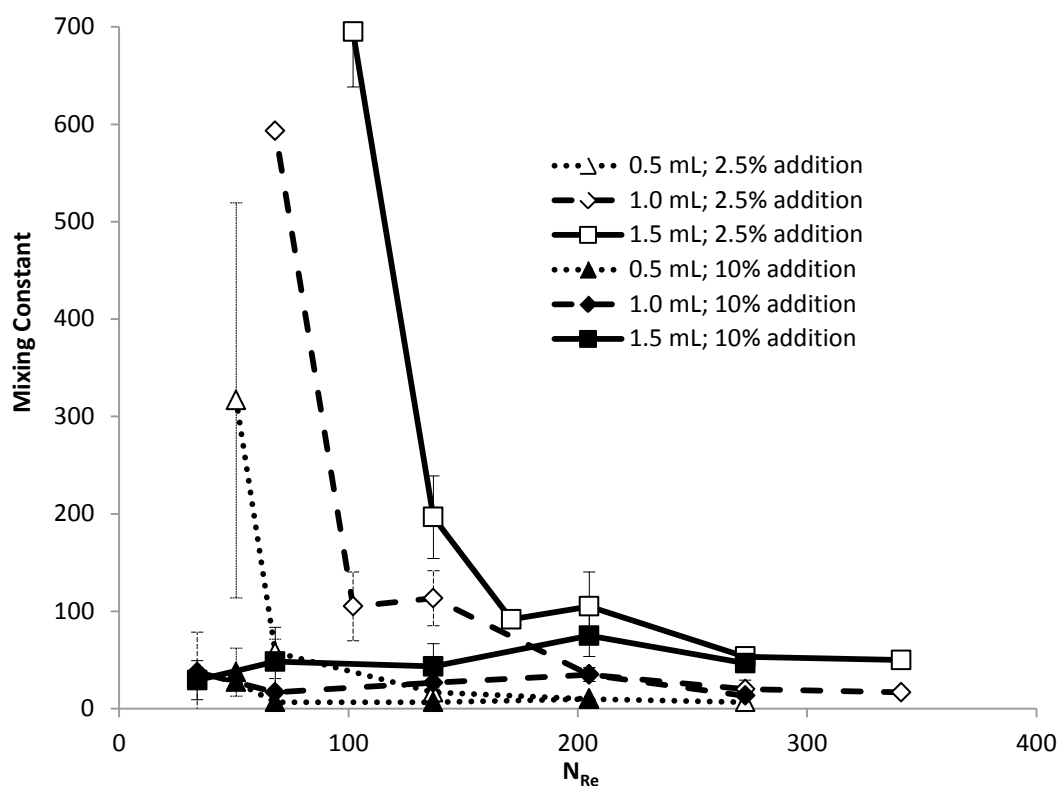


Figure 4.2. Mixing constant (95% mixed) as a function of Reynolds number (N_{Re}), measured in duplicate in the USD system using iodometry. Liquid volumes of 0.5, 1.0, and 1.5 mL with Z/T ratios of 0.9, 1.8, and 2.7, respectively, were employed with percentage by volume additions of 2.5% (v/v) and 10% (v/v). Each condition was in duplicate and the error bars denote the standard deviation. For N_{Re} calculations, $\eta = 0.002 \text{ Pa s}$ and $\rho = 1010 \text{ kg m}^{-3}$.

4.4.3 Engineering Characterisation

Because of the design constraints in the USD system, there are few published correlations fully applicable. The D/T ratio of 0.8 is larger than most studies have examined, where an upper limit of 0.5-0.7 is typically encountered. Few studies have evaluated such small clearances or tank designs with hemispherical floors. Fluid dynamics in the transitional regime are more varied and

configuration-dependent than in the viscosity-independent turbulent regimes. This is perhaps one reason for the markedly fewer hydrodynamic correlations available for transitional regimes than for fully turbulent flows. As a result, we have had to rely on engineering calculations based on studies not entirely representative of the present USD system. Two examples of such limitations and our approach to resolve them are exemplified by regime analysis and N_p .

4.4.3.1 Regime Analysis

Commercial-scale reactors are characterised by fully turbulent flow while Pilot-scale reactors tend to reside in the upper transitional regime. Mixing scale-up in the transitional regime ($100 < N_{Re} < 10,000$) has markedly different rules than in the turbulent regime ($N_{Re} \geq 10,000$) (Grenville et al., 2004). In this study, the USD system is characterised by $N_{Re} \leq 341$, nominally placing it in the lower transitional range. However, the following evidence suggests that turbulent-like environments may exist in the microwell. In the turbulent regime, the mixing constant is independent of N_{Re} (Doran, 1995; Grenville et al., 2004). Inspection of Figure 4.2 shows that where $N_{Re} > 270$ (*i.e.* $N \geq 13 \text{ s}^{-1}$), the mixing constants curves flatten, behaviour consistent with turbulent conditions. Corroboration of the presence of turbulent conditions was found when the blend time data was fitted to a set of eight published turbulent and transitional correlations for baffled tanks. The data for mixing constant closely matched the turbulent correlations (Table 4.2a). Similarly, the extracted N_p 's were unrealistic when the transitional correlations were employed (Table 4.2b)

These findings are consistent with Hill et al., who measured turbulent fluctuating rms velocity profiles in reactors characterised by $4000 \leq N_{Re} \leq 11,000$ (Hall et al., 2005). Reactors of 35, 45, and 60 mm diameter were compared at constant P/V_{avg} and the two smaller reactors had turbulent conditions, suggesting that turbulence may occur at lower N_{Re} as reactor dimensions decrease.

Table 4.2. Mixing constants (θt) in the USD system. Two different stirrer speeds were used for each volume scale evaluated (0.5 mL: 10, 13, 10 s^{-1} ; 1.0 mL: 13, 17 10 s^{-1}) with each stirrer speed evaluated in duplicate. Mixing constants were calculated for the respective USD configurations based on nine independent published correlations spanning the transitional and turbulent regimes and assuming $N_p = 1$ (transitional: (Grenville et al., 2004); turbulent: (Grenville et al., 2004; Hiraoka and Ito, 1977; Kresta et al., 2006; Nienow, 1997; Norwood and Metzner, 1960; Prochazka and Landau, 1961; Ruszkowski, 1994; Sano and Usui, 1985; Shiue and Wong, 1984). Alternatively, using experimental mixing times for the same set of mixing experiments described above, we solved for N_p using published correlations between mixing time and N_p (Grenville et al., 2004; Kresta et al., 2006; Nienow, 1997; Sano and Usui, 1985; Van de Vusse, 1955). “N” refers to the number of different correlations averaged for the calculation of θt and N_p . The errors represent the standard deviation.

1.0 mL	0.5 mL	Regime	Details
Average θt			
18 ± 2	8.4 ± 2.3	Turbulent?	Experimental (2 rpm, duplicate)
8.8 ± 3.9	7.5 ± 2.8	Turbulent	Correlations with $N_p=1$ (N=8)
90 ± 14	116 ± 24	Transitional	Correlations with $N_p=1$ (N=1)
Average N_p			
0.3 ± 0.2	1.0 ± 0.9	Turbulent	Correlations (N=6)
11 ± 1	53 ± 7	Transitional	Correlations (N=1)

4.4.3.2 Power Number (N_p)

The technical difficulty in measuring torque or making other physical measurements at scales less than 1 mL means that there are very few citations of stir bar power numbers. The lone reference located for a magnetic stir bar assigned $N_p = 1.2$, although no hardware details were given, limiting its applicability (Kresta and Brodkey, 2004).

A consideration of paddle impellers suggests that the N_p of rod-like stir bars should be < 2 . Stir bars loosely resemble paddles ($N_p = 2$) in design though the sloped facets of the stir bar should translate to

relatively decreased drag resistance and lower N_p . For paddle impellers, large D/T ratios, similar to the USD system decreased N_p from 2 to 0.7-0.8 in the turbulent regime (Van de Vusse, 1955). Moreover, the very small clearance in the stirred microplate would likely lead to further suppression of N_p (Armenante and Change, 1998; Nienow, 1968).

If the hydrodynamics of the USD system are not turbulent, extrapolating N_p to the transitional regime (from turbulent reference values) is ambiguous and depends in part on impeller type (Couper et al., 2010; Hemrajani and Tatterson, 2004; Leentvaar and Ywema, 1980). However, there are many sources suggesting a mild depression of N_p is observed in the transitional regime when compared to the fully turbulent condition. Rushton showed that when N_{Re} was between 100 and 10,000, the N_p was lower than the corresponding constant value in the turbulent regime, a finding corroborated in a recent review by Ghotlie et al. and others (Afshar Ghotli et al., 2013; Rushton et al., 1950; Van de Vusse, 1955). These analyses are directionally useful and further support the notion that the N_p of the magnetic stirrer in our system is significantly less than 2.

One approach for estimating N_p is to deduce it from the empirical relationship between mixing constants and reactor parameters (Tatterson and Kyser, 1991). To assess the suitability of this approach, the blend time data from Figure 4.2 using the two highest impeller speed at 0.5 mL and 1.0 mL liquid volumes was fit to turbulent and transitional correlations (N=8)(Table 4.2). In a similar manner, we used the turbulent correlations that included an N_p term (N=6) to calculate the average N_p for the magnetic stir bar to be 0.7 ± 0.7 . An effective lower limit of 0.2 for N_p applies as lower drag coefficients have not been reported in literature for any impeller geometry (Couper et al., 2010; Doran, 1995; Hemrajani and Tatterson, 2004; Post, 2010). This mixing time-derived estimate of N_p combined with the literature inferences described above led us to assign $N_p=1$ for the magnetic stir bar in the ultra scale-down HTPC system when $N \geq 10 \text{ s}^{-1}$. To the best of our knowledge, this is the first published N_p for a characterised magnetic stir bar and will be of practical value to other researchers who are interested in calculating power input in a baffled system agitated with a stir bar.

4.4.3.3 Heat Transfer

In Figure 4.3, the heating performance of the USD flocculation apparatus in achieving an arbitrary 50°C set point was measured. The utilisation of copper shot to fill the air voids between base of the microplate base and the floor of the heating block greatly improved the heat transfer rate. The addition of aluminium sealing tape and an aluminium shroud provided insulation and enabled the target temperature range to be attained much more quickly. The foil tape was demonstrated to produce marginally faster heating than the aluminium tent alone (data not shown).

There was a minor effect of volume on the heating performance with larger volumes requiring more time to heat. For mixing and heating performance, 0.75 mL of liquid represents an ideal volume for HTPD. With this configuration, 30 minutes is required to attain a set point of 50°C, which is comparable to larger scale reactors. Maintaining similar heating profiles and hence, similar isothermal aging times, help minimize heat transfer-related scaling artefacts.

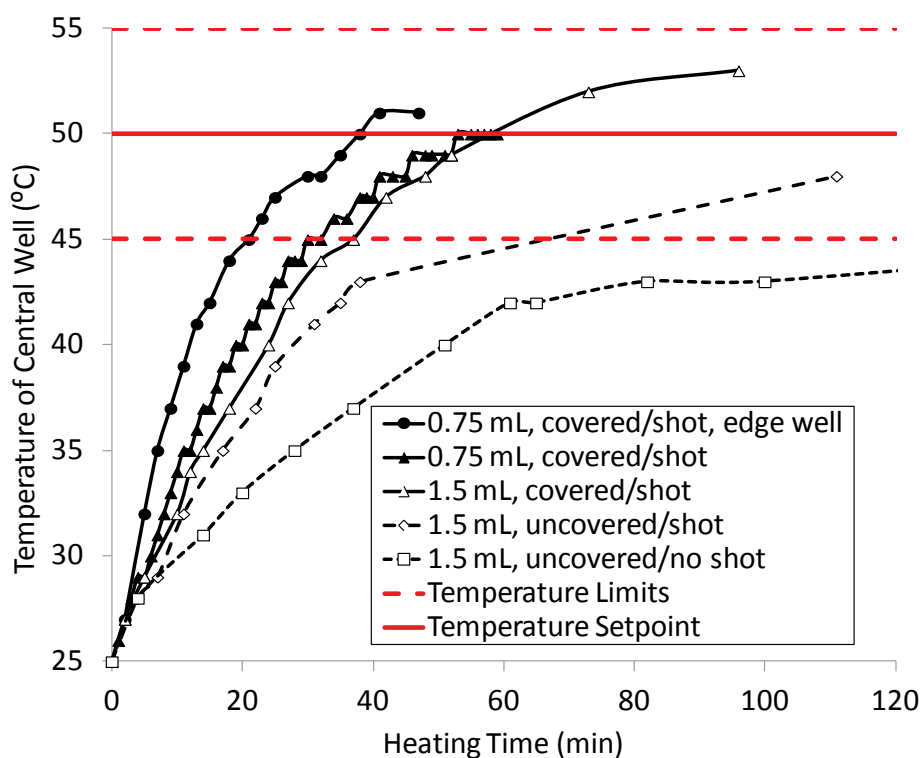


Figure 4.3. Heat transfer in the microplate for different volumes with various insulation configurations. The same volume of water (see legend) was added to all 96 wells. The temperature target was $50^{\circ}\text{C} \pm 5^{\circ}\text{C}$ and the starting water temperature was 25°C . The temperature was measured with a small wire thermocouple set in a central (E6) or an edge (A1)(where noted in legend) well of the microplate to monitor the slowest and fastest heating times, respectively. “Shot” refers to the presence of a bed of conductive copper shot (Figure 4.1) and “covered” refers to the presence of an aluminium sealant over the microplate and an aluminium shroud over the microplate and heating block.

4.4.3.4 Hydrodynamics

For some engineering characteristics, the microplate system can approach conditions present in the larger scale systems (Table 4.1). P/V_{avg} can be matched owing to the small volume and high rotational speeds. Indeed, the P/V in the impeller swept volume, P/V_{imp} , a measure of the maximum local

energy dissipation rate (ϵ_{\max}), can be set to match or greatly exceed large scale reactors owing to the high ratio of impeller swept volume to total volume. Similarly, the Kolmogorov micro-scale of turbulence, λ_{Kavg} and/or λ_{Kimp} , can be made equivalent between scales, whether the turbulence field is restricted to the impeller-swept zone or includes the entire tank. Maintaining this characteristic constant with scale-up increases the probability that particles of similar size will be sustained by meso-mixing during the aging process.

The heterogeneity of energy dissipation throughout the reactor differs greatly with scale-up, especially between the USD and Pilot-scale reactors qualified in this investigation. This is important because the regions of higher ϵ and accordingly smaller characteristic scales of turbulence are more likely to determine floc strength and size distributions than the respective regions defined by low values of ϵ . The maximum ratio of local to average energy dissipation rate ($\frac{\epsilon_{\max}}{\epsilon_{\text{avg}}}$) found across the reactor volume decreases with decreasing scale and with increasing D/T (Geisler et al., 1994; Hall et al., 2005)(Table 4.1). One reason for this is that the USD system has a very high D/T ratio, leading to more uniform distribution of energy dissipation rates across the vessel. Conversely, commercial-scale reactors have much smaller impeller-swept zones and consequently, much greater variation of energy dissipation rates across the tank volume. The flocs will experience the full range of conditions during the aging processes and this divergence between scales can affect floc morphology. Since ϵ_{\max} in the USD system is a smaller multiple of ϵ_{avg} than in larger scale systems, selection of an ϵ_{avg} condition in the USD vessel that approximates the most aggressive condition in the larger reactor (*i.e.* ϵ_{\max}) is critical. This relationship forms the foundation for scale-up by maintaining P/V_{imp} , as the impeller swept volume is the zone characterised by the highest shear and largest ϵ .

Shear rates and energy dissipation rates drive mass transfer in stirred vessels but it is more difficult to match shear than ϵ when scaling between reactors (Geisler et al., 1994). Maximum shear rates, which are proportional to v_{tip} , increase with scale, while the mean shear rate can decrease (Hemrajani and Tatterson, 2004; Metzner and Taylor, 1960). The v_{tip} of commercial-scale reactors are often defined by fixed gearboxes that dictate a minimum N and hence a minimum v_{tip} . The minimum value of v_{tip} is generally large, rendering scaling by constant v_{tip} impractical in many cases. In our current work, v_{tip}

was the same order of magnitude in all systems, but even when maximally powered at 17 s^{-1} , the USD stir bar value was lower than the large scale systems by a factor of ≥ 2 (Table 4.1). Indeed, the maximum turbulent shear stress, normalized for tip speed ($\frac{\tau_{turb}}{\rho v_{tip}^2}$), in the USD reactor was calculated to be up to 1/6 lower than in the largest reactors (Table 4.1). The consequence of lower, albeit more uniform shear rates present in HTPC reactors can lead to alterations in particle breakup and re-formation processes.

The engineering characterisation has provided insight into hydrodynamic differences between USD and large-scale reactors. In general, in the USD reactor, mixing times will be shorter; energy dissipation, eddy size, and shear rates will be lower and have less heterogeneity; turbulent-like conditions will exist; and heat transfer rates will be marginally slower. With careful system design and modulation of operating parameters, the hydrodynamic environments between USD and large-scale differences can be minimized. Square cross-section microwells have been deduced to be a reasonable representation of a baffled cylindrical tank with a single central impeller. The complex interplay between these hydrodynamic parameters and their effect on particle populations and associated centrifugation and/or filtration operations, explain the need to evaluate empirically different scaling heuristics.

4.4.4 Demonstrating Industrial Platform Scalability

The establishment of a platform approach for the development of particle conditioning operations requires that a variety of feedstreams be tested during the initial development phase. In doing so, the industrial practitioner meets an array of large-scale equipment that differ from lab to lab, manufacturing suite to manufacturing suite, internal site to internal site; with system differences potentially exacerbated if contract manufacturing organizations are involved. This description reflects the reality of many industrial operations: geometric similarity of stirred tanks upon scale-up should not be expected and often time might not be logistically possible. Hence, it is critical that scaling approaches designed for industrial processes accommodate this situation and strive to be applicable to as broad a range of vessels as possible.

Fortunately, as is evident in Table 4.1, if the feedstreams share a few common fluid properties, groups of scaling terms can be matched simultaneously. If feedstreams have similar physicochemical characteristics such as viscosity and density and if aging times are standardised, matching of P/V will result in comparable Kolmogorov characteristics lengths, Camp numbers, and integrated liquid stress factors. This is true whether P/V (and derivative values) are averaged over the entire stirred tank or limited to the impeller-swept volume. In addition, holding factors such as blend time constant during scale-up is so limiting as to be impractical, thereby reducing the design choices the process designer must make.

4.4.5 Particle Conditioning with Polysaccharides

This section will examine four examples where HTPC with CPS was scaled up to Pilot-scale. The aim was to align responses hypothesised to be dominated by thermodynamic equilibria, such as impurity removal, product yield, and quality with more hydrodynamically sensitive responses such as particle distributions and clarification between HTPC and Pilot-scale. In the first two examples (Figures 4.4-4.7), the scalability of impurity, product yield, and product quality (*i.e.* MW) responses was examined across a full factorial experimental space. In the third example (Figure 4.8), particle characterisation was used to identify improved scaling heuristics. In the final example, centrifugal effects were decoupled from flocculation effects while illustrating how HTPC can be employed to identify operating windows of operations.

4.4.5.1 Flocculation with *Staphylococcal CPS (SA1)*

Using SA1 broth, a full factorial HTPC screen was run at the 1.2 mL scale (Table 4.1: B), with a subset of conditions performed in 3.5 L reactors (Table 4.1: A), representing a 3-log scaling factor.

Operational parameters were based on prior experience and ensured vigorous mixing as determined visually. There was no effort made to utilise a specific scaling rule. The filtered contour plot of product yield in Figure 4.4a allows a point-to-point comparison while the full contour plot in Figure 4.4b describes the broader knowledge space.

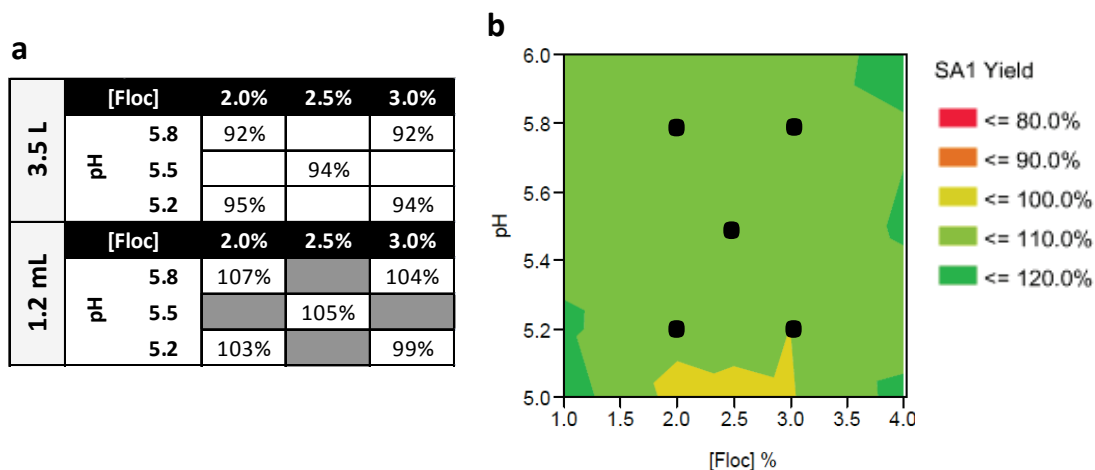


Figure 4.4a, b. CPS yield (percentage of load control) in the supernatant as a function of the floc agent concentration and pH during the flocculation process for staphylococcal CPS SA1. Results for identical conditions at the 1.2 mL (average of duplicates) and 3.5 L scales (single measurement) are presented in the matrix on the left, with gray boxes denoting 1.2 mL data withheld to maintain the comparison pattern (4.4a). Conditional formatting was not employed because the values are considered to be within the error of the assay. Full factorial results for the 1.2 mL system (average of duplicates) are provided in the contour plot on the right where floc agent percentage = 1.0, 2.0, 2.5, 3.0, 4.0, pH = 5.0, 5.2, 5.5, 5.8, 6.0, and black squares represent conditions (single measurement) tested at the 3.5 L scale (4.4b).

The recovery of product was comparable between the two scales. The slight difference in mean yield between the two scales is due to analytical imprecision in determining titre in complex load samples. Product quality, as informed by MW was measured for the same conditions (Figure 4.5). Normalized MW were comparable between the two scales and were not influenced across the tested operating ranges (Figure 4.5). As with MW, r_{rms} did not change across the test range, indicating that the conformation of the polysaccharides were not affected by these conditions (data not shown). Finding that product yield and quality were constant across the experimental space enabled the optimization of the step to be performed with respect to impurity clearance.

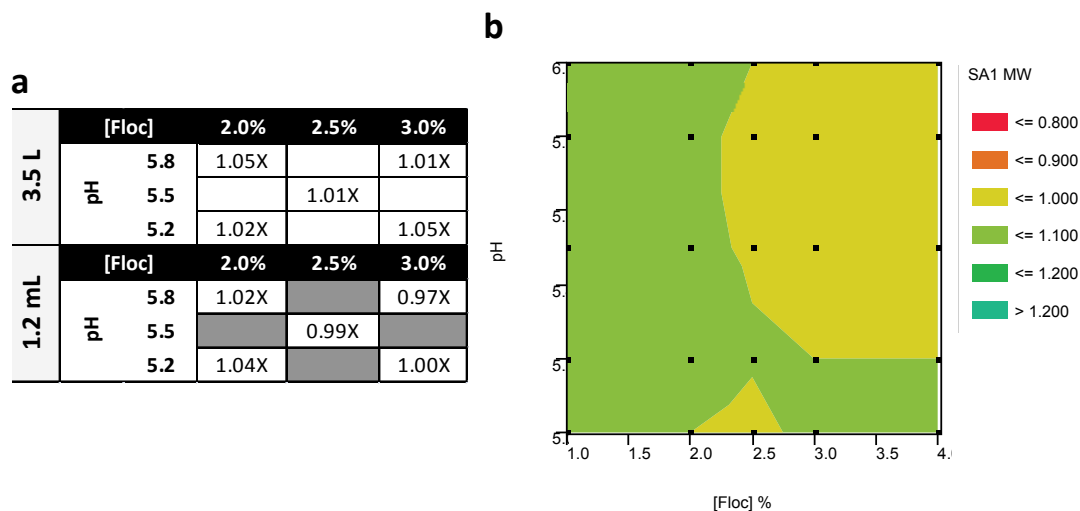


Figure 4.5a, b. CPS MW (relative to the mean MW for both scales at 2.5% floc agent concentration/pH 5.5) in the supernatant as a function of the floc agent concentration and pH during the flocculation process for staphylococcal CPS SA1. Results for identical conditions at the 1.2 mL (average of duplicates) and 3.5 L scales (single measurement) are presented in the matrix on the left, with gray boxes denoting data withheld to maintain the comparison pattern (4.5a). Conditional formatting was not employed because the values are considered to be within the error of the assay. Full factorial results for the 1.2 mL system (average of duplicates) are provided in the contour plot on the right where floc agent percentage = 1.0, 2.0, 2.5, 3.0, 4.0, pH = 5.0, 5.2, 5.5, 5.8, 6.0, and black squares represent data points used to generate contour plots at the 1.2 mL scale (4.5b).

Protein concentrations were constant across the screen. Responses that shift significantly across the experimental space are needed to test scalability rigorously. DNA clearance was the response with the largest change across the experimental space and is detailed in Figure 4.6. DNA clearance was a strong function of pH and floc agent concentration with better removal observed at lower pHs and higher floc agent concentrations. Very similar absolute values and trends were observed at both scales. Spectroscopic measurements of turbidity also exhibited variability across the experimental space highlighted in Figure 4.6 and like DNA, showed good comparability between scales (data not shown).

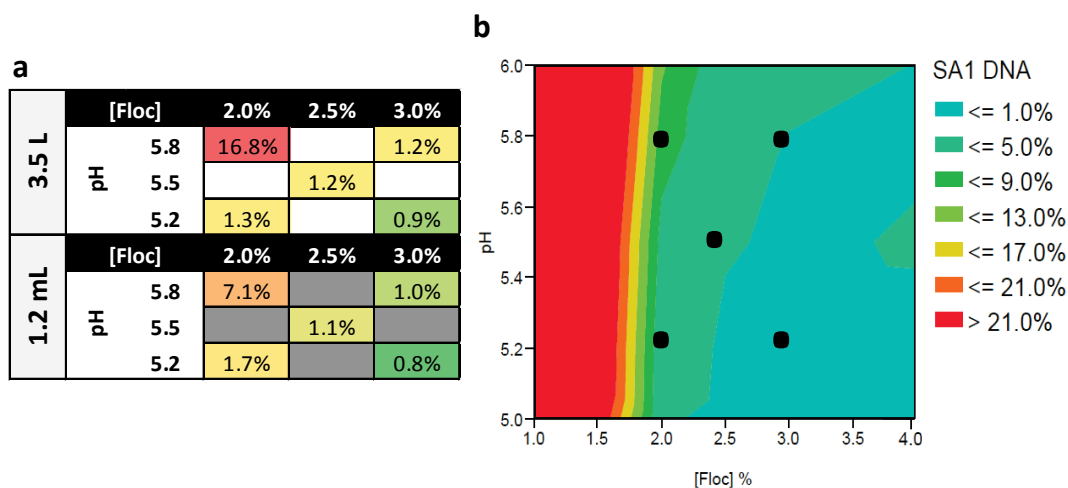


Figure 4.6a, b. DNA clearance (percentage of load control) in the supernatant as a function of the floc agent concentration and pH during the flocculation process for staphylococcal CPS SA1. Results for identical conditions at the 1.2 mL (average of duplicates) and 3.5 L scales (single measurement) are presented in the matrix on the left, with gray boxes denoting data withheld to maintain an identical comparison pattern (4.6a). In 4.6a, conditional formatting was performed as a single group to facilitate inter-scale comparison. Full factorial results for the 1.2 mL system (average of duplicates) are provided in the contour plot on the right where floc agent percentage = 0, 1.0, 2.0, 2.3, 2.5, 2.7, 3.0, 4.0, pH = 5.0, 5.3, 5.5, 5.7, 6.0 (4.6b). The large black squares represent conditions run at the 1.2 mL and 3.5 L scales.

In Figure 4.6a, a performance cliff was identified with the HTPC screening. The cliff occurred in an area just outside the process acceptable ranges (PAR) that were tested at Pilot-scale (Figure 4.6b). Due to limited resources, testing a broad operating parameter range outside of the design space is not routinely done at Pilot-scale. HTPC allows for the generation of this additional information, which informs how an initial design space could be adjusted to improve robustness.

With SA1, the performance of the USD system generally matched the Pilot-scale system. Product yield, product quality (MW, r_{rms}), and protein clearance (data not shown) were consistent between scales and conditions. A broad range of responses was observed for DNA clearance, with consistent

removal demonstrated between scales, meeting the most rigorous requirements for USD platforms. A 2-log removal factor for DNA was achieved at both scales. This value is substantial for a single stage particle conditioning step and approaches the selectivity achieved with chromatographic separations (Bonnerjea et al., 1986). This result underscores the performance that can be achieved with particle conditioning when conditions are optimized with HTPC.

4.4.5.2 Flocculation with *Staphylococcal* CPS (SA2)

A full factorial HTPC screen was run with SA2 broth at the 1.2 mL scale (Table 4.1: C), with a subset of conditions performed in 3.5 L reactors (Table 4.1: B), representing a 3-log scaling factor. The respective DNA clearance is depicted in Figure 4.7. The application dictates which particular scaling approach is appropriate. The studies with SA1 and SA2 utilised set points determined empirically to promote vigorous mixing. In these studies, most data between the 1.2 mL and 3.5 L scales were comparable. The exceptions occurred with DNA clearance for SA2 that, although showing similar trends, yielded inferior removal at the Pilot-scale (Figure 4.7). When further scale-up to clinical-scale reactors was considered, the scale-dependency was more pronounced (data not shown). The discrepancy in DNA removal that occurred in experimental areas defined by the sharpest response gradients was apparent. Results obtained in these areas are the most sensitive to minor offsets in process parameters and altered hydrodynamics between scales. Given the lower energy input in the USD reactor than in the Pilot-scale reactor, it is conceivable that the flocs produced in the USD system were larger (due to less intense mixing than at the 700 L scale) and therefore removed more effectively by the centrifugation step, thereby enhancing purification.

he conditions comprising the sharp response gradients were also characterised by inferior purification at Pilot-scale. This observation might be due to the presence of weaker and more reversible interactions between the particulates constituting the flocs, leading to inferior floc strength. Flocs of reduced mechanical strength are more likely to disintegrate or fragment at larger scales where shear forces are higher, leading to inferior clarification via centrifugation or filtration, which would explain the corresponding decrease in DNA removal that was observed. Hence, the scale differences might be due to the strength of the flocs. To elucidate whether the scaling differences were due to a slower

rate of floc formation, an examination of the flocculation kinetics was undertaken (Appendix 9.6: Flocculation Kinetics at the Micro-scale). Kinetics at the micro-scale were not representative of the larger scale and opportunities to measure kinetics at larger scale were not available, thus scaling approaches were further investigated.

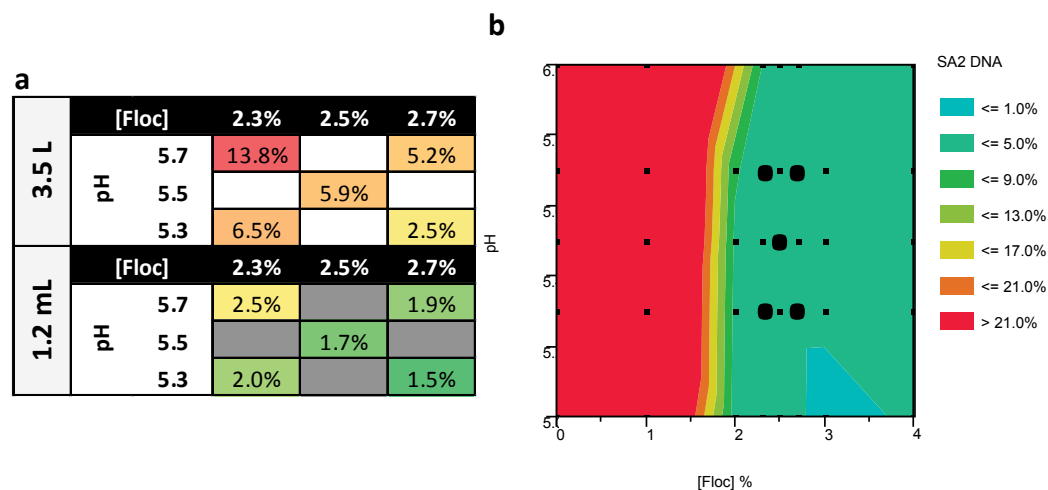


Figure 4.7a, b. DNA clearance (percentage of load control) in the supernatant as a function of the floc agent concentration and pH during the flocculation process for staphylococcal CPS SA2. Results for identical conditions at the 1.2 mL (average of duplicates) and 3.5 L scales (single measurement) are presented in the matrix on the left, with gray boxes denoting data withheld to maintain an identical comparison pattern (4.7a). In 4.7a, conditional formatting was performed as a single group to facilitate inter-scale comparison. Full factorial results for the 1.2 mL system (average of duplicates) are provided in the contour plot on the right where floc agent percentage = 0, 1.0, 2.0, 2.3, 2.5, 2.7, 3.0, 4.0, pH = 5.0, 5.3, 5.5, 5.7, 6.0, with each condition represented by small black squares (4.7b). The large black rounded squares represent conditions run at the 1.2 mL and 3.5 L scales.

TOverall, impurity clearance, product yield, and product quality were comparable between scales except for the noted DNA differences. Although minor, these discrepancies underscored the need to develop a rational basis for scaling up of particle conditioning processes, supported with scale-up

data. In order to assess scaling approaches and to investigate the differences conferred by different bacterial and polysaccharide serogroups, several additional scale-up studies were performed.

4.4.5.3 Flocculation with Meningococcal CPS

To address the effect of hydrodynamic differences on floc particle populations, we measured particle size distributions for flocculated MnC broth under a range of conditions. Previous experience had identified particle characterisation of the aged flocs as the most sensitive measurement to processing conditions (DNA removal was equivalent between scales) and therefore the best surrogate for assessing scaling fidelity.

Particle properties are critical for effective downstream clarification, whether by centrifugation and/or depth filtration. Particle concentration is informative for assessing the extent of flocculation and corresponding purity after bucket centrifugation. However, particle concentration might be altered during downstream operations at larger scales due to phenomena such as shear-induced fragmentation of particulates. The volume-average mean size ($D[4,3]$) of particles largely determines the centrifugation efficiency, given the size dependency expressed in Stokes' Law. Large particles can also blind downstream depth filters, leading to cake formation and decreased throughput (Singh et al., 2013). For filterability, the number-average mean size ($D[1,0]$) is more informative. This value indicates the size of the bulk of the particles that can bind to and plug the filter. In conjunction with particle concentration, a mean number-average particle size provides information on relative surface area, which have been correlated with pressure increases in depth filters (Darby and Lawler, 1990). In addition, the smallest particles ($< 2 \mu\text{m}$), typically the most abundant in a heterogeneous floc preparation, can pass through filters leading to undesirable residual turbidity.

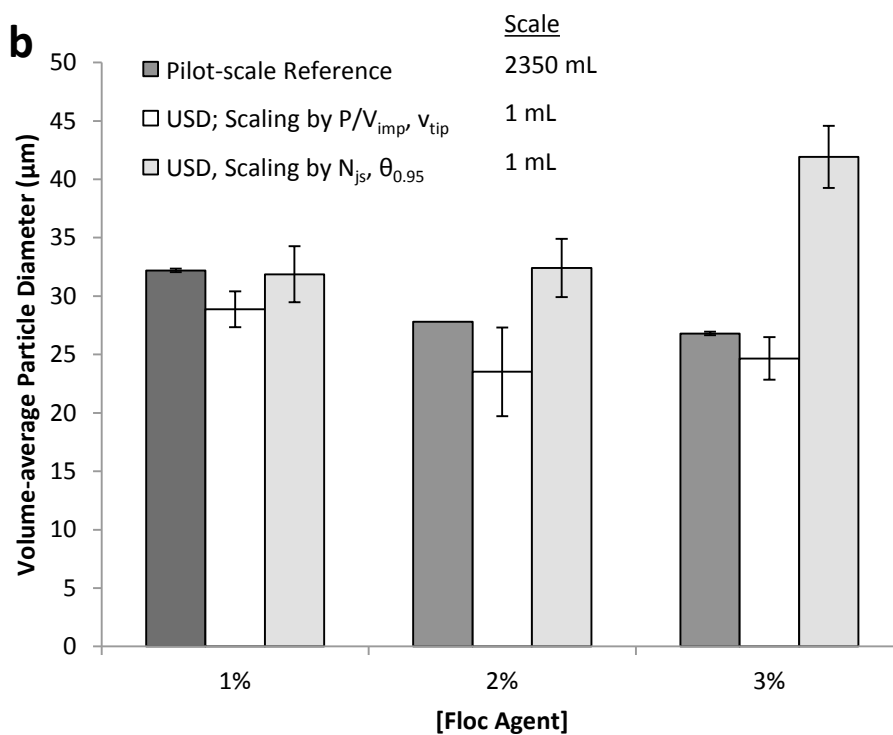
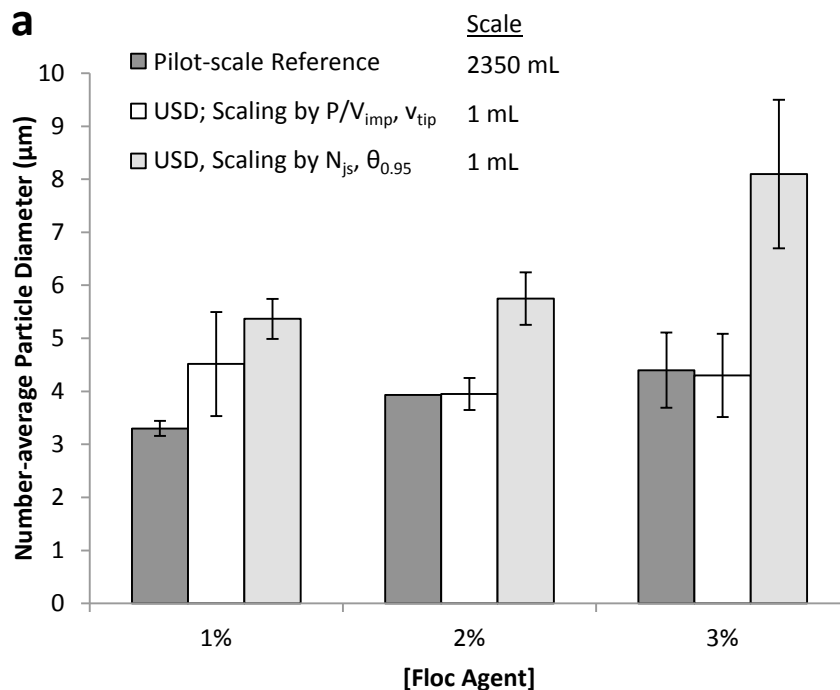
Mixing parameters were scaled by maintaining N_{js} , the just suspended stirrer speed, which equates to the minimum energy input required to ensure that particles remain suspended and hence, the maximum surface area of particles is available for mass transfer or reaction (Atiemo-Obeng et al., 2004). Determination of N_{js} relied on a visually determined Zwietering criterion. Because the feedstreams and aging times at both particle conditioning scales were identical, coincidentally, this

scaling approach matched P/V_{avg} and λ_{kavg} (Table 4.1: C, D). Time-integrated forms of these scaling terms such E_f , Ca were also kept constant.

Fast blend times in HTPC and extreme energy demands at large-scale preclude the maintenance of blend time during scale-up to very large commercial stirred tanks. However, scaling by N_{js} , the stirrer speed needed to provide the minimum amount of lift to keep all particles suspended, offered comparable blend times across the vessels.

4.4.5.3.1 Scaling by N_{js} and Blend Time

To assess the suitability of scaling by N_{js} (and blend time across a limited scale range), flocculation with meningococcal CPS broth was performed as described in Table 4.1: C, D. Meningococcal broth was flocculated in 1.2 mL and 2.4 L reactors (Table 4.1: C, D). Full factorial HTPC screen with factors of pH and floc agent concentration was performed (Figure 4.8). In general, similar trends were seen at both scales, with size and counts increasing with increasing floc agent concentration and pH having no significant effects. However, when scaling by N_{js} , the particle sizes (both number- and volume-average) and concentrations differed markedly between the 1.2 mL and 2.4 L scales and grew worse as the floc agent concentration increased. Under these conditions, particles were larger in size and fewer in number in the 1.2 mL vessel than at the 2.4 L scale. Critically, the percentage solids for a given condition at both scales were comparable. This indicated that the difference was due not to the mass of material partitioning between the scales, but the larger hydrodynamic forces that were breaking, eroding, and re-forming the particles at the 2.4 L scale.



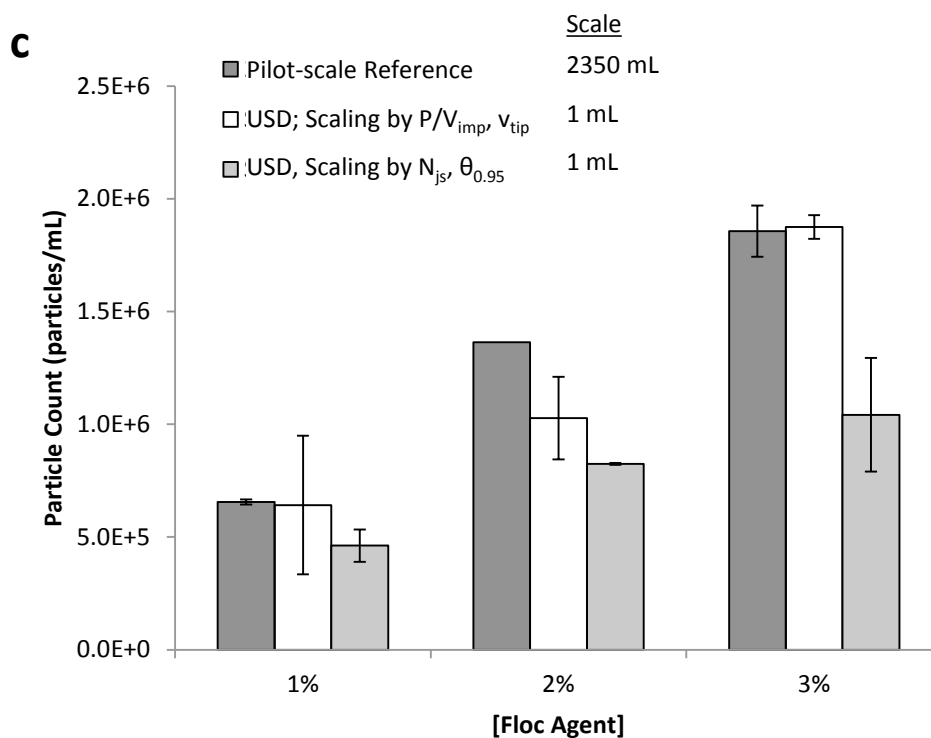


Figure 4.8a, b, c. Scaling by N_{js} , P/V_{avg} , λ_K , E_f , Ca , or v_{tip} , P/V_{imp} , λ_{kimp} : Effect of scaling meningococcal flocculation using different scaling rules on MFI-derived particle characterisation. Number-average particle diameters (4.8a), volume-average particle diameters (4.8b), and concentrations of the raw floc suspension diluted 100-fold diluted (4.8c). The pH did not influence results and for a given floc agent concentration, the results for all pH set points were averaged (three wells for each USD point; two reactors for each Pilot-scale point). The error bars denote the standard deviation. For HTPC, a full factorial screen was performed with floc agent percentage = 1.0, 2.0, 3.0 and pH = 4.5, 5.0, 5.5. For Pilot-scale, the floc agent percentage/pH conditions were 1.0/pH 4.5, 1.0/pH 5.5; 2.0/pH 5.0, and 3.0/pH 4.5; 3.0/pH 5.5.

4.4.5.3.2 Scaling by P/V_{imp}

As shown in Figure 4.8, the results obtained when scaling with constant N_{js} suggested that the power input and/or impeller-induced shear in the USD flocculation reactors were low relative to the 2.4 L scale environment. To increase unit energy input, three changes to the USD system were made: the

working volume was reduced to increase P/V , the stirrer speed was increased to increase P/V and tip speed, and orbital shaking during initial mixing was replaced with magnetic stirring. These combined changes ensured that the P/V_{imp} in the two systems was matched for the subsequent trial.

Flocculation was repeated with the refined operating conditions and the same feed material at the 1 mL scale and compared to the previous results at the 2.4 L scale (Table 4.1: E, D; Figure 4.8).

Clarification and impurity removal were again comparable between scales (data not shown). In general, the higher powered USD system, which matched the v_{tip} and P/V_{imp} in the Pilot-scale reactor produced particles significantly smaller in size and higher in particle concentration than the lower powered USD system scaled by N_{js} (Table 4.1: E, C). This was true for number- or volume-based size distributions and was seen across the distribution of particles. Moreover, there was a convergence of mean particle size and counts between the 0.8 mL and the 2.4 L reactors, when P/V_{imp} was maintained between the systems. By matching P/V_{imp} and v_{tip} during the mixing step of particle conditioning, the particle counts and mean particle sizes (number- and volume-average) were similar between USD and Pilot-scale. This outcome suggests that absent differences in floc strength, downstream clarification of these suspensions would have comparable performance.

We conclude that differences in the particle populations were driven by differential hydrodynamic environments. This phenomenon is consistent with enhanced particle breakup mediated by increased levels of input energy and shear. P/V_{imp} and v_{tip} characterise the most vigorous local environments that a given particle will be exposed to during aging. Since all flocs will pass through the impeller zone multiple times during the aging process, it is reasonable that the local energy dissipation (therefore characteristic scale of turbulent eddies) and maximum shear rates will be decisive factors in determining the extent of particle break-up. This critical relationship may explain why scaling flocculation by holding P/V_{imp} and/or v_{tip} constant proved the most successful scaling strategy. The number of passes a particle makes through the impeller region will be a function of aging time. Therefore, the time-integrated factors, $P/V_{imp} t$ or $\overline{G}_{imp} t$ may represent the most relevant permutations on P/V_{imp} . Alternatively, a scaling factor of $v_{tip} t$ is equally supported by the data.

Changing to scaling by constant time-integrated v_{tip} or P/V_{imp} enabled the USD system to produce particles similar in characteristics to the Pilot-scale reactor, which differed by a scaling factor of 3100X. This outcome approached the most stringent USD goal of achieving accurate absolute values and did so for the most scale-sensitive assay.

4.4.5.4 Flocculation with Pneumococcal CPS

With scaling established between the USD system and small Pilot-scale models using staphylococcal and meningococcal feedstreams and maintaining P/V_{imp} or v_{tip} , the scalability from HTPC to a larger, 13 L Pilot-scale reactor (Table 1: F) was explored with a pneumococcal broth that contained a neutral CPS.

4.4.5.4.1 Effect of Centrifugation Conditions

The 13 L floc reactor produced sufficient material to run a semi-continuous disk stack centrifuge (DSC). This enabled a further refinement of the HTPC model to connect the clarification of batch centrifugation to semi-continuous centrifugation (Figure 4.9). As described in Methods, the operational parameters of the microplate centrifuge were optimized to match the clarification performance of the DSC for a crude pneumococcal floc sample.

Crude flocs from three Pilot-scale preps of pneumococcal flocs were spun independently in a CSC-6 DSC (Figure 4.9, dark gray bars) and in a swinging bucket centrifuge fitted with microplate adapters (Figure 4.9, light gray bars). The yield (data not shown), purity, and clarification results obtained with both types of centrifugation equipment were equivalent (Figure 4.9). The CSC-6 was operated at Q/Σ of 8.1×10^{-9} m/s. To match performance, the microplate centrifuge required Q/Σ of 4.4×10^{-8} m/s (Russell et al., 2007). As has been observed with PEG- and ammonium sulphate-precipitated yeast protein, scaling centrifugation by maintaining Q/Σ in a swinging bucket centrifuge leads to slight over-clarification (Maybury et al., 2000). The shear present in a DSC has been shown to degrade precipitated material during processing (Boychyn et al., 2004). Demonstrating the low sensitivity of this particular flocculation system to shear from centrifugation enabled the effective decoupling of flocculation effects from the centrifugation effects for this pneumococcal trial. This may seem

counter-intuitive based on previous work but under these conditions and with this particular serotype, there was no discernible difference whether a low shear swinging bucket centrifuge or a higher shear DSC was employed (Boychyn et al., 2000; Chatel et al., 2014; Maybury et al., 2000; Tait et al., 2009).

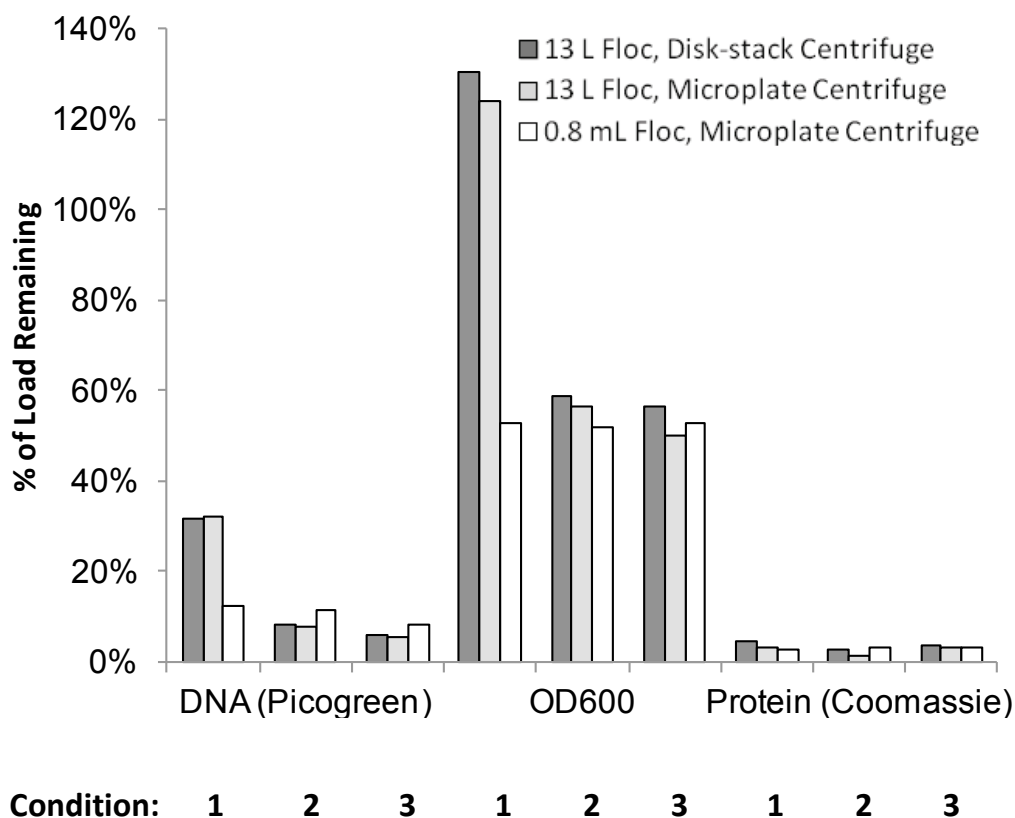


Figure 4.9. Scaling by P/V_{avg} , λ_{kavg} , E_f , and/or Ca: Flocculations with a neutral pneumococcal CPS were performed at the 13 L scale (single measurement) and centrifuged in a semi-continuous disk-stack (dark gray bars) or in a swinging bucket (light gray bars) centrifuge. Flocculation was also performed under equivalent conditions at the 0.8 mL scale (in triplicate) and centrifuged in a swinging bucket centrifuge (white bars). The three conditions run at Pilot-scale were 2% floc agent concentration combined with one of three pH/Ca conditions: (1) pH 3.7/Ca = 6.5×10^5 ; (2) pH 3.5/Ca = 9.7×10^5 ; and (3) pH 3.2/Ca = 1.3×10^6

4.4.5.4.2 Scaling by P/V_{avg}

To assess the influence of pH and Ca, three conditions were scaled down from a 13 L bioreactor to HTPC (Table 4.1: E, F)(Figure 4.9: white and dark gray bars, respectively). Mixing parameters were scaled by maintaining P/V_{avg} and Ca during the aging process. Because feedstreams were constant and mixing times were fixed, Ca, E_{fr} and λ_{kavg} were also maintained (Table 4.1: E, F). The Pilot-scale reactor was operated in the turbulent regime and was geometrically similar (*i.e.* equivalent Z/T, D/T, and impeller parameters) to commercial-scale (Table 4.1: A), providing good confidence in the scalability of the results to commercial-scale (Kresta and Brodkey, 2004). In these trials, the product recovery was excellent and the impurity clearance of DNA and protein were substantial. Moderate clarification, as determined by A_{600} , was observed although this method was characterised by low sensitivity and tended to underestimate solids removal. Importantly, yield, protein, DNA clearance, and turbidity were equivalent between the two scales for two of the three tested conditions, which included the centerpoint. As will be discussed later, the condition which lay in a region where responses were strongly dependent on small changes in factors (*i.e.* Condition 1), did not appear to scale well.

4.4.5.4.3 Effect of Camp Number

To maximize floc strength, many flocculation processes are designed to achieve $Ca \geq 10^5$ (Bell et al., 1983). In order to probe the effect of Ca on the entire pH and floc agent concentration experimental space, a three factor, full factorial design was performed at the 0.8 mL scale (Table 4.3). The same outputs examined in Figure 4.9 were measured and are reported in Table 4.3. Lowering the pH had a pronounced effect on all three impurity responses, while increasing the floc agent concentration and/or increasing the aging parameter, Ca, improved purity to a lesser extent. Clarification enhancements mediated through Ca or floc agent concentration were most significant in areas where overall flocculation performance was inferior, such as the region characterised by low floc agent concentration and higher pH (*e.g.* pH 3.7, 4.0). As with the staphylococcal CPS examples (Figure 4.6 & 4.7), HTPC enabled the presence of a performance cliff to be resolved thoroughly.

Statistical models of the responses were generated with standard DOE analysis (Figure 4.10).

Table 4.3. A full factorial flocculation study at the 0.8 mL scale was performed with a neutral pneumococcal CPS. Results are illustrated for clarification (A_{600}) (4.3a), DNA clearance (4.3b), and protein clearance (4.3c) in the centrate as a function of the flocc agent concentration, pH, and Ca. Values are given as percentage of load control. For each assay, conditional formatting was performed as a single group to facilitate inter-scale comparisons, where cells in white are BLOQ or discarded samples. The cells outlined in blue represent the conditions in Figure 4.9, albeit with data from USD- instead of Pilot-scale. For comparison purposes, the last row of data in each matrix shows the corresponding performance of the 13-L reactors spun in a DSC (Figure 4.9). Each condition was run once.

a

% A_{600}	Gt	6.5×10^5			9.7×10^5			1.3×10^6		
	[Floc agent]	1%	2%	3%	1%	2%	3%	1%	2%	3%
pH	4	129%	59%	56%	125%	58%	55%	111%	56%	55%
	3.7	116%	53%	50%	107%	53%	51%	91%	53%	51%
	3.5	54%	51%	49%	54%	52%	50%	55%	52%	50%
	3.2	52%	51%	48%	53%	51%		53%	52%	50%
	3	52%	49%	48%	53%	51%	49%	53%	50%	51%
13 L-Scale:			130%			59%			56%	

b

% DNA	Gt	6.5×10^5			9.7×10^5			1.3×10^6		
	[Floc agent]	1%	2%	3%	1%	2%	3%	1%	2%	3%
pH	4	112%	99%	26%	100%	101%	26%	109%	103%	31%
	3.7	52%	13%	7%	41%	14%	7%	42%	14%	8%
	3.5	13%	8%	6%	13%	8%	6%	13%	9%	6%
	3.2	8%	7%	5%	6%	6%		7%	6%	5%
	3	6%	5%	5%	6%	6%	5%	7%	5%	5%
13 L-Scale:			32%			8%			5%	

c

% Protein	Gt	6.5×10^5			9.7×10^5			1.3×10^6		
	[Floc agent]	1%	2%	3%	1%	2%	3%	1%	2%	3%
pH	4	8.7%	3%	2%	7.0%	2%	3%	6.2%	3%	2%
	3.7	6.5%	3%	3%	5.1%	2%	4%	4.7%	2%	3%
	3.5	3%	3%	4%	3%	3%	4%	3%	3%	3%
	3.2	3%	3%	4%	3%	4%		3%	4%	4%
	3	3%	4%	4%	3%	4%	4%	4%	4%	4%
13 L-Scale:			4.7%			3%			4%	

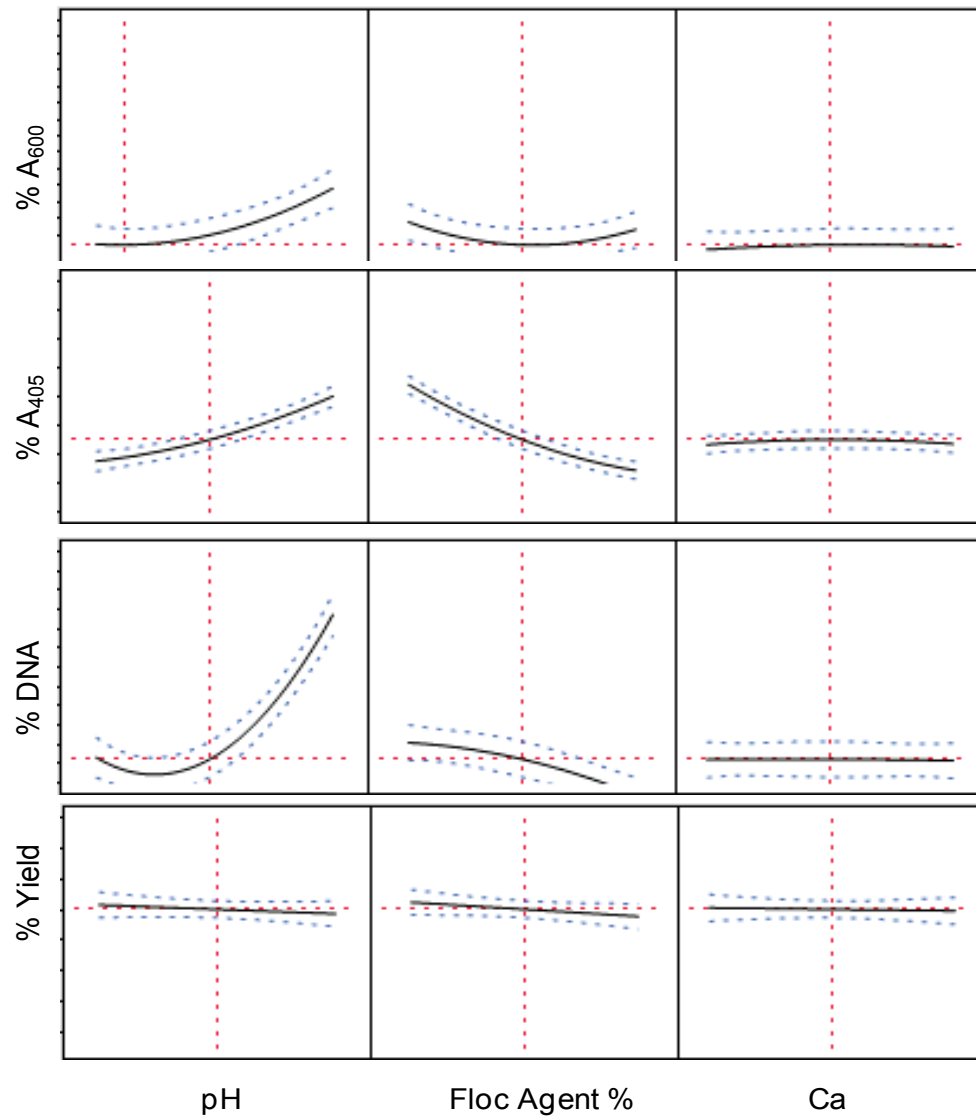


Figure 4.10. Statistical analyses from the full factorial HTPC with the neutral pneumococcal CPS (see Table 4.2). Effects plots for three factors where y-axis is percentage of load control remaining for four different responses. Protein clearance trends were not included because too many values were BLOQ to give trend lines for the full experimental window.

Ca had no effect on yield or DNA removal but improved the levels of protein clearance (Figure 4.10). However, the relative effect of Ca was substantially less than pH or floc agent concentration. In addition, although not evident in Figure 4.10, increasing Ca improved clarification for conditions at high pH (*i.e.* pH 3.7, 4.0).

A condition residing in both a region of inferior robustness and a sharp response gradient (*i.e.* pH 3.7, 2.0 % floc agent concentration) was scaled up to the 13 L scale. Clarification deteriorated with scale. The rich data afforded by HTPC enabled a better understanding of why the purification of this condition was more difficult to scale. This region is characterised by poor robustness because it encompasses a performance cliff. Table 4.3 clearly shows that the problematic condition resided in an experimental area where slight changes in input factors, set points, buffers, etc. would have a dramatic effect on the responses. Such areas are best avoided for a production process but useful for exacting tests of scalability. A similar outcome was obtained for this flocculation condition irrespective of the centrifuge employed for clarification, suggesting that P/V_{avg} , λ_K , and Ca were not optimal as the scaling metric for this pneumococcal serotype.

With scale-up by constant P/V_{avg} , λ_K , and Ca , several hydrodynamic properties changed (Table 4.1: E & F). Both the maximum turbulent shear stress in the tank ($\tau_{turb}/\rho v_{tip}^2$) and v_{tip} increased with scale. These changes would have altered the capability of the environment to support equivalent floc populations at two different scales, potentially leading to smaller particles and degraded purification at larger scale. Conversely, other parameters indicated conditions that would promote persistence of larger particles. The maximum ratio of energy dissipation rates present $(\epsilon_{loc}/\epsilon_{avg})_{max}$ was elevated for the Pilot-scale reactor, indicating the presence of regions of lower energy dissipation rates than in the USD model. The blend time increased markedly which may have further contributed to the formation of larger flocs, particularly since the Damköhler number was much greater than 1. Conceivably, these properties would have enabled the persistence of larger particles, which would have been readily removed by the low-shear batch centrifugation step leading to improved purification; however, the opposite effect was observed. Hence, the likely importance of $(\epsilon_{loc}/\epsilon_{avg})_{max}$ and blend time as scaling determinants diminished.

There are several ways to improve scalability. A tenable approach to bring the scales into closer alignment would be to scale by maintaining v_{tip} or P/V_{imp} constant, which would simultaneously increase shear stress and energy dissipation rates. Moreover, since aging time was consequential for performance, using the time-integrated variant of these two parameters would be warranted.

Alternatively, modifying the Camp number to substitute P/V_{imp} or v_{tip} for P/V_{avg} would preserve the correction for rheological effects. The influence of viscosity and density on the scaling of particle conditioning is unknown, besides what is reported in the literature for non-capsular polysaccharide systems (Doran, 1995).

The consistency of results between both scales in Table 4.3 qualified HTPC as a suitable scale-down model for the Pilot-scale system. Subsequently, a robust condition (Figure 4.9, Condition 2; Table 4.3) was scaled up to the 700-L scale and equivalent performance was demonstrated at all scales from 0.6 mL up to 700 L of broth, a 6 log range (Figure 4.11).

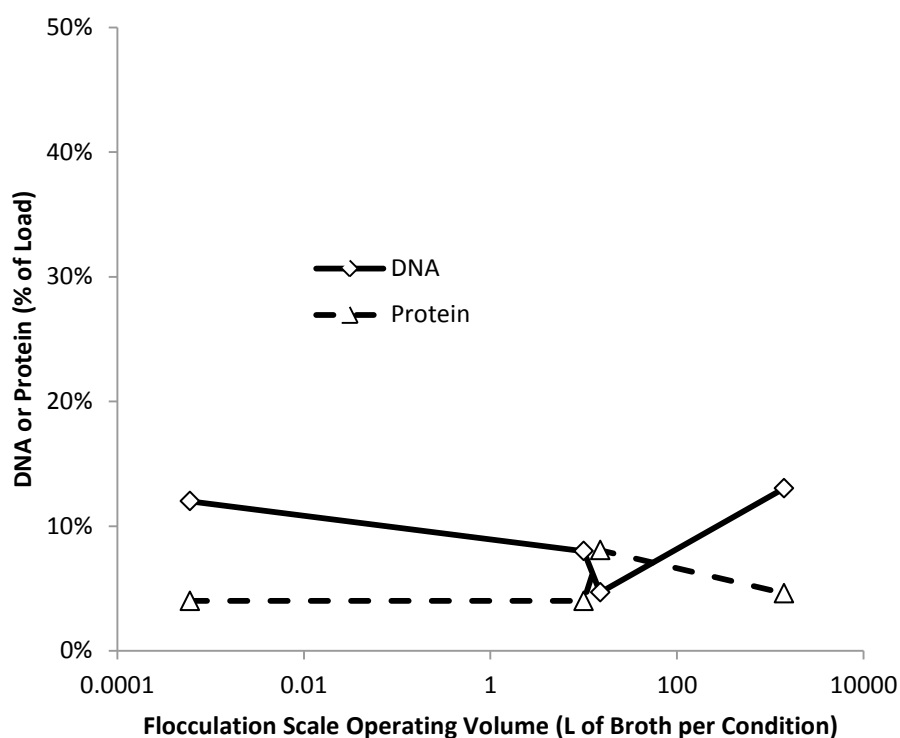


Figure 4.11. Scale-up of impurity removal from a particle conditioning step for a neutral pneumococcal CPS at 0.6 mL to 700 L. The condition tested at all scales was 2% floc agent concentration, pH 3.5, with $Ca = 6.5 \times 10^5$. USD points were in duplicate and all other points were single measurements.

Figure 4.11 substantiates the use of HTPC to emulate accurately clinical-scale performance. For DNA clearance and protein clearance, HTPC matched the performance of the largest scale and the intermediate scale condition from which the HTPC feed was drawn. The shift in performance at the intermediate scale may be due to many factors. There can be significant batch-batch variability in a process, especially across scales, tanks, cell line age, though the specific reason(s) for the range of performance observed intermediate scale are unknown. Given the variability inherent in scale-up and the equivalence of the three datasets, the Figure 4.11 is considered strong evidence of predictive and consistent scale-up from HTPC to production-scale.

HTPC can help fulfil some elements of Quality by Design. The high resolution performance context provided by HTPC enables the rapid identification of a design space that is large enough to provide ample process robustness. Appendix 8: Validation explores how the previous results can be implemented in a QbD framework for determination of a design space. Information from other sources regarding filtration, centrifugation, stability, etc. can be combined with the HTPC output to identify operating windows that deliver acceptable performance.

4.4.5.5 Do All Floccs Have the Same Composition?

Consideration of the divergent behaviour of assay responses offers insights into how different molecular classes are participating in the composition of the floccs. Neither DNA removal nor CPS yield were enhanced by increasing Ca (Figure 4.10). Moreover, in none of the described HTPC studies did CPS recovery vary across the experimental space. Therefore, it appears that CPS did not participate in most of the floccs and DNA was incorporated into floccs of large enough size and/or sufficient strength to enable straightforward centrifugal removal. Conversely, increasing Ca increased both clarification and protein removal for the trial with pneumococcal broth (Table 4.3). One explanation for this behaviour is that protein and possibly other unknown species contributing to turbidity form weaker floccs or reside on the outside of flocc particulates, both of which would be more sensitive to rearrangement from the hydrodynamic fields present during conditioning. The restructuring results in stronger floccs with properties more amenable to removal by centrifugation. This phenomenon could be compounded by slow flocculation kinetics for the protein impurities, where steady state

might not be reached until at least 120 minutes. Beyond offering mechanistic insights, these results underscore the importance of multi-faceted analyses when undertaking scaling exercises and of utilizing assays that are fit for purpose. Chemical assays are useful for tracking the population of a given molecular class but give only a narrow representation of the particle conditioning process and may be misleading if that molecular class is not evenly distributed (*e.g.* protein vs. DNA) among all the flocs. Conversely, particle characterisation of flocs is a non-specific technique that is insensitive to the differential composition of flocs. Particle sizing offers a general and very sensitive method for assessing the suitability of a scaling metric.

4.4.6 Sources of Scaling Discrepancies

In general, differences between scales were minor but it is instructive to consider potential sources of divergence. When the USD system was not operated to maintain P/V_{imp} or v_{tip} with the Pilot-scale reactor, it was effectively underpowered, leading to over-purification. For example, when the SA2 process was scaled up to the 1,000 L scale, the DNA in the centrifuged flocculated stream was found to be approximately 17% of the load (compared to 2% in the USD model; Figure 4.7). As with SA2, the HTPC results for SA1 were slightly more pure than the Pilot-scale reactor SA1 (Figure 4.7). Scaling by v_{tip} or P/V_{imp} instead of P/V_{avg} would have generated greater quantities of small particles that would be less efficiently removed by centrifugation, leading to decreases in HTPC purification and in these examples, greater consistency between the performance at both scales.

Conditions residing in regions of sharp response gradients are very sensitive to errors, noise, and variability in input factors, set points, buffers, etc. For instance, slight offsets between pH electrodes or titration endpoints and the innate variability in the titrations (*e.g.* concentration, volumes, etc.) can have pronounced effects on results. Because of a lack of commercially available means to measure rapidly pH in a microplate, the USD titrations relied on percentage by volume additions based on off-line titrations. This method might have introduced a significant source of error, especially in areas of sharp response gradients. The multitude of points generated with HTPC and the duplicates utilised in these studies ($RSD \leq 15\%$) mitigates against one bad HTPC datum misleading developers but do not preclude systematic offsets or anomalous large-scale data that are not typically run in duplicate.

Hardware non-idealities influence the scalability of centrifugation performance. In the case of particle conditioning for pneumococcal CPS, the Q/Σ required for equivalent clarification in the microplate centrifuge was slightly higher than what was used in the DSC. While an offset in this direction was expected, the impact of process factors (floc agent, species, molecular structure, class of molecules, etc.) on the magnitude of the offset are unknown and deserve additional research. These considerations suggest that for optimal scale comparability, different flocs might require different Q/Σ offsets between batch and continuous centrifuges. However, practical constraints often demand fixed set points and scaling strategies, with manufacturers often willing to accept the incidental performance variability that will derive.

As posited for staphylococcal kinetic experiments, flocs formed under weaker conditions (*i.e.* higher pH, lower floc agent concentrations) may be characterised by slower kinetics or reduced floc strength, which renders scale-up of these conditions particularly challenging (Appendix 9.6: Flocculation Kinetics at the Micro-scale). Floc strength could be improved by augmenting Ca through extending the aging process and intensifying agitation. Additionally, system differences between the two scales might be implicated as reports have highlighted that turbidity (*i.e.* clarification) can change as function of impeller type when Ca is held constant (Letterman et al., 1973).

Finally, when comparing scaling rules using different streams, it is possible that subtleties between the streams bias a particular scaling rule. For example, the centrifugation results suggest that flocs from the neutral pneumococcal CPS stream were shear-insensitive (Figure 4.9) but this has not been studied extensively for other CPS serotypes. Treating CPS broth from different species or serotypes as a single class of test molecules is convenient for the purpose of platform establishment but may miss important CPS-specific scaling effects.

When factoring all of the sources of errors and the unknowns present during the initial adoption of a novel HTPD platform, it may be prudent to confirm the HTPC results with lab-scale data at the edges of the design space. This would also allow for testing of attributes that cannot be tested at the micro-scale, such as filterability.

4.5 Chapter Summary

The overarching objective of this body of work was to develop and characterise a system for high throughput particle conditioning. A consideration of the engineering and scale-up context for HTPC was undertaken and key scale-related differences mitigated through system design where possible. Using diverse CPS from three bacterial species, HTPC was then demonstrated to be comparable to Pilot-scale, effectively qualifying the scale-down model. Product yield, product quality, multi-faceted impurity removal, floc particle characteristics, and clarification were proven scalable responses. A comparison of potential scaling rules suggests that the most consistent scale-up is achieved by maintaining constant P/V_{imp} and/or tip speed. Time-integration of either parameter (*i.e.* $P/V_{imp} t$, $\bar{G}_{imp} t$, and $v_{tip} t$) is supported by time-sensitive clarification and protein clearance results. It was found that evaluating scalability in experimental areas where a response changes sharply as a function of input parameter(s) represents the most rigorous test for the suitability of a given scaling rule.

The novel system and methods of HTPC enable the assessment of flocculation and centrifugation performance with up to 96 conditions in parallel. The described system forms the basis for platform workflows, enabling one scientist to develop a robust particle conditioning operation in less than one week with 50 mL of feed.

5 High Throughput Depth Filtration

5.1 Introduction

Depth filtration is a key purification unit operation and the final step in particle conditioning processes. Depth filters effect separations through simple steric retention or when impregnated with adsorbents, a combination of steric and chemical retention. Depth filters are commonly employed for clarification or for capture of solid product. Alternatively, the adsorptive properties of certain filters offer the potential for targeted removal of impurities at any location in a purification train and therefore, can serve as a polishing step.

There is currently no way to evaluate depth filtration at the micro-scale with constant flux operation. The smallest commercially available depth filters have areas of 23 cm² and 25 cm² and are offered by MerckMillipore and 3M, respectively. In order to achieve a typical capacity of 200 L m⁻², 0.5 L of feed would be required. As described in 1.9.4, several groups have proposed designs for assessing filtration at smaller scales, with most focused on the scale-down of membrane separations (Chandler and Zydney, 2004; Jackson et al., 2006; Vandezande et al., 2005). Only Lau et al. investigated depth filtration but applicability is limited due to the utilisation of a vacuum as the liquid driving force (Lau et al., 2013). Vacuum filtration offers little control over residence time and departs from standard industrial practise where depth filtration is operated at constant flux.

Depth filtration represents a gap in the suite of USD purification technology. A means to assess rapidly filterability at the micro-scale would bridge this technology gap. High throughput depth filtration using USD technology, HTDF, would open up many applications by increasing parallelization and by reducing the labour resource required. Potential applications can be classified broadly as screening, scaling, characterisation, and sample prep. Diverse filtration media could be screened and conditions optimized through modulation of operational parameters or feed properties (*i.e.* pH, conductivity, etc.). Laboratory qualification of clinical production processes could be expedited and concluded with less material. HTDF could enable the production of representative feedstreams

earlier in the development cycle, leading to more nuanced development of downstream operations. Indeed, process mapping of experimental spaces, potentially as an element of QbD, would be possible. Established process would also benefit as process upsets or deviations encountered at manufacturing scale could be quickly scaled-down for investigation. Finally, HTDF requiring only a few mL of feed would address a gap in sample preparation for analytical assays.

Depth filtration is complex and limited foundational data has hindered performance optimization of these operations. Partly responsible is the mixed-mode binding functionality of several popular media, which can be complex to untangle. The result has been limited mechanistic understanding, leading to media selection and respective filtration conditions based on historical set points or vendor recommendations. Advent of HTDF would enable deeper understanding and more informed optimization activities.

5.1.1 Scale-down Models

At the outset of this thesis, the options to scale-down USD depth filtration were limited and comprised essentially three options (Table 5.1).

Table 5.1. Available options for scale-down of depth filtration. D = diameter of filter element; CSA = cross-sectional area of filter element (Jackson et al., 2006).

	D (cm)	CSA (cm ²)	Volume (mL) Required for Processing of:	
			200 L m ⁻²	1000 L m ⁻²
Commercial bench-scale	NA	270	5,400	27,000
Commercial Small-scale	NA	23	460	2,300
Pfizer internal	1.8	2.6	52	260
Jackson et al.	0.6	0.28	5.6	28
Novel design	0.53	0.22	4.4	22

In collaboration with Bend Research, Pfizer had developed previously a small-scale filter holder (2.6 cm²) that enabled filtration with a single filter. As part of this thesis, the scalability and application of

this device was assessed. A USD filtration device devised by Jackson et al. and proven for membrane filtration was available in the Department of Biochemical Engineering at UCL (Jackson et al., 2006; Kong et al., 2010). An evaluation was undertaken to determine whether thick and heterogeneous depth filters could be accommodated within the unit and was followed by a performance evaluation. If these two technologies proved inadequate, a third option entailed the *de novo* design and development of a micro-scale system for depth filtration. The objective would be to filter eight or more depth filters in parallel using less than 10 mL per filter channel.

5.1.2 Challenges

5.1.2.1 Commercial

Given the potential utility of USD HTDF, it is curious that the market had not filled the technological void; especially as disposable products would result, ensuring a steady revenue stream. In consulting with two major filtration companies, two key obstacles were relayed. The first was the perceived limited market for a HTDF device. One leading company mentioned that the number of units they would sell would not offset the development costs of bringing such a device to the market. Under these circumstances, there would need to be a strong commercial incentive to undertake this project, such as growing their market share. This incentive did not exist because, paradoxically, if a leading company had a dominant market share, making it easier to compare the respective offerings from a competitor would be counter-productive. For the other vendor who possessed scarcer R&D resources, the technical challenge combined with the multitude of media offered made such a project exceptionally daunting. The other challenge was both media vendor and institutional scepticism that it was possible to obtain satisfactory precision at the micro-scale.

5.1.2.2 Engineering

The design of a micro-scale depth filtration device requires the advent and integration of several components. A method must be devised to cut swatches of media reproducibly from a larger sheet. This approach must be high throughput and convenient for the end user. Sealing the media in the

device is also challenging. The ratios of the seal and edge areas to filter surface area are much higher than in larger scale devices, with any structural perturbation induced by a seal or edge having a relatively amplified effect. The edges must be sealed because the layered media structure facilitates radial flow. The top and bottom of the media must be sealed carefully as compression will distort the media and reduce permeability. These scale-related complications ensure that the sealing mechanism will be different from larger devices where compression is used to prevent radial flow. The system must deliver a specified flow rate and record feed pressure, with automation preferable. If pump slippage with increasing feed pressure is an issue, a feedback loop must modulate the pump rate. The entire device must support ≥ 8 filters in parallel and enable the collection of filtrate, preferably in fractions. Perhaps the most challenging feature is modularity. The device must be as “universal” as possible with respect to filtration media. This goal is particularly daunting since filtration media vary in height, surface roughness, porosity, compressibility, morphology, and some applications employ multiple layers in series.

A key issue when scaling down depth filtration is precision. Depth filtration media are comprised of irregular layers of substrate and are very heterogeneous. The performance of a large-scale device represents the average performance of this substrate. As the scale decreases, the likelihood increases that increasingly small swatches will not be representative of the larger sheet. Inter-device precision was found to be $\pm 30\%$ when Mini capsule filters (24 cm^2) containing A1HC filter drawn from the same lot were run in replicate (Lutz et al., 2009). If this imprecision were predominantly due to the media heterogeneity, then inferior reproducibility would be seen as one scales down further.

5.1.2.3 Scalability

It is accepted that owing to the aforementioned challenges, USD depth filtration may not yield P_{\max} values or filtrate quality that can be scaled directly to production-scale. The accuracy of the system will ultimately determine which applications can be supported. If the directionality of response matches larger scales, then screening experiments for media or parameters would be justified. If the magnitude of the response is proportional to the response at larger scale, then HTDF could be used to home in on regions of optimal performance. With this level of performance, scaling factors would

need to be produced for the optimized condition at lab-scale. The most rigorous threshold, accurately predicting large-scale results, would enable HTDF to be used for formal process qualification studies and to supplant lab-scale as the developmental model used for scaling to production. A fixed scaling factor might be needed to connect the USD performance to larger scales.

5.1.2.4 Predicting Filterability

The need for HTDF would be reduced if a surrogate measure of filterability could be established. Extensive industrial experience suggests that turbidimetric and spectroscopic measurements can be misleading. Data from particle characterisation instruments (*e.g.* size, concentration, shape, etc.) are potential predictors of filterability. Light scattering techniques struggle to deconvolute complex streams with multimodal particle distributions but imaging-based technologies have yet to be evaluated comprehensively.

5.1.2.5 Clarity Assays

Capacity and filtrate quality are the principal metrics used to assess depth filtration. In USD depth filtration, the filtrate volumes are less than the minimum volume (*i.e.* approximately 7 mL) required for the industry standard nephelometric measurement (*i.e.* Hach NTU). This constraint necessitates an alternative clarity measurement. An ideal substitute would require ≤ 300 μL and be high throughput to support USD filtrate fractionation. A Hach nephelometer quantifies scattering at 90° , which makes plate-based measurements impractical and raises concerns over comparability of technology. Many studies have employed visible (400-670 nm) or near infrared (730-970 nm) spectroscopy to assess turbidity (Balasundaram et al., 2011; Boychyn et al., 2000; Riske et al., 2007). Indeed, optical density at 600 nm is correlated with cell density for microbial fermentation (Mukhopadhyay, 2008). These spectroscopic approaches require only 150 μL of material, are compatible with microplates, and are high throughput. A microplate-based nephelometric instrument (*i.e.* Nephelostar) would be ideal but correlation with Hach nephelometers has not been established. Many researchers have used particle characterisation to understand clarification but this approach has not been harnessed for the purpose of clarity determination (Chatel et al., 2014; Fisher

and Glatz, 1988a; Fisher and Glatz, 1988b; Singh et al., 2013; Walther et al., 2014). For clarity measurements, particle counts from dynamic light scattering (DLS) or particle concentrations (derived from image analysis) may have value.

5.2 Aim and Objectives

The overarching aim of this chapter is to enable high throughput depth filtration at the micro-scale.

To achieve these goals, several aspects of USD filtration are explored:

1. Capacity in various 96-well filterplates and particle characterization are examined as surrogates for filterability.
2. Pre-existing scale-down devices are evaluated as scale-down models:
 - a. a custom small-scale filtration device available at Pfizer
 - b. a vacuum-driven filtration device available at UCL.
3. The design and engineering of a novel, high throughput, USD device for depth filtration is described. Several filters are employed to qualify the accuracy, precision, and reproducibility of the HTDF device while demonstrating modularity across diverse depth media morphologies.
4. Four orthogonal clarity measurements are compared to standard lab-scale measurements to identify which micro-scale measurements are suitable HT replacements for current practises.

5.3 Materials and Methods

The identities of products and filters were redacted in 5.4.2.2.2.

5.3.1 Materials

All common chemicals were commercial analytical grade. Nalgene 0.22 μm polyethersulfone or cellulose filters (Thermo Fisher Scientific, Waltham, MA) were used interchangeably for filtration.

Biological solutions were not filtered except as described.

Harvest and concentrate material from Chinese Hamster Ovary (CHO) cell culture of mAbs and in-process pools of CPS from serotypes of *S. aureus* were provided kindly by Pfizer R&D. All sugars have D and α structural configuration.

5.3.2 Filtration Systems

Depth filtration is run at constant flux until completion, typically, when feed volume is exhausted or a pressure maximum is reached. In this body of work, the standard sequence of operation was to install filters, flush with water, vent to remove any entrapped air, flush with water to measure permeability, and then prime with feed up to the filter.

5.3.2.1 Load Material

Recombinant CHO cell culture used for the production of humanized monoclonal antibodies was centrifuged in a DSC and served as the feed stream for A1HC, X0HC, 30SP, and 60SP testing. Whole cell lysate of harvest material was generated with a freeze-thaw cycle. After centrifugation to sediment intact cells, the supernatant was spiked in the concentrate in order to degrade filterability. A single stream was composed to provide fouling at a target volume processed for both 30SP and 60SP sterile filters but a 3-fold dilution in PBS was required for X0HC, C0HC, D0HC, and CE50 filtration. These feeds were used for all filtration studies, except where noted. Hereafter, these feeds will be referred to as concentrate.

5.3.2.2 Laboratory-scale Filtration

Commercially available lab-scale devices served as the performance benchmark. Capsules with 25 cm² filter area of single-layer 30SP (BC0025L30SP, 3M, St. Paul, MN) or 60SP media (BC0025L60SP, 3M) or Micropods with 23 cm² filter area of two-layer A1HC (MA1HC23CL3, MerckMillipore, Billerica, MA) or X0HC (MA1HC23CL3, MerckMillipore) were employed as appropriate. Large lab-scale pods (270 cm², MerckMillipore) were used for the initial scale-down trials with X0HC. Pressure was monitored with SciPres digital pressure transducers (Scilog, Madison, WI) and flow rates were measured with graduated cylinders.

5.3.2.3 Generation of Filtrate Samples for Clarity Measurements

CHO centrate was filtered with 23 cm² Micropods of X0HC (< 0.1 µm nominal rating, MX0HC23CL3), C0HC (0.2-3 µm nominal rating, MC0HC23CL3), D0HC (0.6-9 µm nominal rating, MD0HC23CL3), and CE50 (0.6-1.0 µm nominal rating, MCE5023CL3) filters manufactured by MerckMillipore. The CE50 filter was solely a steric filter whereas the other media were impregnated with DE particles. After flushing with 100 L m⁻² of water, filters were challenged at a flux of 0.0556 L s⁻¹ m⁻² until the feed pressure reached 241 kPa or 280 L m⁻² of feed had been filtered. Filtrate was fractionated into 30 mL aliquots for immediate analysis with the proceeding battery of clarity measurements described in 5.3.3.

5.3.2.4 Filterplates

Filterplates were evaluated as a rapid assessment of relative filterability. The filters given in Table 5.2 were screened. Centrifugation conditions were determined independently for each plate by spinning four samples of differing filterability until partial filtration of all samples had occurred. If all samples filtered completely, the test was repeated with less aggressive centrifugation conditions until the aforementioned condition was met. Centrifugation at 20°C in a swinging bucket centrifuge fitted with microplate adapters (5810R, Eppendorf, Hamburg, Germany) was typically accomplished in ≤ 3 minutes, except for VPro and Ultracel 10 filters, which required up to 60 minutes for adequate volumes to be permeated.

Table 5.2. Filterplates used for filterability correlation work. NMWCO = nominal molecular weight cut-off, PVDF = polyvinylidene fluoride, PP = polypropylene, CA = cellulose acetate and cellulose nitrate

Name	Material	Porosity	N	Time	Vendor	Part #
Philoc VPro MultiScreen	PES	20 nm	34 s^{-1}	2 min	MerckMillipore	00114073PU
Unifilter	PP	0.25/0.45 μm	8.3 s^{-1}	1 min	GE (Whatman)	7770-0062
MCE MultiScreen	CA	0.45 μm	1.7 s^{-1}	1 min	MerckMillipore	MSHA S45 10
Ultracel 10 MultiScreen	Regenerated cellulose	10 kDa NMWCO	37.5 s^{-1}	35 min	MerckMillipore	MAUF01010
Unifilter	PP	0.45 μm	8.3 s^{-1}	1 min	GE (Whatman)	7700-2805
GV MultiScreen	PVDF	0.22 μm	1.7 s^{-1}	3 min	MerckMillipore	MSGVN2210
Unifilter	DE81 DEAE cellulose	NA	NA	NA	GE (Whatman)	7700-4313
Unifilter	PP	25-30	NA	NA	GE (Whatman)	7700-3304
Unifilter	PP	25	NA	NA	GE (Whatman)	7700-1804

5.3.2.5 Pre-existing Pfizer Device

The internal Pfizer filtration device is a two-piece filter housing assembled with a tri-clamp. Media discs measuring 1.8 cm in diameter must be cut with a hollow punch. The discs are inserted into the device and are supported underneath by a steel screen. Plastic rings can be inserted to increase media height, thereby improving sealing.

5.3.2.6 UCL Constant Vacuum USD Device

The constant vacuum-driven USD device was designed by Jackson et al. and designed for membrane filters (Jackson et al., 2006; Kong et al., 2010). The device is also able to accommodate the media heights typical of single and dual layer depth filtration. In brief, filters are cut and installed into a threaded holder seated in a vacuum manifold. A maximum of two filters discs were run simultaneously in the device. This constraint was imposed to improve control.

Filter discs, 0.6 cm in diameter, were cut out of square media stock with a sharpened hollow punch mounted on an overhead drill press. A cardboard and cork composite backing was necessary to minimize distortion of media during the cutting process. To prevent deterioration during long-term storage, discs had to be stored in a desiccated environment. Each filter was weighed after cutting.

Two filters were tested with the UCL filtration device: a two-layer A1HC diatomaceous earth depth filter (MerckMillipore, Billerica, MA) and an adsorptive filter. A1HC filters were flushed initially with $> 100 \text{ L m}^{-2}$ of RODI under 70 kPa vacuum. After evacuation, the mAb concentrate was processed at 70 kPa vacuum until flux was greatly reduced, indicating V_{max} . A_{405} was used to measure clarity of the filtrate.

5.3.2.7 Novel Constant Flux USD Device

A micro-scale depth filtration device was designed, fabricated, and developed in collaboration with Bend Research Inc. (Bend, Oregon). Many design iterations were required before the final design was attained. These included several models that sought to isolate a small section of a larger filter substrate using surface seals. These designs were not robust as radial flow was observed eventually in all designs. In addition, the variable compressibility of different media led to differential deformation under the axial load of the seals, thereby altering porosity and filtration performance.

5.3.2.7.1 Fabrication

The final design enabled the parallel depth filtration of eight filters with a nominal circular area of 0.22 cm^2 per filter. The maximum feed pressure was 280 kPa. Filter discs were cut with a laser operated at 300 W, 100 Hz, 20% duty, and 3.8 cm s^{-1} cutting velocity (Figure 5.1). To avoid charring, an atmosphere of 0.2 MPa nitrogen gas was required during cutting. Filter discs were embedded in epoxy (K20 Conap Easyepoxy, Cytec Industries Inc., Woodland Park, NJ). After the application of epoxy in a mould, a flat plastic washer was depressed into the surface. This provided uniform topography for the top O-ring to seal. The bottom of the filter “puck” (Figure 5.1) was flat due to flush mating of the epoxy with the mould. During puck fabrication, care was taken to avoid setting epoxy on top of the filter, to coat the edge of the filter comprehensively, to minimize floating of the filter disc during

epoxy addition or excessive disc depression, and to ensure the washer was parallel with the mould floor.

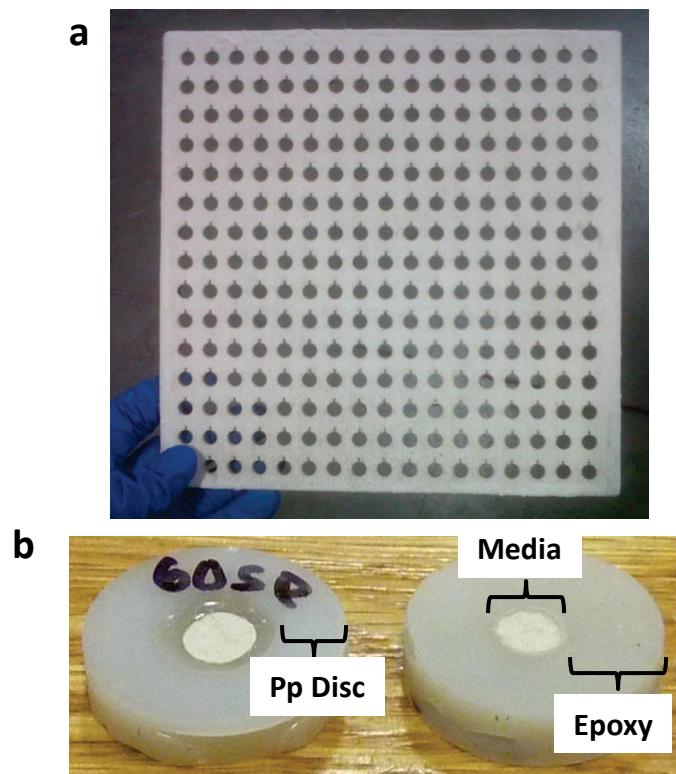
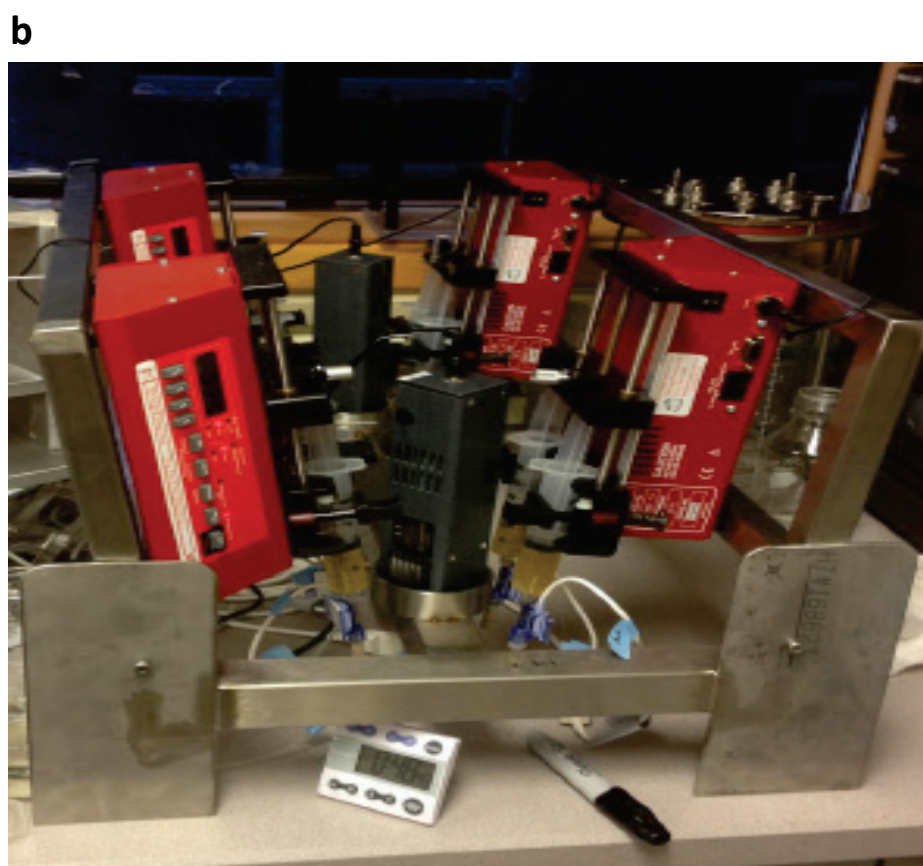
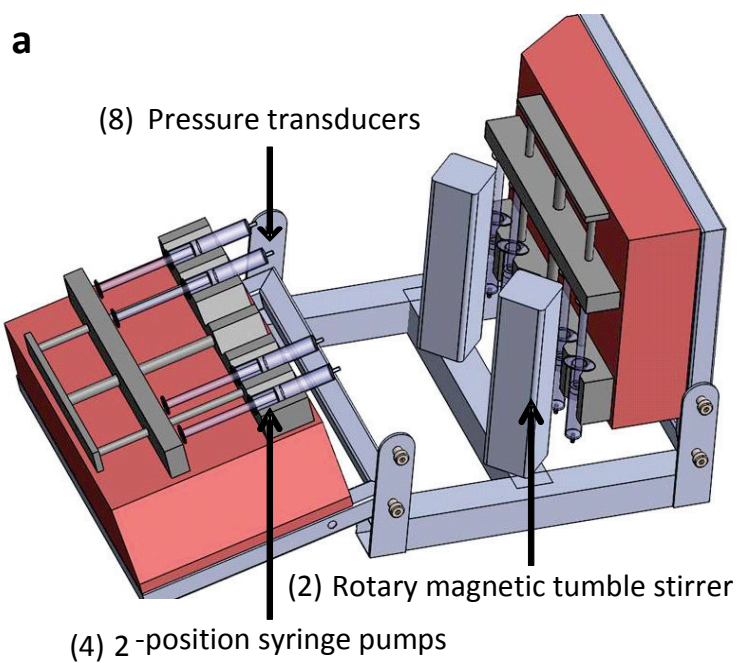


Figure 5.1a, b. Media substrate after laser cutting of 255 filter discs (5.1a). Filter pucks: depth filter discs embedded in epoxy with an embedded flat plastic washer serving as the top sealing surface (5.1b). Top (left) and bottom (right) faces of filter puck are depicted in 5.1b.

5.3.2.7.2 Integrated Device

The final device was comprised of four syringe pumps, with each capable of driving two syringes (Figure 5.2).



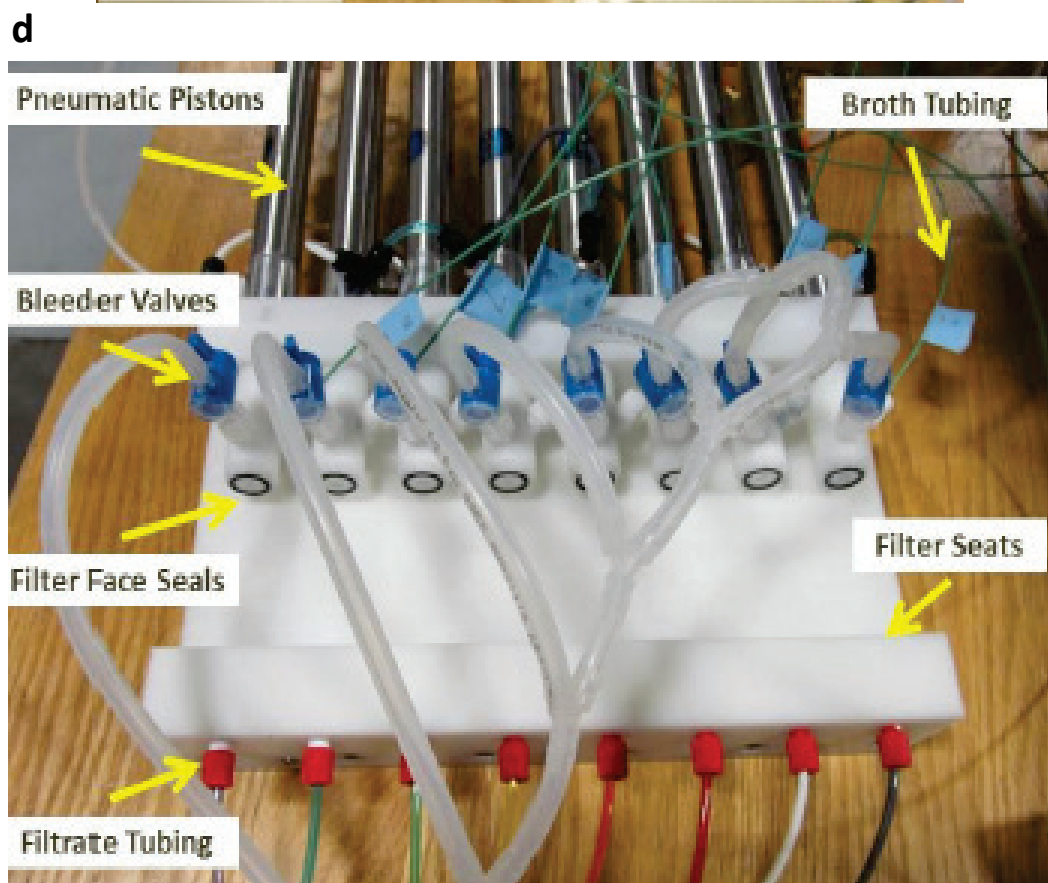
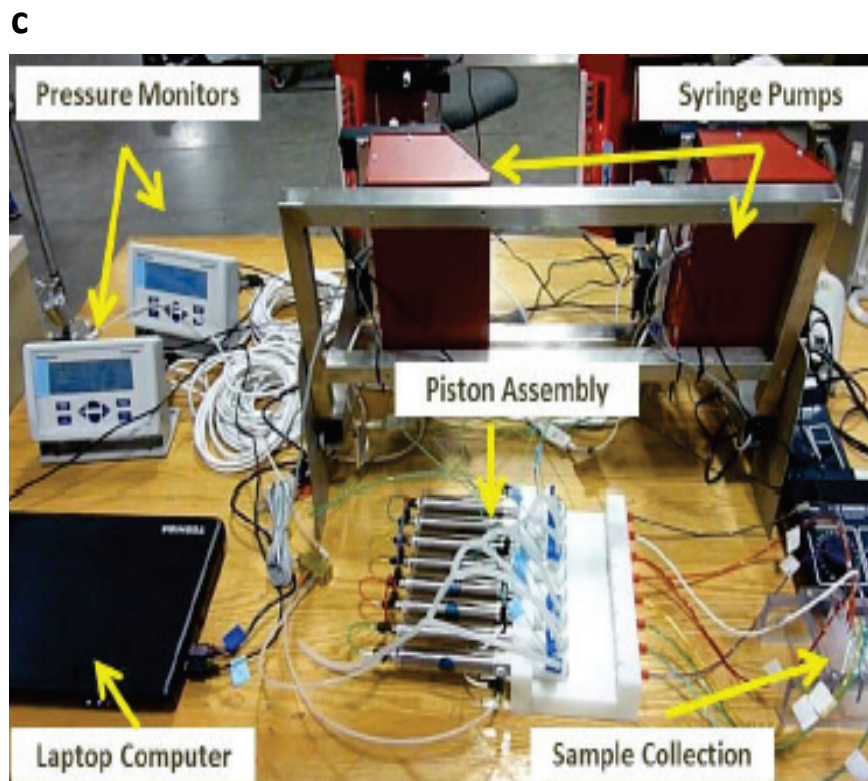


Figure 5.2a, b, c, d. Final micro-scale depth filtration device. Schematic of pump, syringe, and pressure transducer sub-assembly (5.2a), pump, syringe, and pressure transducer sub-assembly (5.2b), complete layout of all components of device (5.2c), and filter manifold (5.2d).

A PTFE-coated, neodymium iron boron magnetic stirrer disc (8 mm D, 1.8 mm thick, VP 772DP-N42-8-2, V&P Scientific, San Diego, CA) was installed inside each syringe. When driven by one of two external magnets (Multi Stirrus, V&P Scientific), rotation of the stir elements ensured homogeneity of the feed material during filter loading. Each syringe was connected to a digital pressure transducer (PRESS-S-000, Pendotech, Princeton, NJ) which was connected to the filter assembly via 0.7 mm inner diameter HPLC tubing. The filter assembly housed eight filtration pucks, sealed on the top face with EPDM double-seal O-rings (1.1 cm ID, 1.4 cm OD, McMaster-Carr, Princeton, NJ) and standard silicon O-rings on the bottom face. A three-way valve connected the solids holding volume upstream of the filter to a waste line that could be used to purge air or liquids without traversing the filter puck. Filtrate lines were routed to a manual microplate fraction collector. Pump control and pressure data recording via pressure monitors were integrated with a custom MATLAB program run from a laptop.

5.3.2.7.3 Generic Operation

The syringes were loaded with RODI and the filters installed in the housing. RODI was then primed up to the filter using the vent filters. A volume of RODI $> 100 \text{ L m}^{-2}$ was flushed through each filter at 400 L m^{-2} . After equilibration, backpressure measurements were made at fixed flux set points up to 1000 L m^{-2} . Feed solutions were then loaded into the syringes. The system was primed up to the filter surface using the vent valves and the run was initiated.

5.3.2.7.4 Specific Operation

30SP and 60SP steric depth filters and XOHC adsorptive filters were evaluated. Different lots of media were used at lab-scale and in HTDF. Feed material was loaded until $\geq 170 \text{ kDa}$ feed pressure was achieved. Fractions or whole pools of filtrate were taken where appropriate and clarity was measured using one or more of the clarity measurements as detailed in 5.3.3.

5.3.2.8 Sterile Filtration at Constant Pressure

As part of a particle conditioning DOE study, filtration across a $0.22 \mu\text{m}$ filter (47 mm, Durapore PVDF, MerckMillipore, Billerica, MA) was evaluated. The samples were drawn from the centrate following particle conditioning of a staphylococcal CPS broth. The flux was set to generate 69 kPa of feed

pressure at the outset of the operation. As the filter plugged progressively, flux was maintained until the pressure exceeded 138 kPa. From this point forward, the flux was throttled to prevent further increases in pressure.

5.3.3 Clarity Measurements

5.3.3.1 Turbidity

5.3.3.1.1 Hach Turbidity

A portable turbidimeter (2100P, Hach, Loveland, CO) was used with a minimum volume of 7 mL per sample. Duplicate measurements were made with the average value reported. Except where noted, “turbidity” values are referred to in units of nephelometric turbidity units (NTU) and are measured with a Hach turbidimeter.

5.3.3.1.2 Nephelostar Turbidity

A Nephelostar Galaxy (BMG Labtech, Ortengberg, Germany) was used for microplate-based turbidity measurements. 200 μ L of sample was loaded into an acrylic microplate (Costar 3635; Corning, Corning, NY). Standards of 1, 10, 20, and 200 NTU were run in duplicate to generate a standard curve. Gain was normalized before each run.

5.3.3.2 Spectrophotometric (A_{405} , A_{600})

A_{260} , A_{405} , and A_{600} of 300 μ L of supernatant were read using a spectrophotometric plate reader. Acrylic microplates (Costar 3635) were used for all absorbance measurements. All spectroscopic measurements were made using a spectrophotometric plate reader (Spectramax M3; Molecular Devices, Sunnyvale, CA) except for results with the constant vacuum-driven USD device, for which a Safire II microplate spectrophotometer (Safire II, Tecan, Switzerland) was employed.

5.3.3.3 Particle Characterisation by Micro Flow Imaging

Particle characterisation and sizing was performed with a Micro Flow Imager (MFI) with Bot1 autosampler (5200; 1-70 μ m; Protein Simple, Santa Clara, CA). Loads were diluted 100-fold in PBS but

filtrate samples were analysed neat. Analysis was limited to 50,000 particles per sample with particles excluded that spanned the edge of the micrograph.

5.4 Results and Discussion

5.4.1 Correlates of Filterability

The principal impetus to develop high throughput filtration is the simple fact that without actually running the filter, one generally does not know which feeds will plug a given filter. If it were possible to make a simple measurement that is predictive of filterability, much of the need for high throughput filtration would be eliminated. To explore this possibility, four samples that spanned a range of filterability were considered (Figure 5.3). A broad range of plugging is encompassed by the samples A-D. These four samples were analysed extensively to determine if differences in physical properties could be detected that would correlate with the relative filterability illustrated in Figure 5.3. In addition to the proceeding section, potential correlations between filterability and A_{600} , A_{405} , turbidity, and DLS of samples A-D (filtrate and centrate) were evaluated (data not shown). However, none was found, leaving particle characterisation as the sole method that provided measurements correlating to filterability.

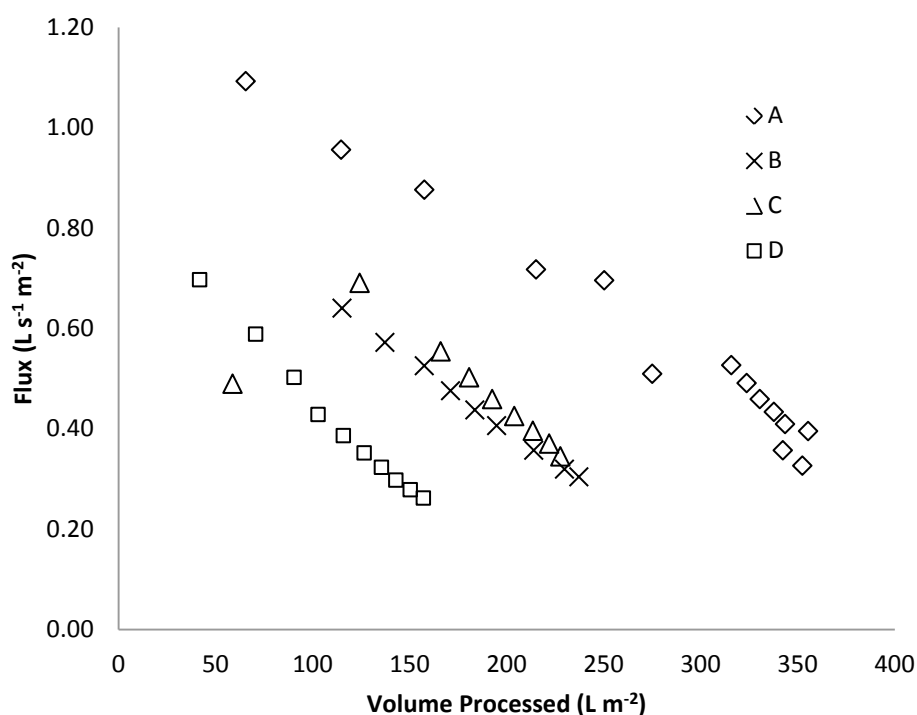


Figure 5.3. Changes in filtration flux at nominal constant feed pressure with four staphylococcal concentrate samples at 17 cm²-scale (47 mm discs). As the filter plugged, the flux had to be decreased to prevent over-pressurization. The relative filterability is A > B = C > D.

5.4.1.1 Particle Characterisation

Particles larger than 0.2 μm should be retained by sterilizing grade 0.22 μm filters. The available technology for characterisation of particles 0.1-1 μm in diameter is not reliable for the accurate quantification of particles and is not amenable to high throughput analysis of volumes ≤ 1 mL. The Micro Flow Imager 5200 with bot1 autosampler (Protein Simple) is a high throughput particle analyser that characterises particles with a diameter range of 1-70 μm . The technology is based on image analysis and therefore, can interrogate complex samples without concern for the accuracy of deconvolution algorithms, as afflicts light scattering. To examine whether particles ≥ 1 μm were responsible for the filter plugging depicted in Figure 5.3, samples A-D were analysed with the MFI (Figure 5.4).

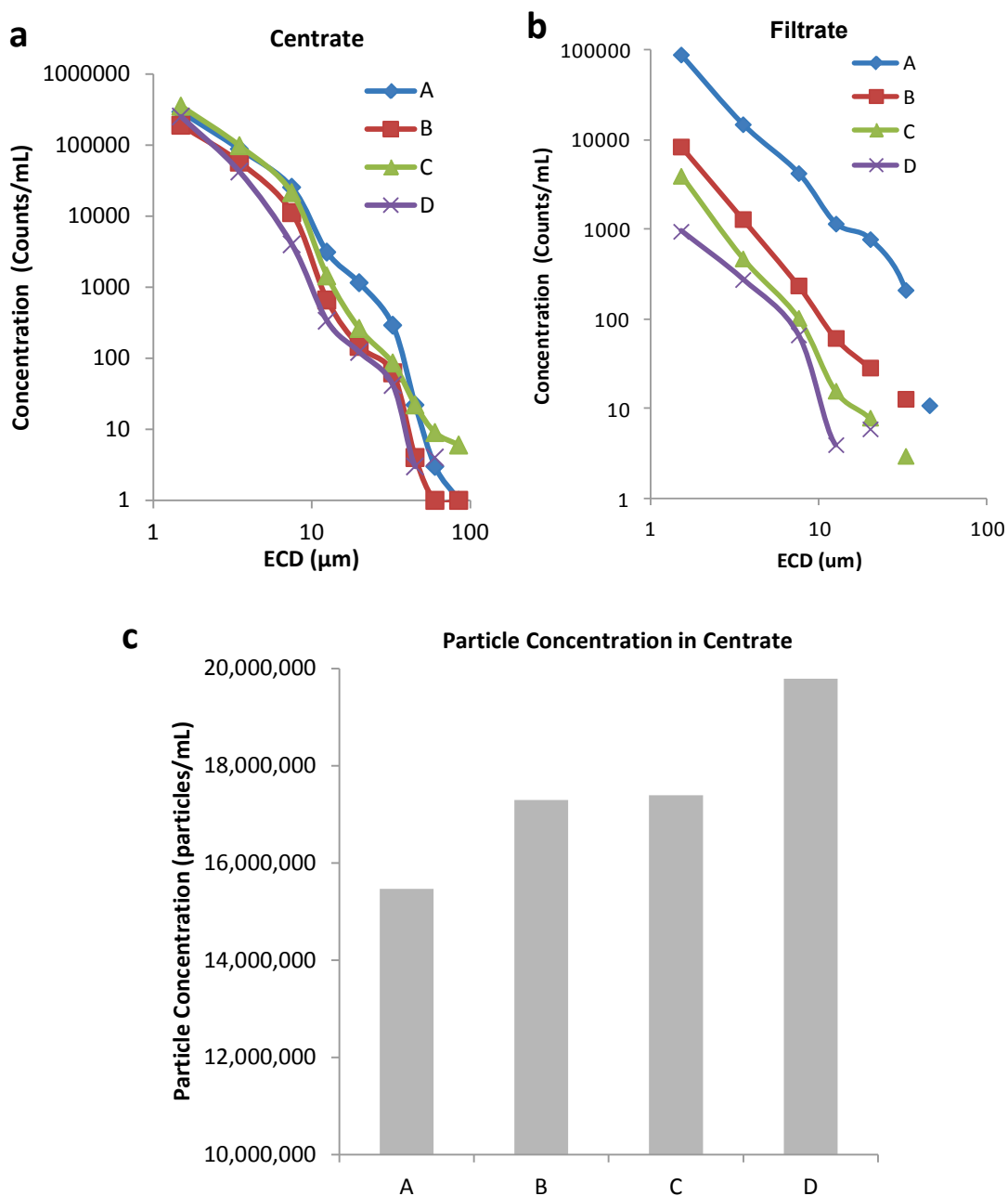


Figure 5.4a, b, c. Correlating particle properties measured with MFI with 0.22 μm filterability. A histogram of particles in the centrate (*i.e.* load) (5.4a), in the filtrate (5.4b), and the total particle concentrations of particles with diameters 1-70 μm (5.4c).

Particles in the sample affording the best filterability (A) had more large particles in the centrate than did samples B-D. For the least filterable sample (D), the opposite was true with the centrate from this sample having the least number of large particles. Inspection of the filtrate showed that the particle

concentration of particles 2-100 μm in diameter was higher in samples with better filterability (5.4b). The most promising correlate for filterability is total particle concentration, of which the vast majority are 1-2 μm in diameter. As seen in Figure 5.4c, the fewest particles are observed in sample A and the most are found in sample D. Moreover, samples B and C, which filtered equally well, have comparable particle concentrations. Additional particle analyses showed that the largest difference in particle concentration between the samples was observed for the particles $< 2 \mu\text{m}$ (data not shown). Hence, the number of particles $< 2 \mu\text{m}$ are implicated in the poor filterability of 0.2 μm Durapore filters.

These phenomena are likely due to several factors: (i) a plugged filter exhibits a smaller mean pore size due to fouling, (ii) a fouled filter has higher surface velocity on the few remaining open pores leading to increased shear and particle fragmentation, and (iii) the filters that plugged earliest were operated at higher pressures for longer periods, leading to greater overall degradation of the particles that were retained initially (Darby and Lawler, 1990; Kim and Tobiasson, 2004).

As this work was performed to assess the filterability of 0.2 μm filters, it is unclear if this finding extends to depth filters. It does implicate particle distribution; however, as an important factor in filter plugging.

5.4.1.2 Filterplates

Many commercial filterplates are available and are designed for rapid sample prep. At the outset of this study, the intra-well precision for a given plate and the relative consistency of different plates, vendors, media, etc. were unknown. Samples A-D were filtered through the plates with centrifugation conditions modulated so filtration of the full volume was not achieved. The filtrate volume was proportional to filterability, with greater volume indicating a more filterable stream. Filtration volume was estimated by measuring liquid height in a microwell using absorbance at 990 nm. Using this approach, samples A-D were filtered through a plethora of filterplates, using custom centrifugation settings (Figure 5.5).

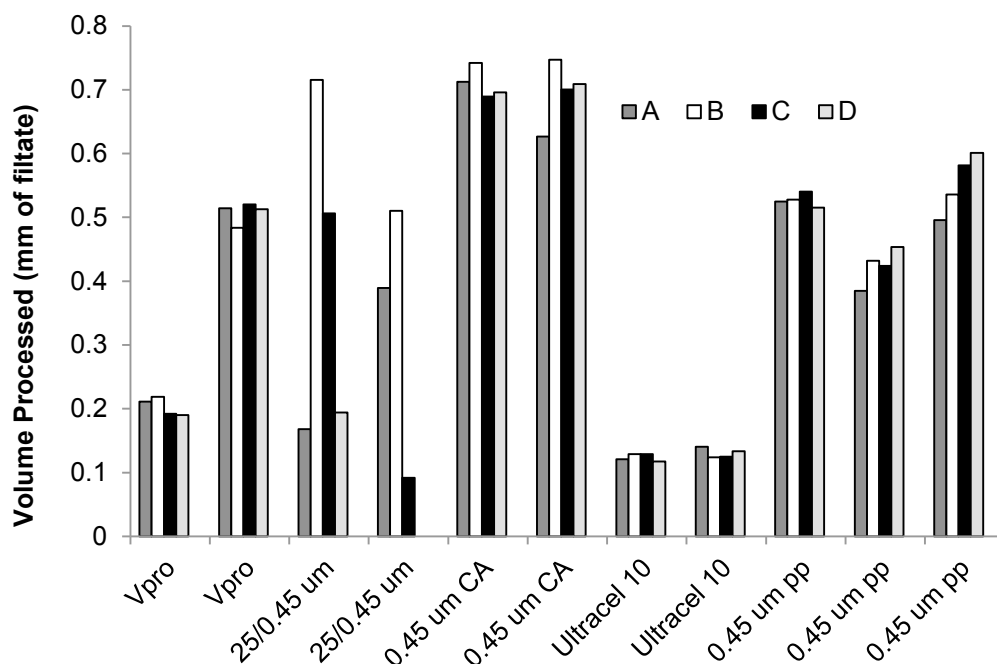


Figure 5.5. Relative filterability of samples A-D in various filterplates. Filterplates are described in 5.2. All points were run once except where filters are listed twice on the x-axis to indicate that a run was repeated.

The results from the filterplate study were disappointing. Most of the plates, particularly those from Whatman, exhibited large intra-well variability, in which cases the data were not presented in Figure 5.5. Where reproducibility was better, either there were negligible differences in filtrate volumes or the differences were not correlated with filterability. Initially, VPro showed promising results but upon repeating the trial, the initial weak correlation disappeared. These failings, combined with the lack of filterplates designed for depth filtration, necessitated consideration of alternative options.

5.4.2 Pre-existing Scale-down Options

Three experimental scale-down devices were evaluated prior to the decision to design a new micro-scale depth filtration device. The aims were to ascertain the utility of existing devices and where appropriate to determine the reproducibility of cutting small areas of media. Given the 30% variability reported with previous MerckMillipore 24 cm² depth filters, a central question was

whether the inherent heterogeneity in pad construction would render scale-down impractical, even in a hypothetically perfect scale-down device (Lutz et al., 2009). High variance would require the averaging of many replicate micro-scale runs, thereby negating any advantage in feed volume requirements or productivity.

5.4.2.1 Pre-existing Pfizer Device

Pfizer had previously developed a device in collaboration with Bend Research, Inc. The device was a single holder accommodating filters with the dimensions given in Table 5.1. Since the performance of this device had not been evaluated thoroughly, a study was performed to evaluate the consistency of replicate filtration runs and to determine the scalability of X0HC filtration. The filters were loaded with CHO centrate until pressure became asymptotic. Figure 5.6 contains a summary plot of filtration hydraulics.

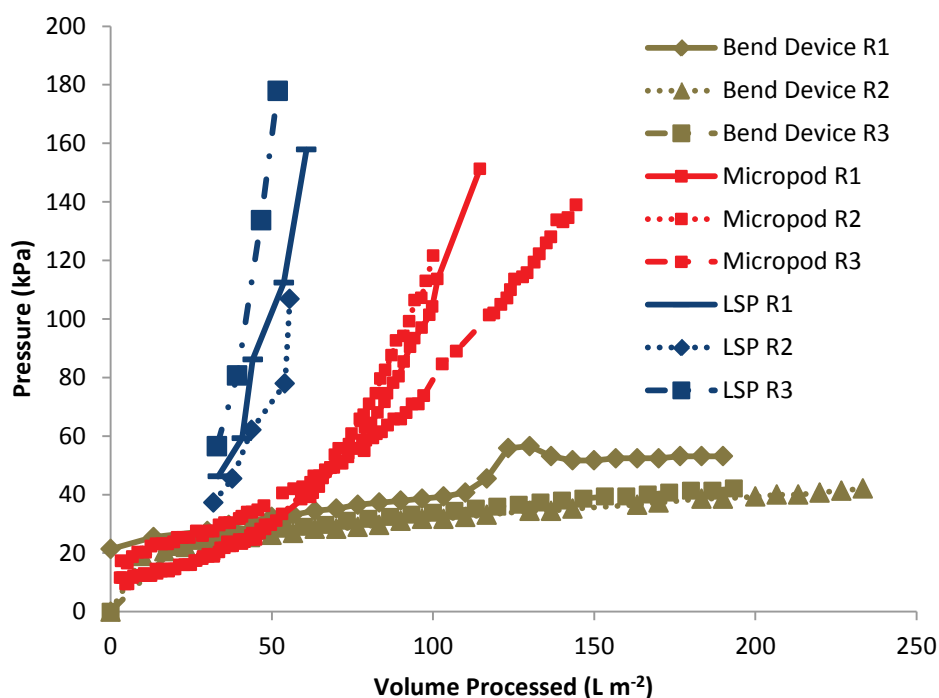


Figure 5.6. Hydraulic profiles for 270 cm² lab-scale pods (LSP), 23 cm² Micropods, and 2.6 cm² internal Pfizer device (Bend device) replicates. The trials with the Micropods and the Bend device utilised the same lot of media whereas the LSP were manufactured from three different lots of media.

The filtration performance was different at each scale with filter capacity inversely proportional to scale. The internal Pfizer device failed to plug, possibly due to fissures created in the media during the punching process used to cut discs from media sheets. At 140 kPa backpressure, the average capacities of the Micropods and LSPs were 186 L m^{-2} and 57 L m^{-2} , respectively. The filtrate was clearer for the LSPs too, with a mean turbidity of 4.2 NTU compared to 6.2 NTU for the Micropods. The discrepancy between the Micropods and LSP was unexpected. The feed vessels for the Micropods were not constantly stirred during loading, though they were for the LSP and for the runs with the internal Pfizer device. Solids may have settled out of the Micropod feeds, leading to improved capacity.

Precision was acceptable for all the devices in the study. For LSPs, the RSD for capacity and filtrate clarity was 16% and 13%, respectively. These filters were drawn from different batches of media, further indicating that inter-media variability was minimal. Inter-media variability must be higher than intra-batch variability as the former has the same sources of error due to media heterogeneity and device imprecision plus the contributions from media sourcing. Intra-batch variability for the media was represented by the Micropods, where the RSD for volume processed and filtrate clarity were 23% and 16%, respectively. This precision is superior to the values reported by Lutz et al. and may indicate that the Micropod, a successor to the devices used in their study, is more reproducible than its predecessor (Lutz et al., 2009). These findings increased optimism that scale-down below areas of 23 cm^2 could produce sufficiently precise results.

5.4.2.2 UCL Constant Vacuum Device

A device designed for membrane filtration was available for testing at UCL (Jackson et al., 2006; Kong et al., 2010). Using two different filters, a study was conducted to evaluate filter scalability and reproducibility. In addition, since the cutting process was implicated in the failure of the internal Pfizer device, development work focused on improving this process. Subsequent to this work, Lau et al. demonstrated that this USD device could be used for single layer non-adsorptive depth filters (Lau et al., 2013).

5.4.2.2.1 Diatomaceous Earth Filters

A1HC is a two-layer depth filter with adsorptive and steric properties integrated with an additional membrane layer positioned beneath the depth media. The bottom membrane layer, RW01, was excluded from this study. DE60 and DE75, the two discrete depth media constituting A1HC media were cut with a rotating, sharpened hollow punch. For DE60 and DE75, the cut disc masses had a RSD of 4% and 5%, respectively. This precision indicated that the cutting approach was isolating consistent amounts of media. The two layers were operated in tandem.

The two A1HC layers were challenged with CHO centrate. During each A1HC run, the filters plugged, leading to a sharp reduction in permeation rate. Hydraulic profiles were consistent between each well. To compare the data and better understand the nature of the fouling, the data was transformed using two different filtration models: gradual pore plugging and cake filtration (Figure 5.7). A better fit was obtained with the gradual pore plugging model. This suggests that the particulates are becoming entrained in the pores leading to a gradual reduction in porosity until complete blocking occurs. It also contextualizes the data given in Figure 5.5 by providing a mechanism through which differential particle populations influence filterability. However, the cake filtration model fit the data well enough to suggest that cake buildup is also occurring, although to a lesser extent. This indicated a secondary plugging mechanism and underscored the complexity of depth filtration processes.

The gradual pore plugging model enabled the extraction of an average V_{max} value. The V_{max} was 77 $L\ m^{-2}$ with a RSD of 15%, indicating consistent performance. In conjunction with the consistency data in Figure 5.6, this result demonstrated definitively that micro-scale depth filtration was technically possible, even given the heterogeneity of raw materials.

Water permeability was highly variable per well, with a RSD of 47%. To determine if the unique morphology of each filter cutout was contributing to inter-run variability, the V_{max} and permeability (y-intercept) values obtained with centrate were compared against the respective water permeability values (Figure 5.8).

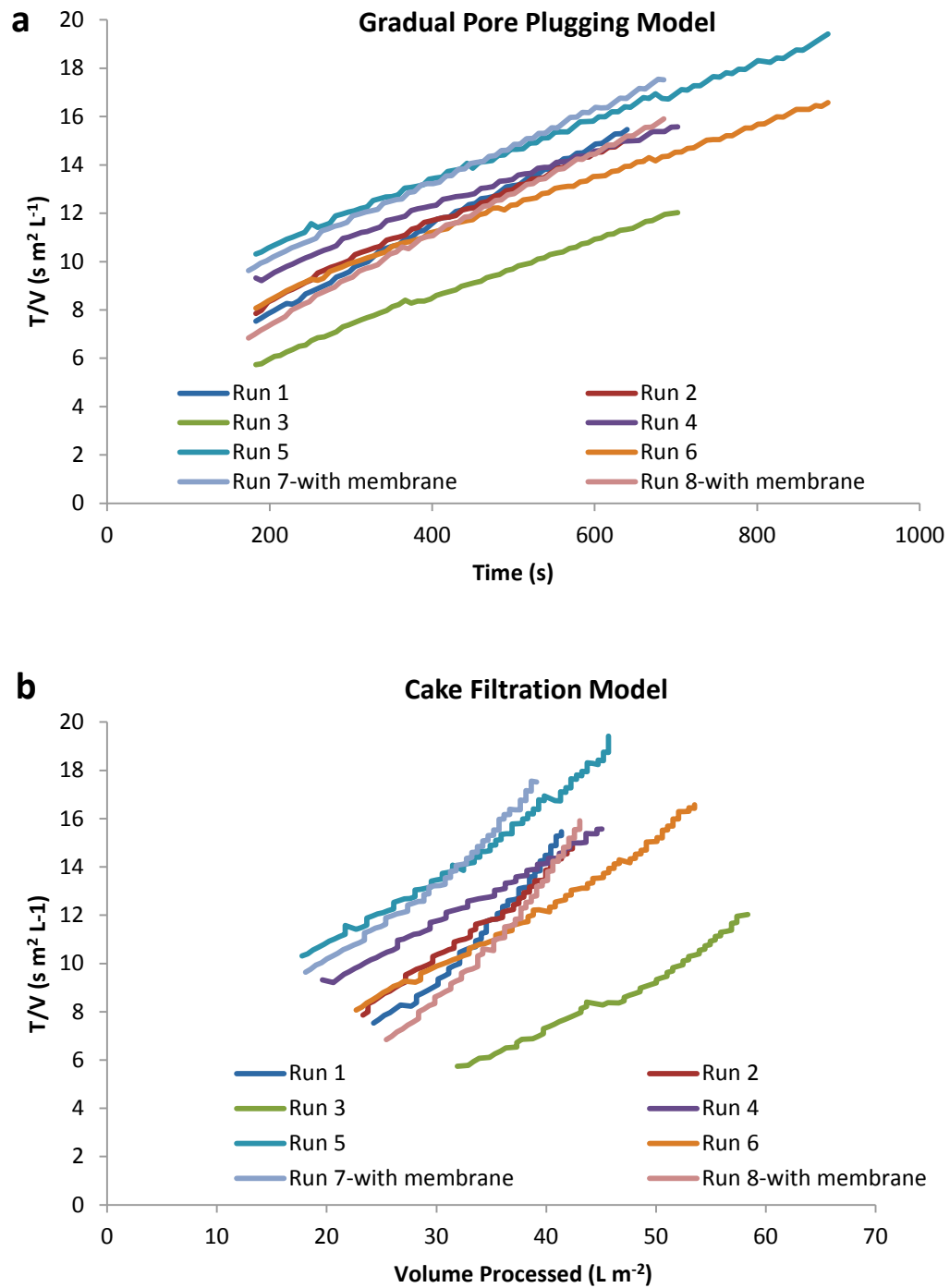


Figure 5.7a, b. A1HC depth filtration in constant vacuum USD device. Hydraulic data was fitted to the gradual pore plugging model (5.7a) or cake filtration model (5.7b). Data at the beginning of the run was excluded because the vacuum had not formed completely.

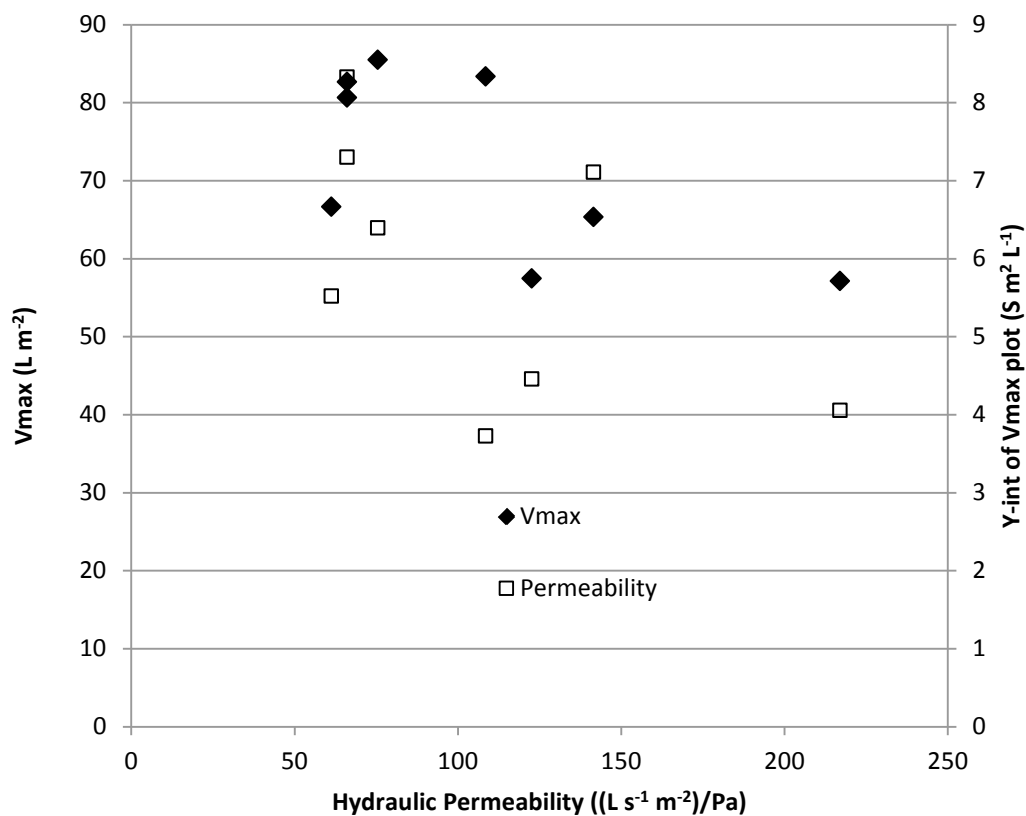


Figure 5.8. Correlation of water permeability of A1HC with the filtration performance obtained with CHO centrate. Data from eight independent filtrations were included in this plot.

It is evident that water permeability was predictive of neither V_{max} nor hydraulic permeability for the centrate load. The media may have not been “wet” fully due to the low permeability of A1HC combined with the maximum vacuum pressure (700 mbar) achievable with the USD device. An alternative explanation is that the binding of sample components to the adsorbent sites in the media altered the hydrodynamics. Irrespective of the underlying mechanism, this result undermined the utility of water permeability measurements with this device and media combination.

5.4.2.2.2 Adsorptive Removal

An adsorptive filter was tested in the UCL device (data not shown). The water permeability was a good predictor of flux obtained with the in-process CPS pool. The correspondence between water

permeability and process flux is believed to be due to a media structure that is more porous than A1HC. In this filter trial, removal of a specific impurity was dependent on contact time. Variability in filter permeability introduced inconsistent residence times, which led to inconsistent removal. The constant vacuum design of the UCL device did not offer direct control of residence time, making applications with adsorptive filters untenable. Hence, it was decided that the UCL device did not meet our micro-scale filtration needs.

5.4.3 Novel Micro-scale Depth Filtration Device

Testing of the aforementioned devices proved that depth media possessed satisfactory spatial heterogeneity to warrant further scale-down and highlighted the need to operate at constant flux. To design, fabricate, and develop novel USD depth filtration technology, a partnership between Pfizer and Bend Research, Inc. was created. My role included proposing, securing funding, and leading the project, but decisions and direction were decided by a collaborative, interdisciplinary team. As such, it was not a design determined solely by the thesis team.

5.4.3.1 Device Design and Engineering

Development of a suitable device took many design iterations, which are beyond the scope of this document. A concise summary follows. To avoid media cutting, initial efforts sought to isolate a small cylinder of media from a larger substrate using a variety of seal configurations on the top and bottom surfaces. Radial flow was excessive and the compressibility of the media altered filtration properties when under the axial load of the seal. These properties were filter media-specific, frustrating attempts for a universal device. As described in section 5.3.2.6, the final design included cutting filter discs to the desired size, sealing the edges of the media with epoxy, and forming sealing surfaces against a washer seal (top) and epoxy surface (bottom), thereby avoiding any media compression.

Samples of the engineering elements that underpinned design parameters and that I was solely responsible for are included in Appendix 9.7: Engineering of USD Depth Filtration Device.

5.4.3.2 Filtration Performance

The qualification of the HTDF device included several objectives: (i) filter puck manufacture had to be executed consistently, (ii) the precision of filtration performance between channels had to be established to qualify that a single run or two would yield representative results, (iii) performance, as measured with hydrodynamics and filtrate quality, would need to be scalable, and (iv) employment of steric and adsorptive media, with different porosities, compressibility, and materials of construction would need to demonstrate modularity.

5.4.3.2.1 Steric Filters

Non-adsorptive media characterized by different porosities were tested in the micro-scale depth filtration device. For 30SP and 60SP, the nominal retention ratings are 0.5-5 μm and 0.2-5 μm , respectively. In addition, 30SP is more compressible than 60SP. To benchmark performance, water permeability of the media was first measured (Figure 5.9).

The water permeability of 60SP ($613 \text{ L s}^{-1} \text{ m}^{-2}/\text{Pa} \pm 14\%$) at the micro-scale was indistinguishable from lab-scale ($762 \text{ L s}^{-1} \text{ m}^{-2}/\text{Pa} \pm 14\%$). Surprisingly, the precision was equivalent, suggesting that some of the noise at lab-scale is due to device design or scale-dependent operational constraints such as flow rate control. The water permeability of 30SP was approximately 4-fold higher than 60SP, consistent with the greater porosity and retention rating of this filter. Ascertaining the exact accessible filtration area of the USD filter discs was challenging due to slight variations in cutting, depth of epoxy penetration into the edges of the media, and variable heights of filter disc. To achieve equivalent water permeability based on the average values for 60SP, the effective filter area would calculate to be 0.19 cm^2 .

The two steric depth filters were challenged with centrate at two scales (Figure 5.10).

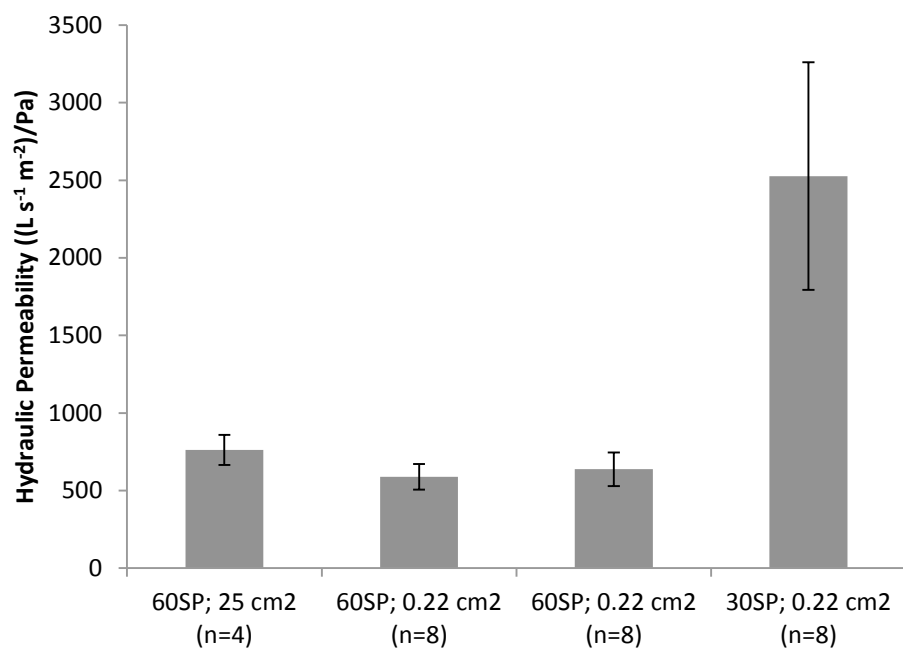
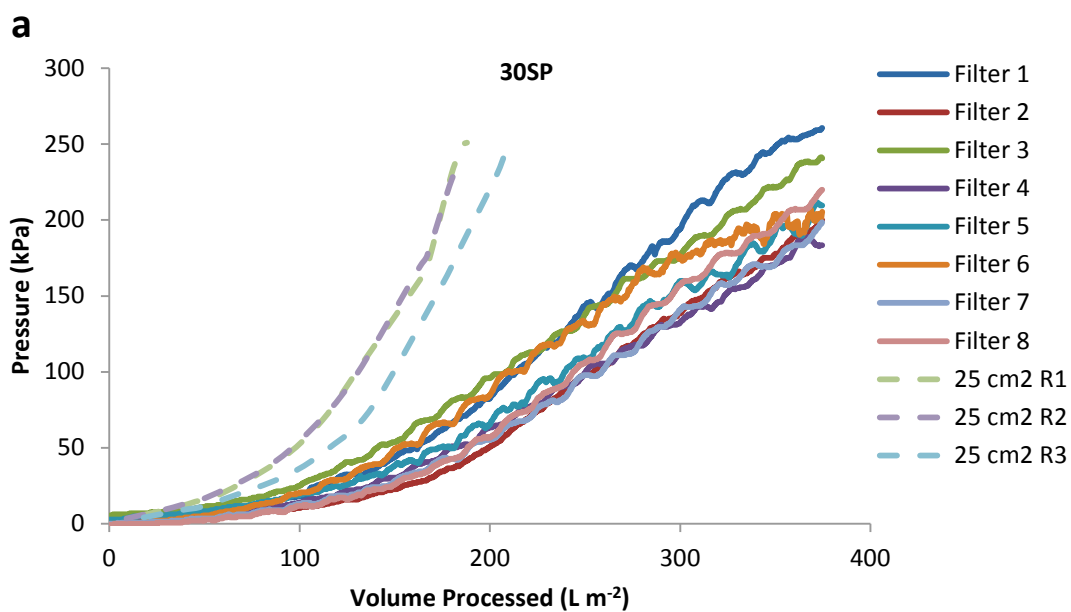


Figure 5.9. Water permeability of steric depth filtration media. The number in parentheses refers to the number of replicates that were averaged. Error bars represent the standard deviation of replicates. Permeability at lab-scale for 30SP was not included because the lab-scale pressure transducers offered neither adequate precision nor accuracy at the very low pressures characteristic of this particular hydraulic permeability testing.



b

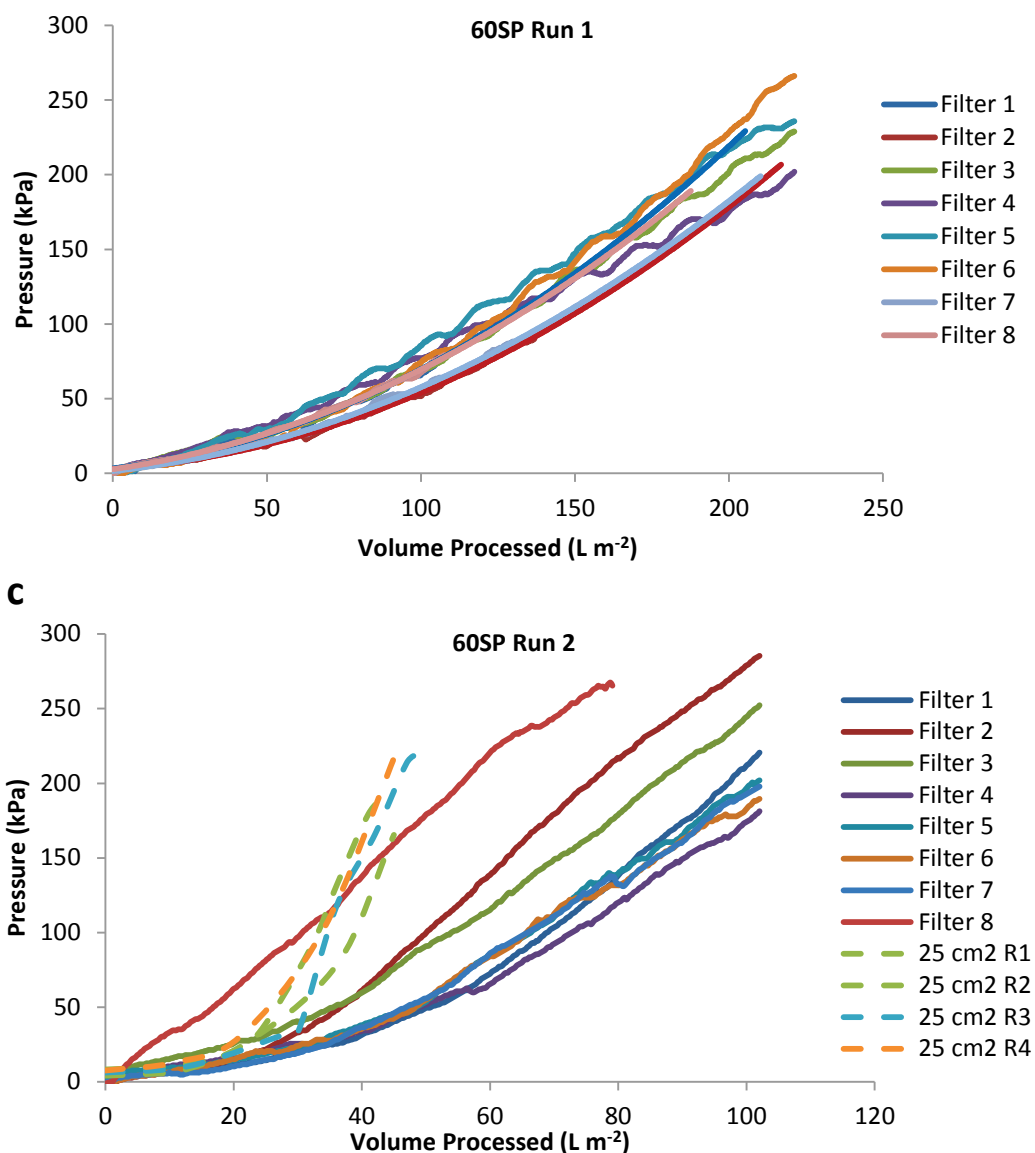


Figure 5.10a, b, c. Hydrodynamics during mAb concentrate filtration at USD- (solid lines) and lab-(dashed lines) scales for 30SP (5.10a), 60SP with freshly thawed concentrate (5.10b), and 60SP with thawed concentrate held for several hours at room temperature (5.10c). The dotted lines in 5.10b are extrapolations of polynomial fits for truncated filtration runs. Due to the complexity and rich growth potential of the feed material, capacity was a function of load hold time, thus requiring careful experimental planning.

Several commonalities were present in the filtration performance. Qualitatively, the precision of HTDF was excellent and the hydrodynamic profiles were consistent. Occasionally, a filter plugged earlier than the average of the HTDF set, likely due to filter heterogeneity or epoxy ingress as opposed

to a key area of concern: bypass between the epoxy and filter material, which would have been manifested as greater capacity. When comparing the two media, plugging across both scales occurred at a similar relative capacity, with 30SP filters exhibiting greater capacity than 60SP. Conversely, plugging occurred earlier at lab-scale than with HTDF. The performance can be quantified by calculating capacity at 170 kPa (Figure 5.11).

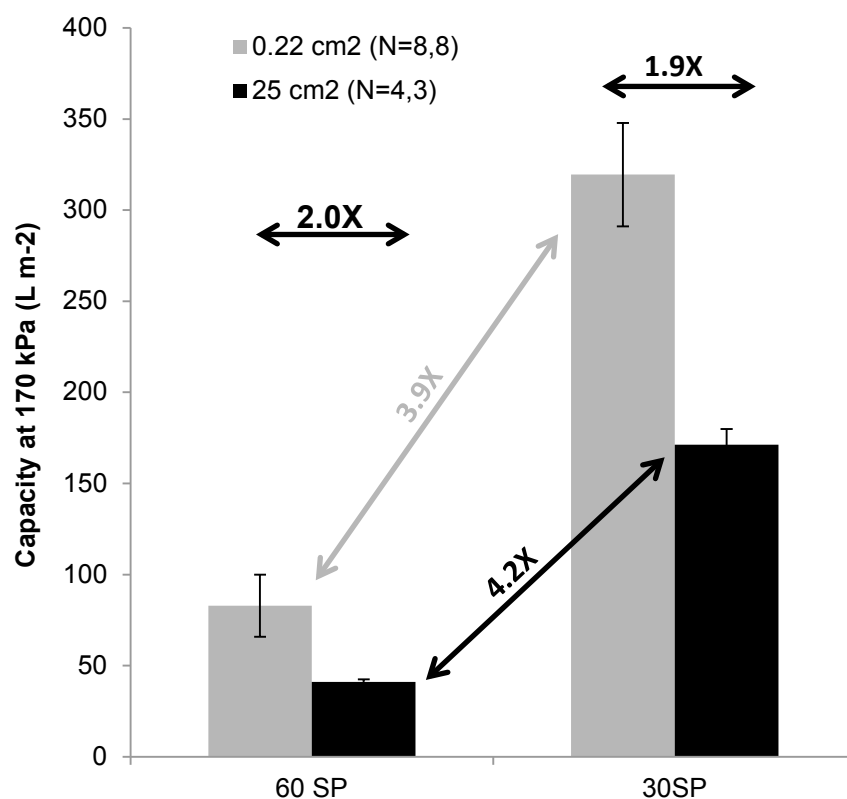


Figure 5.11. Capacity achieved at 170 kPa pressure with steric depth filters at two scales. Error bars represent the standard deviation of replicates (0.2 cm² scale: 30SP: N = 8, 60SP: N = 8; 25 cm² scale: 30SP: N = 3, 60SP: N = 4). Black and gray diagonal arrows/font show the quotients of the capacity differences between the two filters for a given scale. Horizontal black arrows and large black font provide the scaling factors between the two scales for each filter.

For both media, capacity at USD-scale exceeded lab-scale. Overall, the measurements were consistent and suggested a scaling factor of 2X between USD and lab-scale for this class of media. 30SP provided the best capacity, providing approximately 4X better capacity at both scales. As

expected, lower precision was observed with the USD runs, presumably due to spatial heterogeneity of the media, which is inversely proportional to the physical size of the filter sample. The consistency of the proportions, both between media and between scales indicated that HTDF provided repeatable relative scaling but a scaling factor (2X) was required to predict larger scale performance. HTDF achieved the goal of providing proportional performance to larger scales. When combined with a scaling factor, HTDF can be used to predict accurately capacity at larger scale.

Besides capacity, filtrate clarity is a critical performance attribute for depth filtration (Figure 5.12).

Improved filtrate clarity was observed with lab-scale experiments. This is consistent with the lower capacity achieved, suggesting solids loading capacity of the filters at both scales was more comparable than the capacity data suggested. At lab-scale, the reproducibility of filtrate clarity was also more consistent than at USD-scale. In practical terms, the scale-difference is negligible when viewed as a percentage of load turbidity or A_{600} values.

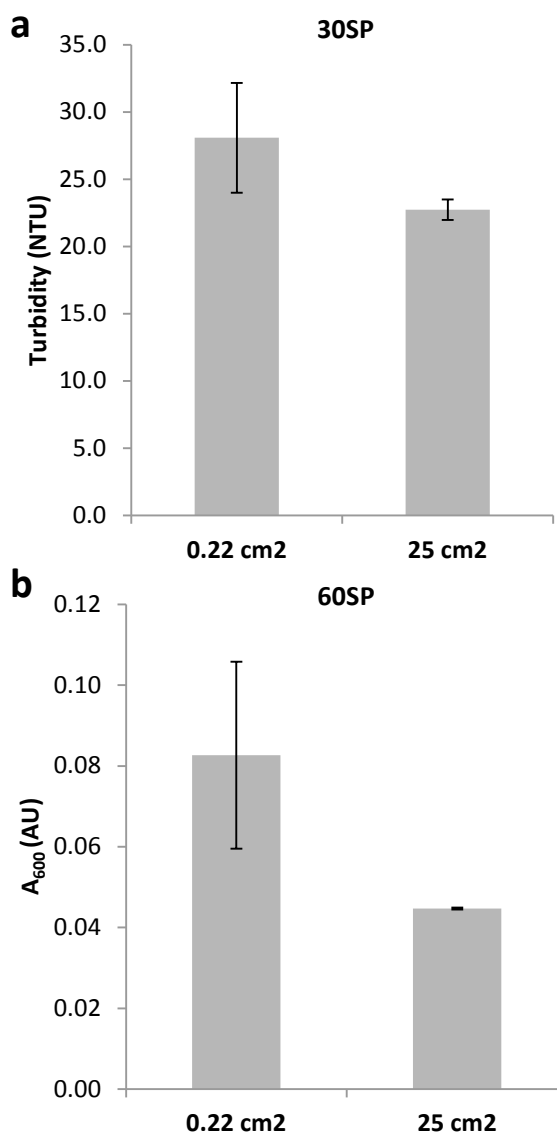


Figure 5.12a, b. Filtrate clarity of filtration scale-down. Mean turbidity of 30SP filtrate (5.12a) and 60SP filtrate (5.12b) at two scales. Error bars denote the standard deviation of replicates (0.2 cm² scale: 30SP: N = 8, 60SP: N = 8; 25 cm² scale: 30SP: N = 3, 60SP: N = 4). For the 60SP, A₆₀₀ measurements are given in lieu of turbidity measurements because HTDF filtrate volumes were too low for turbidimetric measurements. Load turbidities for 30SP and 60SP runs were 710 and 454 NTU, respectively. The corresponding load A₆₀₀ values were 0.68 and 0.60, respectively.

5.4.3.2.2 Adsorptive Filters

Conceptually, steric depth filters should be easier to scale than adsorptive depth filters, which combine steric retention with adsorptive media. Adsorptive capability is usually conferred through the impregnation of particles such as diatomaceous earth and is complicated by the addition of charged binders. As such, adsorptive filters represent a more challenging composite filter to scale-down. In addition, a popular adsorptive depth filter, XOHC, is comprised of two layers instead of the single layer of the 30SP and 60SP filters.

Filter pucks were produced for each layer of XOHC. A two-layer filter sandwich was composed by stacking two filter pucks in the HTDF holder, separated by a double O-ring seal. This configuration was more sensitive to filter pucks that did not have parallel sealing surfaces. The filtration performance of XOHC at USD- and lab-scale was compared with a complex centrate stream composed of CHO mAb centrate (Figure 5.13). With XOHC, the filtration hydrodynamics and plugging profiles were equivalent between the two scales. The RSD of capacity for lab-scale devices was 7% (and 5% for a related study ($n=3$; data not shown)). As with the steric filters, the precision declined slightly at the micro-scale. However, the RSD was still 16% at the micro-scale, consistent enough for a user to have confidence in a solitary screening data point.

The filtrate clarity for both runs is given in Figure 5.14. The filtrate clarity was comparable between the three runs at each scale. The precision of A_{600} measurements was 9% and 5% for the 0.22 cm² and 23 cm² scales, respectively.

The results with two steric filters and an adsorptive filter demonstrate that the constant flux USD device can reliably scale-down depth filtration. For the 30SP and 60SP, accurate scale-down required a scaling factor of 2 and resulted in marginally less turbid samples at the micro-scale. For XOHC, accurate scale-down was achieved without any scaling factor except standard filtration scaling by unit filter area. The clarity of HTDF-derived, XOHC filtrate samples was comparable to lab-scale. The basis for the scaling differences between the two classes of filters is unknown. It may be due to structural differences between the two broad classes of media or the scaling factor may turn out to be specific for each filter, device, or vendor. Additional research is required to deepen this understanding.

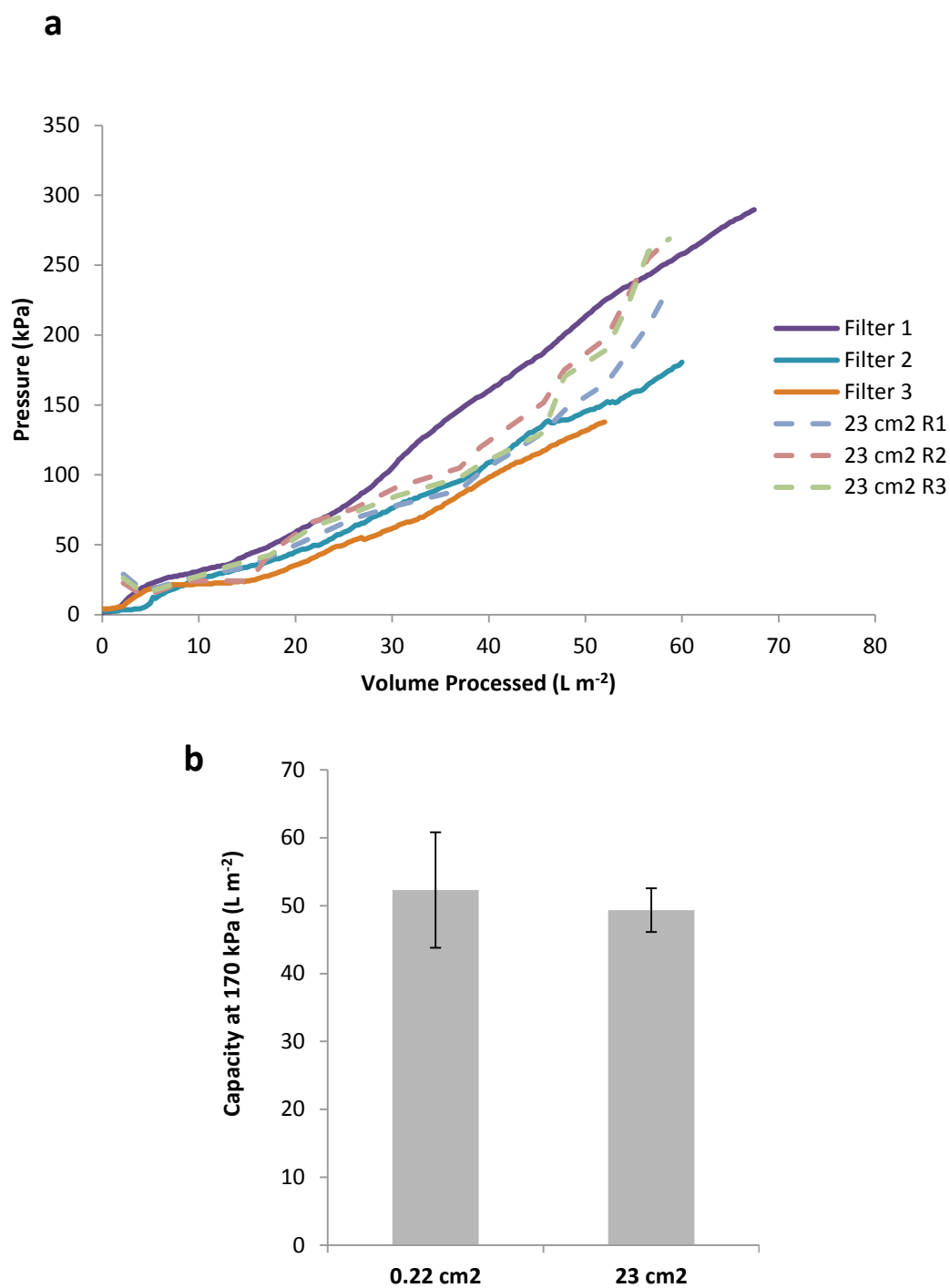


Figure 5.13a, b. XOHC filtration at USD- and lab-scale. Filtration hydrodynamics at 0.22 cm² scale (N = 3, connected data points) and 23 cm² scale (N = 3, unconnected data points) (5.13a) and filter capacity at 170 kPa (5.13b). Error bars denote the standard deviation of replicates.

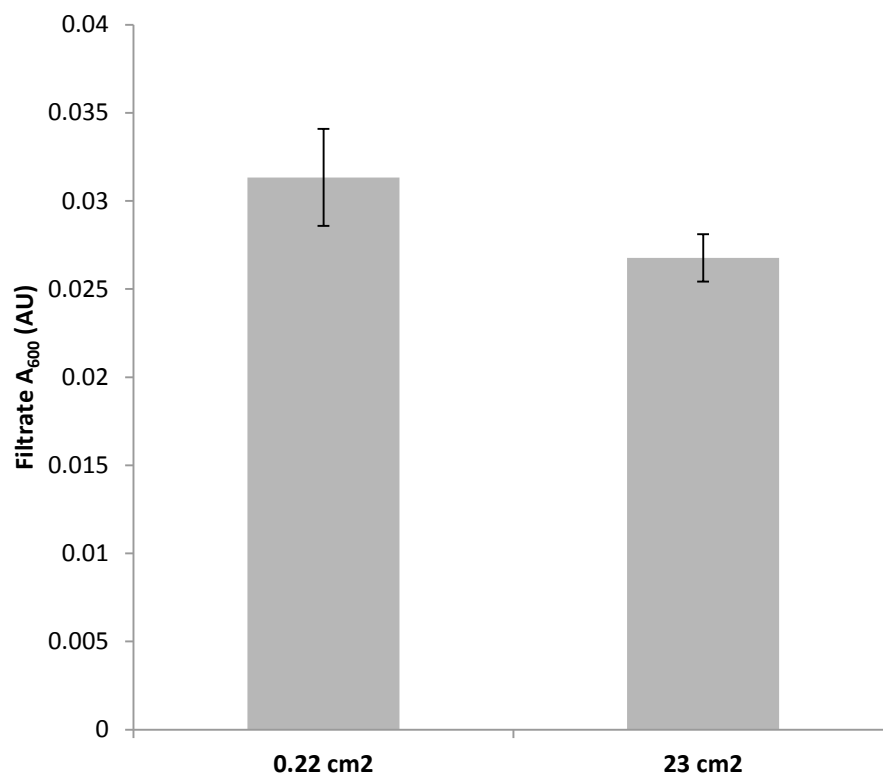


Figure 5.14. Filtrate clarity of X0HC runs. A_{600} in filtrate of runs at 0.22 cm² (N = 3) and 23 cm² (N = 3) scales. The A_{600} of the load was 0.55 AU.

5.4.4 Micro-scale Clarity Measurements

The advent of HTDF and HTPC has exposed an acute need for meaningful measurements of clarity at the micro-scale. The ideal assay would be correlated to historical measurements, require < 1 mL of sample, and offer microplate-based measurements. Samples characterised by a broad range of clarity were systematically analysed with A_{405} , A_{600} , MFI particle characterisation, Hach turbidity, and Nephelostar turbidity. A comprehensive analysis of these studies is given in Appendix 9.8:

Correlations between Clarity Measurements. As a result of these studies, three measurements are proposed for future work at the micro-scale: (i) Nephelostar NTU to provide a NTU value that provides context to people familiar with larger scale measurements, (ii) A_{600} because where $NTU > 20$, A_{600} is proportional to Hach NTU and can be measured rapidly with the same sample plate used in the Nephelostar, and (iii) MFI particle counts/size because these properties offer the most sensitive

measurement and can facilitate mechanistic insight where necessary. With this set of three complementary clarity assays, many samples can be measured and analysed quickly, using < 1 mL of sample.

5.5 Chapter Summary

This chapter described the development and qualification of an automated system for high throughput USD depth filtration. The filtration area is 2 logs less than the smallest commercially available devices, opening up applications including filter screening, capacity optimization, and rapid sample prep. The 8-channel system has been qualified for two steric and one adsorptive depth filtration media. Comparisons with lab-scale benchmarks have demonstrated that the USD system can accurately emulate results at larger scale including both hydrodynamics and filtrate clarity. No one measurement has been determined to give a full picture of clarity and at a minimum, a combination of turbidity and MFI particle characterisation would be best.

In researching HTDF, it became apparent that meaningful micro-scale measurements of clarity were needed. Diverse technology including multiple nephelometers, absorbance at multiple wavelengths, and particle characterisation by image analysis and dynamic light scattering were compared systematically. Nephelostar turbidity, A_{600} , and particle concentration by MFI offered the most utility for HTDF while providing comparability with the existing knowledge base at larger scales.

The need for high throughput micro-scale depth filtration and clarity measurements would be lessened if a capability to predict filterability existed. To explore this area, feed samples representing several levels of filterability were assessed analytically. The samples were analysed by the battery of micro-scale clarity measurements and processed through a variety of filterplates. Of the assays, only MFI particle counts, specifically particles 1-2 μm in diameter, correlated with filterability. Filterplates were found to be too variable or to offer no useful differentiation of the feedstreams. Additional research in this area has the potential to transform filtration development.

This thesis chapter has detailed successful attempts to enable high throughput depth filtration at the micro-scale, to identify meaningful and rapid microplate assays for filtrate clarity, and to begin the development of characterisation approaches that will enable the prediction of filterability based on sample properties alone.

6 Conclusions and Future Work

6.1 Conclusion

The development of purification processes for multivalent polysaccharide vaccines has required substantial resources, owing to the complexity and sheer number of unique molecular entities included in a single conjugated polysaccharide vaccine product. Technologies to streamline process development will reduce the time and expense to bring new vaccines to the clinic, thereby increasing vaccine availability to the global market.

6.1.1 High Throughput Analytics

The advent of HTPD approaches is dependent on the availability of relevant HT analytical capabilities.

6.1.1.1 *Product Quantification and Quality*

Several high throughput methods were developed to quantify product titre, with an emphasis on methods specific to a particular carbohydrate structure. In the first approach, a phenol sulphuric acid assay was adapted to a microplate, providing a broad spectrum assay for pentoses and hexoses. However, the employment of toxic reagents limited the applicability of this approach and made integration with an open liquid handling system infeasible. To overcome these limitations, a novel analytical application of Hb was devised to precipitate anionic polysaccharides, resulting in turbidity that was proportional to product concentration. Negligible reactivity with neutral polysaccharides combined with an extent of reaction correlated to the polysaccharide charge density indicated electrostatic interactions were predominant. A final high throughput titre assay adapted SEC-MALS, conventionally run with HPLC, to UPLC. This approach enabled multiplexed determination of polysaccharide titre and product quality attributes, MW and r_{rms} .

6.1.1.2 Impurity Determination

Capsular polysaccharides must be separated from many impurities, requiring a suite of high throughput impurity analytics for thorough sample interrogation. Of particular interest, the compatibility (cross-reactivity, interference, etc.) of assays with CPS and various sample matrix components was evaluated. Standard approaches for protein quantification, based on Bradford and BCA, were assessed. DNA was measured with Picogreen where cross-reactivity with CPS, necessitated dilution strategies. A commercial endotoxin assay was simplified and shown to be suitable for use with CPS. Combined with standard spectrophotometric approaches for relatively clean streams, a fit-for-purpose suite of high throughput biochemical analytics was qualified for deployment in HTPD with CPS. Collectively, these analytics have resulted in an over 10-fold savings in labour and a similar reduction in overall costs while decreasing analytical turnaround time by weeks.

6.1.2 High Throughput Particle Conditioning

USD systems were designed for the high throughput development of particle conditioning operations: flocculation, particle aging, and centrifugation. Microplate-based workflows were developed that required 600 uL of feed per condition, enabling the parallel screening of up to 80 conditions. An emphasis on selecting off-the-shelf components ensured that this system could be utilised by researchers elsewhere. The mean precision between duplicate conditions was found to be < 15% RSD for the set of high throughput analytics. An engineering characterisation of hydrodynamics supported the design of the USD system and enabled a mechanistic comparison with several larger scales. Blend time studies demonstrated that turbulent conditions persisted in the USD microwell, contrary to conventional Reynolds number analysis. In addition, the N_p of the magnetic stir bar was determined to be 1.0, the first characterized instance of a stir bar N_p . These findings will facilitate the engineering analyses of future USD applications.

The performance of particle conditioning processes was compared at USD- and Pilot-scale. Diverse polysaccharides from three bacterial species were evaluated using full factorial particle conditioning DOEs with pH, floc agent concentration, and/or aging time as factors. Product yield and MW were

equivalent at both scales. DNA and protein clearance were similar between scales except in regions where impurity responses were highly sensitive to slight changes in input factors, in which slight differences were observed. All three primary factors influenced purity. Particle characteristics were dependent on the hydrodynamic scaling rule. Scaling by constant v_{tip} , P/V_{imp} and time-integrated permutations on these values yielded consistent particle sizes and particle concentrations in both HTPC and Pilot systems. Standard DOE analysis was implemented for HTPC, leading to statistical modelling and delineation of a QbD design space. Models for individual responses were integrated to illuminate multi-dimensional windows of operation. Scaling centrifugation by Sigma theory provided consistent results, indicating that the flocs were insensitive to shear in the DSC. Overall, HTPC provided comparable results to Pilot-scale with respect to product yield, product quality, impurity clearance, and particle characterisation.

6.1.3 High Throughput Depth Filtration

Depth filtration performance is a key factor in optimizing particle conditioning. Indeed, depth filtration is prevalent in biotechnology purification processes but the smallest commercial systems require 0.5 L to assess depth filterability. Custom USD devices produced by Pfizer and the Department of Biochemical Engineering at UCL were evaluated and found to be inadequate for the relevant depth filtration applications. To address this technology gap, a bespoke novel system for high throughput USD depth filtration, HTDF, was developed using 0.2 cm² cross-sectional area per filter and requiring 4 mL of feed material to achieve a desired target capacity of 200 L m⁻². Eight streams can be filtered in parallel with automated operation and collection of pressure data. Key engineering properties were matched to those characteristic of large-scale devices to assist scale-down. The technology is modular with respect to filter media, accommodating a broad range of media compositions, porosity, and surface topography. The performance of two steric depth filtration media was compared in the USD and commercially available lab-scale devices. HTDF yielded filtrates of comparable clarity and slightly higher capacity than lab-scale filters. Precision of 20% RSD was achieved, better than the published precision for lab-scale filtration devices. These results

demonstrated that micro-scale devices provide meaningful scale-down with comparable performance to larger-scale.

6.1.4 Final Conclusion

In this dissertation, we have designed, developed, and qualified systems and approaches to enable high throughput particle conditioning and depth filtration for capsular polysaccharides. These technologies will reduce the resource investment and increase the richness of data produced in process development. The investments made in developing generic and modular systems suggest that these approaches will be applicable to a wider spectrum of molecules, specifically proteins and products derived from mammalian cell culture.

6.2 Future Work

This research has demonstrated the utility of HTPD using USD approaches for particle conditioning and depth filtration. To further this understanding, additional research is warranted in the following areas:

6.2.1 High Throughput Analytics

Solutions for rapid analysis of yield and impurity were developed along with MALS-based measures of product quality. Additional high throughput assays of CPS quality would be useful. In particular, assays for quantifying the amount and location of O-acetylation and N-acetylation are laborious and typically require complex procedures such as nuclear magnetic resonance. Simplification of quality assays would expand the potential scope for HTPD.

MFI offers a high throughput approach for assessing particles 1-70 μm in size. The available technologies for analysis of particles $< 1 \mu\text{m}$ in size are lacking, requiring either meticulous sample preparation or simple sample matrices. A technology for high throughput particle characterization for assessing the amount, size, and morphology of particles 0.1-1.0 μm in diameter would yield insight that would be helpful in delineating how floc distributions affect filtration.

6.2.2 High Throughput Particle Conditioning

6.2.2.1 *Deepening Understanding of Scalability*

HTPC was proven a high fidelity USD model for Pilot-scale particle conditioning of CPS. Additional verification of scaling rules would be prudent. The applicability of Sigma theory for centrifugation scaling with CPS should be evaluated more thoroughly, particularly where DSCs are employed.

Additional studies could decouple the relative suitability of v_{tip} , P/V_{imp} , and time-integrated forms of these parameters for the scaling of hydrodynamic conditions. An examination of any CPS-dependency of these heuristics would establish the versatility of these scaling rules. Since particle properties were the most scale-dependent property, additional characterisation of particles at several

larger scales would be valuable. This would enable a mechanistic analysis of particle size, size, and the interplay of dynamic aging processes. Deepening the understanding of how different measures of clarity interrelate also would be beneficial.

6.2.2.2 *Measuring Clarity*

Significant progress was made in correlating the diverse measurements available for measuring clarity but the relationships are complex. Nonlinearity in assay responses characterised by turbidity ≤ 15 NTU warrants further investigation. The correlation of MFI particle counts with filterability should be developed for different media. Moreover, growing the understanding of the relationship between filter composition and the salient physical properties that influence relative filterability is a fertile area for exploration.

6.2.2.3 *Predicting Clarification*

The connection between flocculation conditions and downstream clarification via centrifugation and depth filtration is complex. Studies should seek to establish which particle properties relate to shear sensitivity, floc strength, and the capacity of particles to survive centrifugation intact. It would be useful to develop a HT method for applying controlled shear to flocs in order to estimate floc strength. Extending this understanding to connect flocculation conditions to the depth filtration performance of the respective centrate would be pivotal. Ideally, such investigations would enable one to predict depth filtration based on the particle characteristics of the flocs. Accordingly, resources should be invested in technology to predict filterability. Progress in this area would fill out response gaps in the current HTPC state and eliminate the need to perform HTDF with each floc study.

6.2.2.4 *Structure-function Relationships*

CPS are ripe for investigations into how CPS structure informs purification behaviour. The rheology of CPS spans a broad spectrum yet the molecular underpinnings are opaque. Little is known about the

structural basis for the differential shear-sensitivity of CPS and the influence on processability. In-process stability is likely affected by CPS conformation. Illuminating these areas would increase biophysical understanding and lead to the development of more sophisticated predictive tools for process development.

6.2.2.5 Expand Applications

The operational envelope for which HTPC is qualified should be expanded. Additional flocculation and precipitation agents should be integrated into HTPC to enable their reliable and routine use (*i.e.* in platform screens). The scalability of HTPC results should be evaluated with various molecular modalities, including proteins, virus-like particles, viruses, and DNA. The clarification of very high cell density mammalian cell cultures is a specific application in which HTPC shows promise.

6.2.3 High Throughput Depth Filtration

HTDF would benefit from additional development. Three types of depth filtration media have been qualified with the HTDF technology. Proving the scalability of filtration performance for additional depth filtration media would increase the screening capability of the apparatus. There appear to be media- and/or device-specific influences on scaling parameters and understanding these relationships would increase confidence in scaling predictions. The HTDF device created for this study was a beta prototype. A “next generation” version could be designed to streamline the manufacture of filter pucks, improve software functionality, automate water flush functions, and incorporate other minor hardware modifications.

6.2.4 Final Thoughts

There is a tremendous potential to build on these initial HTPC and HTDF platforms. Modest additional investments along with the appropriate focus can yield process insight that will expand the state-of-the-art and maintain UCL’s and Pfizer’s leadership in this area.

7 References

- Adam O, Vercellone A, Paul F, Monsan PF, Puzo G. 1995. A nondegradative route for the removal of endotoxin from exopolysaccharides. *Anal Biochem* **225**:321-327.
- Afshar Ghotli R, Raman A, Ibrahim S, Baroutian S. 2013. Liquid-liquid mixing in stirred vessels: a review. *Chem Eng Commun* **200**:595-627.
- Agbenorhevi JK, Kontogiorgos V. 2010. Polysaccharide determination in protein/polysaccharide mixtures for phase-diagram construction. *Carbohydr Polym* **81**:849-854.
- Ahmad SS, Dalby PA. 2011. Thermodynamic parameters for salt-induced reversible protein precipitation from automated microscale experiments. *Biotechnol Bioeng* **108**:322-332.
- Al-Tawfiq J, Clark T, Memish Z. 2010. Meningococcal disease: the organism, clinical presentation, and worldwide epidemiology. *J Travel Med* **17 Suppl**:3-8.
- Ambler C. 1959. The theory of scaling up laboratory data for the sedimentation type centrifuge. *J Biochem Microbiol Technol Eng* **1**:185-205.
- Anderson P, Smith DH. 1977. Isolation of the capsular polysaccharide from culture supernatant of *Haemophilus influenzae* type b. *Infect Immun* **15**:472-7.
- Armenante P, Change G. 1998. Power consumption in agitated vessels provided with multiple-disk turbines. *Ind Eng Chem Res* **37**:284-291.
- Astronomo RD, Burton DR. 2010. Carbohydrate vaccines: developing sweet solutions to sticky situations? *Nat Rev Drug Discov* **9**:308-324.
- Atiemo-Obeng V, Penney W, Armenante P. 2004. Solid-liquid Mixing. In: Paul, E, Atiemo-Obeng, V, Kresta, S, editors. *Handbook of Industrial Mixing: Science and Practice*. John Wiley & Sons, pp. 543-584.
- Aucamp JP, Cosme AM, Lye GJ, Dalby P a. 2005. High-throughput measurement of protein stability in microtiter plates. *Biotechnol Bioeng* **89**:599-607.
- Awtrey A, Connick R. 1951. The rate law and mechanism of the reaction of iodine with thiosulfate ion: the formation of the intermediate $S_2O_3I^-$. *JACS* **73**:1341-1348.
- Badmington F, Wilkins R, Payne M, Honig E. 1995. Vmax testing for practical microfiltration train scale-up in biopharmaceutical processing. *Pharm Technol*:64-76.
- Bae K, Choi J, Jang Y, Ahn S, Hur B. 2009. Innovative vaccine production technologies: the evolution and value of vaccine production technologies. *Arch Pharm Res* **32**:465-480.
- Balasundaram B, Sachdeva S, Bracewell DG. 2011. Dual salt precipitation for the recovery of a recombinant protein from *Escherichia coli*. *Biotechnol Prog* **27**:1306-14.

- Ball TK, Saurugger PN, Benedik MJ. 1987. The extracellular nuclease gene of *Serratia marcescens* and its secretion from *Escherichia coli*. *Gene* **57**:183-192.
- Bao H, Li L, Gan LH, Zhang H. 2008. Interactions between ionic surfactants and polysaccharides in aqueous solutions. *Macromolecules* **41**:9406-9412.
- Bardotti A, Averani G, Berti F, Berti S, Carinci V, D'Ascenzi S, Fabbri B, Giannini S, Giannozzi A, Magagnoli C, Proietti D, Norelli F, Rappuoli R, Ricci S, Costantino P. 2008. Physicochemical characterisation of glycoconjugate vaccines for prevention of meningococcal diseases. *Vaccine* **26**:2284-96.
- Bardotti A, Averani G, Berti F, Berti S, Galli C, Giannini S, Fabbri B, Proietti D, Ravenscroft N, Ricci S. 2005. Size determination of bacterial capsular oligosaccharides used to prepare conjugate vaccines against *Neisseria meningitidis* groups Y and W135. *Vaccine* **23**:1887-1899.
- Baruque-Ramos J, Hiss H, Dearauz L, Mota R, Riccisilva M, Dapaz M, Tanizaki M, Raw I. 2005. Polysaccharide production of (Serogroup C) in batch and fed-batch cultivations. *Biochem Eng J* **23**:231-240.
- Batchelor G. 1947. Kolmogoroff's theory of locally isotropic turbulence. *Proc Cambridge Phil Soc* **43**:533-559.
- Bell DJ, Dunnill P. 1982. Shear disruption of soya protein precipitate particles and the effect of aging in a stirred tank. *Biotechnol Bioeng* **24**:1271-1285.
- Bell DJ, Heywood-Waddington D, Hoare M. 1982. The density of protein precipitates and its effect on centrifugal sedimentation. *Biotech Bioeng* **24**:127-141.
- Bell DJ, Hoare M, Dunnill P. 1983. The formation of protein precipitates and their centrifugal recovery. In: . *Downstream processing*. Springer Berlin Heidelberg, pp. 1-72.
- Belter P, Cussler E, Hu W. 1988. Precipitation. In: . *Bioseparations; Downstream Processing for Biotechnology*. New York: John Wiley & Sons, pp. 21-236.
- Berrill A, Ho S, Bracewell D. 2008. Ultra scale-down to define and improve the relationship between flocculation and disc-stack centrifugation. *Biotechnol Prog* **24**:426-431.
- Berry DS, Lynn F, Lee C-hung, Frasch CE, Bash MC. 2002. Effect of O-acetylation of *Neisseria meningitidis* serogroup A capsular polysaccharide on development of functional immune responses. *Infect Immun* **70**:3707-3713.
- Bhambure R, Kumar K, Rathore A. 2011. High throughput process development for biopharmaceutical drug substances. *Trends Biotechnol* **29**:127-135.
- Biddlecombe R, Pleasance S. 1999. Automated protein precipitation by filtration in the 96-well format. *J Chromatogr B* **734**:257-65.
- Bill and Melinda Gates Foundation. 2014. Vaccine delivery strategy overview. <http://www.gatesfoundation.org/What-We-Do/Global-Development/Vaccine-Delivery>.
- Bio Rad. 2008. Bradford Protein Assay. *Cold Spring Harbor Protocols*. Hercules. Vol. 2006.
- BioPartners S. 2011. Focus on cost of goods during process development. <http://www.syncobiopartners.com/modules/cms/rubriek113.aspx?CatID=55>.

- Biswas SC, Chatteraj DK. 1997. Polysaccharide-surfactant interaction. 2. Binding of cationic surfactants to carboxymethyl cellulose and dextrin. *Langmuir* **13**:4512-4519.
- Black S, Shinefield H, Fireman B, Lewis E, Ray P, Hansen JR, Elvin L, Ensor KM, Hackell J, Siber G, Malinoski F, Madore D, Chang I, Kohberger R, Watson W, Austrian R, Edwards K. 2000. Efficacy, safety and immunogenicity of heptavalent pneumococcal conjugate vaccine in children. *Pediatr Infect Dis J* **19**:187-95.
- Bonnerjea J. 1988. Affinity flocculation of yeast cell debris by carbohydrate-specific compounds. *Enzyme Microb Tech* **10**:357-360.
- Bonnerjea J, Oh S, Hoare M. 1986. Protein purification: The right step at the right time. *Nature Biotech* **4**:954-956.
- Boychyn M, Doyle W, Bulmer M, More J, Hoare M. 2000. Laboratory scaledown of protein purification processes involving fractional precipitation and centrifugal recovery. *Biotechnol Bioeng* **69**:1-10.
- Boychyn M, Yim S, Bulmer M, More J, Bracewell D, Hoare M. 2004. Performance prediction of industrial centrifuges using scale-down models. *Bioprocess Biosyst Eng* **26**:385-91.
- Boychyn M, Yim S, Shamlou P, Bulmer M, More J, Hoare M. 2001. Characterization of flow intensity in continuous centrifuges for the development of laboratory mimics. *Chem Eng Sci* **56**:4759-4770.
- Bradford MM. 1976. A rapid and sensitive method for the quantitation of microgram quantities of protein utilizing the principle of protein-dye binding. *Anal Biochem* **72**:248-254.
- Brodsky Y, Zhang C, Yigzaw Y, Vedantham G. 2012. Caprylic acid precipitation method for impurity reduction: an alternative to conventional chromatography for monoclonal antibody purification. *Biotechnol Bioeng* **109**:2589-2598.
- Brons C, Olieman C. 1983. Study of the high-performance liquid chromatography separation of reducing sugars, applied to the determination of lactose in milk. *J Chromatogr A* **259**:79-86.
- Brown RE, Jarvis KL, Hyland KJ. 1989. Protein measurement using bicinchoninic acid: elimination of interfering substances. *Anal Biochem* **180**:136-9.
- Buckland B. 2014. Development and scale-up of an insect cell culture-based process for making Flubluk, the first FDA-licensed recombinant influenza vaccine. In: . *Vaccine Technology V*. Playa del Carmen, Mexico: Protein Sciences.
- Buxbaum E. 2003. Cationic electrophoresis and electrotransfer of membrane glycoproteins. *Anal Biochem* **314**:70-76.
- Camp T, Conklin G. 1970. Towards a rational jar test for coagulation. *Jour NEWWA* **84**:325-338.
- Camp T, Stein P. 1943. Velocity gradients and internal work in fluid motion. *J Boston Soc Civ Eng* **1**:219-237.
- Centers for Disease Control. 2002. Progress toward elimination of Haemophilus influenzae Type b invasive disease among infants and children -- United States, 1998-2000. *MMWR Morb Mortal Wkly Rep* **51**:234-237.
- Centers for Disease Control. 2005. Prevention and control of meningococcal disease. *MMWR Morb Mortal Wkly Rep* **54**:1-21.

- Centers for Disease Control. 2010a. Licensure of a meningococcal conjugate vaccine (Menveo) and guidance for use — advisory committee on immunization practices (ACIP). *MMWR Morb Mortal Wkly Rep* **59**:273.
- Centers for Disease Control. 2010b. Active Bacterial Core Surveillance (ABCs) Report, Emerging Infections Program Network, *Neisseria meningitidis*.
- Cepria G, Castillo JR. 1997. Surface plasmon resonance-based detection. An alternative to refractive index detection in high-performance liquid chromatography. *J Chromatogr A* **759**:27-35.
- Chakraborty T, Chakraborty I, Ghosh S. 2006. Sodium carboxymethylcellulose-CTAB interaction: a detailed thermodynamic study of polymer-surfactant interaction with opposite charges. *Langmuir* **22**:9905-13.
- Chan G, Booth AJ, Mannweiler K, Hoare M. 2006. Ultra scale-down studies of the effect of flow and impact conditions during *E. coli* cell processing. *Biotechnol Bioeng* **95**:671-683.
- Chandler M, Zydney A. 2004. High throughput screening for membrane process development. *J Membr Sci* **237**:181-188.
- Chandramohan D, Hodgson A, Coleman P, Baiden R, Asante K, Awine E, Owusu-Agyei S, Boutriau D, Nelson CB, Greenwood B. 2007. An evaluation of the immunogenicity and safety of a new trivalent meningococcal polysaccharide vaccine. *Vaccine* **25 Suppl 1**:A83-91.
- Chatel A, Kumpalume P, Hoare M. 2014. Ultra scale-down characterization of the impact of conditioning methods for harvested cell broths on clarification by continuous centrifugation-Recovery of domain antibodies from rec *E. coli*. *Biotechnol Bioeng* **111**:913-924.
- Chen PS, Toribara TY, Warner H. 1956. Microdetermination of phosphorus in organic compounds. *Anal Chem* **28**:1756-1758.
- Chhatre S, Titchener-Hooker NJ. 2009. Review: Microscale methods for high-throughput chromatography development in the pharmaceutical industry. *J Chem Technol Biotechnol* **84**:927-940.
- Coffman JL, Kramarczyk JF, Kelley BD. 2008. High-throughput screening of chromatographic separations: I. Method development and column modeling. *Biotechnol Bioeng* **100**:605-18.
- Cohn EJ. 1925. The physical chemistry of proteins. In: . *Physiol Rev* **5**, p. 349.
- Compton SJ, Jones C. 1985. Mechanism of dye response and interference in the Bradford protein assay. *Anal Biochem* **151**:369-74.
- Costantino P. 2002. Capsular polysaccharide solubilisation and combination vaccine. European Patent EP2216044A1.
- Costantino P. 2006. Purification of streptococcal capsular polysaccharide. World Intellectual Property Organization WO 2006-082527 A2.
- Costantino P, Norelli F, Giannozzi A, D'Ascenzi S, Bartoloni A, Kaur S, Tang D, Seid R, Viti S, Paffetti R, Bigio M, Pennatini C, Averani G, Guarnieri V, Gallo E, Ravenscroft N, Lazzeroni C, Rappuoli R, Ceccarini C. 1999. Size fractionation of bacterial capsular polysaccharides for their use in conjugate vaccines. *Vaccine* **17**:1251-1263.

- Costantino P, Viti S, Podda A, Velmonte MA, Nencioni L, Rappuoli R. 1992. Development and phase 1 clinical testing of a conjugate vaccine against meningococcus A and C. *Vaccine* **10**:691-698.
- Couper J, Penney W, Fair J, Wales S. 2010. Mixing and agitation. In: . *Chemical Process Equipment* 2nd ed. Elsevier, Vol. 3, pp. 273-324.
- Crittenden J, Trussel R, Rhodes D, Tchobanoglous G. 2005. Coagulation, mixing, and flocculation. In: . *Water Treatment-Principles and Design* 2nd editio. John Wiley and Sons, pp. 643-711.
- Cruz-Leal Y, Menéndez T, Coizeau E, Espinosa RR, Canaan L, Blanco F, Carmenate T, Chang J, Quiñones D, Tamargo I, Cremata J, Verez-Bencomo V, Guillén G. 2006. Enzyme-linked immunosorbent assay for quantitative determination of capsular polysaccharide production in *Streptococcus pneumoniae* clinical isolates. *Biotechnol Appl Biochem* **44**:101-108.
- Cuesta G, Suarez N, Bessio MI, Ferreira F, Massaldi H. 2003. Quantitative determination of pneumococcal capsular polysaccharide serotype 14 using a modification of phenol-sulfuric acid method. *J Microbiol Methods* **52**:69-73.
- Cuo J. 1977. Patent: Isolation and purification of polyribosyl ribitol phosphate from haemophilus influenzae tybe b. United States US4220717.
- Dambra A, Baugher JE, Concannon PE, Pon R a, Michon F. 1997. Direct and indirect methods for molar-mass analysis of fragments of the capsular polysaccharide of Haemophilus influenzae type b. *Anal Biochem* **250**:228-36.
- Dambra A, Soika M, Morgan L, Faust S, Arnold F. 2000. Absolute molecular-size and molar-mass analysis of meningococcal and pneumococcal conjugates and polysaccharide intermediates by size-exclusion chromatography with detection by multiangle light-scattering photometry and differential refractometry. *Dev Biol (Basel)* **103**:241-242.
- Darby J, Lawler D. 1990. Ripening in depth filtration: Effect of particle size on removal and head loss. *Environ Sci Technol* **24**:1069-1079.
- Dascenzi S. 2006. Analysis of mannosamine-containing capsular saccharides. US 2010/0022015 A1.
- Ding JL, Ho B. 2001. A new era in pyrogen testing. *Trends Biotechnol* **19**:277-81.
- Doran P. 1995. *Bioprocess Engineering Principles*. San Diego: Academic Press.
- Dreywood R. 1946. Qualitative test for carbohydrate material. *Ind Eng Chem Res* **18**.
- DuBois M, Gilles K a., Hamilton JK, Rebers P a., Smith F. 1956. Colorimetric method for determination of sugars and related substances. *Anal Chem* **28**:350-356.
- Dubois M, Gilles K, Hamilton J, Rebers P, Smith F. 1951. A colorimetric method for determination of sugars. *Nature* **4265**:167.
- Ducoste JJ, Clark MM. 1998. The influence of tank size and impeller geometry on turbulent flocculation: I. Experimental. *Environ Eng Sci* **15**:215-224.
- European Medicines Agency. 2009. Assessment report for Menveo.
- European Pharmacopoeia. 2005a. Limits: Haemophilus Type B conjugate vaccine.

- European Pharmacopoeia. 2005b. Limits: Typhoid polysaccharide vaccine.
- European Pharmacopoeia. 2005c. Assays: Nucleic acids/phosphorus/O-acetylation in polysaccharide vaccines. *Test*.
- European Pharmacopoeia. 2005d. Assays: Sialic acids in polysaccharide vaccines. *Test*.
- Fisher R, Glatz C. 1988a. Polyelectrolyte precipitation of proteins: II. Models of the particle size distributions. *Biotechnol Bioeng* **32**:786-796.
- Fisher R, Glatz C, Murphy P. 1986. Effects of mixing during acid addition on fractionally precipitated protein. *Biotechnol Bioeng* **28**:1056-1063.
- Fisher RR, Glatz CE. 1988b. Polyelectrolyte precipitation of proteins: I. The effects of reactor conditions*. *Biotechnol Bioeng* **32**:777-785.
- Food and Drug Administration United States. 1993. Summary for Basis of Approval of ActHIB.
- Food and Drug Administration United States. 2010a. Summary Basis for Regulatory Action (MenVeo).
- Food and Drug Administration United States. 2010b. Highlights of prescribing information (MenVeo). *Highlights of prescribing information*.
<http://www.fda.gov/downloads/biologicsbloodvaccines/vaccines/approvedproducts/ucm201349.pdf>.
- Fox JD, Robyt JF. 1991. Miniaturization of three carbohydrate analyses using a microsample plate reader. *Anal Biochem* **195**:93-96.
- Francois R. 1987. Strength of aluminum hydroxide flocs. *Wat Res* **21**:1023-1030.
- Frasch CE. 1990. Production and control of Neisseria meningitidis vaccines. In: Mizrahi, A, editor. *Advances in Biotechnological Processes: Bacterial Vaccines, Vol 13*. New York: John Wiley & Sons, Vol. 13, pp. 123-145.
- Frasch CE. 2009. Preparation of bacterial polysaccharide-protein conjugates: Analytical and manufacturing challenges. *Vaccine* **27**:6468-6470.
- Fundin J, Hansson P, Brown W, Lidegran I. 1997. Poly(acrylic acid)-cetyltrimethylammonium bromide interactions using dynamic and static light scattering and time-resolved fluorescence quenching. *Macromolecules* **30**:1118-1126.
- GAVI Alliance Secretariat. 2014. Annual report on advance market commitment for pneumococcal vaccines.
- Gagnon P. 2012. Technology trends in antibody purification. *J Chromatogr A* **1221**:57-70.
- Geisler R, Krebs R, Forschner P. 1994. Local turbulent shear stress in stirred vessels and its significant for different mixing tasks. *Inst Chem Eng Symp Ser* **136**:243-250.
- Genco RJ, Emmings FG, Evans RT, Apicella M. 1976. Purification, characterization, and immunogenicity of cell-associated glucan from Streptococcus mutans. *J Dent Res* **55**:C115-q20.
- Gold R, Lepow ML, Goldschneider I, Gotschlich EC. 1977. Immune response of human infants to polysaccharide vaccines of groups A and C Neisseria meningitidis. *J Infect Dis* **136**:S31-S35.

- Gotschlich EC, Goldschneider I, Artenstein MS. 1969a. Human immunity to the meningococcus IV. Immunogenicity of Group A and Group C meningococcal polysaccharides in human volunteers. *J Exp Med* **129**:1367-1384.
- Gotschlich EC, Liu TY, Artenstein MD. 1969b. Human immunity to the meningococcus. *J Exp Med*:1349-1365.
- Granoff DM. 2009. Relative importance of complement-mediated bactericidal and opsonic activity for protection against meningococcal disease. *Vaccine* **27**:B117-B125.
- Granoff DM, Goies EG, Munson RS. 1984. Immunogenicity of Haemophilus influenzae type B polysaccharide-diphtheria toxoid conjugate vaccine in adults. *J Pediatr* **105**:222-27.
- Gregory J. 2009. Monitoring particle aggregation processes. *Adv Colloid Interface Sci* **147-148**:109-23.
- Grenville R, Nienow A, Grenville R. 2004. Blending of Miscible Liquids. In: Paul, E, Atiemo-Obeng, V, Kresta, S, editors. *Handbook of Industrial Mixing: Science and Practice*. John Wiley & Sons, pp. 507-542.
- Gudlavalleti SK, Lee C-hung, Norris SE, Paul-satyaseela M, Vann WF, Frasch CE. 2007. Comparison of Neisseria meningitidis serogroup W135 polysaccharide – tetanus toxoid conjugate vaccines made by periodate activation of O-acetylated, non-O-acetylated and chemically de-O-acetylated polysaccharide. *Vaccine* **25**:7972-7980.
- Guo Y, Anderson R, Mciver J, Gupta RK, Siber GR. 1998. A simple and rapid method for measuring unconjugated capsular polysaccharide (PRP) of Haemophilus influenzae type b in PRP-tetanus toxoid conjugate vaccine. *Biologicals* **26**:33-38.
- Hall JF, Barigou M, Simmons MJH, Stitt EH. 2005. Comparative study of different mixing strategies in small high throughput experimentation reactors. *Chem Eng Sci* **60**:2355-2368.
- Hanning A, Roeraade J. 1997. A spectroscopic refractometer for temperature-independent refractive index detection. *Anal Chem* **69**:1496-1503.
- Hansson P, Almgren M. 1996. Interaction of CnTAB with sodium (carboxymethyl) cellulose: effect of polyion linear charge density on binding isotherms and surfactant aggregation number. *J Phys Chem* **3654**:9038-9046.
- Harden VP, Harris J. 1952. The isoelectric point of bacterial cells. *J Bacteriol* **65**:198-202.
- Harrison LH, Trotter CL, Ramsay ME. 2009. Global epidemiology of meningococcal disease. *Vaccine* **27 Suppl 2**:B51-63.
- Hecht M-L, Stallforth P, Silva DV, Adibekian A, Seeberger PH. 2009. Recent advances in carbohydrate-based vaccines. *Curr Opin Chem Biol* **13**:354-9.
- Helting T, Kumpe M. 1978. A sensitive method for the determination of the molecular size of meningococcal polysaccharide vaccine. *J Biol Stand* **6**:111-115.
- Hemrajani R, Tatterson G. 2004. Mechanically Stirred Vessels. In: Paul, E, Atiemo-Obeng, V, Kresta, S, editors. *Handbook of Industrial Mixing: Science and Practice*. John Wiley & Sons, pp. 345-390.
- Hestrin S. 1949. The reaction of acetylcholine and other carboxylic acid derivatives with hydroxylamine and its analytical application. *J Biol Chem* **180**:249-261.

- Hiraoka S, Ito R. 1977. Simple relationship between power input and mixing time in turbulent agitated vessel. *J Chem Eng Jpn* **10**:75-77.
- Hoare M, Dunnill P, Bell D. 1983. Reactor design for protein precipitation and its effect on centrifugal separation. *Ann N Y Acad Sci*:254-269.
- Hutchinson N, Bingham N, Murrell N, Farid S, Hoare M. 2006. Shear stress analysis of mammalian cell suspensions for prediction of industrial centrifugation and its verification. *Biotechnol Bioeng* **95**:483-491.
- Ibrahim S, Nienow A. 1999. Comparing impeller performance for solid-suspension in the transitional flow regime with newtonian fluids. *Trans IChemE* **77**:721-727.
- Irving M, Krueger CA, Wade JV, Hodges JC, Leopold K, Collins N, Chan C, Shaqair S, Shornikov A, Yan B. 1998. High-throughput purification of combinatorial libraries II: Automated separation of single diastereomers from a 4-amido-pyrrolidone library containing intentional diastereomer pairs. *J Comb Chem* **6**:478-86.
- Iyer HV, Przybycien TM. 1995. Metal affinity protein precipitation: effects of mixing, protein concentration, and modifiers on protein fractionation. *Biotechnol Bioeng* **48**:324-32.
- Jackson NB, Liddell JM, Lye GJ. 2006. An automated microscale technique for the quantitative and parallel analysis of microfiltration operations. *J Membr Sci* **276**:31-41.
- Jenner E. 1798. An inquiry into the causes and effects of variolae vaccinae. *Search*. London: Sampson Low.
- Jones C. 2005a. Vaccines based on the cell surface carbohydrates of pathogenic bacteria. *An Acad Bras Cienc* **77**:293-324.
- Jones C. 2005b. NMR assays for carbohydrate-based vaccines. *J Pharm Biomed Anal* **38**:840-50.
- Jones C, Lemercinier X. 2002. Use and validation of NMR assays for the identity and O-acetyl content of capsular polysaccharides from *Neisseria meningitidis* used in vaccine manufacture. *J Pharm Biomed Anal* **30**:1233-47.
- Joshi VS, Bajaj IB, Survase SA, Singhal RS, Kennedy JF. 2009. Meningococcal polysaccharide vaccines: A review. *Carbohydr Polym* **75**:553-565.
- Jumel K, Ho MM, Bolgiano B. 2002. Evaluation of meningococcal C oligosaccharide conjugate vaccines by size-exclusion chromatography/multi-angle laser light scattering. *Biotechnol Appl Biochem* **36**:219-226.
- Jódar L, Griffiths E, Feavers I. 2004. Scientific challenges for the quality control and production of group C meningococcal conjugate vaccines. *Vaccine* **22**:1047-53.
- Kachel V, Sindelar G, Grimm S. 2006. High-throughput isolation of ultra-pure plasmid DNA by a robotic system. *BMC Biotechnol* **6**:1-8.
- Kamerling JP, Schauer R, Shukla AK, Stoll S, Halbeek HV, Vliegenthart FG. 1987. Migration of O-acetyl groups in N,O-acetylneuraminic acids. *Eur J. Biochem* **162**:601-607.
- Kang YK, Hamzik J, Felo M, Qi B, Lee J, Ng S, Liebisch G, Shanhsaz B, Singh N, Persaud K, Ludwig DL, Balderes P. 2013. Development of a novel and efficient cell culture flocculation process using a

- stimulus responsive polymer to streamline antibody purification processes. *Biotechnol Bioeng* **110**:2928-2937.
- Kao G. 2004. Quantification of O-acetyl, N-acetyl and phosphate groups and determination of the extent of O-acetylation in bacterial vaccine polysaccharides by high-performance anion-exchange chromatography with conductivity detection (HPAEC-CD). *Vaccine* **22**:335-344.
- Kelley BD, Switzer M, Bastek P, Kramarczyk JF, Molnar K, Yu T, Coffman J. 2008. High-throughput screening of chromatographic separations: IV. Ion-exchange. *Biotechnol Bioeng* **100**:950-63.
- Kempken R, Preissmann A, Berthold W. 1995. Assessment of a disc stack centrifuge for use in mammalian cell separation. *Biotechnol Bioeng* **46**:132-8.
- Kim JS, Laskowich ER, Arumugham RG, Kaiser RE, MacMichael GJ. 2005. Determination of saccharide content in pneumococcal polysaccharides and conjugate vaccines by GC-MSD. *Anal Biochem* **347**:262-274.
- Kim J, Tobiasson JE. 2004. Particles in filter effluent: the roles of deposition and detachment. *Environ Sci Technol* **38**:6132-8.
- Knevelman C, Davies J, Allen L, Titchener-Hooker NJ. 2010. High-throughput screening techniques for rapid PEG-based precipitation of IgG4 mAb from clarified cell culture supernatant. *Biotechnol Prog* **26**:697-705.
- Kolmogorov A, Levin V (translation). 1991. Turbulence and stochastic process: dissipation of energy in the locally isotropic turbulence. *Proc: Math and Phys Sci* **434**:15-17.
- Komorowska-Rycerz A, Bruhl A, Krauze R. 1966. Fractionation of tetanus toxoid by gel filtration. *Bull Acad Pol Sci Biol* **14**:81-84.
- Kong S, Aucamp J, Titchener-Hooker NJ. 2010. Studies on membrane sterile filtration of plasmid DNA using an automated multiwell technique. *J Membr Sci* **353**:144-150.
- Konop AJ, Colby RH. 1999. Role of condensed counterions in the thermodynamics of surfactant micelle formation with and without oppositely charged polyelectrolytes. *Langmuir* **15**:58-65.
- Kramarczyk JF, Kelley BD, Coffman JL. 2008. High-throughput screening of chromatographic separations: II. Hydrophobic interaction. *Biotechnol Bioeng* **100**:707-20.
- Kresta SM, Brodkey R. 2004. Turbulence in Mixing Applications. In: Paul, E, Atiemo-Obeng, V, Kresta, S, editors. *Handbook of Industrial Mixing: Science and Practice*. John Wiley & Sons, pp. 19-87.
- Kresta SM, Mao D, Roussinova V. 2006. Batch blend time in square stirred tanks. *Chem Eng Sci* **61**:2823-2825.
- LaForce FM, Konde K, Viviani S, Préziosi M-P. 2007. The Meningitis Vaccine Project. *Vaccine* **25 Suppl 1**:A97-100.
- Laskin A. 1988. *Advances in Applied Microbiology*. Ed. A. Laskin 33rd ed. London: Academic Press.
- Lattanzi M, Giudice G del. 2002. Meningitis C vaccine: North American vaccine. *Curr Opin Investig Drugs* **1**:51-53.

- Lau EC, Kong S, McNulty S, Entwisle C, McIlgorm A, Dalton K, Hoare M. 2013. An ultra scale-down characterization of low shear stress primary recovery stages to enhance selectivity of fusion protein recovery from its molecular variants. *Biotechnol Bioeng* **110**:1973-1983.
- Laurentin A, Edwards CA. 2003. A microtiter modification of the anthrone-sulfuric acid colorimetric assay for glucose-based carbohydrates. *Anal Biochem* **315**:143-145.
- Lee C, Frasch CE. 2001. Quantification of bacterial polysaccharides by the purpald assay: measurement of periodate-generated formaldehyde from glycol in the repeating unit. *Anal Biochem* **296**:73-82.
- Leentvaar J, Ywema TSJ. 1980. Some dimensionless parameters of impeller power in coagulation-flocculation processes. *Wat Res* **14**:135-140.
- Lemercinier X, Jones C. 1996. Full ¹H NMR assignment and detailed O-acetylation patterns of capsular polysaccharides from *Neisseria meningitidis* used in vaccine production. *Carbohydr Res* **296**:83-96.
- Letterman R, Quon J, Gemmell R. 1973. Influence of rapid-mix parameters on flocculation. *JAWWA* **65**:716-722.
- Li Y, Xu G, Wu D, Sui W. 2007. The aggregation behavior between anionic carboxymethylchitosan and cetyltrimethylammonium bromide: MesoDyn simulation and experiments. *Eur Polym J* **43**:2690-2698.
- Lindberg B, Lönngrén J, Powell D. 1977. Structural studies on the specific type-14 pneumococcal polysaccharide. *Carbohydr Res* **58**:177-86.
- Liu H, Dasgupta PK. 1994. Dual-wavelength photometry with light emitting diodes. Compensation of refractive index and turbidity effects in flow-injection analysis. *Anly Chim Acta* **289**:347-353.
- Liu H, Ma J, Winter C, Bayer R. 2010. Recovery and purification process development for monoclonal antibody production. *mAbs* **2**:480-499.
- Lonza. 2007. Pyrogene recombinant Factor C endotoxin detection system. Walkersville, MD: Lonza.
- Lundqvist H, Eliasson A-charlotte, Olofsson G. 2002. Binding of hexadecyltrimethylammonium bromide to starch polysaccharides. Part I. Surface tension measurements. *Carbohydr Polym* **49**:43-55.
- Lutz H, Abbott I, Blanchard M, Paramalli A, Setiabudi G, Chiruvolu V, Noguchi M. 2009. Considerations for scaling-up depth filtration of harvested cell culture fluid. *BioPharm Int* **22**:58-66.
- Löffelholz C, Husemann U, Greller G, Meusel W, Kauling J, Ay P, Kraume M, Eibl R, Eibl D. 2013. Bioengineering parameters for single-use bioreactors: Overview and evaluation of suitable methods. *Chem Ing Tech* **85**:40-56.
- Ma J, Shi J, Le H, Cho R, Huang JC-jou, Miao S, Wong BK. 2008. A fully automated plasma protein precipitation sample preparation method for LC-MS/MS bioanalysis. *J Chromatogr B* **862**:219-26.

- Ma J, Hoang H, Myint T, Peram T, Fahrner R, Chou JH. 2010. Using precipitation by polyamines as an alternative to chromatographic separation in antibody purification processes. *J Chromatogr B* **878**:798-806.
- Mandell GL, Bennett JE, Dolin R. 2004. Mandell, Douglas, and Bennett's Principles & Practice of Infectious Diseases 6th ed. Churchill Livingstone.
- Markets and Markets. 2013. Vaccine Market, MD2020.
- Masuko T, Minami A, Iwasaki N, Majima T, Nishimura S-I, Lee YC. 2005. Carbohydrate analysis by a phenol-sulfuric acid method in microplate format. *Anal Biochem* **339**:69-72.
- Maulik S, Jana P, Moulik S, Chattoraj D. 1995. Biopolymer-surfactant interaction. I. Kinetics of binding of cetyltrimethyl ammonium bromide with carboxymethyl cellulose. *Biopolymers* **35**:533-541.
- Maybury J, Hoare M, Dunnill P. 2000. The use of laboratory centrifugation studies to predict performance of industrial machines: studies of shear-insensitive and shear-sensitive materials. *Biotechnol Bioeng* **67**:265-273.
- Mayor S. 2010. New meningococcal A vaccine is being introduced into Africa. *Br Med J*.
- McAleer WJ, B BE, Maigetter RZ, Wampler DE, J MW, Hilleman MR. 1984. Human hepatitis B vaccine from recombinant yeast. *Nature* **307**:178-179.
- McCauley J a, Mancinelli RJ, Downing GV, Robbins JB. 1981. Molecular size characterization of bacterial capsular polysaccharide vaccines with Sepharose CL-2B. *J Biol Stand* **9**:461-8.
- Meningitis Vaccine Project. 2011. Meningitis vaccine project timeline. <http://www.meningvax.org/timeline.php>.
- Merson JR, Bojanic D. 1990. Multiwell assay tray assembly. GB2243446A.
- Metzner A, Taylor J. 1960. Flow patterns in agitated vessels. *AIChE J* **6**:109-114.
- Milburn P, Bonnerjea J, Hoare M, Dunnill P. 1990. Selective flocculation of nucleic acids, lipids, and colloidal particles from a yeast cell homogenate by polyethyleneimine, and its scale-up. *Enzyme Microb Tech* **12**:527-32.
- Mukhopadhyay TK. 2008. Rapid vaccine development using a microscale platform; University College London.
- Nagata S, Yanagimoto M, Yokoyama T. 1957. A study on the mixing of high viscosity liquid. *Kagaku Kogaku* **21**:278.
- Neal G, Christie J, Keshavarz-Moore E, Shamlou PA. 2003. Ultra scale-down approach for the prediction of full-scale recovery of ovine polyclonal immunoglobulins used in the manufacture of snake venom-specific Fab fragment. *Biotechnol Bioeng* **81**:149-57.
- Nfor BK, Hylkema NN, Wiedhaup KR, Verhaert PD, van der Wielen, Luuk A Ottens M. 2011. High-throughput protein precipitation and hydrophobic interaction chromatography: Salt effects and thermodynamic interrelation. *J Chromatogr A* **1218**:8958-8973.
- Nienow A. 1968. Suspension of solid particles in turbine agitated baffled vessels. *Chem Eng Sci* **23**:1453-1459.

- Nienow A. 1997. On impeller circulation and mixing effectiveness in the turbulent flow regime. *Chem Eng Sci* **52**:2557-2565.
- Norwood K, Metzner A. 1960. Flow patterns and mixing rates in agitated vessels. *AIChE J* **6**:432-437.
- Noyes A, Boesch A, Godavarti R, Titchener-Hooker N, Coffman J, Mukhopadhyay T. 2013. High throughput quantification of capsular polysaccharides for multivalent vaccines using precipitation with a cationic surfactant. *Vaccine* **31**:5659-65.
- Noyes A, Godavarti R, Titchener-Hooker N, Coffman J, Mukhopadhyay T. 2014. Quantitative high throughput analytics to support polysaccharide production process development. *Vaccine* **32**:2819-2828.
- Nunnally BK, Yao K. 2007. The use of capillary electrophoresis in vaccines. *Anal Lett* **40**:615-627.
- Osborne T, Harris I. 1903. The precipitation limits with ammonium sulphate of some vegetable proteins. *J Am Chem Soc* **25**:837-842.
- Patel M, Mulhall H, Al-Quatani K, Lewis M, Wall I. 2011. Muscle-derived precursor cells isolated on the basis of differential adhesion properties respond differently to capillary flow. *Biotechnol Lett* **33**:1481-6.
- Pato TP, Barbosa A de PR, da Silva Junior JG. 2006. Purification of capsular polysaccharide from *Neisseria meningitidis* serogroup C by liquid chromatography. *J Chromatogr B* **832**:262-7.
- Paz MFD, Baruque-Ramos J, Hiss H, Vicentin MA, Leal MB, Raw I. 2003. Polysaccharide production in batch process of *Neisseria meningitidis* serogroup C comparing Frantz, modified Frantz and Catlin 6 cultivation media. *Braz J Microbiol* **34**:27-32.
- Pearson FC, Bohon J, Lee W, Bruszer G, Sagona M, Jakubowski G, Dawe R, Morrison D, Dinarello C. 1984. Characterization of *Limulus* amoebocyte lysate-reactive material from hollow-fiber dialyzers. *Appl Environ Microbiol* **48**:1189-96.
- Peng SX, Branch TM, King SL. 2001. Fully automated 96-well liquid-liquid extraction for analysis of biological samples by liquid chromatography with tandem mass spectrometry. *Anal Chem* **73**:708-14.
- Pfizer Corporation. 2011. Pfizer Press Release: Jan 2, 2011. New York.
- Plotkin SA. 2005. Vaccines: past, present and future. *Nat Med* **11**:S5-11.
- Plumb JE, Yost SE. 1996. Molecular size characterization of *Haemophilus influenzae* type b polysaccharide-protein conjugate vaccines. *Vaccine* **14**:399-404.
- Pollard AJ, Frasch C. 2001. Development of natural immunity to *Neisseria meningitidis*. *Vaccine* **19**:1327-46.
- Post T. 2010. Understand the real world of mixing. *CEP*:25-32.
- Preaud J. 2010. Development of MenAfriVac in India: an example of efficient technology transfer to develop a needed vaccine. In: . *Workshop on Technology Transfer*, pp. 1-31.
- Prochazka J, Landau J. 1961. Studies on mixing. XII. Homogenation of miscible liquids in the turbulent region. *Coll Czech Chem Commun* **26**:2961-2973.

- Pujar NS, Huang NF, Daniels CL, Dieter L, Gayton MG, Lee AL. 2004. Base hydrolysis of phosphodiester bonds in pneumococcal polysaccharides. *Biopolymers* **75**:71-84.
- Rao P, Pattabiraman TN. 1989. Reevaluation of the phenol-sulfuric acid reaction for the estimation of hexoses and pentoses. *Anal Biochem* **181**:18-22.
- Ravenscroft N, Hearshaw M, Mattick C, Martino A, Feavers I, Bolgiano B, Suresh K, Beri S, Goel A, Kapre S, Préaud J-marie, Viviani S. 2007. Physicochemical and immunological characterization of the drug product (final lot) of a meningococcal group A conjugate vaccine. In: . *Clinical Trials*, p. 1.
- Rayat A, Lye G, Micheletti M. 2014. A novel microscale crossflow device for rapid evaluation of microfiltration processes. *J Membr Sci* **284-293**.
- Reingold A, Hightower AW, Bolan GA, Jones EE, Tiendrebeogo H, Broome CV, Ajello GW, Adamsbaum C, Phillips C, Yada A. 1985. Age-specific differences in duration of clinical protection after vaccination with meningococcal polysaccharide A vaccine. *Lancet* **July 20**:114-118.
- Ricci S, Bardotti A, D'Ascenzi S, Ravenscroft N. 2001. Development of a new method for the quantitative analysis of the extracellular polysaccharide of *Neisseria meningitidis* serogroup A by use of high-performance anion-exchange chromatography with pulsed-amperometric detection. *Vaccine* **19**:1989-1997.
- Riske F, Schroeder J, Belliveau J, Kang X, Kutzko J, Menon MK. 2007. The use of chitosan as a flocculant in mammalian cell culture dramatically improves clarification throughput without adversely impacting monoclonal antibody recovery. *J Biotechnol* **128**:813-23.
- Robbins JB, Austria R, J LC, Rastogi SC, Schiffman G, Hinrichsen J, Makela PH, Broome CV, Facklam RR, Tiesjema RH, Parke JCJ. 1983. Considerations for formulating the second-generation polysaccharide vaccine with emphasis on the cross-reactive types within groups. *J Infect Dis* **148**:1136-1159.
- Roberts IS. 1996. The biochemistry and genetics of capsular polysaccharide production in bacteria. *Annu Rev Microbiol* **50**:285-315.
- Roe J. 1955. The determination of sugar in blood and spinal fluid with anthrone reagent. *J Biol Chem* **212**:335-343.
- Rouan MC, Buffet C, Marfil F, Humbert H, Maurer G. 2001. Plasma deproteinization by precipitation and filtration in the 96-well format. *J Pharm Biomed Anal* **25**:995-1000.
- Roush DJ, Lu Y. 2008. Advances in primary recovery: centrifugation and membrane technology. *Biotechnol Prog* **24**:488-495.
- Rushton J, Costich E, Everett H. 1950. Power characteristics of mixing impellers, part II. *Chem Eng Prog* **46**:467-476.
- Russell W, Wang A, Rathore A, Russell E. 2007. Harvest of a therapeutic protein product from high cell density fermentation broths: principals and case study. In: Shukla, A, Etzel, M, Gadam, S, editors. *Bioseparations for the Biopharmaceutical Industry*. Taylor & Francis, pp. 1-58.
- Ruszkowski S. 1994. A rational method for measuring blending performance, and comparison of different impeller types. *Inst Chem Eng Symp Ser* **136**:283-291.

- Saha SK, Brewer CF. 1994. Determination of the concentrations of oligosaccharides, complex type carbohydrates, and glycoproteins using the phenol-sulfuric acid method. *Carbohydr Res* **254**:157-167.
- Salt D, Hay S, Thomas O, Hoare M, Dunnill P. 1995. Selective flocculation of cellular contaminants from soluble proteins using polyethyleneimine: A study of several organisms and polymer molecular weights. *Enzyme Microb Tech* **17**:107-113.
- Sano Y, Usui H. 1985. Interrelations among mixing time, power number and discharge flow rate number in baffled mixing vessels. *J Chem Eng Jpn* **18**:47-52.
- Schneerson R, Barrera O, Sutton A, Robbins JB. 1980. Preparation, characterization, and immunogenicity of Haemophilus influenzae type b polysaccharide-protein conjugate. *J Exp Med* **152**:361-377.
- Shan J, Xia J, Guo Y, Zhang X. 1996. Flocculation of cell, cell debris and soluble protein with methacryloyloxyethyl trimethylammonium chloride-acrylonitrile copolymer. *J Biotechnol* **49**:173-178.
- Sheth RD, Madan B, Chen W, Cramer S. 2013. High throughput screening for the development of a monoclonal antibody affinity precipitation step using ELP-Z stimuli responsive biopolymers. *Biotechnol Bioeng* **110**:2664-2676.
- Shiue S, Wong C. 1984. Homogenization efficiency of various agitators in liquid blending. *Can J Chem Eng* **62**:602-609.
- Siddiqi SF, Titchener-Hooker NJ, Shamlou P a. 1997. High pressure disruption of yeast cells: The use of scale down operations for the prediction of protein release and cell debris size distribution. *Biotechnol Bioeng* **55**:642-9.
- Sieberz J, Stanislawski B, Wohlgemuth K, Schembecker G. 2014. Identification of parameter interactions influencing the precipitation of a monoclonal antibody with anionic polyelectrolytes. *Sep Purif Technol* **127**:165-173.
- Singer V, Jones L, Yue S, Haugland R. 1997. Characterization of Picogreen reagent and development of a fluorescent-based solution assay for double-stranded DNA quantitation. *Anal Biochem* **249**:228-238.
- Singh N, Pizzelli K, Romero JK, Chrostowski J, Evangelist G, Hamzik J, Soice N, Cheng KS. 2013. Clarification of recombinant proteins from high cell density mammalian cell culture systems using new improved depth filters. *Biotechnol Bioeng* **110**:1964-72.
- Smith P, Krohn R, Hermanson G, Mallia A, Gartner F, Provenzano M, Fujimoto E, Goeke N, Olson B, Klenk D. 1985. Measurement of protein using bicinchonic acid. *Anal Biochem* **150**:76-85.
- Stephens DS. 2007. Conquering the meningococcus. *FEMS Microbiol Rev* **31**:3-14.
- Stephens P. 2014. Vaccine R&D: past performance is no guide to the future. *Vaccine* **32**:2139-42.
- Stone AL, Szu SC. 1988. Application of optical properties of the Vi capsular polysaccharide for quantitation of the Vi antigen in vaccines for typhoid fever. *J Clin Microbiol* **26**:719-25.
- Svennerholm L. 1957. Quantitative estimation of sialic acids II: A colorimetric resorcinol-hydrochloric acid method. *Biochim Biophys Acta* **24**:604-611.

- Tait A, Aucamp J, Bugeon A, Hoare M. 2009. Ultra scale-down prediction using microwell technology of the industrial scale clarification characteristics by centrifugation of mammalian cell broths. *Biotechnol Bioeng* **104**:321-31.
- Takahashi K, Takahata Y, Yokota T, Konno H. 1985. Mixing of two miscible highly newtonian liquids in a helical ribbon agitator. *J Chem Eng Jpn* **18**:159-162.
- Tan LK, Carlone GM, Borrow R. 2010. Advances in the development of vaccines against *Neisseria meningitidis*. *N Engl J Med* **362**:1511-20.
- Tanizaki MM, Garcia LR, Ramos JB, Leite LC, Hiss H, Furuta JA, Cabrera-Crespo J, Raw I. 1996. Purification of meningococcal group C polysaccharide procedure suitable for scale-up. *J Microbiol Methods* **27**:19-23.
- Tattersson G, Kyser E. 1991. Mixing in fed-batch and continuous flow processes in nonstandard geometries. *AIChE J* **37**:269-273.
- Thermo Scientific. 2007. Pierce BCA Protein Assay Kit. *Test*. Rockford, IL. Vol. 0747.
- Thommes J, Etzel M. 2007. Alternatives to chromatographic separations. *Biotechnol Prog*:42-45.
- Titchener-Hooker N, Dunnill P, Hoare M. 2008. Micro biochemical engineering to accelerate the design of industrial-scale downstream processes for biopharmaceutical proteins. *Biotechnol Bioeng* **100**:473-487.
- Townsend A. 1976. *The Structure of Turbulent Shear Flow*. Ed. G Batchelor, J Miles. Cambridge University Press.
- Trautmann M, Ghandchi A, Held T, Cryz SJ, Cross AS. 1991. An enzyme-linked immunosorbent assay for the detection of soluble *Klebsiella pneumoniae* capsular polysaccharide. *J Microbiol Methods* **13**:305-313.
- Treier K, Hansen S, Richter C, Diederich P, Hubbuch J, Lester P. 2012. High-throughput methods for miniaturization and automation of monoclonal antibody purification processes. *Biotechnol Prog* **28**:723-32.
- Tsai C-ming, Gu X-xing, Byrd RA. 1994. Quantification of polysaccharide in *Haemophilus influenzae* type b conjugate and polysaccharide vaccines chromatography with pulsed amperometric detection. *Vaccine* **12**:700-706.
- Turula VE, Gore T, Singh S, Arumugham RG. 2010. Automation of the anthrone assay for carbohydrate concentration determinations. *Anal Chem* **82**:1786-92.
- Tustian AD, Salte H, Willoughby N, Hassan I, Rose MH, Baganz F, Hoare M, Titchener-Hooker NJ. 2007. Adapted ultra scale-down approach for predicting the centrifugal separation behavior of high cell density cultures. *Biotechnol Prog* **23**:1404-10.
- Tzeng Y-ling, Noble C, Stephens DS. 2003. Genetic basis for biosynthesis of the (α1-4)-linked N-acetyl-D-glucosamine 1-phosphate capsule of *Neisseria meningitidis* serogroup X. *Infect Immun* **71**:6712-6720.
- Vandezande P, Gevers L, Paul J, Vankelecom I, Jacobs P. 2005. High throughput screening for rapid development of membranes and membrane processes. *J Membr Sci* **250**:305-310.

- Verez-Bencomo V, Fernández-Santana V, Hardy E, Toledo ME, Rodríguez MC, Heynngnezz L, Rodríguez A, Baly A, Herrera L, Izquierdo M, Villar A, Valdés Y, Cosme K, Deler ML, Montane M, Garcia E, Ramos A, Aguilar A, Medina E, Toraño G, Sosa I, Hernandez I, Martínez R, Muzachio A, Carmenates A, Costa L, Cardoso F, Campa C, Diaz M, Roy R. 2004. A synthetic conjugate polysaccharide vaccine against *Haemophilus influenzae* type b. *Science* **305**:522-5.
- Van de Vusse J. 1955. Mixing by agitation of miscible liquids, part II. *Chem Eng Sci* **4**:209-220.
- WHO. 1980. Annex 6: Requirements for meningococcal polysaccharide vaccine.
- WHO Expert Committee on Biological Standardization. 2006. Recommendations to assure the quality, safety, and efficacy of group A meningococcal conjugate. *WHO*.
- WHO Expert Committee on Biological Standardization. 2009. Recommendations to assure the quality, safety and efficacy of pneumococcal conjugate vaccines. *WHO*.
- WHO Technical Report Series, No 840 1994. 1994. Annex 1: Requirements for Vi polysaccharide typhoid vaccine.
- WHO Technical Report Series, No. 897 2000. 2000. Annex 1: Recommendations for the production and control of *Haemophilus influenzae* type b conjugate vaccines.
- WHO Technical Report, Series No. 924 2004. 2004. Annex 2: Recommendations for the production and control of meningococcal group C conjugate vaccines. *Controlled Clinical Trials*.
- Walter RE, Cramer JA, Tse FLS. 2001. Comparison of manual protein precipitation (ppt) versus a new small volume ppt 96-well filter plate to decrease sample preparation time. *J Pharm Biomed Anal* **25**:331-337.
- Walther C, Mayer S, Trefilov A, Sekot G, Hahn R, Jungbauer A, Dürauer A. 2014. Prediction of inclusion body solubilization from shaken to stirred reactors. *Biotechnol Bioeng* **111**:84-94.
- Wang H, Loganathan D, Linhardt R. 1991. Determination of the pKa of glucuronic acid and the carboxy groups of heparin by ¹³C-nuclear-magnetic-resonance spectroscopy. *Biochemistry* **278**:689-95.
- Washabaugh M. 2014. Applying quality by design to vaccine and viral biopharmaceuticals: highlights, lesson learned and observations involving a seasonal vaccine. In: . *Vaccine Technology V*. Playa del Carmen, Mexico: MedImmune.
- Whitfield C, Valvano M. 1993. Biosynthesis and expression of cell-surface polysaccharides in Gram-negative bacteria. In: . *Advances in Microbial Physiology*, Vol. 35, pp. 135-246.
- Wickramasinghe SR, Han B, Akeprathumchai S, Jaganjac A, Qian X. 2005. Modeling flocculation of biological cells. *Powder Technol* **156**:146-153.
- Wiechelmann KJ, Braun RD, Fitzpatrick JD. 1988. Investigation of the bicinchoninic acid protein assay: identification of the groups responsible for color formation. *Anal Biochem* **175**:231-7.
- Wiendahl M, Volker C, Husemann I, Krarup J, Staby A, Scholl S, Hubbuch J. 2009. A novel method to evaluate protein solubility using a high throughput screening approach. *Chem Eng Sci* **64**:3778-3788.
- World Health Organization. 1967. Annex 2: Requirements for meningococcal polysaccharide vaccine.

- World Health Organization. 2006. Temperature sensitivity of vaccines. *World Health*.
- Xi X, Wei X, Wang Y, Chu Q, Xiao J. 2010. Determination of tea polysaccharides in *Camellia sinensis* by a modified phenol-sulfuric acid method. *Arch Biol Sci* **62**:669-676.
- Yang J, Chen S, Fang Y. 2009. Viscosity study of interactions between sodium alginate and CTAB in dilute solutions at different pH values. *Carbohydr Polym* **75**:333-337.
- Yang W. 2011. Nucleases: diversity of structure, function and mechanism. *Q Rev Biophys* **44**:1-93.
- Yoshimoto N, Minakuchi K, Itoh D, Isakari Y, Yamamoto S. 2013. High throughput process development methods for chromatography and precipitation of proteins: Advantages and precautions. *Eng Life Sci* **13**:446-455.
- Zaman F, Allan CM, Ho SV. 2009. Ultra scale-down approaches for clarification of mammalian cell culture broths in disc-stack centrifuges. *Biotechnol Prog* **25**:1709-16.
- Zhou G, Kresta SM. 1996. Impact of tank geometry on the maximum turbulence energy dissipation rate for impellers. *AIChE J* **42**:2476-2490.
- Zimmer SM, Stephens DS. 2004. Meningococcal conjugate vaccines. *Expert Opin Pharmacother* **5**:855-63.
- Zon G, Szu SC, Egan W, Robbins JD, Robbins JB. 1982. Hydrolytic stability of pneumococcal group 6 (type 6A and 6B) capsular polysaccharides. *Infect Immun* **37**:89-103.
- Zoro BJH, Owen S, Drake R a L, Mason C, Hoare M. 2009. Regenerative medicine bioprocessing: concentration and behavior of adherent cell suspensions and pastes. *Biotechnol Bioeng* **103**:1236-47.
- Zubay G, Strominger J. 1988. Biochemistry. In: Zubay, G, editor. *Biochemistry* New York. McMillan, pp. 131-153.
- Zwietering T. 1958. Suspending of solid particles in liquid by agitators. *Chem Eng Sci* **8**:244-253.

8 Appendix A - Validation

8.1 Research Objectives

It has proven challenging to manufacture and develop production processes for multivalent, polysaccharide vaccines. Although certain unit operations have been common to multiple polysaccharide serotypes and standardization has been practised where possible, custom processes have been required for many polysaccharide serotypes. In addition, it has been observed that particular serotypes can present unique and unforeseen challenges such as high viscosity, poor stability, inconsistent behaviour, etc. This research aims to accelerate the development of purification processes for multivalent polysaccharide vaccines through the application of HTPD. To accomplish this, we first developed an analytical platform customized for polysaccharide vaccines. Next, we applied the analytical toolbox to design high throughput screens that enable the development of unit operations at the micro-scale. Owing to the prevalence of particle conditioning (*i.e.* flocculation/precipitation, aging, centrifugation, and filtration) in vaccine production, we focused on this series of interdependent unit operations. To provide confidence in the relevance of the USD output, the microplate-based results were scaled to Pilot-scale, which is representative of performance in clinical and commercial manufacturing. Several competing scaling rules were evaluated to identify which offered the most comparable performance between scales. Commercially available polysaccharides and relevant internal products constituted representative feedstreams.

8.2 Significance of Research

A rapid, modular approach for developing purification processes for polysaccharides at the micro-scale will greatly enhance productivity, reduce development costs, and speed the development of novel polysaccharide vaccines. The richer contextual data afforded by HTPD will increase process understanding, leading to enhanced process robustness. Drug substance batches will meet specifications more consistently, ultimately leading to the generation of safer medicines. Project

expenses will decrease due to fewer failed batches and an augmented capability to progress more projects with fewer people. Lower development costs per project will reduce the risk inherent in taking on new projects, thereby enabling companies to support more candidates in late-phase clinical trials. Although, HTPD will decrease the costs associated with purification development and production, it is unlikely to affect the price of approved drugs in developed countries. This paradox is explained by the insignificance of the cost of manufacturing biopharmaceuticals relative to the expenses associated with conducting clinical trials. An exception where lower COGS might possibly translate into greater access of treatment is with vaccines for developing countries. In these cases, the number of doses included with a donation or bulk purchase of vaccines is a stronger function of COGS. Outside of these areas, the benefits of HTPD reside in faster time-to-market, higher project carrying capacity for companies, enhanced process robustness and understanding, and more consistent drug substances.

8.3 Key Validation Issues

8.3.1 Overview

The critical objective for biopharmaceutical companies is to produce safe, consistent, and efficacious medicine. A key element in this process is validation, the documented development, qualification, and control of production processes for clinical and commercial drug products. As it applies to USD technology such as HTPC and HTDF, validation can be construed as process development and process characterisation. The former is focused on acquiring information relevant for process design early in the development cycle, typically utilizing broad experimental spaces and ultimately leading to optimization studies. The latter emphasizes fidelity with large-scale performance, since well-understood and qualified scaling is a requisite for understanding operating spaces.

Process development of a purification step encompasses the identification of parameters that affect critical quality attributes (CQA) such as purity, quality, and consistency. Process economics and facility utilisation require an emphasis on yield maximisation. To achieve these goals, flocculation requires the specification and control of myriad parameters and set points. Needlessly controlling

parameters that neither affects a validated state (*i.e.* affecting critical quality attributes) nor key process economics (*e.g.* yield, process duration, facility utilisation, etc.) is undesirable. Previous experience, scientific judgment, risk assessments, and factorial screening studies (many factors; usually two levels per factor) are effective tools for determining which parameters affect a process. Although hard data often represent the most compelling evidence, resource constraints confine the breadth of the experimental set. HTPD provides an opportunity to increase the number of factors screened, test conditions outside of process acceptable ranges, evaluate a greater number of two- and three-way effects, and more thoroughly assess non-critical factors that that may change product profile without affecting critical quality attributes. For optimization with DOE approaches, HTPD enables the inclusion of more levels for significant parameters, allowing higher resolution when estimating effects. Amongst the advantages of higher resolution are: greater confidence in the operating window, an enhanced capability to delineate in which regions of a multi-factorial space a factor is significant, and the potential to 'see' areas where operating ranges can be extended while maintaining CQAs.

8.3.2 High Throughput Particle Conditioning Case Study

The utility of higher resolution experimental designs can be illustrated with a HTPC case study. A selection of results from the 45-condition pneumococcal HTPC study described in Section 4.4.5.4 was integrated with conventional DOE analysis for process validation. In this example, the CQA was percentage of load DNA remaining in the centrate following flocculation. A Pareto plot was used to identify pH and floc agent concentration as the significant factors at the $p < 0.05$ level (Figure 8.1). Clearly, floc agent concentration and pH are the most important factors to control. The presence of an interaction between these two factors was also confirmed, which had been suggested by several of the contour plots provided in Section 4.4.5.

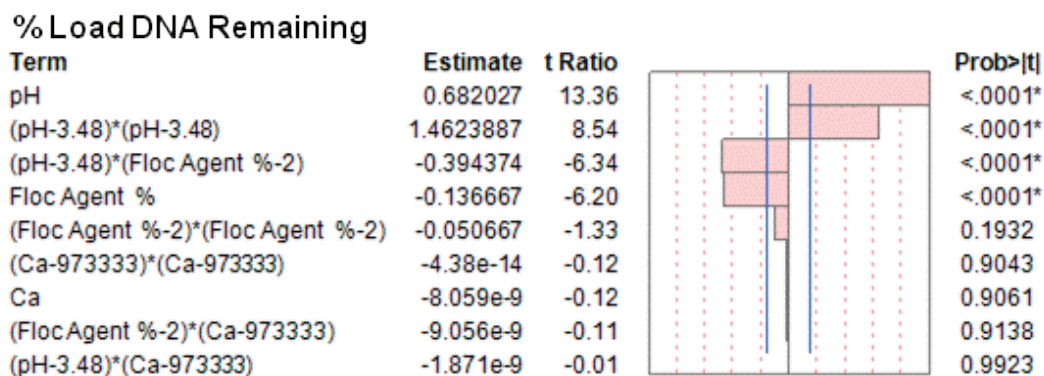


Figure 8.1. Pareto plot for percentage of DNA remaining after particle conditioning relative to load control (data in Table 4.3)

8.3.2.1 Quality by Design

HTPC is effective in demarcating regions where a given level of performance can be achieved. To illustrate this attribute, the previous example was analysed using a QbD framework. A statistical model was constructed for DNA clearance and used to identify a rectangular design space where CQA metrics of < 10% of load DNA remaining were met (Figure 8.2). The corresponding pH and floc agent concentration ranges defined the process acceptable range (PAR). From the design space, a smaller operational space was designated as the control space for manufacturing and the normal operating ranges (NOR) for the two parameters specified. If the USD model was qualified or related to qualified lab-scale models, the design space could be used in support of regulatory filings. Regulatory pathways exist for the approval of design spaces and HTPC can provide substantiation of parameter range selection.

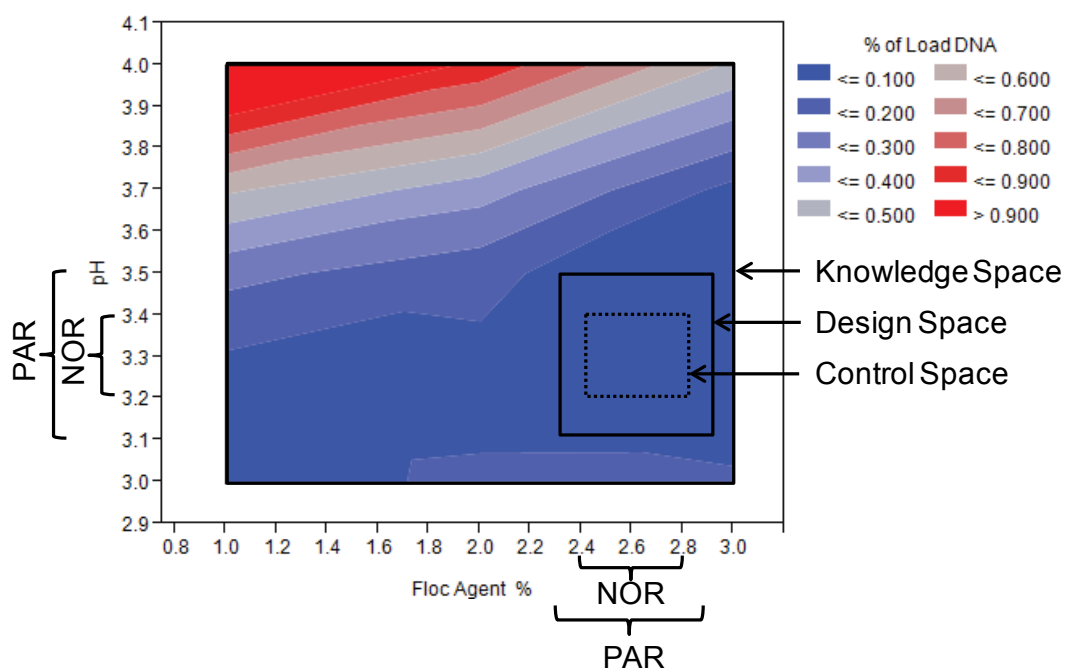


Figure 8.2. Contour plot model of DNA clearance (percentage of load control) for HTPC with neutral pneumococcal CPS. Only significant ($p < 0.05$) primary factors were included in the analysis. Potential QbD knowledge, design, and control spaces are delineated along with the respective PARs ($\text{pH} = 3.3 \pm 0.2$; floc agent = 2.6 ± 0.3) and NORs ($\text{pH} = 3.3 \pm 0.1$; floc agent = 2.6 ± 0.2).

8.3.2.2 Windows of Operation

The totality of information generated with HTPC can be integrated to establish windows of operation that deliver acceptable performance. In addition, information from other sources regarding filtration, centrifugation, stability, etc. can be combined with HTPC outputs to determine regions of optimum performance. Such a holistic approach is illustrated in Figure 6.3 where the multifaceted impurity clearance responses were combined with prior filtration experience to define a satisfactory window of operation. The translation of HTPC into operating windows enables the rapid identification of a design space that is large enough to provide ample process robustness. HTPC also succeeded in identifying a parameter (*i.e.* Ca) that could be modulated to increase the size of the operating window if necessary.

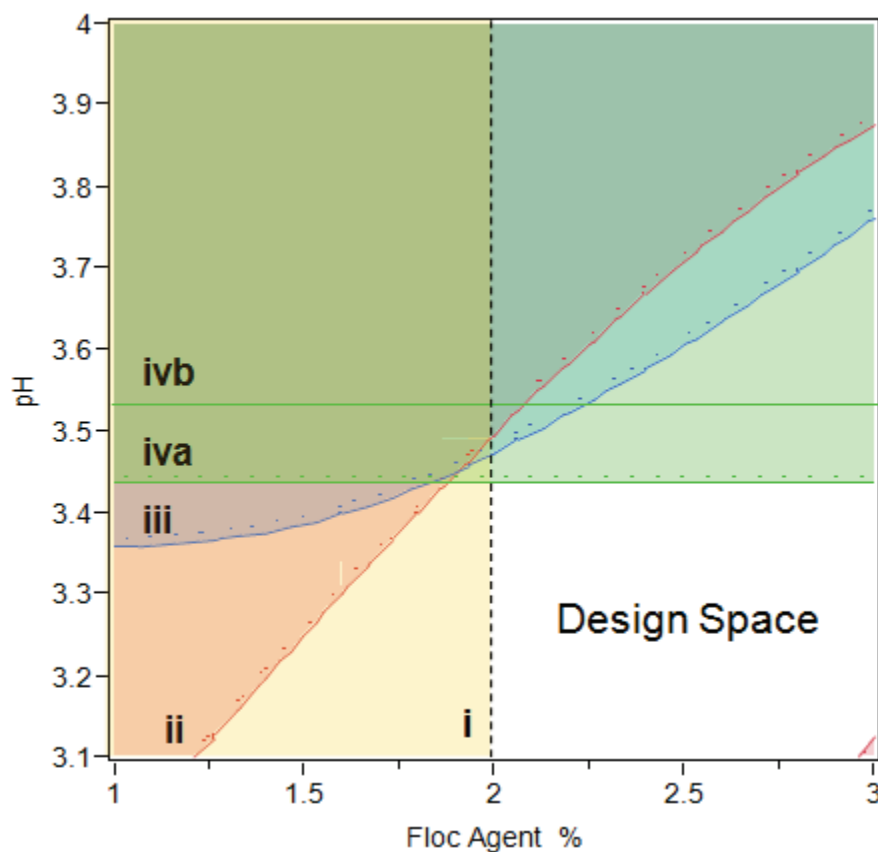


Figure 8.3. Window of operation for a particle conditioning operation with a neutral pneumococcal CPS where $Ca = 6.5 \times 10^5$. The un-shaded area delineates the operating region where acceptable performance was achieved as defined by: desirable downstream filtration performance (i), $\leq 10\%$ of load DNA (ii), $< 50\%$ of load A_{600} (iii), and $\leq 3\%$ of load protein (iva). If Ca was increased to 1.3×10^6 (ivb), the operating window would expand upward, owing to improved protein clearance.

The central validation challenge in process development is to identify a process train that will consistently produce a drug product with adequate safety and consistent target product profile. For a given process train, there will be several individual unit operations that must be developed. These unit operations will be inter-dependent and require validation in the context of the surrounding unit operations, a process referred to as linkage analysis. Particle conditioning embodies this inter-dependency because the purification of the flocculation step is dependent on how effectively the

downstream centrifugation and filtration steps are able to remove the flocs. Flocculation conditions that produce flocs of decreased strength will detrimentally affect the clarification obtained with centrifuges. In addition, sub-optimal conditions for a centrifuge can disaggregate flocs, leading to decreased purification and possibly lower capacity on subsequent depth and sterile filters. The interplay between unit operations is a critical consideration for validation.

8.4 Regulatory Concerns

There are few regulatory obstacles to the uptake of HTPC and other forms of HTPD. The multi-faceted issue that does arise is the extent to which HTPD data can be used in regulatory filings, particularly as a substitute for traditional small-scale models.

8.4.1 Scaling Models

Qualified small-scale models are the linchpins of process characterization activities that enable results garnered in the development lab to be used to define clinical and commercial manufacturing operations. To qualify a small-scale model as representative of larger scale operations, purification performance such as yield and purity must match between scales. Operational characteristics must be similar and a scaling methodology established. For many separation technologies, including chromatography and filtration, scaling rules are well-accepted (Titchener-Hooker et al., 2008). For particle conditioning, there is less consensus, specifically for how to scale centrifugation and flocculation. Scaling centrifugation by maintaining Q/Σ offers a credible scaling option, although additional evidence for this particular application (molecule class, flocculant, etc.) is desirable (Ambler, 1959; Boychyn et al., 2000; Boychyn et al., 2004). Multiple competing heuristics for ensuring consistent performance of flocculation across scales have been proposed and discussed in the context of HTPC (1.8.1.1). To address this knowledge gap, this thesis compared several different scaling methodologies and succeeded in identifying several approaches that were supported with case studies. When combined with scaling approaches for particle removal via centrifugation and/or filtration, we have identified and proffered corroborating evidence in support of a holistic scaling methodology for particle conditioning. As this conclusion was determined only recently, there may

be additional onus on firms, relative to other separation technologies, to substantiate the scaling methodology in their regulatory applications.

8.4.2 Limitations to Scale Equivalence

Irrespective of purification technology, scale-down models cannot incorporate all aspects of larger scale operations. For HTPC, the limitations inherent in a microplate-based approach can be greater than for scale-down with other unit operations. Some examples include:

- Materials of construction
- Equipment dimensions and ratios. Discrepancies in reactor configuration can produce substantially different hydrodynamic environments and flow patterns. Since mixing is critical to the initiation and conditioning of flocculation, this can impart scale-dependent performance differences. For HTPC, system differences can be mitigated through selection of suitable hardware and operating parameters. Scale-related hydrodynamic differences are intrinsic to the scale-up of all modes of purification. These issues are surmountable as these are already encountered when scaling within a facility or changing production sites
- Operating parameters that are discretely controlled at larger scale but are not available for active control within a USD system, such as rate of titrant addition, location of titrant addition (*i.e.* surface vs. submerged), heat transfer rates, and impeller type. If these are significant factors for a given particle conditioning process, one would need to rely on testing at a larger scale or other mitigation strategies. Although some of the aforementioned parameters may possess significance, their relative significance may make an examination of their magnitude of effect unnecessary. Fortunately, the performance of many particle conditioning process is driven largely by equilibrium descriptors such as pH, floc agent concentration, ionic strength, and aging time
- Many dynamic real-time *in situ* measurements are not possible during flocculation, including particle size, pH, and conductivity
- For centrifugation and depth filtration, it is currently infeasible to:
 - shear < 1 mL of sample to a level characteristic of a DSC

- measure turbidity with established technology (*i.e.* Hach)
 - measure sterile filtration capacity
- Capability for linkage analysis is hindered by the small volumes intrinsic to USD approaches. Linkage studies could be used to demonstrate clearance of floc agents or to show that a performance difference observed was eliminated through the process-dampening effects of a downstream unit operation. Depending on the assay, floc agent removal studies may be possible with HTPC but options for downstream processing are quite limited

Many of these issues will be resolved eventually with additional technology innovation but presently, USD models are lacking in these areas. If these factors are found to be critical to the performance of an application, this would hinder the utilisation of USD models in regulatory filings.

8.4.3 Looking to the Future

We are not yet at the point where the development, optimization, and qualification of a clinical-scale application will be performed exclusively with USD approaches. For the near future, the most optimistic scenarios leverage HTPC for scouting, development, and optimization but assume some intermediate scales will be used, at least for verification studies. In such a paradigm, HTPC is the focal point of development efforts but bench-scale models are still employed for verification and to test parameters that cannot be accurately emulated at the micro-scale. Accordingly, HTPC is valuable for process development but until additional scalability data is generated, has more limited utility for process characterisation. Although excellent HTPC precision/reproducibility has been observed during this thesis, replicates of conditions could be employed to further increase confidence in results.

Elements of QbD form an important role in validation but wholesale implementation of QbD holds an uncertain future. In certain instances, the benefits offered by the filing of design spaces via a formal QbD regulatory filing have been justified. Conversely, even if a design space is not bounded by straight lines or a rectangular operating window, the benefits of specifying an accurate contour may not be worth the regulatory burden or the operational complexity of attempting to implement a nuanced operating window. These observations have consequences for HTPD that explores wide

operating ranges, especially where failure is sought. The generation of deep process understanding afforded by these tools leads to more robust processes, but the details may not be worth disclosing to myriad regulatory agencies. HTPC can promote the utilisation of QbD elements to inform development but will likely be included only in abbreviated form in regulatory filings.

8.5 Chapter Summary

To fulfil the obligation for process validation, each organization will make the set of choices that are appropriate to their specific circumstances. The suitability of the choices will be assessed by regulatory agencies during formal application submission and review. While conservative in nature, regulators nevertheless expect a continual evolution and deepening sophistication of practise from manufacturers. In some cases, the obligatory evolution can be synergistic with cost-conscious efforts to streamline development activities. In other cases, the need for continuous improvement creates a tension that can be at least partly resolved through adoption of sophisticated, data-rich, practises such as HTPD. The larger number of data points offered by HTPC enable more process combinations to be examined, leading to greater process understanding. The result is the definition of an operating window that is underpinned by deeper process understanding.

The accepted scale-down of chromatographic processes to microplate batch binds and mini-columns offers a glimpse to how much value can derive from embracing an USD technology. Similarly, HTPC will reduce developmental resources, provide greater process understanding, and ultimately lead to more robust processes. While some obstacles remain, HTPC and its substituent components have the potential to revolutionize how the industry conducts process development.

9 Appendix B – Supplementary Data

9.1 *Neisseria Meningitidis* Case Study

9.1.1 Meningococcal Pathogenesis

N. meningitidis is a Gram-negative, aerobic bacterium. Meningococcal meningitis is acquired through direct contact with respiratory fluids. Humans are the only known carrier of *N. meningitidis*, with nasopharyngeal colonization present in at least 10% of adults (Pollard and Frasch, 2001). Although mucosal carriage is usually asymptomatic; infection of the blood or cerebrospinal fluid is pathogenic (Al-Tawfiq et al., 2010; Tan et al., 2010). Upon infection of internal systems, clearance of exogenous *N. meningitidis* is effected through opsonisation, complement-mediated serum bactericidal activity, phagocytosis, or a combination of these mechanisms (Granoff, 2009; Stephens, 2007). For many individuals, clearance is inadequate as fatality occurs in 10-14% of cases with 11-19% of survivors experiencing serious sequelae such as hearing loss, limb loss, and cognitive deficits (Centers for Disease Control, 2005).

9.1.2 Meningococcal Epidemiology

Thirteen serotypes of *N. meningitidis* have been classified based on antigenic and chemical differences in the CPS. However, meningococcal infections in humans are predominantly caused by serotypes A, B, C, W-135, X, and Y (Frasch, 1990; Stephens, 2007). All of the infectious serotypes possess CPS and it is believed that this attribute helps minimize complement activation (Tan et al., 2010). The prevalence of serotypes is strongly delineated by geography (Figure 9.1). For example in the United States in 2007, the serotype profile of classified meningococcal infections was 32% B, 28% C, 37% Y, and 4% other. Contrast that with Africa, where almost all outbreaks have been caused by serotype A and are usually associated with widespread infection and death (Centers for Disease Control, 2010b; Mayor, 2010). In 1996-97, an epidemic of meningococcal serotype A infected 250,000 people, resulting in 25,000 deaths (Mayor, 2010). The global epidemiology is further complicated by serotype distribution being dependent on age group (Centers for Disease Control,

2005). The uneven global distribution of serotypes combined with an evolving epidemiology has led to a profusion of vaccines (Table 9.1).



Figure 9.1. Distribution of *N. meningitidis* serotypes around the world (Harrison et al. 2009).

Serotypes A, C, W-135, and Y have been the target of most prophylactic efforts to produce a polysaccharide vaccine. In Table 9.1, it is evident that the development of meningococcal vaccines progressed from monovalent to multivalent CPS and finally to CPS conjugates. As mentioned in section 1.3.3, the most recent vaccine development activity has focused on producing a low cost serotype A CPS conjugate vaccine for use in Africa where most of the deaths occur.

Table 9.1. Meningococcal vaccine development (Centers for Disease Control, 2005; Chandramohan et al., 2007; Food and Drug Administration United States, 2010a; Gold et al., 1977; Lattanzi and Giudice, 2002; Meningitis Vaccine Project, 2011; Stephens, 2007; Zimmer and Stephens, 2004).

Naked Polysaccharides				
Valency	Serotype(s)	Brand Name	Manufacturer	Approval Date
Mono-	A	N/A	N/A	1971 (US)
Mono-	C	N/A	N/A	1971 (US)
Di-	A, C	Mencevax AC	GlaxoSmithKline	N/A
Di-	A,C	Mengivac A+C,	Sanofi Aventis (Aventis Pasteur)	N/A
Di-	B ² , C	VA-MENGOB-BC	Cuba	1989 (Cuba)
Tri-	A,C,W-135	Mencevax ACW	GlaxoSmithKline	2003 (Belgium)
Tetra-	A, C, Y, W-135	Menomune	Sanofi Aventis	1981 (US)
Tetra	A,C,W-135, Y	Mencevax ACYW	GlaxoSmithKline	N/A
Polysaccharide-Conjugates				
Valency	Serotype(s) (conjugate protein)	Brand Name	Manufacturer	Approval Date (country)
Mono-	C (CRM ₁₉₇)	Meningitec	Pfizer (Wyeth)	1999 (UK)
Mono-	C (CRM ₁₉₇)	Menjugate	Novartis (Chiron)	1999 (UK)
Mono	C ¹ (tetanus toxoid)	NeisVac-C	Baxter	2000 (UK)
Mono-	A (tetanus toxoid)	MenAfriVac	Meningitis Vaccine Project	2010 (WHO)
Tetra-	A, C, Y, W-135 (diphtheria toxoid)	Menactra	Sanofi Aventis	2005 (US)
Tetra-	A, C, Y, W-135 (CRM ₁₉₇)	Menveo	Novartis	2010 (US)

¹NeisVac is de O-acetylated; ²Vaccines to Hepatitis B have been developed by several countries (e.g.

Cuba, Norway, New Zealand, etc.) but were restricted to local strains of serogroup B.

9.1.3 Meningococcal Glycobiology

In *N. meningitidis*, a complex cellular envelope surrounds the cell (Figure 9.2). The innermost layer is a phospholipid bilayer and is surrounded by a peptidoglycan cell wall and an outer cell wall. These structures serve to give the bacteria structural integrity (Pollard and Frasch, 2001).

Lipopolysaccharides (*i.e.* endotoxin) and a membrane comprise the outer cell wall with the CPS forming the outer layer of this superstructure. Meningococcal CPS is covalently bound to phospholipid or lipid A molecules in the outer cell wall (Whitfield and Valvano, 1993).

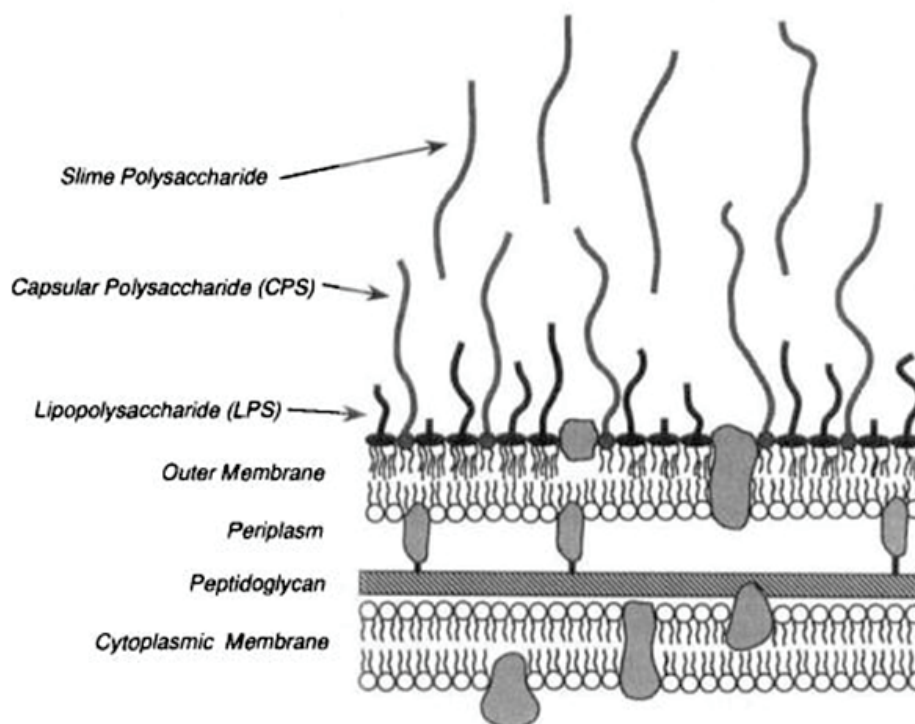


Figure 9.2. Outer cellular structure of *N. meningitidis* (Whitfield and Valvano, 1993).

The serotypes of *N. meningitidis* are classified by structure. A consolidated description of the serotype-specific repeating oligosaccharides is provided in Table 9.2. The CPS identified in Table 9.2 share many properties. When purified, each polysaccharide is a linear homopolymer of repeating mono- or disaccharides (Joshi et al., 2009). The profusion of hydroxyls in each sugar ensures that the molecules are highly hydrated. Serotypes C, Y, and W-135 all contain sialic acid and hence have a negatively charged carboxylic group in physiological conditions. Similarly, the phosphodiester bond of Mn A is negatively charged.

The levels of O-acetylation and their significance vary among the meningococcal polysaccharides. O-acetylation has not been found to be important for generating a protective immunological response in Mn C and Mn W135 (Jones and Lemercinier, 2002). Conversely, the pattern of O-acetylation comprises immunologically active epitopes in Mn A (Berry et al., 2002). Antibodies specific for O-acetylation epitopes tend to be of low avidity compared with the high affinity antibodies that bind to the polysaccharide backbone (Jones, 2005a). O-acetylation has been shown to be labile under

bioprocessing conditions: groups can be lost or migrate position (Lemerclinier and Jones, 1996). For these reasons, this characteristic has historically been monitored for regulatory purposes in vaccine release specifications for CPS vaccines.

Table 9.2. Repeating structures of pathogenic *N. meningitidis* CPS. All sugars have D and α structural configuration (Food and Drug Administration United States, 2010a; Jones and Lemerclinier, 2002; Joshi et al., 2009; Lemerclinier and Jones, 1996; Tzeng et al., 2003).

Serotype	Repeating Motif	Range of O-acetylation (%) (average)	O-acetylation Position(s)
A	(1,6)N-acetylmannosamine phosphate	81-95% (88%)	O3
C	(2,9)N-acetylneuraminic acid	76-96% (90%)	O7/O8
Y	(4)N-acetylneuraminic acid (2→6)-glucose-(1→	38-84% (49%)	O7/O9
W-135	(4)N-acetylneuraminic acid-(2→6)-galactose-(1→	60-86% (66%)	O7/O9

9.2 Holistic Purification Process Development for CPS

There has been limited research aimed at improving existing production purification processes for capsular polysaccharides from *N. meningitidis* (Table 9.3).

Table 9.3. Summary of research into downstream processing of meningococcal polysaccharide: (s) indicates solid is product containing and (l) indicates liquid is product containing. Centrifugation is integral to each precipitation step. Table is colour-coded per this legend:

Chromatography
Precipitation
Tangential Flow Filtration
Extraction

Sero-type	Mn A/Mn B/Mn C	Mn C	Mn C
Order of Operation →	Ppt with 0.10% (w/v) CTAB; CF at 20,000 g for 5 min (s)	Spin to remove cells (l)	Ppt with 0.10% (w/v) CTAB; CF at 15,000 g for 30 min (s)
	Homogenization with H ₂ O and spin at 13,000 g for 10 min (s)	UF (100 kDa)	Resuspension in 1.0 M CaCl ₂ ; spin at 15,000 g for 30 (l)
	Resuspension in 0.9 M CaCl ₂ -CF at 13,000 g for 15 min; repeat 3X (l)	0.5% DOC at 50°C	Ppt DNA with 25% EtOH; incubate 1 h; CF at 15000 g for 30 min (l)
	Ppt DNA with 25% EtOH, cool to 4°C for 3 h, CF at 13000 g for 15 min (l)	DF at 50°C (100 kDa)	Ppt with 80% EtOH to remove CaCl ₂ /detergent; incubate O/N; CF at 15,000 g for 30 min(s)
	Ppt with 80% EtOH to remove CaCl ₂ /detergent; CF at 2,000 g for 10 min (s)	Bind/Elute AEX with Source 15Q	Resuspension in 20 mM Tris, pH 8.5; degrade protein with proteinase K, trypsin, and nagarase O/N; repeat for 4 h
	Wash ppt with 100% EtOH (3X), acetone (2X), diethyl ether (2X), spinning at 13,000 g for 10 min, and dried	SEC with Sepharose CL-4B	Add DOC and incubate for 30 min at 60°C; sonicate for 15 min.
	Resuspension in 0.1 M Na acet.; pH 6.8, CF at 100,000 g for 2 h to remove protein (l)	DF	UF (100 kDa MWCO) to remove LPS and small proteins
	Resuspension with chloroform/butanol (5:1); CF at 13,000 g for 10 min (6X) (l)		DF with 5 DV of 20 mM Tris, 2 mM EDTA; 0.5% DOC; 3 CV w/o DOC; 3 CV H ₂ O
	Ppt with 80% EtOH; CF at 2,000 g for 10 min (s); resuspend with sat. NaAc., pH 7.0		
	Ppt with 80% EtOH; CF at 2,000 g for 10 min (s)		
	Resuspend with H ₂ O; UltraCF at 100,000 g for 2 h (l)		
	Ppt with 80% EtOH; CF at 2,000 g for 10 min (s)		
	Wash with 100% EtOH (3X), acetone (2X), and dry		
Perfor- mance	N/A	Yield: 67%; 0;1% Protein: 0.1%; Nucleic acid: 0.5%; MW = 452 kDa	Yield: 50%; Protein: 1.3%; Nucleic acid: 1.2%; Kd > 0.30
Ref.	(Gotschlich et al., 1969b)	(Pato et al., 2006)	(Tanizaki et al., 1996)

CTAB = cetyltrimethylammonium bromide; Ref = reference; ppt = precipitation, LPS =

lipopolysaccharide; Inact. = inactivation agent; CF = centrifugation; DOC = deoxycholate; O/N=

overnight

The research outlined in Table 9.3 focused on the integration of improvements into a coherent downstream purification process. In general, this body of work sought to improve the precipitation, centrifugation, and filtration steps. Tanizaki *et al.* added proteases and a negatively-charged detergent to eliminate phenol extraction and also substituted tangential flow filtration for ultracentrifugation (Tanizaki et al., 1996). Although the resulting process was greatly simplified, the addition of exogenous enzymes would be problematic for commercial manufacture. Furthermore, the final purity achieved was inadequate for a vaccine. Pato *et al.* avoided the addition of enzymes and opted to purify with a chromatographically intensive process (Pato et al., 2006). This approach eliminated the polysaccharide precipitation step. The result is a greatly simplified process although the resins selected are expensive and not conducive to straightforward scale-up. Source resin has a bead diameter of 15 μm and forms packed beds of low permeability requiring equipment with very high pressure ratings. The complexity of scaling SEC stems from the difficulty in maintaining efficiency, resolution, and linear velocity in larger diameter columns. Nevertheless, patent applications and product literature from Novartis indicate similar interest in chromatography for polysaccharide purification (Costantino et al., 1999; Food and Drug Administration United States, 2010b). Although suffering some limitations, these developmental efforts do signal a shift in the approach to polysaccharide purification towards integration of advancements in purification technology.

9.3 Protein Assays

BSA standard curves for the Bradford and BCA assays are given in Figure 9.3. The response of BSA in the BCA assay resulted in a stronger absorbance signal (A_{562}) than in the Bradford assay ($A_{595-990}$). The optimum mathematical fits for the standard curves were polynomial and linear for the BCA and Bradford assays, respectively. The accuracy of the Bradford assay reached a maximum when a dynamic range of 0.0-0.5 mg/mL BSA was employed. This range could be expanded but small decreases in accuracy were observed. The effects on precision of using different wavelengths for the Bradford assay are shown in Figure 9.4.

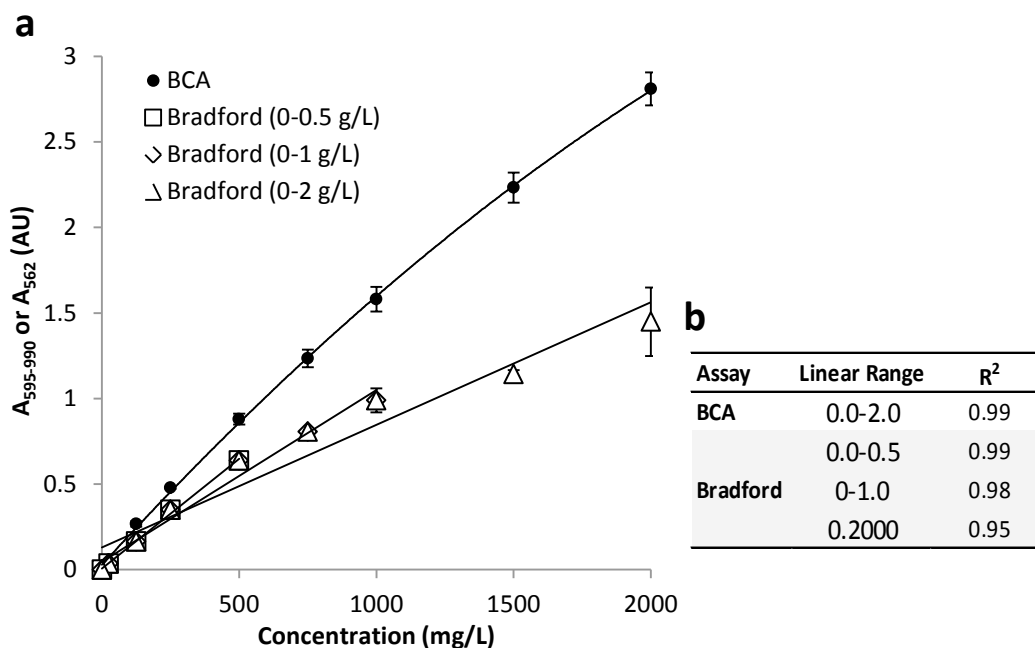


Figure 9.3. Standard curves (9.3a) and statistical effect (9.3b) of adjusting the dynamic range of BSA in the protein assays. Bradford utilised $A_{595-995}$ and BCA utilised A_{562} . N = 4 for each curve.

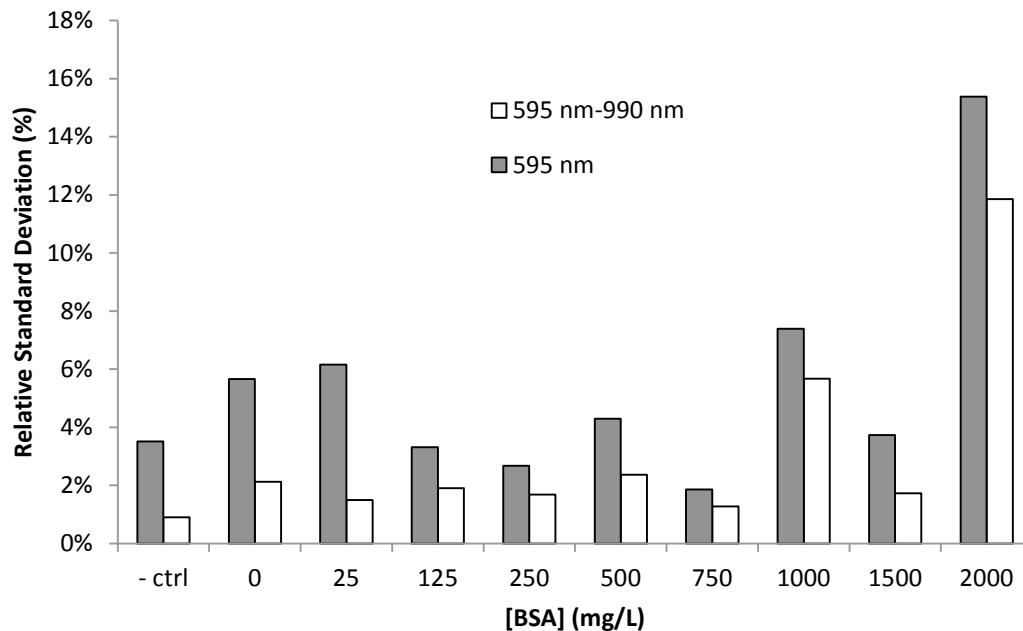


Figure 9.4. Relative standard deviation of two different measurement parameters for generating standard curves with the Bradford assay. N = 4 for each method.

Clearly, using the A_{990} correction for turbidity improves the precision of the Bradford assay. The standard curves in the Bradford assay for a library of carbohydrates and potential process impurities are illustrated in Figure 9.5. Only proteins and DNA to a significantly lesser extent react in the Bradford assay.

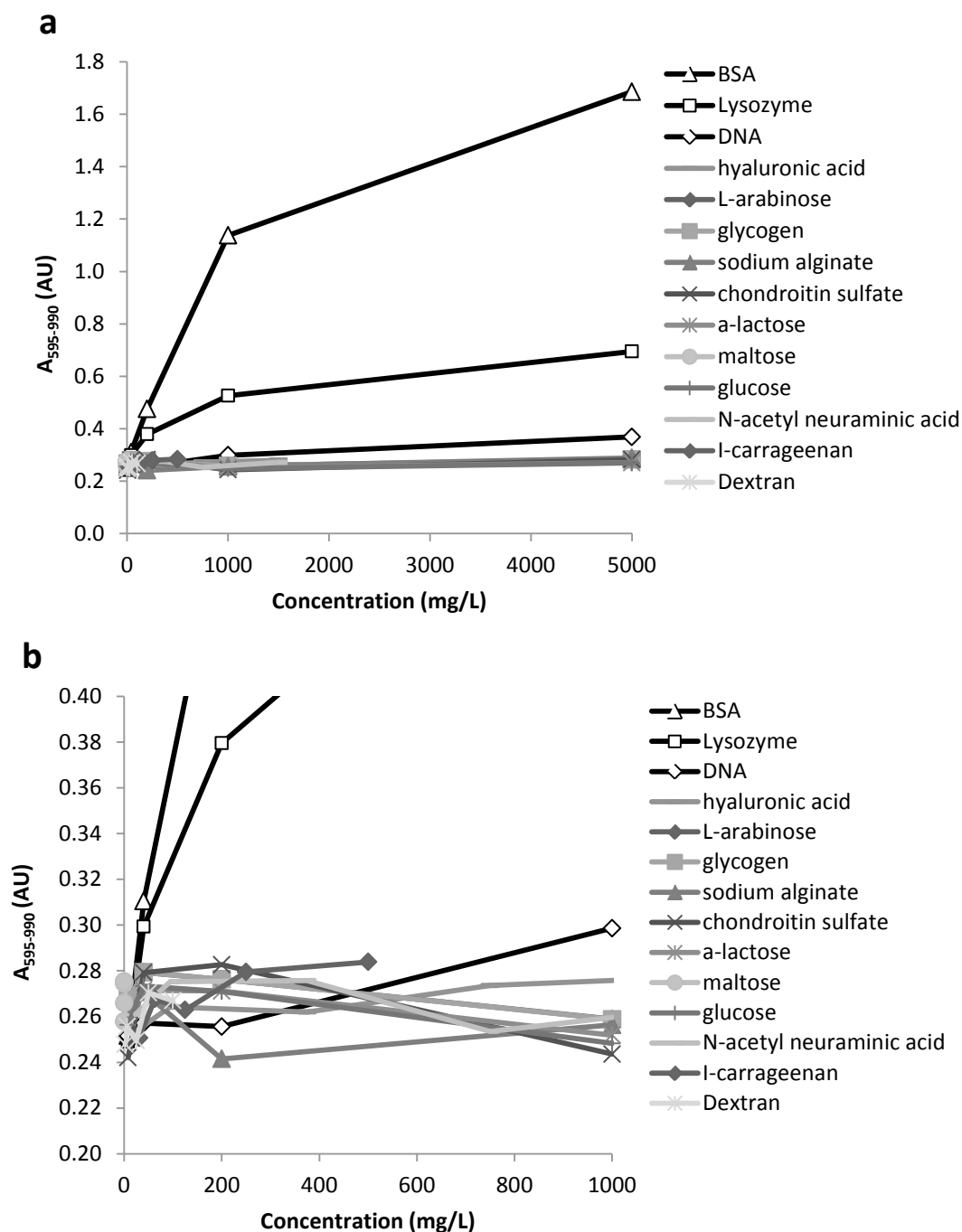


Figure 9.5a, b. Standard curves generated with the Bradford assay for assorted carbohydrates and compounds typically found in microbial broths (9.5a). Zoomed in section of Figure 9.5a (9.5b).

9.4 Differential Assay for Carbohydrates

Given the contrasting responses of reducing sugars in the two proteins assays, an effort was made to use the differential signal to measure the titre of a reducing sugar. First, the capability to sum the reactive components of multi-component mixtures was examined. The slopes of the standard curves for glucose and BSA were independently measured with the BCA assay, with the sum equalling 1.56 AU/(mg/mL). A standard curve for samples consisting of 50:50 BSA:glucose was generated and was characterised by a slope of 1.31 AU/(mg/mL), 18% below the expected value.

In a subsequent examination of the differential approach, glucose was spiked to a final concentration of 1 mg/mL in solutions containing from 0.02-0.50 mg/mL BSA (Figure 9.6). The amount of glucose was calculated from the difference of the BCA and Bradford signal. This was achieved by using a calibration equation derived from the BSA standard curve (to measure glucose in units of mg/mL BSA) and normalizing by the ratio of the slopes of the glucose and BSA standard curves. This conversion was necessary because each molecular species generates a unique signal:concentration ratio in the BCA and Bradford assays. The outcome of these experiments was an estimation of 0.724 ± 0.152 mg/mL of glucose as displayed in Table 9.4. This result was imprecise and significantly below the expected concentration of 1 mg/mL. The high variance and inaccuracy may be due to additive errors present when using multiple assay measurements for a single differential measurement.

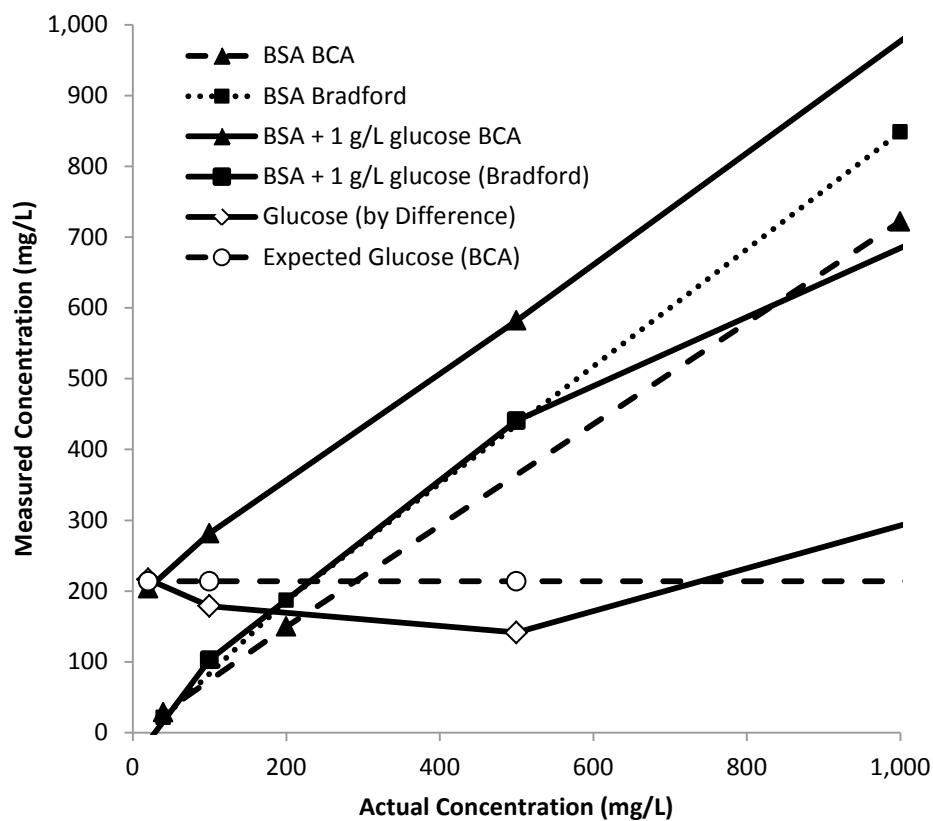


Figure 9.6. Determination of reducing sugar concentration through differential analysis of orthogonal protein assays. Standard curves with pure BSA (dashed lines) and an additional 1 g/L glucose present (solid lines) were run in the Bradford and BCA assays. The horizontal dashed line represents the BCA response for 1 g/L glucose and the starred dataset is the experimental equivalent derived from the differential use of the two protein assays.

Table 9.4. Amount of glucose calculated from differential method. Measured in BSA samples spiked with 1 mg/mL Glc.

[BSA] (mg/L BSA)	500	100	20	4	Average	Σ
[Glucose] (as mg/L BSA)	141	179	216	118	179	38
[Glucose] (as mg/L glucose)	572	724	877	478	724	153

This trial indicated that the differential use of the two assays was neither accurate nor robust enough for estimating sugar concentrations. Equally problematic was that both protein assays reacted with an intensity that was dependent on the protein composition. If the relative reactivity of a given sample in the two assays varied sharply, it would hinder the utilisation of this approach. This would be particularly vexing for purification development where protein compositions could differ markedly across a microplate due to selective purification. The contrasting slopes for lysozyme and BSA standard curves when measured in both protein assays in Figure 2.4 provides an indication of the noise that could be encountered. For these reasons, the differential method for reducing sugar quantification was deemed better suited to highly purified samples, drawn from further downstream in the purification process.

9.5 Phase Separation Assay

Standard curves in the Hb phase separation assay were produced with Mn C and Mn Y drug substance. Each CPS was serially diluted into 25 mM sodium phosphate, pH 7.2 in the presence of 10, 50, 100, 200, 300, or 400 mM NaCl in the background buffer. The range and precision of the phase separation assay were determined by measuring the light scattering without correction for blanks or negative controls. The data for each CPS concentration (with varying [NaCl]) was averaged and plotted against reference concentrations determined with manufacturing SOPs.

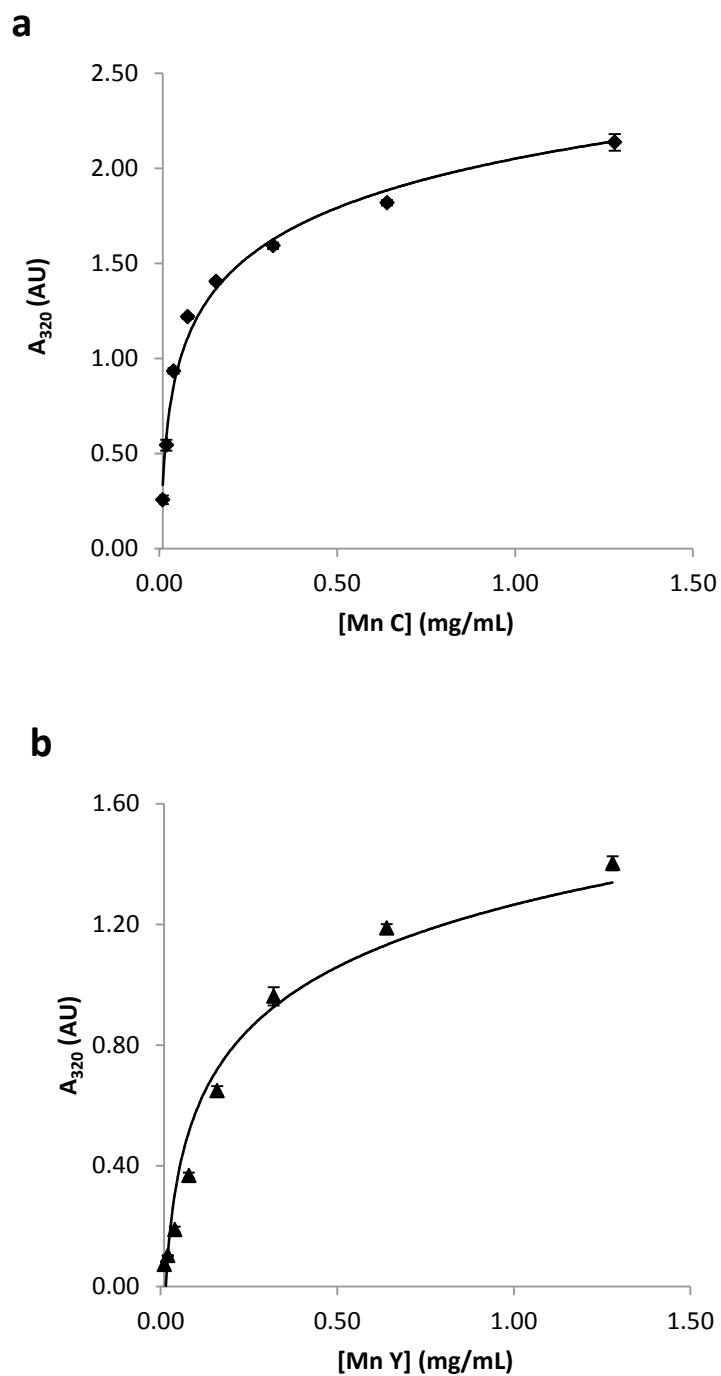


Figure 9.7a, b. Precision ($N = 6$) and dynamic range of phase separation assay for Mn C (9.7a) and Mn Y (9.7b). Initial [NaCl] = 10-400 mM NaCl. As per the standard assay procedure, samples were batch-desalted in a microplate. Error bars represent standard deviation of replicates ($N = 6$).

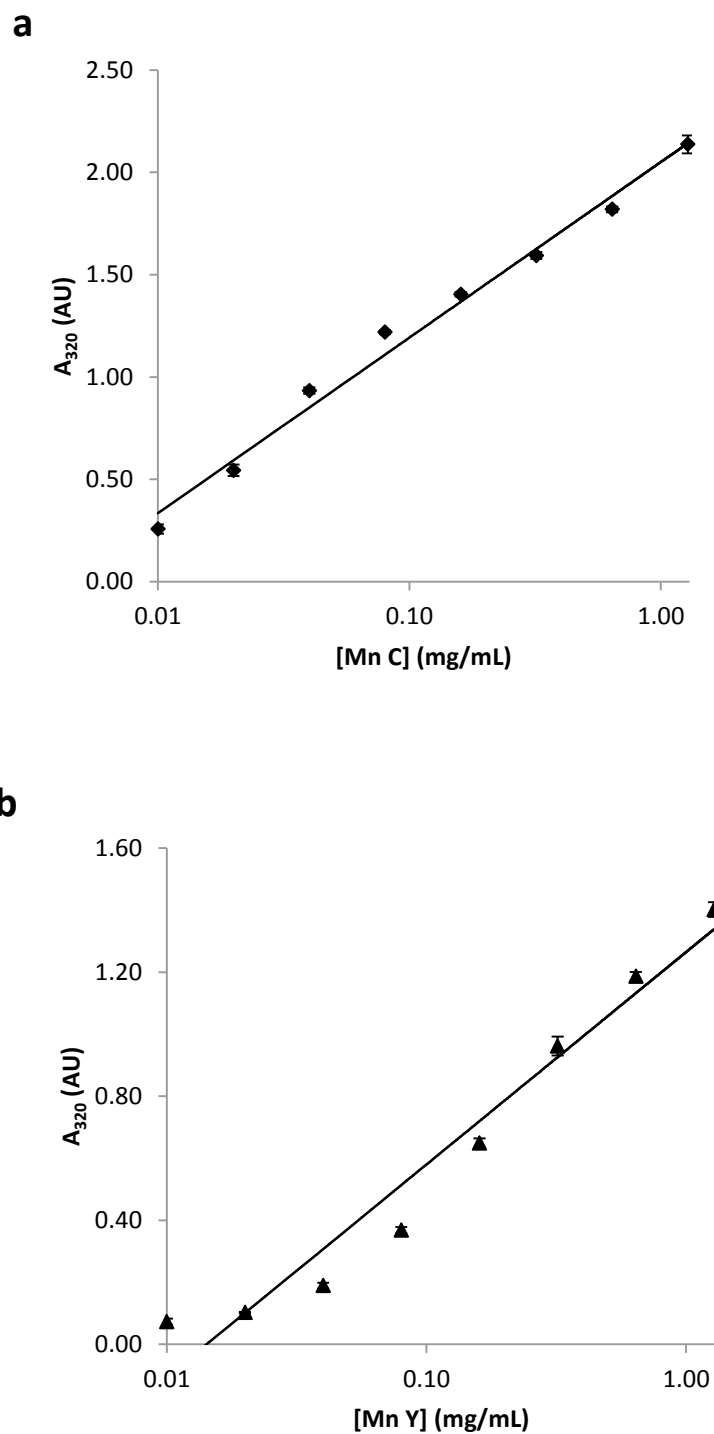


Figure 9.8a b. Figure 9.7 plotted on a semi-log-transformed plot. The following equations define the lines: Mn C: $y = 0.37 \ln(x) + 1.27$, $R^2 = 0.99$; Mn Y: $y = 0.30 \ln(x) + 1.27$, $R^2 = 0.96$. Error bars represent standard deviation of replicates ($N = 6$).

9.6 Flocculation Kinetics at the Micro-scale

The flocculation kinetics of the floc agent with two different staphylococcal serotypes were examined in a 10 mL microplate (Figure 9.9).

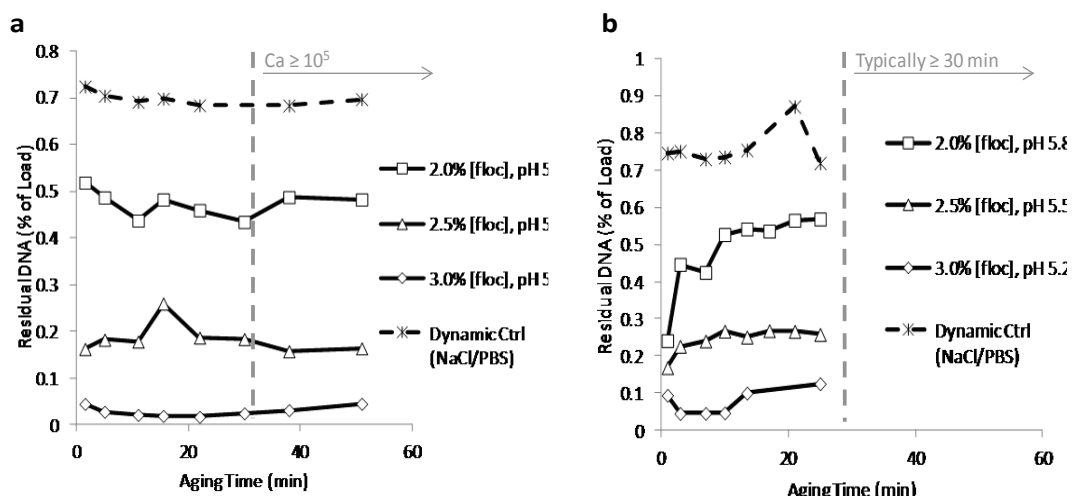


Figure 9.9a, b. Kinetic curves for the flocculation of staphylococcal CPS SA1 (9.9a) and SA2 (9.9b) during dynamic aging steps. Three flocculation conditions and a dynamic control were evaluated during the development of a steady state. The dynamic control substituted an equal volume of PBS and 5 M NaCl for the titrant and floc agent, respectively. The vertical dashed lines denote the aging time beyond which $Ca \geq 10^5$, a value associated with maximal floc strength.

Using the same load for each serotype, flocculation was performed at three conditions, which had previously been shown to span a broad spectrum of DNA clearances (Figure 4.6, 4.7). With SA1, the flocculation reached equilibrium within five minutes (Figure 9.9a). Although different levels of purification were achieved, negligible differences in rates were observed between the three conditions tested. For SA2, equilibrium was also attained within five minutes, however changes in the early flocculation rates differed between the three conditions tested (Figure 9.9b). The worst-case flocculation condition (*i.e.* 2.0%, pH 5.8) was characterised by slower kinetics.

In general the reaction kinetics for this type of flocculant, which were not measured directly in this study, are quite fast, occurring in < 5 s (Kresta and Brodkey, 2004). Hence, the high Damköhler number (*i.e.* mixing time/reaction time) suggests the rate of flocculation is dictated by mixing and therefore, is dependent on diffusion and turbulence. Indeed, slower flocculation kinetics occurred in a condition (*i.e.* 2.0%, pH 5.8) that was characterised by a relatively low percentage solids, floc size, and particle concentration. It is likely that this condition had a higher viscosity than the other two conditions due to the presence of more un-flocculated particles such as nucleic acids, leading to mixing constraints. For weaker flocculation conditions, the nascent flocs might also be characterised by lower floc strengths, leading to extended restructuring processes and requiring more time to achieve hydrodynamically stable floc structures. In Figure 9.9, it is evident that even for the kinetically slower flocculation condition, steady-state is established well before the completion of the aging step in a process designed to achieve $Ca \geq 10^5$, the minimum Ca found to deliver superior floc strength and stability (Bell and Dunnill, 1982).

The kinetic studies illuminate some of the processes integral to particle conditioning but as they are applicable only to the system in which they were tested, they cannot explain the differences in DNA clearance observed across scales for the staphylococcal CPS.

9.7 Engineering of USD Depth Filtration Device

9.7.1 Tubing Diameter

An important specification for the USD depth filtration device was the tubing size to used to connect the syringe pumps and the filter manifold. Clearly, tubing length should be as short as possible to minimize hold-up volume. Tubing 1.5 mm in inner diameter (ID) was chosen arbitrarily, employed in early designs, and not remarked upon. The basis for the determination of the optimal inner diameter of the tubing was unclear: holdup volume should be minimized but with narrow bore, pressure limitations or particle blockages can arise. The effect of shear on particulates in the feed was unknown, much less the ancillary effect on filtration. To assist with the determination of optimum tubing ID, data was gathered from larger scales systems in use at Pfizer (Table 9.5).

Table 9.5. Engineering characteristics of depth filtrations systems at several scales (Chan et al., 2006; Patel et al., 2011; Zoro et al., 2009).

Regime			Assumes $J = 0.0556 \text{ L s}^{-1} \text{ m}^{-2}$, $\eta = 0.003 \text{ kg m}^{-1} \text{ s}^{-1}$, $\rho = 1000 \text{ kg m}^{-3}$				Option 2	Proposed	Option 3	Option 4	Lab-scale	Lab-scale prep			Pilot-scale				Commercial-scale	
	Filter Cross-Sectional Area	cm^2	0.38	0.38	0.38	0.38	25	170	340	1,000	10,000	10,000	50,000	100,000	330,000					
	Tubing	ID	0.5 mm	0.7 mm	1.0 mm	1/16"	#16	#15	#15	1/2"	1/2"	1"	1"	1"	1"					
	Tubing ID	cm	0.05	0.07	0.10	0.16	0.31	0.48	0.48	1.27	1.27	2.54	2.54	2.54	2.54					
	Length	cm	60	60	60	60	60	60	60	100	100	200	200	200	200					
	Pipe Holdup Volume	$\text{L m}^{-2} \text{ filter}$	3	6	12	32	2	1	0	1	0	1	0	0	0					
	Linear Velocity	cm s^{-1}	1.1	0.5	0.3	0.1	1.8	5.2	10.4	4.4	43.9	11.0	54.8	109.6	233.5					
	Re		2	1	1	1	19	84	167	186	1857	928	4641	9283	19772					
Laminar	Shear Rate at Wall	γ	s^{-1}	172	63	22	5	47	87	174	28	276	35	173	345	736				
	Mean Residence Time	T_r	s	56	109	223	571	33	11	6	23	2	18	4	2	1				
	Mass Average Shear Rate	G_c	s^{-1}	92	33	11	3	25	46	93	15	147	18	92	184	392				
Transitional/ Turbulent	Mass Average Shear Rate	G_c	s^{-1}	6	2	1	0	5	19	49	8	213	20	192	508	1463				
	Pressure Drop in a Pipe	ΔP	mbar	25	7	2	0	1	1	3	0	3	0	3	7	27				

Tubing ID can be consequential, with USD design choices having a major impact on the scalability of physical parameters. Some parameters cannot be matched between USD and other scales, generally because the microscopic IDs required would approach the scale of the particulates and possibly lead to transient blockages. As presented in Table 9.4, USD linear velocities are much lower than in other scales, resulting in much longer residence times. Tubing backpressure is insignificant. The flow regime is laminar in USD and lab-scale, transitional in Pilot, and becomes turbulent at the largest production scales. These differences result in shear rates that are much larger in commercial-scale systems. Using a tubing 0.7 mm in diameter would bring shear in accordance with other scales. It would also lessen scale-related differences in residence time and linear velocity. The effects of these scale-dependent shear differences are difficult to assess definitively but owing to the long residence time, even in a USD environment of similar shear stress to the larger scales, the time-integrated shear will be much higher with potential impact on particulate structures. In some cases, sedimentation of dense particulates could occur. The particle population of particulates with poor mechanical strength would be most affected by these conditions and it is reasonable to assume that these changes would manifest as process differences in some cases. It is interesting to note although the pipe ID at large scale is often dictated by availability or backpressure concerns, the choice can mean the difference between operating in the transitional or turbulent regime.

9.7.2 Solids Holding Capacity

The volume available for holding solids retained on the filter surface must be specified. If one assumes capacities up to 400 L m^{-2} are expected, then a decision is required as to whether the USD filter device will be designed for primary clarification or secondary clarification (after centrifuge) of cell culture or fermentation harvests. The percentage solids for primary and secondary clarification are approximately 5-15% and 0-3%, respectively. Table 9.6 delineates systematically the headspace required for various combinations of solids and volume processed.

Table 9.6. Effect of percentage solids and filter capacity on the height of the solids holding area required.

Assumes the solids holding area is a vertical extension of the accessible filter area.

Height of Solids (cm)		% Solids														Height	
		1%	2%	3%	4%	5%	6%	7%	8%	9%	10%	11%	12%	13%	14%		15%
Filter Challenge (L/m ²)	25	0.0	0.1	0.1	0.1	0.1	0.2	0.2	0.2	0.2	0.3	0.3	0.3	0.3	0.4	0.4	0-1 cm
	50	0.1	0.1	0.2	0.2	0.3	0.3	0.4	0.4	0.5	0.5	0.6	0.6	0.7	0.7	0.8	1-2 cm
	75	0.1	0.2	0.2	0.3	0.4	0.5	0.5	0.6	0.7	0.8	0.8	0.9	1.0	1.1	1.1	2-3 cm
	100	0.1	0.2	0.3	0.4	0.5	0.6	0.7	0.8	0.9	1.0	1.1	1.2	1.3	1.4	1.5	3-4 cm
	125	0.1	0.3	0.4	0.5	0.6	0.8	0.9	1.0	1.1	1.3	1.4	1.5	1.6	1.8	1.9	4-5 cm
	150	0.2	0.3	0.5	0.6	0.8	0.9	1.1	1.2	1.4	1.5	1.7	1.8	2.0	2.1	2.3	5-6 cm
	175	0.2	0.4	0.5	0.7	0.9	1.1	1.2	1.4	1.6	1.8	1.9	2.1	2.3	2.5	2.6	
	200	0.2	0.4	0.6	0.8	1.0	1.2	1.4	1.6	1.8	2.0	2.2	2.4	2.6	2.8	3.0	
	225	0.2	0.5	0.7	0.9	1.1	1.4	1.6	1.8	2.0	2.3	2.5	2.7	2.9	3.2	3.4	
	250	0.3	0.5	0.8	1.0	1.3	1.5	1.8	2.0	2.3	2.5	2.8	3.0	3.3	3.5	3.8	
	275	0.3	0.6	0.8	1.1	1.4	1.7	1.9	2.2	2.5	2.8	3.0	3.3	3.6	3.9	4.1	
	300	0.3	0.6	0.9	1.2	1.5	1.8	2.1	2.4	2.7	3.0	3.3	3.6	3.9	4.2	4.5	
	325	0.3	0.7	1.0	1.3	1.6	2.0	2.3	2.6	2.9	3.3	3.6	3.9	4.2	4.6	4.9	
	350	0.4	0.7	1.1	1.4	1.8	2.1	2.5	2.8	3.2	3.5	3.9	4.2	4.6	4.9	5.3	
	375	0.4	0.8	1.1	1.5	1.9	2.3	2.6	3.0	3.4	3.8	4.1	4.5	4.9	5.3	5.6	
	400	0.4	0.8	1.2	1.6	2.0	2.4	2.8	3.2	3.6	4.0	4.4	4.8	5.2	5.6	6.0	

It is evident that high filter challenges of streams containing substantial percentage solids would require devices with very large (and tall) solids holding area. If the upstream area consists of tubing with a smaller cross-sectional area than the filter, then the heights will be amplified, leading rapidly to excessive backpressure. The key application envisioned for the micro-scale depth filtration device was secondary clarification. As such, solids content should be $\leq 5\%$ solids. Based on prior experience, achieving $\geq 200 \text{ L m}^{-2}$ is highly unlikely with streams of high solids content. These assumptions are borne out by examinations of lab- and Pilot-scale devices offered by 3M and MerckMillipore, where solids holding heights are typically $\leq 1 \text{ cm}$. This analysis, combined with a desire to reduce holdup volume (and related scaling issues), led to the specification of 1 cm of solids holding height. For primary clarification applications, a separate filter manifold with several cm of solids holding height could be fabricated.

9.8 Correlations between Clarity Measurements

To generate samples of varying turbidity, CHO concentrate was filtered independently with X0HC, COHC, D0HC, and CE50 as plotted in Figure 9.10.

The pressure profiles of the four filtration runs are plotted in Figure 9.10.

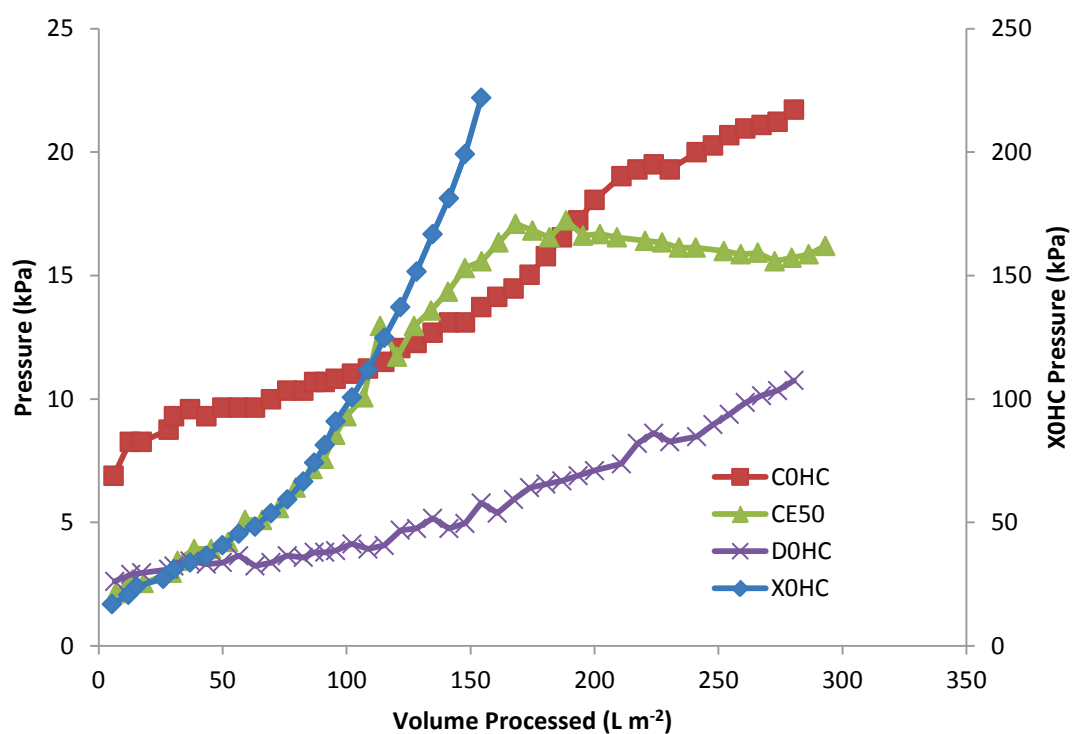


Figure 9.10. Hydraulic profiles for filtration performed with X0HC, C0HC, D0HC, and CE50 depth filters.

X0HC data are plotted on the secondary axis. The slight pressure decline in the second half of the CE50 run was likely due to instrumental error as no other measurement corroborated a performance shift.

X0HC plugged (241 kPa) at approximately 150 L m⁻². The remaining three filters showed slight pressure increases during the runs, but did not exceed 21 kPa. The DE-containing filters plugged relative to their nominal pore size ratings, with smaller pore sizes leading to earlier blockage. Filtrate fractions were collected and analysed with a variety of promising clarity assays.

9.8.1 Nephelometry

Historically, turbidity, as measured with a Hach nephelometer, has been the standard clarity measurement at bench-scale and above. To serve as a benchmark, sequential filtrate samples from the four runs were analysed with a Hach turbidimeter (Figure 9.11).

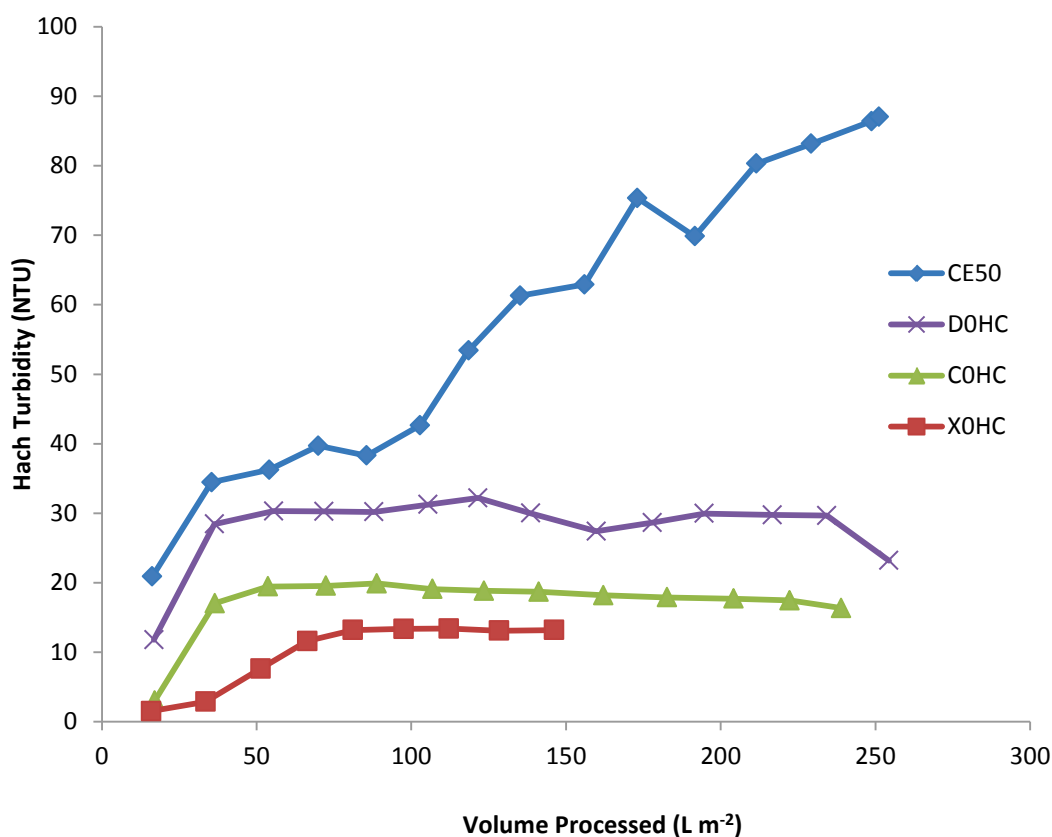


Figure 9.11. Hach turbidity values for filtrate samples during four filter trials. Flux was held constant at $0.0556 \text{ L s}^{-1} \text{ m}^{-2}$. The initial increase in turbidity was due to dilution from the RODI, in which the filters were initially equilibrated.

All the DE-containing filters exhibited flat turbidity profiles, with the level of the plateau dependent on the porosity of the filter. This was true irrespective of significant pressure increase during the run. The turbidity increased throughout the CE50 run, characteristic of breakthrough.

9.8.2 Particle Characterisation

Figure 9.12 provides particle characterisation of the filtrate samples. Particle characterisation is revealing. Particle concentration increased throughout the run for all filters except X0HC. The particle concentrations were proportional to the nominal pore rating for each filter. These data demonstrate that the filtrate composition was changing throughout the runs, in contrast to the trends in Figure 9.11. Particle sizes increased during the CE50 trial but were essentially constant for the adsorptive filters. For these latter filters, these phenomena might have been due to the large amount of small particles disproportionately dominating the number-average size calculation. A difference might have been

observed with volume-average sizes but this analysis was not available with the current MFI software.

The morphologies of the particles in the filtrate were also constant for DE-containing filters but became progressively more skewed and irregular in successive CE50 filtrate fractions (data not shown). The increasing particle counts, size, and irregularity are consistent with breakthrough of CE50.

Mechanistically, as a filter plugs, superficial linear velocities increase, leading to increased shear (Darby and Lawler, 1990; Kim and Tobiason, 2004). When drag exceeds the strength of interaction, particles become dislodged and exit the filter. Larger particles can be fractured by the increased turbulence.

Conversely, particle growth can be driven by the close proximity of particles during filter retention, a process often classified as aggregation. In general, the net results of these phenomena are increases in particle size and particle concentration during breakthrough.

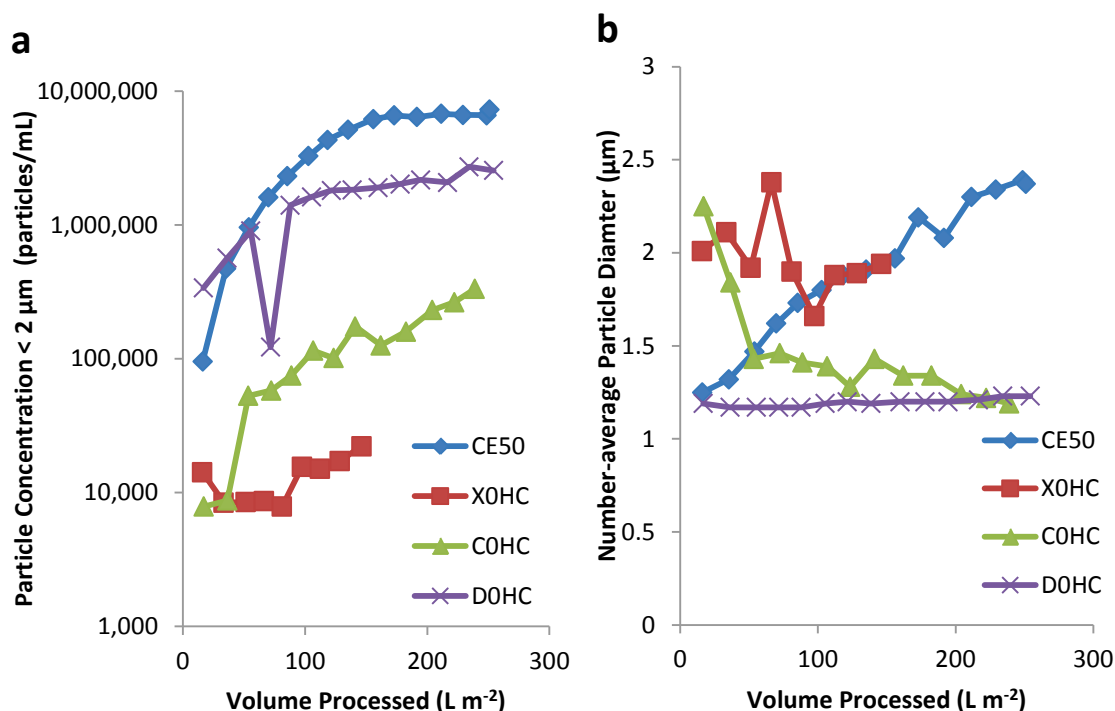


Figure 9.12a, b. Particle characterisation of filtrate samples. Particle concentrations of particles with diameter < 2 μm plotted on a semi-log plot (9.12a) and number-average particle diameter (9.12b).

Particles counts of particles with diameter < 2 μm were virtually indistinguishable from particles 1-70 μm in diameter.

9.8.3 Comparison of Clarification Measurements

Orthogonal clarity measurements for the same set of four filtration run are plotted in Figure 9.13. The relative ordering between the filtrate clarity is consistent for all technologies. Due to limited sensitivity, the Nephelostar did not resolve X0HC from COHC filtrate. The exquisite sensitivity of MFI particle concentrations relative to the other measurements can be appreciated by the much greater range of values spanned, which required a semi-log plot to display adequately.

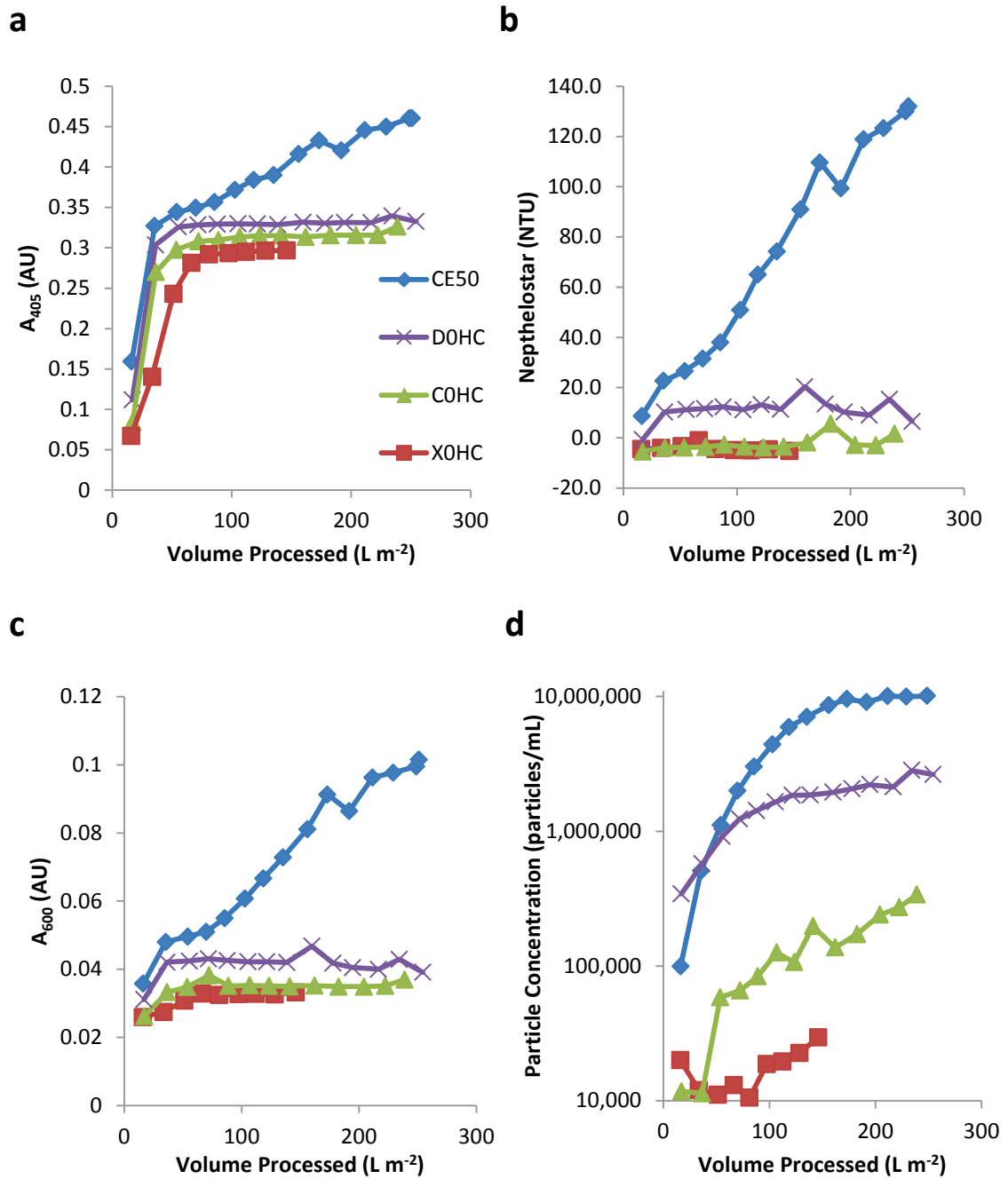


Figure 9.13a, b, c, d. Responses of clarity assays across four filtration runs. Clockwise from the upper left: A_{405} (9.13a), Nephelostar NTU calibrated with 1, 10, 20, and 200 NTU standards (9.13b), MFI particle concentration (9.13c), and A_{600} (9.13d).

9.8.4 Clarity Correlations

Binary correlations were examined for each combination of clarity measurements and several important relationships were noted. Hach and Nephelostar NTU measurements were comparable, though the lower sensitivity limit of the Nephelostar equated to approximately 15-20 NTU (as measured with Hach

turbidimeter). A_{600} was linear with Hach NTU across the full 0-100 NTU range. The response with A_{405} was similar to A_{600} though the relationship grew noisy and markedly deteriorated where Hach turbidity was less than 10-15 NTU. A_{600} was linearly proportional to Nephelostar NTU, although the 0 NTU value equated to 0.04 AU, underscoring the inferior sensitivity limit for the Nephelostar. This suggests a similarity of measurement principle, with differences in the measurement angle potentially influencing sensitivity.

The two most sensitive measurements were Hach NTU and MFI, with their relationship illustrated in Figure 9.14. A general correlation between MFI particle concentration and Hach NTU was present across the full 0-100 NTU range. When delineated by filter, the correlation was highly sensitive to individual particle populations. Indeed, for D0HC and C0HC, the relationship disappeared. For these two filters, particle counts in the filtrate changed by more than 1 log, yet the Hach NTU data suggested consistency. Conversely, for X0HC, particle concentrations did not indicate a systematic shift in particle counts, yet Hach turbidity yielded a range of 0-20 NTU. Particle shapes did not change markedly (data not shown). One plausible explanation for the poor correlation between particle counts and NTU is that the volume-average particle size might have shifted even though the number-average size value was constant.

A comparison of Hach and Nephelostar turbidity values is given in Figure 9.15. The two turbidity measurements yielded comparable values, with the Nephelostar NTU values slightly exceeding the respective Hach measurements. The Hach turbidimeter has superior sensitivity to the Nephelostar. A comparison of Hach NTU values with absorbance measurements is provided in Figure 9.16.

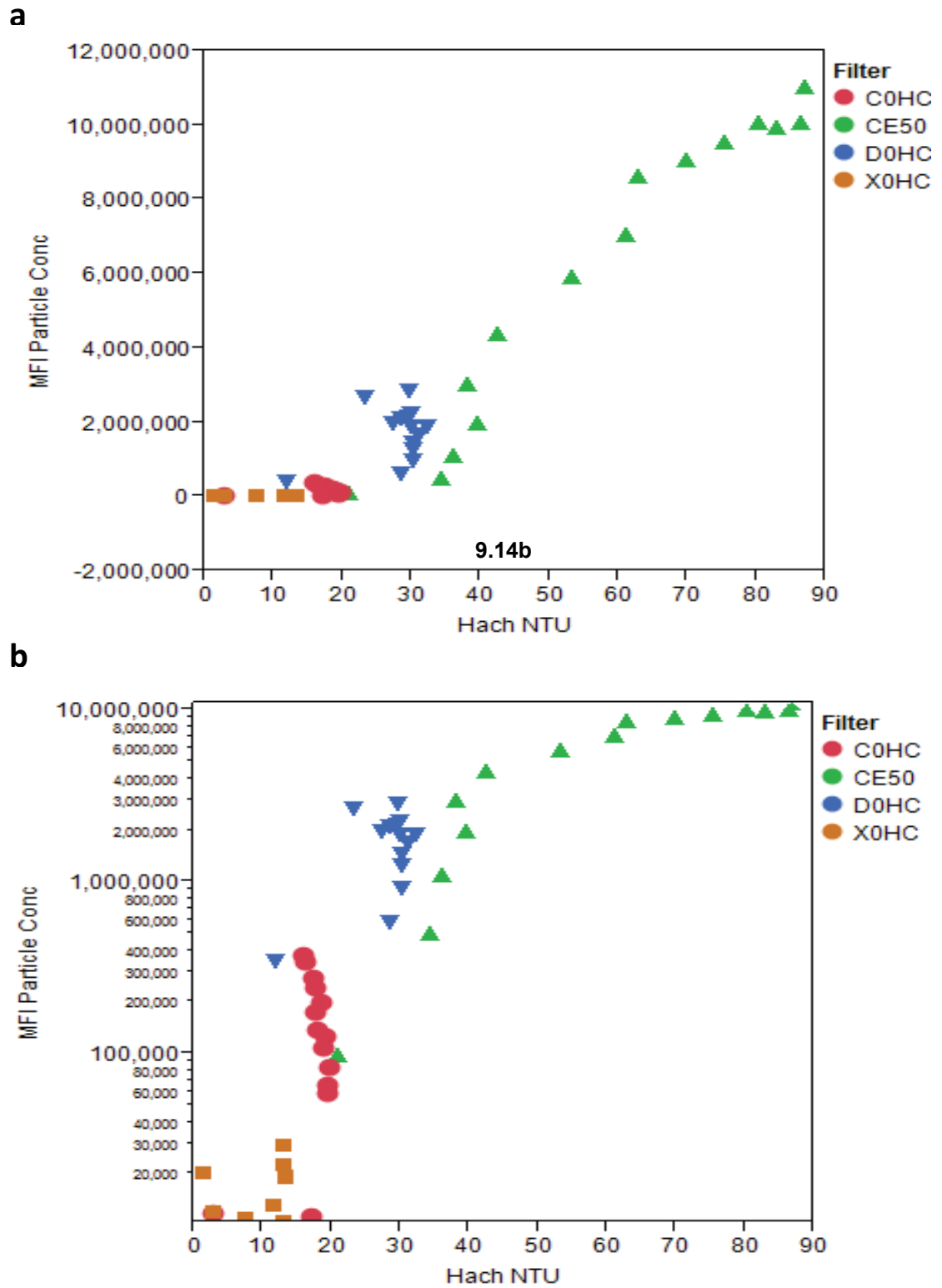


Figure 9.14a, b. Correlation of Hach NTU with MFI particle counts. The particle concentrations in the fractions from each are delineated by colour in a linear plot (9.14a) and semi-log plot (9.14b).

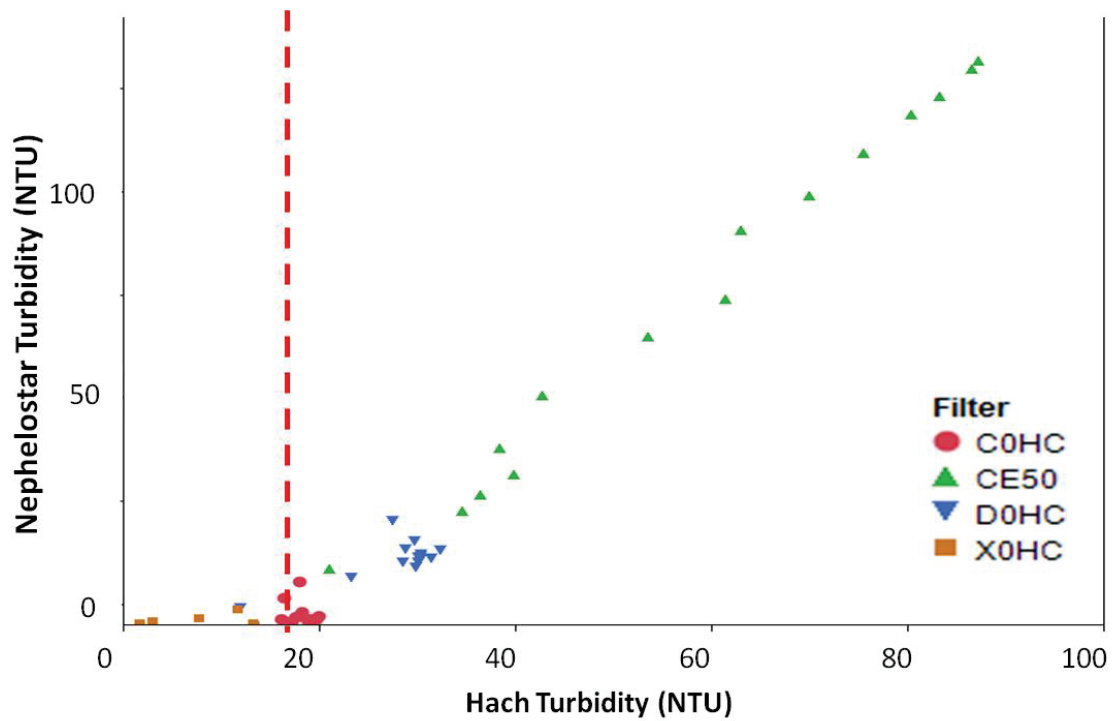


Figure 9.15. Correlation between two nephelometric turbidity measurements. Red line denotes the limit of sensitivity for the Nephelostar. The Nephelostar was calibrated with 1-200 NTU standards. Calibration with 1-20 NTU standards did not improve the sensitivity for relatively clear samples.

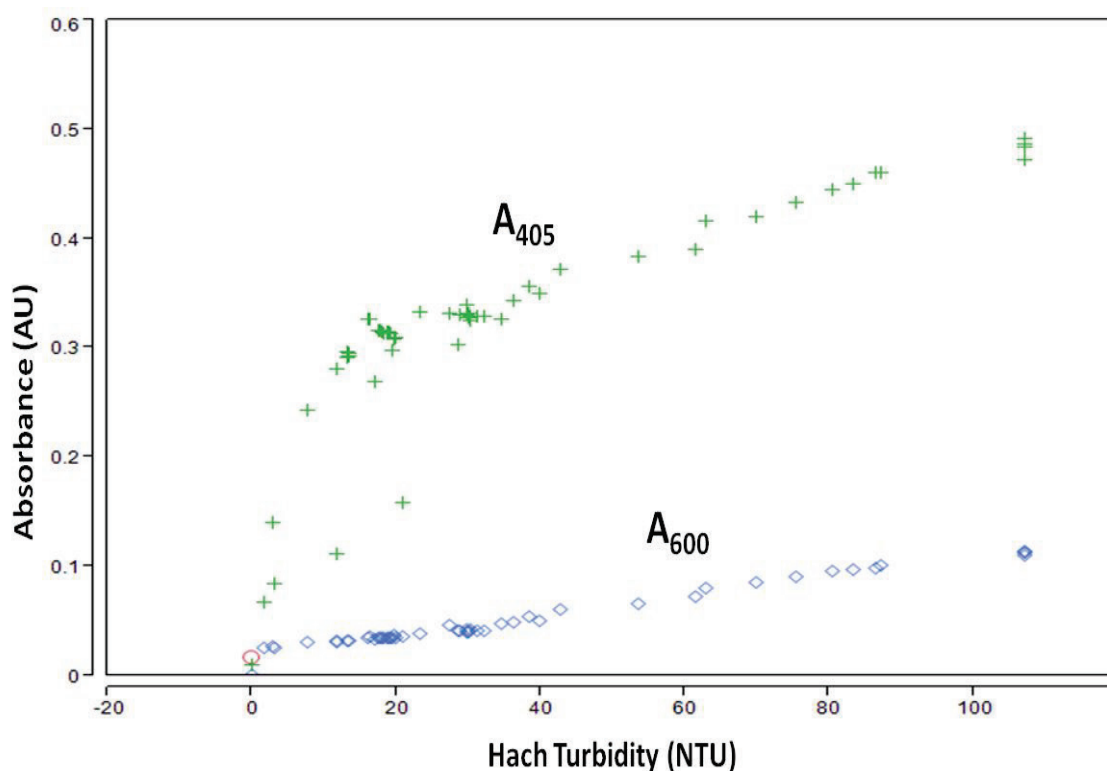


Figure 9.16. Correlations between Hach turbidity and absorbance at two wavelengths: A_{405} (green) and A_{600} (blue).

Linear relationships were observed between absorbance at both wavelengths and Hach NTU. Although the dynamic signal range of A_{600} was lower than A_{405} , it provided superior signal: noise. When turbidity ≤ 10 -15 NTU, the relationship between A_{405} and turbidity shifted, while the noise increased. A_{600} is plotted against the two turbidity measurements in Figure 9.17. Nephelostar NTU values were linearly proportional to A_{600} measurements. Hach NTU was also proportional to A_{600} but the relationship was noisier across the upper turbidity range. However, where Hach turbidity was ≤ 15 -20 NTU, the correlation between A_{600} and Hach NTU was maintained whereas the correlation between A_{600} and Nephelostar NTU disintegrated.

It is clear that clarity is influenced by both the porosity of the filter and the specific characteristics of a particle population. Clarity measurements are typically utilised to provide feedback on a purification process. Establishing a performance correlation between a given clarity attribute and relevant purification performance would identify the most salient measurement to use. Additional work is required to inform this understanding.

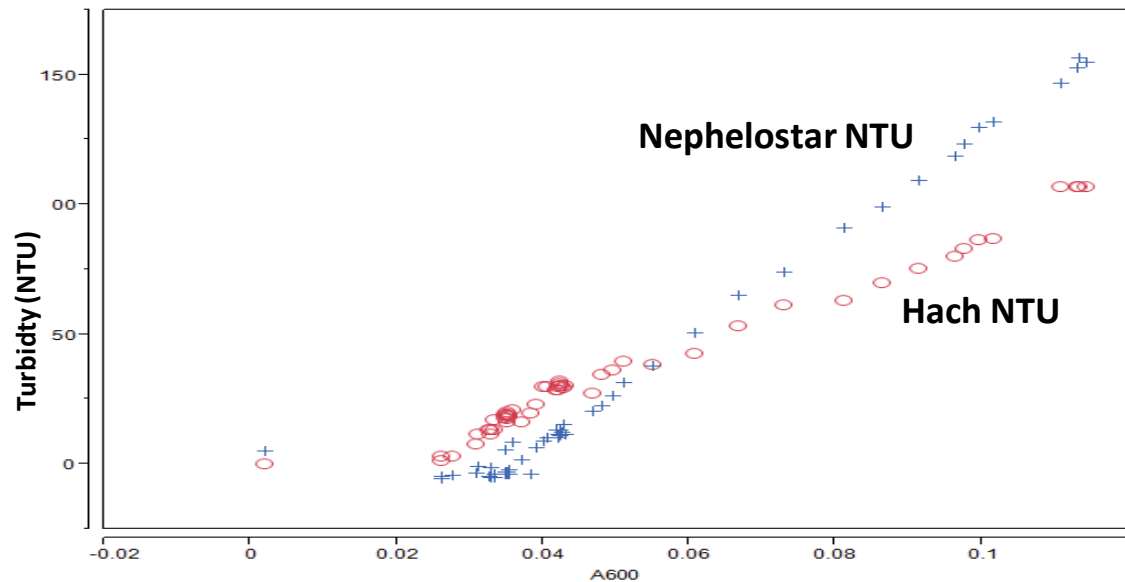


Figure 9.17. Correlations between A_{600} and two nephelometric turbidity measurements: Nephelostar NTU (blue) and Hach NTU (red).

As a result of these studies, three measurements are proposed for future work at the micro-scale: (i) Nephelostar NTU to provide a NTU value that provides context to people familiar with larger scale measurements, (ii) A_{600} because where $NTU > 20$, A_{600} is proportional to Hach NTU and can be measured rapidly with the same sample plate used in the Nephelostar, and (iii) MFI particle counts/size because these properties offer the most sensitive measurement and can facilitate mechanistic insight where necessary. With this set of three complementary clarity assays, many samples can be measured and analysed quickly, using < 1 mL of sample.